THE UNIVERSITY OF ADELAIDE
AUSTRALIA

The Role of Depositional Facies and Uncertainty Assessments in Hydrocarbon Estimates – An Example from the Daralingie Field, Cooper Basin, South Australia, Australia

Mohammad Al-Khalifa

B.Sc. Geology (Hons.)
Master Geology (Hons.)
King Fahad University of Petroleum and Minerals, Saudi Arabia

Australian School of Petroleum
The University of Adelaide

This thesis is submitted in fulfilment of the requirements for the degree of Doctor of Philosophy in the Faculty of Science, The University of Adelaide

December 2005

This dissertation is dedicated to the memory of my parents. Even though you weren't here to see the results, it is because of your love, guidance and your prayers for me, that I became what I am today.

Abstract

In this research a procedure was developed to assess and quantify uncertainties in hydrocarbon estimates related to depositional facies, petrophysical data and gross reservoir volumes. This procedure was applied to the Daralingie Field, which is a mature gas field in the Cooper Basin, South Australia. The aim was to investigate the reasons for an unexpectedly high hydrocarbon recovery factor.

This study was conducted in four phases: reservoir characterisation, stochastic geological modeling, hydrocarbon estimation and uncertainty assessment. The objective of the reservoir characterisation phase was to conduct an integrated reservoir study utilising all available data from Daralingie Field and the surrounding area to build a conceptual geological model. A geological description, based on core analysis, of the facies in the reservoir interval in the Daralingie Field is provided. These facies were matched to their petrophysical log signatures, so facies can be defined based on logs in uncored wells. Extensive work was performed to estimate reservoir geometry by using thickness-to-width ratios plots, net gross ratio plots and modern and ancient analogues. Based on this work, nine facies maps representing the Daralingie Field depositional model are presented. The final outcome of this phase was the building of a new conceptual geological model for Daralingie Field that contains all the available data at the time of the study.

The stochastic modeling phase aimed to generate 3-D petrophysical properties models based on the conceptual geological model created in the reservoir characterisation phase. Different stochastic modeling algorithms were used to generate a range of petrophysical properties. Object based modeling algorithms were used to generate facies-based models based on specific conceptual geological models. The porosity models were generated using a facies based geostatistical algorithm. Several stochastic models constrained by well logs and facies maps were produced.

The hydrocarbon estimates were calculated using different methods such as stochastic modeling and Monte Carlo simulation. The porosity models were generated using different facies percentages while keeping the same facies geometry. The aim of this was to evaluate the impact of facies proportions on hydrocarbon estimates. Cumulative production data were also used to validate volumetric calculations for each model. In the final phase, uncertainty assessments were done to define and quantify the key uncertainties in the hydrocarbon estimates, using a newly developed technique that merges stochastic models with Monte Carlo simulation.

The final results showed that hydrocarbon estimates are highly controlled by facies proportions and the mapped reservoir gross rock volume. The high recovery factors observed in the Daralingie Field were attributed to gas influx coming from deeper Pre-Permian rocks or coming laterally from surrounding fields through faults.

During the course of this work, a geologically driven volumetric (GDV) method has been developed to produce probabilistic hydrocarbon estimates. This method integrates the stochastic modeling method with Monte Carlo simulation to generate hydrocarbon estimates. The GDV method was applied to Daralingie Field and demonstrated advantages over Monte Carlo simulation. The GDV is geologically dependent with lower uncertainty, unlike Monte Carlo estimates that are geologically independent and have higher uncertainty. The GDV is an effective and powerful method to estimate probabilistic hydrocarbons.

Declaration

The work contained in this thesis has not been previously submitted for a degree or a diploma at any other higher education institution. To the best of my knowledge, this thesis contains no material previously published or written by another person except where due reference is made.

I give consent for this copy of my thesis, when deposited in the University Library, being available for loan and photocopying.

1/10/2006

Mohammad Al-Khalifa

ASP, The University of Adelaide
Adelaide, South Australia

Acknowledgements

Acknowledgments are due to Saudi Aramco and especially the Exploration Organization and the Carrier Development Department for giving me the Ph.D. scholarship and for financially supporting me throughout my study in the Australian School of Petroleum (ASP) at the University of Adelaide. Also, I would like to thank Santos Ltd. for providing the Daralingie Field data used in this study and special thanks to Adam Hill, Oki Musakti and Dennis Bennet for their support and cooperation.

I would like to express my profound gratitude and appreciation to my thesis supervisor, Simon Lang, for his guidance and for his review of the manuscript. Sincere thanks are also due to my thesis co-supervisor, Tobias Payenberg, for his excellent advice and comments during the different stages of my research, and thanks to my external supervisor, Hisham Al-Qassab, for his contributions to this work.

A big thank you to John Kaldi for his encouragement to join ASP and to study in Australia. Appreciation and thanks are due to ASP school head, staff and my colleagues, especially Andy Mitchell, Maureen Sutton, Janet Hart, Tetsuya Fujii, Saju Menacherry, Kaia Little, Mohammad Al-Ghamadi, Ali Al-Ghamadi and Sarah Riordan.

During the modeling part of this study, considerable support in modeling with Roxar RMS was provided by Elliott Douglas from Roxar that is highly appreciated. Thanks to Roxar for providing software license to ASP. Also, thanks to Jochen Kassan of Whistler Research for the very useful discussions regarding geological object-oriented modeling. Thanks to Peter Behrenbruch from ASP for the very useful and interesting discussions regarding probabilistic reserves that have profoundly impacted on my research. Special thanks to Carolyn Lang for reviewing and technically editing the manuscript.

Finally, my sincere thanks are extended to my family for their support and patience during this period of study. Also, thanks to my family members and my friends in Saudi Arabia and Australia for their continued encouragement and for keeping in touch with me during these three years of study.

Table of Contents

Chapter 1

Introduction

1.1 Importance of Hydrocarbon Reserves

Hydrocarbon reserves are an estimation of the amount of oil and/or gas than can be produced from a reservoir. Estimates of hydrocarbon reserves have a direct impact on market prices, where the economics of "supply and demand" operate. The economics of whole countries are mainly dependent on these numbers. Furthermore, the share price of oil companies is directly related to their hydrocarbon reserves. Any neglect or poor judgment regarding these reserves estimates may lead to a devastating impact on share value.

Two recent examples of the impact of reserves on company share values are Shell and El Paso. In January 2004, Shell announced a major reclassification of its approved reserves, which led to the reduction of 3.9 billion oil barrels, the equivalent of about 20% of its booked approved reserves. In April 2005, Shell announced that it was cutting its reserves further by 9%. This resulted in not only in the drop of its share price, but in the resignation of the Shell chairman, the head of exploration and production, and the chief financial officer. El Paso reduced its reserve by 41% on February 2004, which resulted in a drop in the company value that amounted to one billion dollars (Behrenbruch, 2005).

Reserve estimates are calculated from geological and engineering parameters with different measurement scales and uncertainties. Furthermore, these estimates can be classified according to geological, engineering and economical factors. Confidence levels in the estimation and classification are highly dependent on the quality of the input data (Garb, 1985).

1.2 Reservoir Characterisation Impact on Hydrocarbon Reserves

Field development projects require a huge financial investment and they are typically based on predictions of future reservoir performance. These predictions are generated from a reservoir simulation model, which is based on a geological model. Consequently, the reliability of the simulation model is highly dependent on the accuracy of the geological model (Jian et al., 2002).

Several challenges, however, are encountered in the creation of a reliable geological model. An important challenge is to build a model with a very limited amount of subsurface information available. Other challenges include defining flow units in the reservoir and identifying reservoir heterogeneities that affect fluid flow (Jian et al., 2002). A flow unit is defined as a volume of reservoir rock that has very similar geological and petrophysical properties that are distinctly different from the fluid flow properties of the other flow units (Aminian et al., 2002). To overcome these challenges, geoscientists conduct integrated reservoir characterisation studies. The literature contains well-documented integrated reservoir studies which have helped in selecting the appropriate plan for reservoir development by improving the quality of the geological model (Meng et al., 2002). Such studies have demonstrated their importance in reservoir management and future development (Ates et al., 2003; Gilman et al., 2002; Marquez et al., 2001; Tye and Hickey, 2001).

One of the important breakthroughs in reservoir characterisation in recent years is high-resolution sequence stratigraphy, using 3D seismic and modern analogues to construct a realistic 3-D conceptual reservoir model which helps in exploration and development (Lang et al., 2002; Strong et al., 2002). Reservoir characterisation studies are usually undertaken to address existing reservoir problems, such as unexpected water production, and to optimise future development plans. Moreover, adequate reservoir characterisation studies may result in an increase in the original hydrocarbon in place (OHIP) estimates. Marquez at al. (2001) conducted such a study, which resulted in an increase of 44% in OHIP. In addition, they defined new areas with significant reserves, which will be

targeted for future development. The success of their study was dependent on integrating data from different sources such as geology and engineering. This process is referred to as data integration in reservoir characterisation.

Data integration has become an important part of reservoir characterisation. It involves merging of information from different branches of geosciences and petroleum engineering (Tahmhane et al., 1999). Data with different measurement scales, such as conceptual geological models, 3-D seismic, flow-meters and well tests have been effectively used in reservoir characterisation studies (Landa et al., 2000; Qassab et al., 2000). Usually the outcome of most integrated reservoir characterisation studies is an integrated 3-D geological model that represents the geologist's understanding of the reservoir. This model will have a large impact on the calculation of OHIP and the expected recovery. Integrated reservoir characterisation studies have become an essential part of hydrocarbon reservoir management and development studies.

1.3 Hydrocarbon Reserve Growth

In 1956 Dr. M. King Hubbert, a geophysicist well known as a world authority on the estimation of energy resources, published his prediction that U.S. oil production would peak in about 1970 and decline afterwards (Laherrer, 1999). His timing for estimated peak production has been proved to be remarkably accurate, although he under estimated the magnitude of the peak (Fig 1.1.) Hubbert based his prediction on the four factors that affect oil production: physics, economics, technology and the volume of unproduced oil (Laherrer, 2000; Taylor, 1997). Among the four factors, advances in technology has contributed the most in increasing the magnitude of U.S. production (Behrenbruch, 2005).

One of the most important technological impacts on hydrocarbon reserves is reserve growth. The term "reserve growth" means the increase in a company's or a country's hydrocarbon reserve. The increase could be due to the addition of new reserves from newly discovered fields or an increase in reserve estimates of existing fields (Beliveau

and Baker, 2003). The addition of reserves from existing fields needs much more justification than the addition from newly discovered fields. Initial reserve estimates tend to be conservative with a high uncertainty associated with them. This is due to the limited data available at the early stage of development and the fear of being too optimistic. It is much more pleasing for management to increase reserves rather than to downgrade the reserves year after year. In order to justify the increase in proven reserves for existing fields, engineers have to rely on acquiring new data and the utilisation of technology.

Technology has improved significantly since the early days of petroleum exploration and production. Structure maps are drawn based on 3-D seismic. Logging tools are much more precise and their measurements are more sensitive to the formation fluids and rocks. Furthermore, the gigantic improvement in computer hardware and software has changed the way that geoscientists work (Beliveau and Baker, 2003).

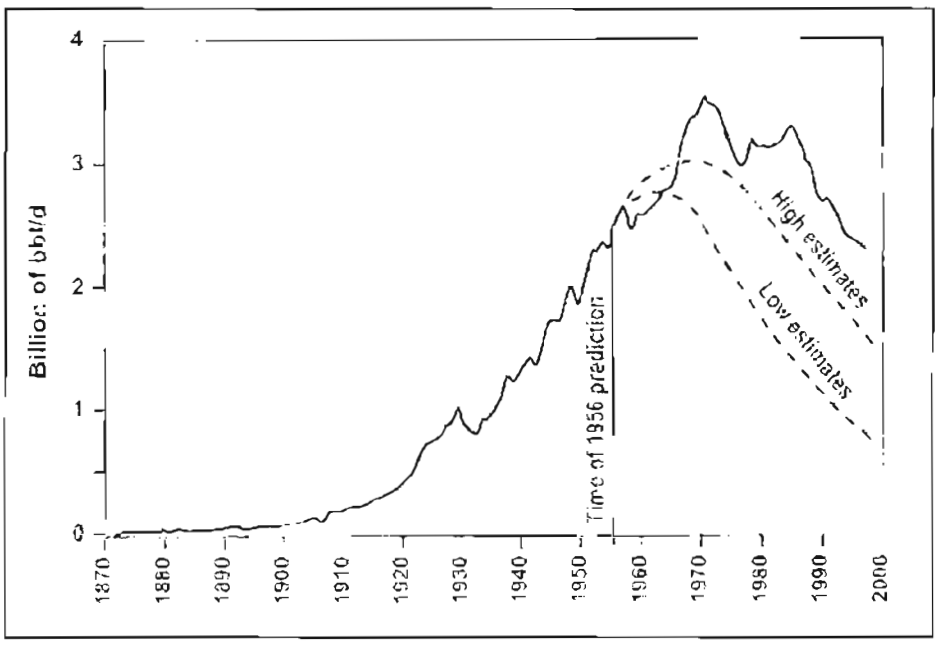

Figure 1.1: U.S. crude oil production from 1870 to 1996 and Hubbert's (1956) prediction for cumulative U.S. crude production. The solid lines are actual production and the dotted lines are Hubbert's predictions. (From Behrenbruch, 2005)

In some cases, such as mature fields, the use of technology along with acquisition of new data, has added considerable reserves. A good example is outlined by Azim et al. (2005) for the Burgan Formation in the Raudhatain and Sabiriyah Fields in North Kuwait. The paper clearly shows that using new techniques in measuring and analysing resistivity logs in a shale/sand sequence resulted in an increase in the reserve and the decrease in its uncertainty.

1.4 Uncertainty in Hydrocarbon Reserves Estimates

Uncertainty is defined as the error difference between estimation and truth and it is very difficult to measure directly, because in most cases the truth in not known (Isaaks and Srivastava, 1989). Uncertainty in 1-D can be very low, whereas in 3-D it increases significantly (Massonnat, 2000). For example, well logs at the well location can be considered as 1-D, whereas a conceptual geological model can be considered as 3-D. There can be few disagreements between geologists while interpreting data at the well location; however, disagreements will increase while interpreting the conceptual geological model. The increase in disagreement is the result of the increase in uncertainty.

Uncertainty in the integrated geological model may come from many sources such as the structural framework and petrophysical properties (Ligero et al., 2003). However, an important source of uncertainty is the conceptual geological model, which is dependent on the geologist's knowledge. This knowledge varies from one geologist to another and is highly influenced by experience and background (Tahmhane et al., 1999). In most of the integrated geological studies, such as in Qassab et al. (2000), only one integrated geological model is presented and used later in building the reservoir simulation model. This integrated geological model does not necessarily represent the actual reservoir; in fact it represents the geologist's imagination of the reservoir. Therefore, there is a need to consider several possible models before deciding on which model to use.

Uncertainty in reserves can be classified into three major types: political, economical and technical (McGilvray and Shuck, 1998). The technical uncertainty can be divided further into engineering and geological types. The geological uncertainty can be studied by using stochastic modeling methods. The stochastic modeling methods have the ability to create many equi-probable realisations from the same geological data. Unfortunately, in the petroleum industry this feature has not been fully utilised, largely due to the length of time required, and only a few number of realisations are selected for history matching. Moreover, usually geological models are upscaled for simulation, which results in the exclusion of fine-scale critical geological heterogeneities (Ates et al., 2003).

1.5 Thesis objectives

The calculation of reserves is a function of geologic, reservoir, operation and economic scenarios. The focus of this thesis is on the geological factors affecting reserves. The main thesis objective is to study the role of depositional facies in the OHIP estimates using a field case study. Also, the thesis will investigate the impact of uncertainty of depositional facies on the final hydrocarbon estimates. Other uncertainties that impact OHIP estimates will be investigated, such as porosity, water saturation and gross rock volume. New methods will be developed to improve the process of OHIP estimation by either stochastic modeling or the Monte Carlo simulation method.

1.6 Case Study

Several field data sets were considered for this research. Daralingie Field was selected because it represents a unique problem in OHIP estimation. Daralingie Field is a mature gas field in the Cooper Basin, South Australia and has produced more gas than originally estimated. As this issue needed special investigation, a carefully designed workflow was set up to fully address this problem and to better understand the reservoir. The Daralingie study was conducted in four phases:

1. Reservoir characterisation
2. Stochastic geological modeling

3. Hydrocarbon estimation
4. Uncertainty assessment.

1.7 Methodology

The objective of the reservoir characterisation phase was to conduct an integrated reservoir study utilising all available data from the Daralingie Field and surrounding area. The first part of this phase included collection and quality checking of all available static data such well logs and cores, and dynamic data such as well tests. This was a critical step, because the subsequent analysis was dependent on the accuracy of these data. Any problems with the data needed to be recognised before the start-up of this project, and subsets of data exported for further analysis. All quality-controlled data was loaded into a Roxar-RMS database at the Australian School of Petroleum for subsequent geological analysis.

The second part in this phase involved the examination of the quality-controlled data to develop a depositional model and a sequence stratigraphic framework for this reservoir. This includes isopach and structure mapping of genetic reservoir intervals. The main outcome was the determination of the relationship between reservoir depositional facies and reservoir flow units. This has led to an improved understanding of reservoir and non-reservoir depositional environments, geometry and connectivity. Flooding surfaces and sequence boundaries were recognised that package successions into genetic intervals, each bounded by unconformities and/or flooding surfaces, equivalent to depositional system tracts. This approach follows the methodology used for the Moomba Area by Strong et al. (2001) and the Baryulah area Study by Lang et al. (2002). Several facies maps were generated for each sequence and they were combined to generate a deterministic conceptual geological model. The final outcome was a 3-D conceptual geological model of the reservoir, represented by a map-set for each systems tract.

The aim of the stochastic modeling phase was to generate 3-D petrophysical properties models for the reservoir based on the conceptual geological model generated in the first

phase. The petrophysical properties (taken from the Santos database) were modeled as facies and porosity.

Different stochastic modeling algorithms were used to generate a range of petrophysical properties. Object-based modeling algorithms were used to generate facies-based models from specific conceptual geological models (i.e. channels belts) using suitable analogues, in contrast to pixel based modeling methods. The porosity models were generated using a facies-based geostatistical algorithm. The final outcome was several stochastic models constrained by well logs and facies maps.

In the third phase, hydrocarbon estimates were calculated using the stochastic porosity models generated in phase-2. These porosity models were generated using different facies percentages while keeping the same facies geometry. The aim of this was to evaluate the impact of facies proportions on hydrocarbon estimates. Furthermore, three volumetric calculations were performed for each porosity model with different fluid contacts. All volumetric calculations were done in RMS version 7.2 for every reservoir interval and every reservoir area. Results were exported as ASCII files and entered manually in an excel sheet for subsequent analysis. Cumulative production data were also used to validate volumetric calculations for each model.

In the final step, uncertainty assessment was undertaken to define and quantify the key uncertainties in the hydrocarbon estimates, using newly developed techniques in Monte Carlo simulation. The results were the development of geologically driven volumetrics methods that estimate reserves through the emphasis of geological knowledge. The final part of this study was the uncertainty analysis of the high recovery factor observed in Daralingie, and a possible explanation for it.

Aminian, K., B. Thomas, and H. I. Bilgesu, 2002, A New Approach for Reservoir Characterization: SPE 78710, SPE Eastern Regional Meeting.

Ates, H., M. Kelkar, and A. Datta-Gupta, 2003, The Description of Reservoir Properties by Integrating Geological, Geophysical and Engineering Data, The University of Tulsa and Texas A&M University, Joint Industry Project, p. pp. 3-16.

Behrenbruch, P., 2005, Short Course Notes, Oil and Gas Resources and Reserves, The Australian School of Petroleum, The University of Adelaide, Adelaide, SA, Australia.

Belivcau, D., and R. Baker, 2003, Reserves Growth: Enigma, Expectation or Fact?: SPE 84144, SPE Annual Technical Conference and Exhibition.

Garb, F. A., 1985, Oil and Gas Reserves Classification, Estimation and Evaluation: Journal of Petroleum Technology, p. pp. 373-390.

Gilman, J. R., H.-Z. Meng, M. J. Uland, P. J. Dzurman, and S. Cosic, 2002, Statistical Ranking of Stochastic Geomodels Using Streamline Simulation: A Field Application: SPE 77374, SPE Annual Technical Conference and Exhibition.

Isaaks, E. H., and R. M. Srivastava, 1989, An Introduction to Applied Geostatistics: New York, USA, Oxford University Press, 561 p.

Jian, F. X., D. K. Larue, A. Castellini, and J. Toldi, 2002, Reservoir Modeling Methods and Characterization Parameters for A Shoreface Reservoir: What is Important for Fluid Flow Performance?: SPE 77428, SPE Annual Technical Conference and Exhibition.

Laherrer, J. H., 2000, Learn Strengths, Weaknesses to Understand Hubber Curve: Oil and Gas Journal, 17 April 2000, p. 63-75.

Landa, J. L., R. N. Home, M. M. Kamal, and C. D. Jenkins, 2000, Reservoir Characterization Constrained to Well-Test Data: A Field Example: SPE Reservoir Evaluation and Engineering, v. 4, p. 325-334.

Lang, S. C., N. Ceglar, S. Forder, G. Spencer, and J. Kassan, 2002, High Resolution Sequence Stratigraphy, Reservoir Analogues, and 3D Seismic Interpretation-Application to Exploration and Reservoir Development in The Baryulah Complex, Cooper Basin, Southwest Queensland: APPEA Journal, v. 42, p. 512-521.

Ligero, E. L., C. Maschio, and D. J. Schiozer, 2003, Quantifying the Impact of Grid Size, Upscaling and Streamline Simulation in the Risk Analysis Applied to Petroleum Field Development: SPE 79677, SPE Reservoir Simulation Symposium.

Marquez, L. J., M. Gonzalez, S. Gamble, E. Gomez, H. A. Vivas, H. M. Bressler, L. S. Jones, S. M. Ali, and G. S. Forrest, 2001, Improved Reservoir Characterization of a Mature Field Through an Integrated Multi-Disciplinary Approach. LL-04 Reservoir, Tia Juana Field, Venezuela: SPE 71355, SPE Annual Technical Conference and Exhibition.

Massonnat, G. J., 2000, Can We Sample the Complete Geological Uncertainty Space in Reservoir-Modeling Uncertainty Estimates?: SPE Journal, v. 5, p. 46-59.

McGilvray, W. G., and R. M. Shuck, 1998, Classification of Reserves: Guidelines and Uncertainty: SPE 39821. SPE International Petroleum Conference and Exhibition.

Meng, H. Z., K. S. Godbey, J. R. Gilman, and M. J. Uland, 2002, Integrated Reservoir Characterization and Simulation for Reservoir Management using a Web-Based

Collaborative Technical Workflow Manager: SPE 77673, SPE Annual Technical Conference and Exhibition.

Qassab, H. M. A., J. Fitzmaurice, Z. A. Al-Ali, M. A. Al-Khalifa, G. A. Aktas, and P. W. Glover, 2000, Cross-Discipline Integration in Reservoir Modeling: The Impact on Fluid Flow Simulation and Reservoir Management: SPE 62902, SPE Annual Technical Conference and Exhibition.

Strong, P. C., G. R. Wood, S. C. Lang, A. Jollands, E. Karalaus, and J. Kassan, 2002, High Resolution Palaeogeographic Mapping of the Fulvial-Lacustrine Patchawarra Formation in the Cooper Basin, South Australia: APPEA Journal, v. 42, p. 65-81.

Tahmhane, D., L. Wang, and P. M. Wong, 1999, The Role of Geology In Stochastic Reservoir Modeling: The Future Trends: SPE 54307, SPE Asia Pacific Oil and Gas Conference and Exhibition.

Taylor, P. J., 1997, Modeling the U.S. Oil Industry: How Much Oil is Left?: Journal of Petroleum Technology, p. 502-507.

Tye, R. S., and J. J. Hickey, 2001, Permeability characterization of distributary mouth bar sandstone in Prudhoe Bay field, Alsaka: How horizontal cores reduce risk in developing deltaic reservoirs: American Association of Petroleum Geologists, v. 85, p. 459-475.

Chapter 2

Case Study-1: Daralingie Field Introduction

2.1 Cooper Basin Review

2.1.1 Tectonics and Stratigraphy

The Cooper Basin is a northeast-trending inter-continental depression covering approximately 130,000 km^2 in northeastern South Australia and southwestern Queensland (Fig. 2.1). It contains up to 1,500 metres (4,900 feet) of Permian-Lower Triassic deposits (Fig. 2.2) (Flottmann et al., 2004). These deposits unconformably overlie the Cambrian-Devonian Warburton Basin and Carboniferous igneous rocks. Also they are unconformably overlain by the Eromanga Basin Jurassic-Cretaceous deposits (Apak et al., 1997).

The Cooper Basin formation started in the earliest Permian. Views of its mechanism vary from the broadly accepted dominantly extensional model to one of strike-slip movement and compression (Brakel and Totterdell, 1996). The basin is divided into six major structural zones: the Gidgealpa-Merrimelia-Innamincka (GMI) and Murteree-Nappacoongee (MN) anticlinal trends, the Patchawarra, Nappamerri and Tennapera Trough, and the northern Cooper Basin (Fig. 2.3) (Nakanishi and Lang, 2002).

The initial sedimentation in the Cooper Basin started with deposition of the Merrimelia Formation, which contains a variety of sub-facies, including glaciofluvial washout, tillite, glaciolacustrine muds and rippled sands. In the Merrimelia Formation, some of the lacustrine muds are rich in algal remains and may be source rocks, whereas some of the better-sorted sands may form locally developed reservoirs. However, more geological studies are needed to locate these plays (Brakel and Totterdell, 1996).

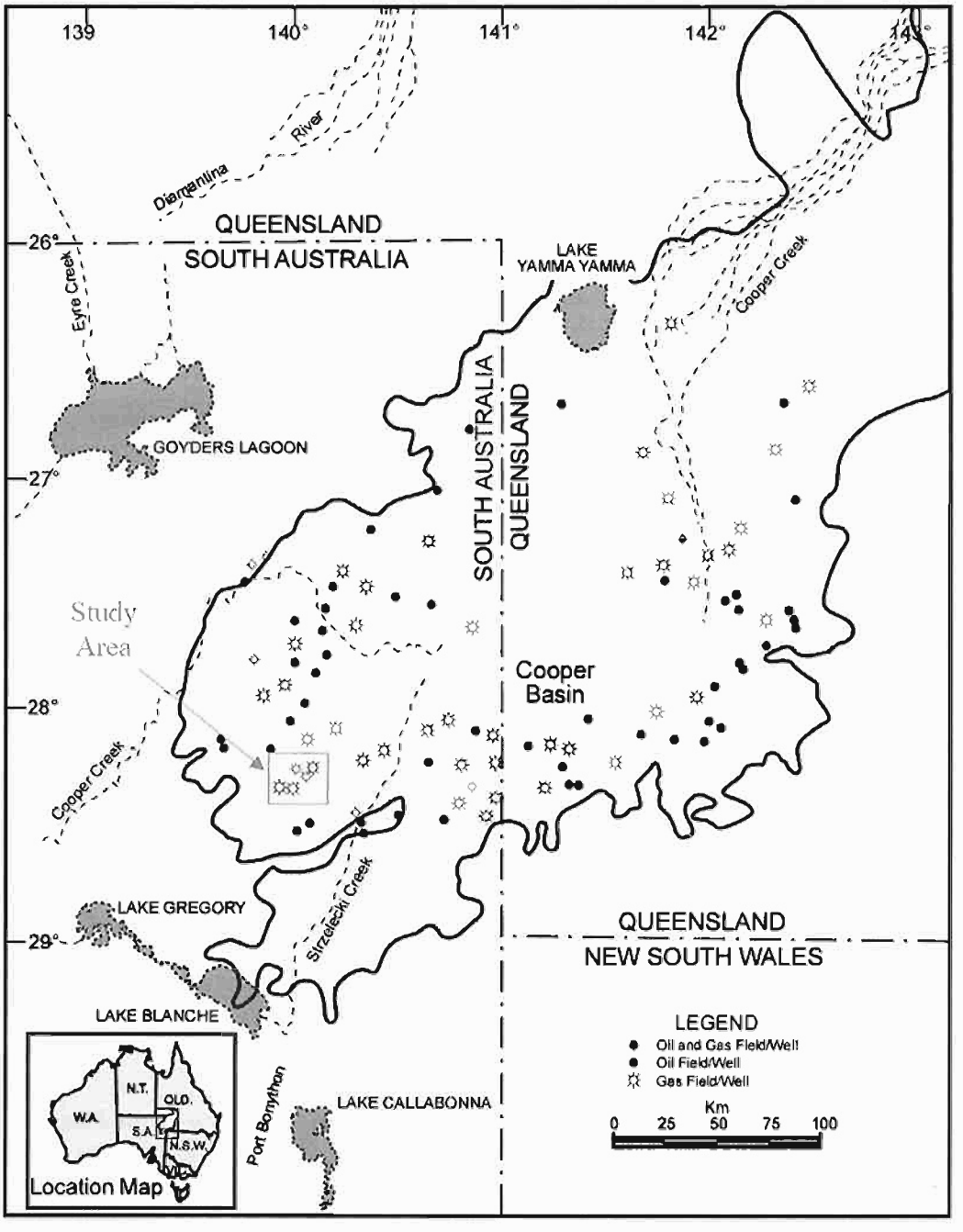

Figure 2.1: Location map showing position of the Cooper Basin in Australia and the location of the study area that includes Daralingie Field and surrounding gas field (modified after Lang et al., 2002).

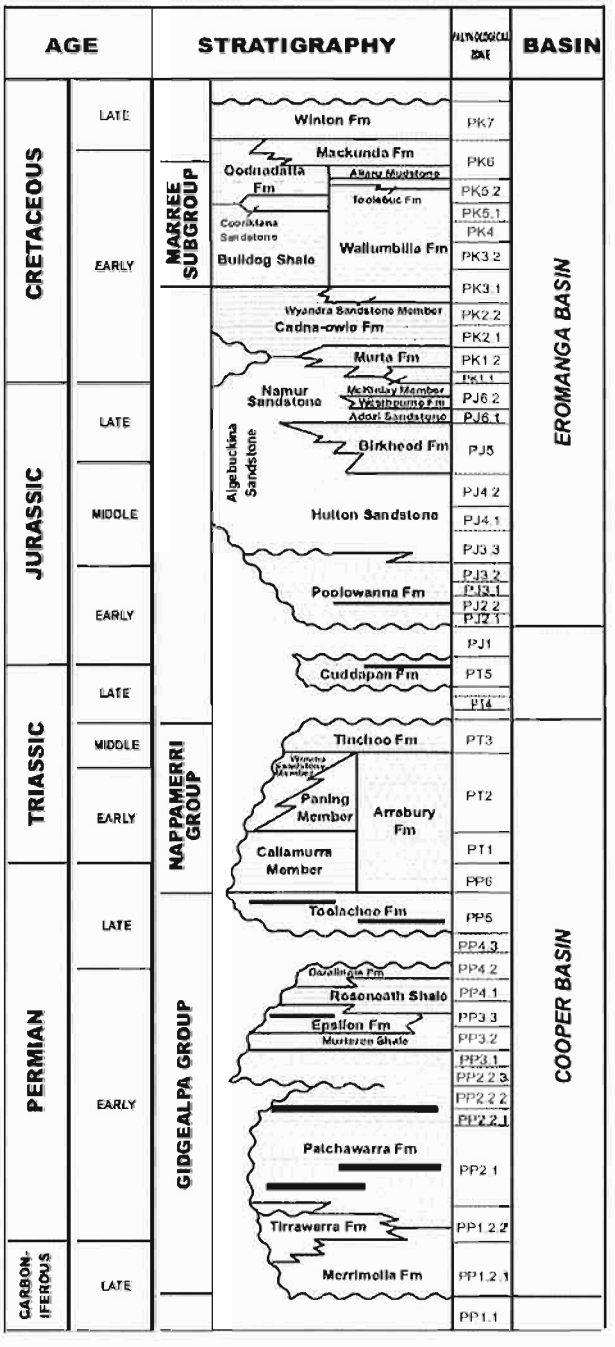

Figure 2.2: Generalised stratigraphic column of the Cooper-Eromanga Basin in northeast South Australia (from Nakanishi et al., 2003).

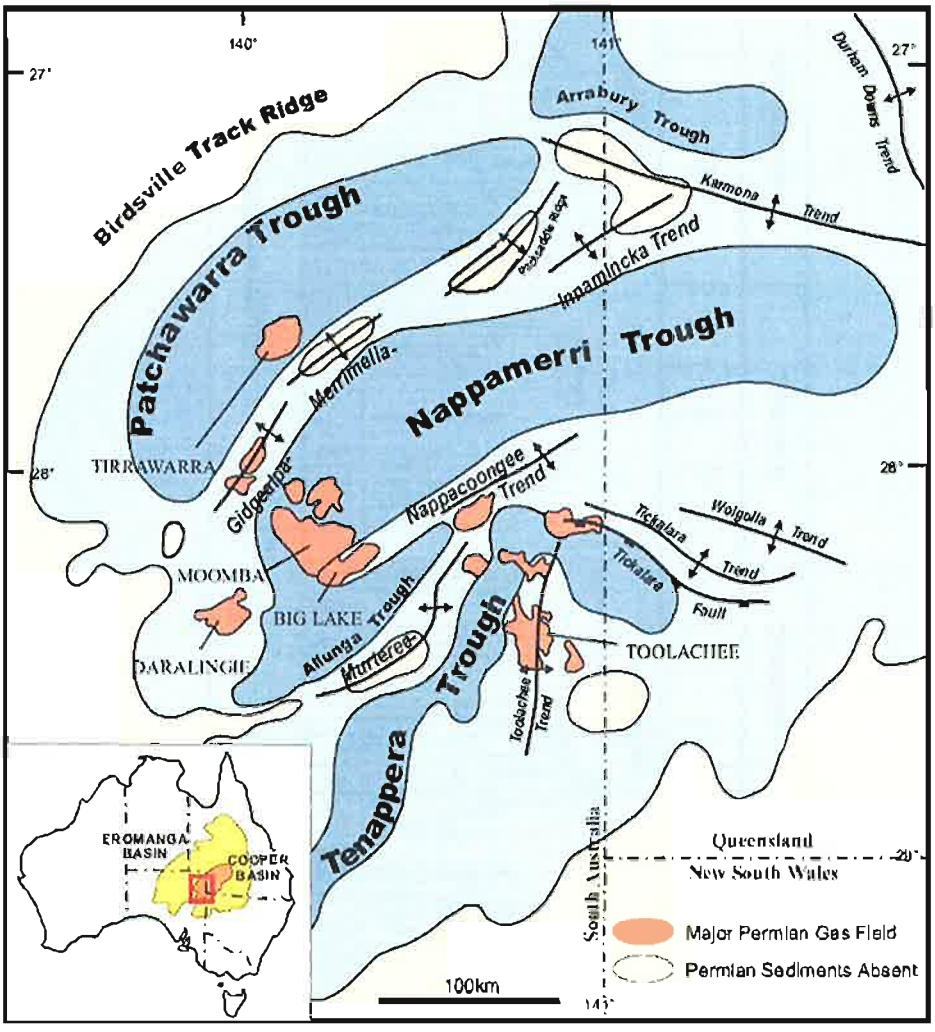

Figure 2.3: Major structural elements of the southern Cooper Basin and the location of the major Permian gas fields (from Nakanishi et al., 2003).

The Merrimelia Formation interfingers with the Tirrawarra Formation. The Tirrawarra Formation is dominated by thick multistorey sandstones, which are typical of low-sinuosity, braided, bedload fluvial channels. Also, it has minor coals that could be the source rocks for hydrocarbons (Brakel and Totterdell, 1996).

The Tirrawarra Formation is overlain by the Patchawarra Formation, which comprises fluvial-deltaic and lacustrine sediments and contains extensive coal sequences. The lacustrine environments were dominant during the deposition of the Murteree Shale, Epsilon Formation, Roseneath Shale and Daralingie Formation (Brakel and Totterdell, 1996). The sequence ends with the major Daralingie unconformity that crosses the basin. The unconformity surface marks the base of the Toolachee Formation, which is comprised of sandstone, local conglomerates and coals (Nakanishi and Lang, 2002). It represents a re-establishment of the fluvial-deltaic environments similar to what existed before the major Daralingie unconformity. The upper sediments in the Cooper Basin consist of the Nappamerri Group, that comprises the Upper Permian to Middle Triassic sandstone and shale of fluvial-lacustrine origin (Flottmann et al., 2004).

2.1.2 Hydrocarbons

Most of the onshore gas and oil production in Australia comes from the Cooper Basin and the overlying Eromanga Basin. Cooper Basin hydrocarbon production comes from Permo-Triassic deposits at depths between 1,830-1,660 metres (6,000-12,000 feet) (Fig. 2.2). The first discovery of natural gas was made at Gidgealpa-2 well in 1963 (Apak et al, 1997). Since then, more than 1,300 wells were drilled and 121 gas-producing fields were discovered in the Cooper Basin. The gas reserve is estimated to be about 85 x 10^9 m^3 (1.089 x10^{10} ft^3)(Brakel and Totterdell, 1996). In the Moomba area, located in South Australia part of the Cooper Basin, several fields have exceeded 10BCF production form the Patchawarra Formation, such as Daralingie Field (162 Bcf), Big Lake Field (24 Bcf) and Moomba Field (16 Bcf) (Strong et al., 2002).

In the Cooper Basin, the main gas reservoirs are within the Patchawarra and Toolachee formations with some gas reservoirs in Tirrawarra/Merrimelia and Epsilon formations. About 30% of the Cooper Basin gas reserves are in the Patchawarra Formation and about 40% is in the Toolachee and Daralingie formations. The Tirrawarra Sandstone in the Tirrawarra Field contains more than 95% of the Cooper Basin oil and about 12% of its gas (Brakel and Totterdell, 1996). Moreover, the deeply fractured rocks of the Permian and the pre-Permian reservoirs in the Cooper Basin contain possible gas reserves (Flottmann et al., 2004).

The Permian succession is thought of as the major source of hydrocarbons in the overlying Eromanga Basin. The Patchawarra, Epsilon, Daralingie and Toolachee formations were deposited as lacustrine deltas or fluvial systems and they contain an abundance of organic source materials. The total reserves of Permian-derived hydrocarbons in the Cooper and Eromanga Basin is more than 5.4 TCF, 430 million barrels of condensate and gas liquids and 140 million barrels of recoverable oil. The Murteree and Roseneath are lacustrine shales and provide the regional seal to the Patchawarra and Epsilon formations (Brakel and Totterdell, 1996).

2.1.3 Patchawarra Formation Chronostratigraphy

This study focuses on the reservoir interval in the upper part of the Early Permian Patchawarra Formation. The Patchawarra chronostratigraphic framework that was adopted for this study was summarised by Strong et al. (2001, 2002). It is based upon the identification of the regional unconformities, widespread lacustrine flooding surfaces, and other local markers (Fig. 2.4). The letter "V" indicates the top surface of the Patchawarra Formation. VC00 is the top regional correlatable lacustrine flooding surface in the Patchawarra Formation. The other flooding surfaces, which typically lie immediately above a coal-prone interval, are indicated by a "VC" prefix and a numerical suffix (i.e. VC25). Regional scale unconformities are denoted by "VU" (e.g. VU45). Higher order unconformities occur within this interval, but they are not necessary regionally widespread.

Local markers, typically lacustrine flooding surfaces, are indicated by the prefix "VL". These surfaces are equivalent to 3rd order flooding surfaces that form boundaries to genetic intervals (some are proxies for systems tracts.) The key interval is the VC15-VC25 succession because it includes the reservoir section. Facies and stratigraphic data from the immediate interval below and above the reservoir are needed, and hence this study examines the VC00-VC35 intervals as a check against mis-correlation.

Each reservoir interval (e.g. VC20-VC25) reflects a balance of the rate of sediment supply and accommodation space (Lang et al., 2001, 2002; Strong et al., 2001, 2002). Where accommodation is temporarily negative, erosion occurs and this is typically followed by a low rate of increase in accommodation, denoted here as a fluvial lowstand systems tract (LST). Where the rate of accommodation increases faster than sediment supply, lacustrine flooding and/or floodplain aggradation and back stepping facies belts occur. These intervals are called transgressive systems tracts (TST). The highstand systems tract (HST) refers to a decelerating increase in accommodation relative to sediment supply, and is associated with rapid lacustrine shoreline progradation and expansion on the alluvial plain.

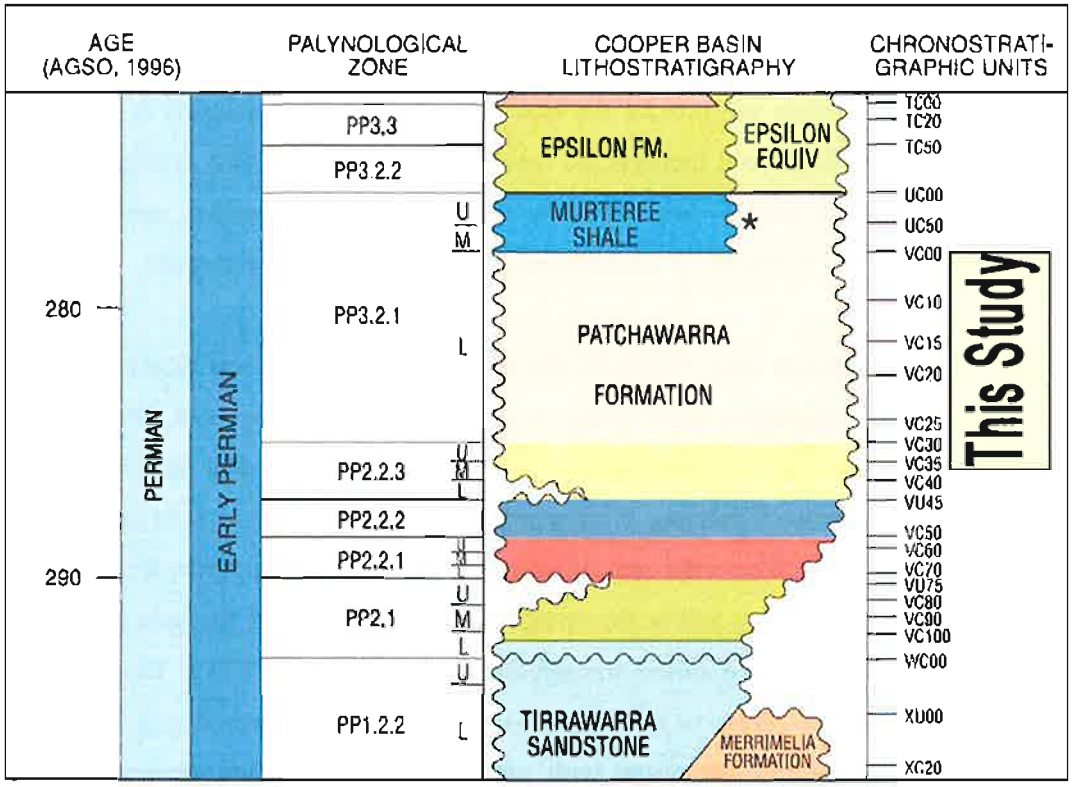

Figure 2.4: Early Permian Chronostratigraphy of the Cooper Basin from Strong et al. (2002). The study interval lies within the Upper Patchawarra Formation, sealed by the Murteree Shale. "VU" refers to known major unconformities, whereas "VC" refers to correlatable flooding surfaces, typically above coal-prone intervals. This study specifically focuses on the VC00-VC35 interval. The VC20-VC25 interval denotes the main reservoir section at the Daralingie Field.

2.2 Study Area and Available Data

2.2.1 Location

The study area is located about 30 km southeast of Moomba Field, Cooper Basin (Fig. 2.1). It includes Daralingie Field and the surrounding area. The main reservoir lies in the upper Patchawarra Formation (VC20-VC25 interval) and is regionally sealed by the Murteree Shale. The field produces gas mainly from the Patchawarra Formation, but has produced from the Epsilon Formation in the past (Hill, 2004). Twenty-seven wells have been drilled in Daralingie Field and sixteen of them have produced gas at some time. Currently, there are five producing wells (Daralingie-1, -9, -11, -12 and –14.)

2.2.2 Well Data

The study area includes fifty-four wells available for the study of which 42 wells lie within the proposed modelling area (Fig. 2.5). Wells that fall in the modeling area are listed in Table 1 and the wells that fall outside the model area are listed in Table 2. Most wells have a complete log suite (i.e. neutron, gamma ray, density porosity) and some have limited logs. In Table 2.1 and 2.2, "All" indicates the presence of a complete suite of logs. Daralingie-9 is shown in Figure 2.6 as an example for the available data across the reservoir.

Depth-surface grids, which were derived from seismic interpretation, were provided by Santos for the Murteree Shale, the VC25 Coal, and the top Pre-Permian-unconformity. The VC25 surface, which is cut by the Pre-Permian unconformity in some areas (Fig. 2.7), was used as the reference horizon in this study. Seismically interpreted fault polygons were also supplied for each of these surfaces. Sequence tops used in this study are based on the Moomba area Patchawarra Study (Strong et al., 2001). They were downloaded from the Santos database and loaded into the Roxar/RMS database. Cored wells were available for examination at the PIRSA Core Library, Glenside, Adelaide.

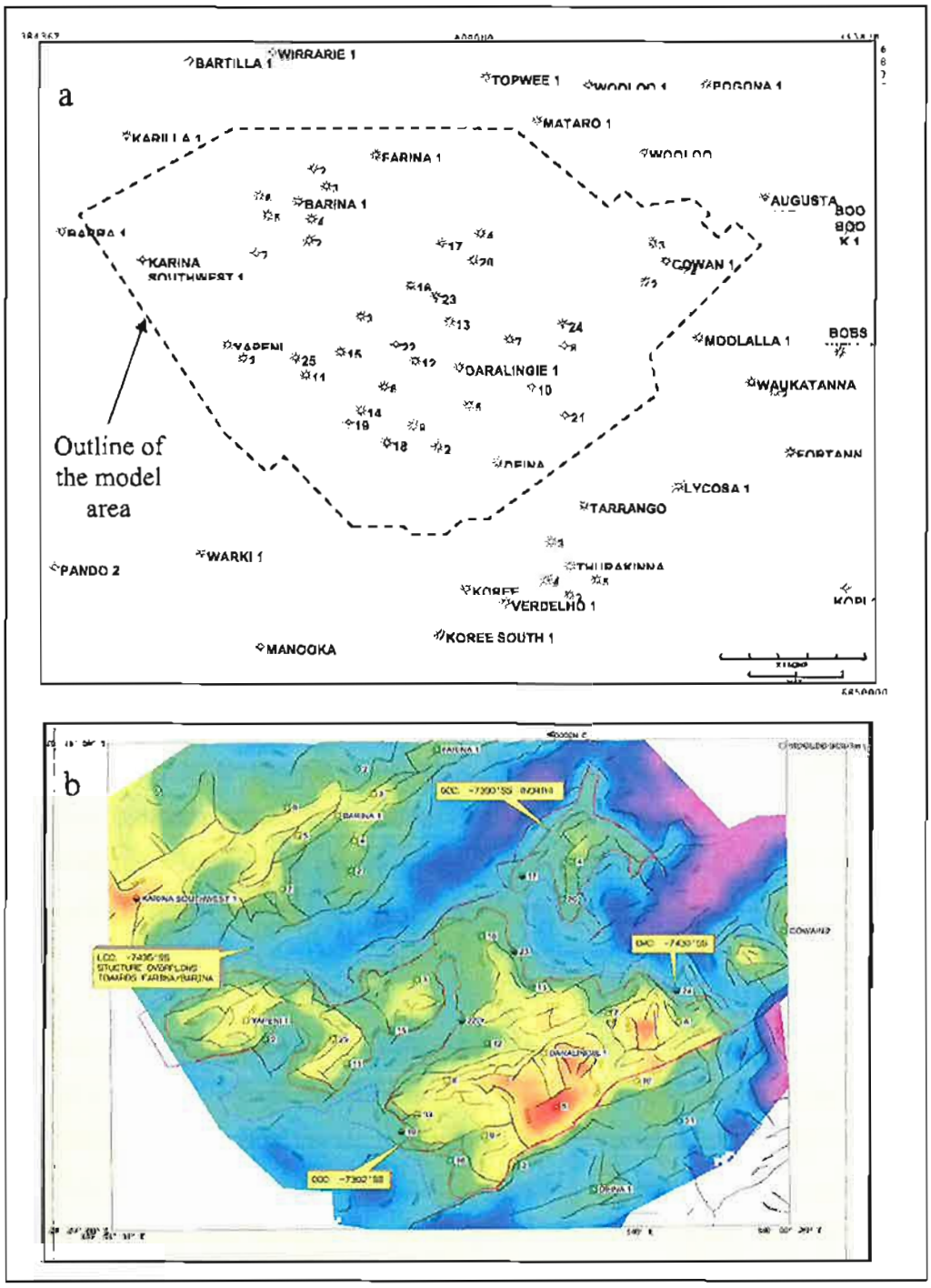

Figure 2.5: a) Daralingie Field and surrounding fields base map showing wells, geological model area and wells included in this study, b) fluid contacts and fault polygons in Daralingie Field highlighted on top VC25 seismic depth map (Hill, 2004). (OWC: Oil Water Contact, GOC: Gas Oil Contact)

Table 2.1: Wells used in model area with available data in each well (* core examined)

Well Name	Logs Available	DSTS	Core
BARINA_1	GR, DT, Resistivity	Yes	No
BARINA_2	GR, DT, Resistivity	Yes	No
BARINA_3	GR, DT, Resistivity	RFT	No
BARINA_4	GR, DT, Resistivity	No	No
BARINA_5	GR, DT, Resistivity	RFT	No
BARINA_6	GR, DT, Resistivity	RFT	No
BARINA_7	GR, DT, Resistivity	RFT	No
COWAN_1	All	No	No
COWAN_2	GR, DT, Resistivity	Yes	No
COWAN_3	All	Yes	No
COWAN_4	GR, DT, Resistivity	Yes	No
DARALINGIE_1	GR, DT, Resistivity	Yes	No
DARALINGIE_10	GR, DT, Resistivity	No	Yes
DARALINGIE_11	All	Yes	No
DARALINGIE_12	GR, DT, Resistivity	Yes	No
DARALINGIE_13	GR, DT, Resistivity	Yes	No
DARALINGIE_14	GR, DT, Resistivity	Yes	No
DARALINGIE_15	GR, DT, Resistivity	Yes	Yes
DARALINGIE_16	All	Yes	No
DARALINGIE_17	All	Yes	No
DARALINGIE_18	All	Yes	No
DARALINGIE_19	All	Yes	Yes*
DARALINGIE_2	GR, DT, Resistivity	Yes	Yes*
DARALINGIE_20	All	Yes	No
DARALINGIE_21	All	Yes	No
DARALINGIE_22	All	Yes	Yes*
DARALINGIE_23	All	Yes	Yes*
DARALINGIE_24	GR, DT, Resistivity	Yes	No
DARALINGIE_25	All	No	No
DARALINGIE_3	All	Yes	Yes
DARALINGIE_4	All	Yes	Yes
DARALINGIE_5	All	No	No
DARALINGIE_6	All	Yes	No
DARALINGIE_7	All	Yes	Yes
DARALINGIE_8	All	Yes	Yes
DARALINGIE_9	All	Yes	Yes*
DEINA_1	All	Yes	No
FARINA_1	GR, DT, Resistivity	Yes	No
FARINA_2	GR, DT, Resistivity	RFT	No
YAPENI_1	All	Yes	No
YAPENI_2	All	Yes	No
KARINA_SOUTHWEST_1	GR, DT, Resistivity	No	No

Table 2.2: Wells used in the study that lie outside model area

Well	Logs Available	DSTS	Cores
MATARO_1	GR, DT, Resistivity	Yes	No
WOOLOO_SOUTH_1	All	Yes	No
AUGUSTA_1ST	All	No	No
MOOLALLA_1	All	No	No
WAUKATANNA_1	All	Yes	No
WAUKATANNA_2	GR only	No	No
BOOB_BOOK_1	GR, DT, Resistivity	No	No
LYCOSA_1	All	No	No
THURAKINNA_1	All	Yes	No
THURAKINNA_2	All	Yes	Yes
KARILLA_1	All	Yes	No
BARRA_1	GR, DT, Resistivity	Yes	No

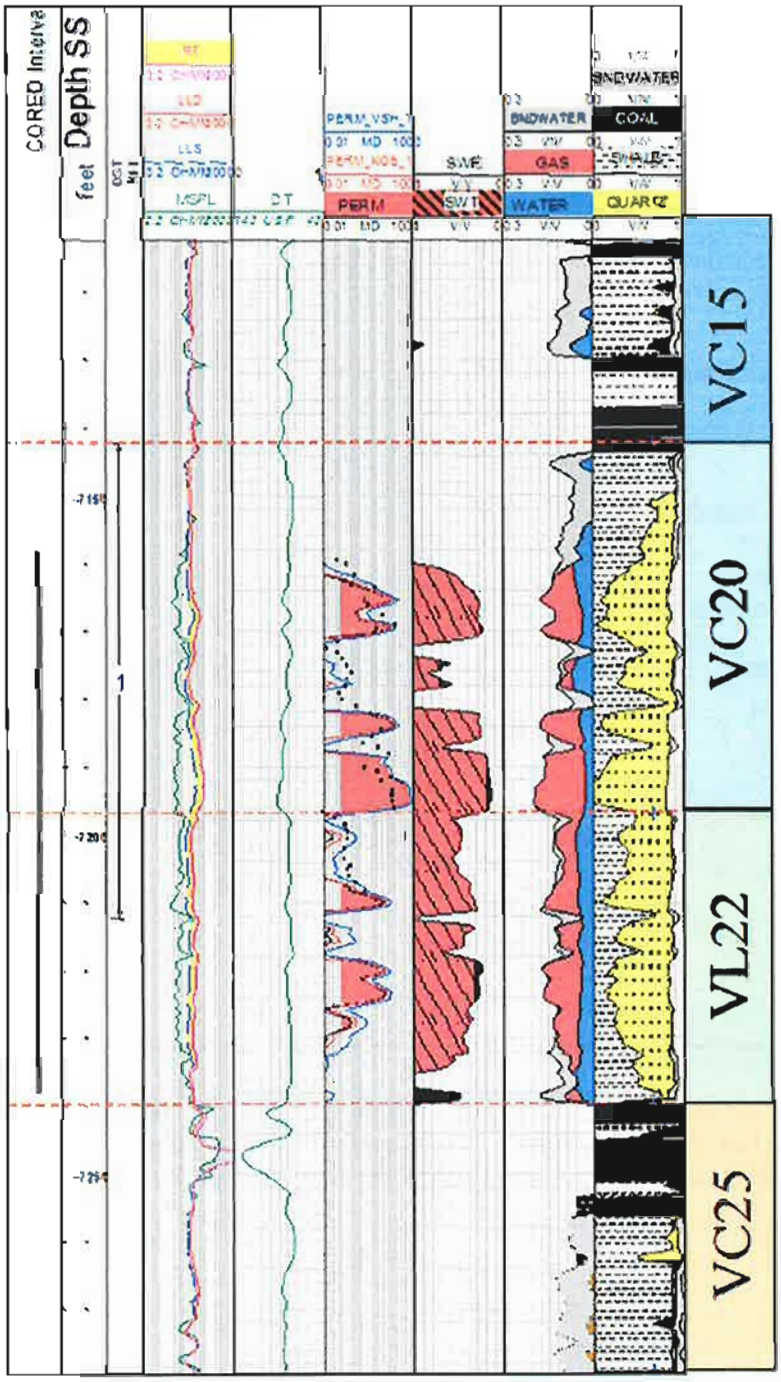

Figure 2.6: Well log for Daralingie-9 showing the main reservoir intervals VC20 and VL22 and showing the cap rock interval VC15. It also shows VC25 coals, which extend throughout the Cooper Basin.

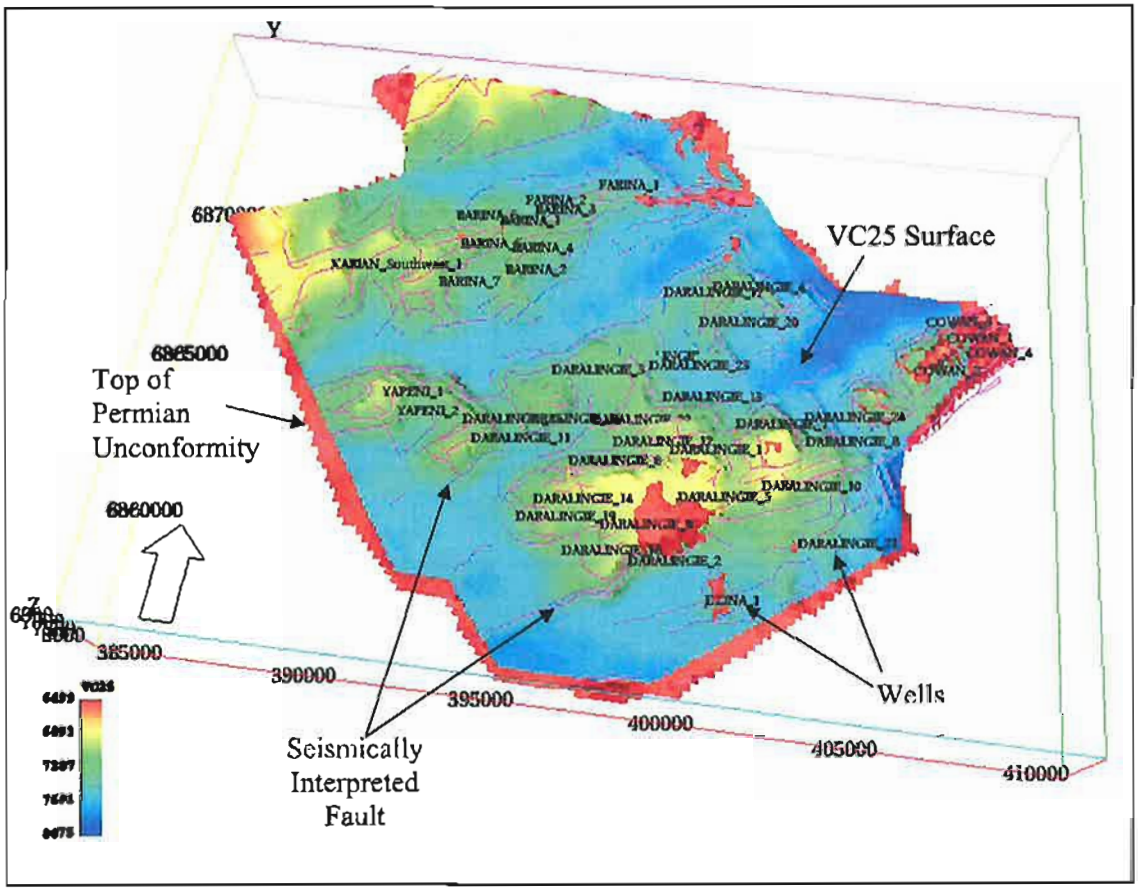

Figure 2.7: 3D view of VC25 and top Permian unconformity surface (shown in red). This unconformity cuts VC25, a seismically derived surface in the Daralinge-5 area and in the Cowan Field, in addition to other small areas within the field. Seismically interpreted faults are also shown.

2.2.3 Production Areas

The Daralingie field is divided into seven separate reservoir areas: DARA Main, DARA 4/20, DARA 11/25, DARA 3, DARA 16, DARA 2 and Yapeni (Fig. 2.7.) The DARA Main is the biggest area and its gas production comes from these wells: D-1, -6, -7, -9, -12, -13, -14, and -15. The DARA 4/20 area production comes from D-4 and -20. The DARA 11/25 area gas production comes from D-11 and -25. Cumulative production data for all reservoir areas, as wells as for individual wells, were provided by Santos for this study, however due to the confidential nature of these they were not included here.

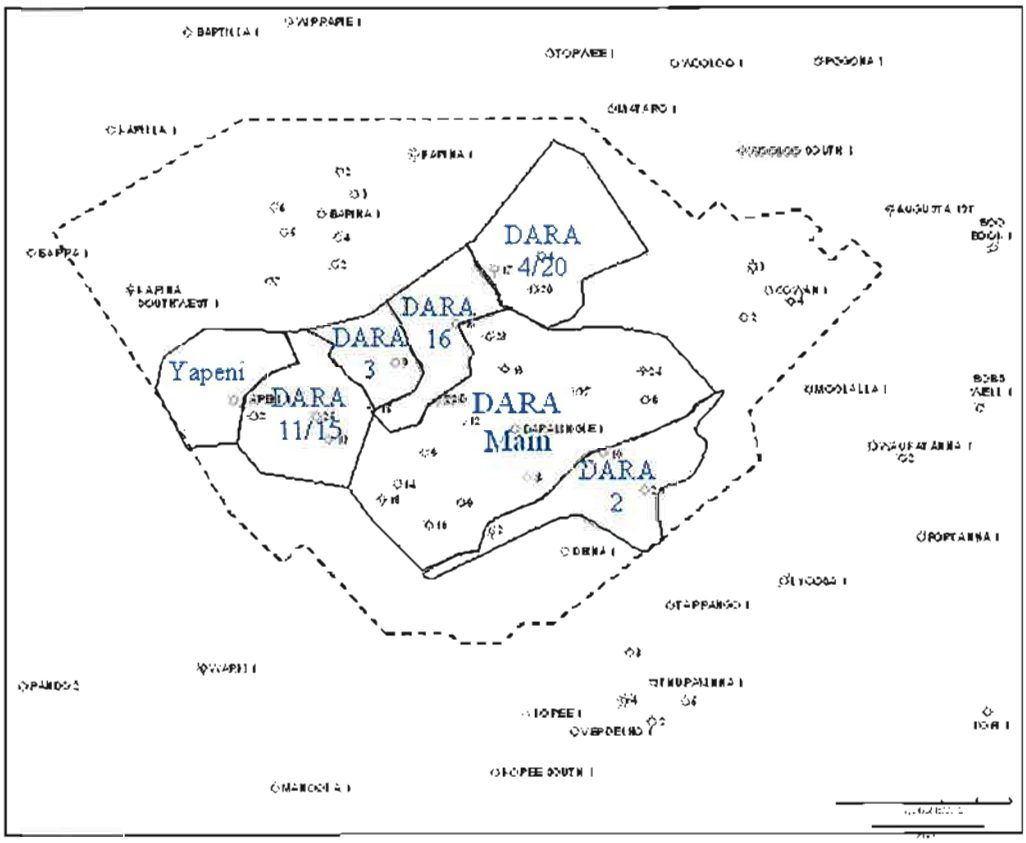

Figure 2.8: The seven production areas for the VC00-VC25 reservoir intervals in the Daralingie Field.

2.2.4 Production Tests

Several drill steam tests (DST) were performed in Daralingie Field (Hill, 2004); the following is a summary of them:

- Daralingie-15: some oil in DST recovery, Core 1 had 31% oil saturation recorded from core plug at base of the VC20 sand and it was considered to be gas saturated
- Daralingie-17: DST oil and water recovered, base of VL22 sand interpreted as wet (possible water breakthrough, though little production to date)
- Daralingie-18: DST oil to surface. Production test was not good, because of heavy waxy oil filled completion after PT.
- Daralingie-19: DST oil, thin sand and good fluorescence in core.
- Daralingie-22: DST Water (5400 feet), however, fluorescence shows in the core are good, though a small zone of washed fluorescence exists (possible water breakthrough?)
- Daralingie-23: DST recovered oil and water, core only just gets base of VL22 sand and has good fluorescence.
- Daralingie-24: Recovered gas/oil/water, lowest known oil (LKO) in Daralingie Field at 7430 feet sub-sea.

2.2.5 Daralingie Field Oil Rim

An oil rim was identified in Daralingie-17. The well test in the main reservoir interval (VC20-VC25) recovered 1140 feet of oil (July 1986) with an API of 38.5. The oil rim was appraised by a number of further wells (Daralingie-18, -19, -22, -23 and –24) and all intersected the oil rim and all of these wells are classified as non-producers of gas (Fig. 2.8) (Hill, 2004).

Daralingie 18 was drilled in August 1987. On DST the well flowed oil to surface at a rate of 584 BPD (plus 0.4 MMcfd of gas). The reservoir sands were found to be depleted and similar in reservoir pressure to the up-dip gas wells. A 27-day production test was conducted followed by a three-day build up test. The well flowed at an average oil rate of 77 BPD with negligible water produced. Ten days after the production test finished, wax-plugging problems were encountered in the well bore. A number of methods were tried, such as hot oil injection and pour point depressant injection, but they were unsuccessful in clearing the wax plugs (Hill, 2004).

The oil rim pressure at Daralingie-18 was about 900 psi depleted, which indicated that gas had been liberated from the oil rim. Furthermore, four separator sample pairs (gas and oil) were taken and analysed. The analysis showed that the oil has bubble point pressure of 3645 psig. Since the pressure at the estimated oil water contact was 3273 psig, it was concluded that two-phase flow had occurred in the reservoir (Santos, 1987). Therefore, the liberated gas had to be taken in account in calculating hydrocarbon volumetrics for VC20-VL22 and VL22-VC25 reservoir intervals.

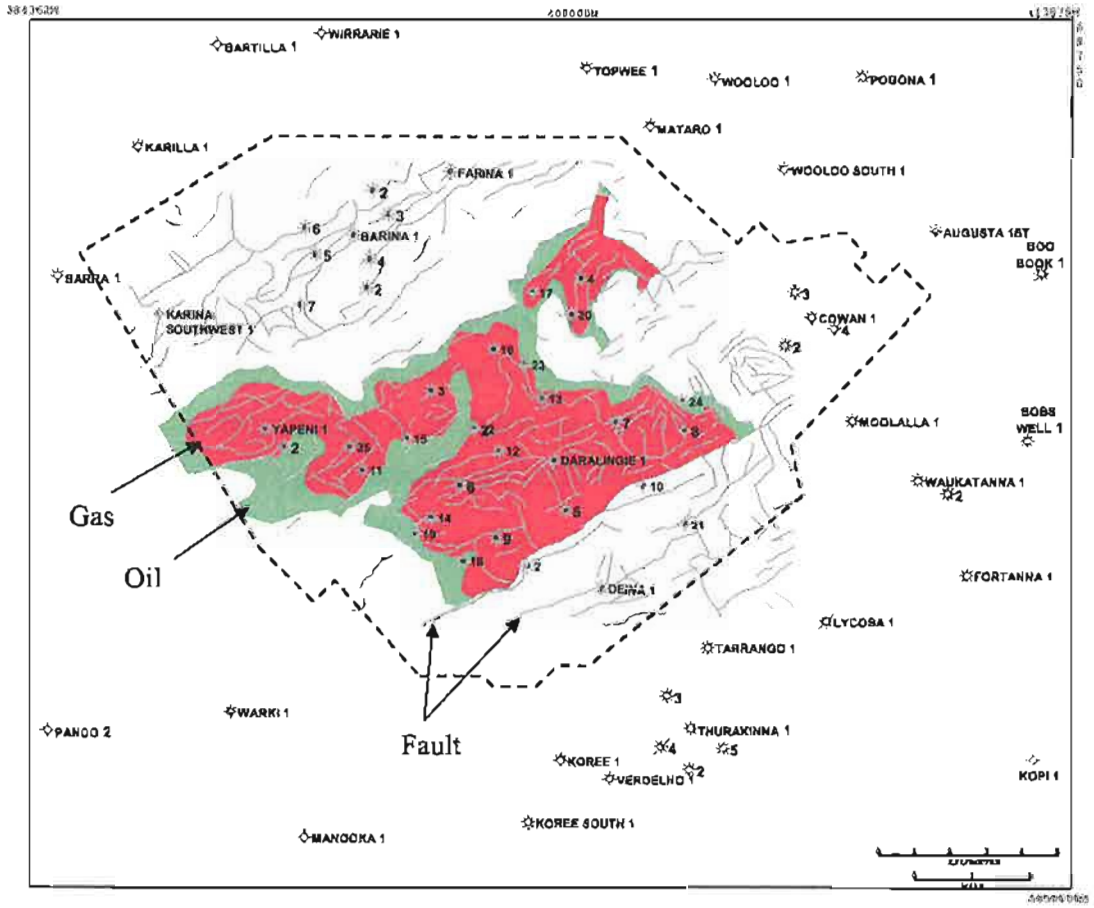

Figure 2.8: Oil rim distribution in Daralingie Field (Hill, 2004). Note that Daralingie-18, -19, -22, -23 and –24 were drilled to delineate the oil rim

2.2.6 Ultimate Development Scenarios

Three different ultimate development scenarios (1P, 2P and 3P) were provided by Hill (2004). Each scenario represents a different fluid contact to account for the liberated gas from the oil rim due to the pressure drop during the field production history. The associated volume of liberated gas was obtained from pressure, volume and temperature (PVT) experimental studies done on D18 oil samples. The calculation was done using current reservoir pressures for 2P and an ultimate abandonment pressure for 3P volumes. The contacts were as follow:

- 1P - (VC20/VL22) gas mapped down to GOC of 7302 feet sub-sea for the DARA Main based on a LKG of 7301 feet sub-sea in Daralinge-12, a highest known oil (HKO) of 7303 feet sub-sea in Daralingie-18 and HKO of 7304 feet sub-sea in the Daraling-23. For the DARA 4/20 area, lowest known gas (LKG) of 7390 feet sub-sea based on GOC of 7390 feet sub-sea in Daralingie-20. For all areas in the Daralingie reservoir an OWC of 7430 feet sub-sea based on Daralingie-24 was used.

- 2P - (VC20/VL22) gas mapped down to GOC (7302 feet sub-sea) plus associated liberated gas at current pressure (626 standard cubic feet/oil barrel (scf/bbl)) for the DARA Main. While in DARA 4/20 area, the GOC was mapped down to 7417 feet sub-sea (gas gradient of 0.05) with the associated liberated gas from the oil rim at 626 scf/bbl.

- 3P - (VC20/VL22) gas mapped down to GOC (7302 feet sub-sea) plus associated liberated gas at abandonment (750 scf/bbl) for the DARA Main. While in DARA 4/20 area, the GOC was mapped down to 7430 feet sub-sea (gas gradient of 0.07) with the associated liberated gas at 750 scf/bbl.

2.2.7 Fluid Petrophysical Properties

J-Functions were not available and no water saturation (Sw) model was built. A constant Sw value of 30% was used above the OWC for the all the calculations. The gas volume factor (Bg) used was 0.0056 and the oil volume factor (Bo) was 1.6750.

2.2.8 Previous volumetric studies

A volumetric estimation for the Daralingie Field was conducted in 1991 (Hill, 2004). Based on these volumetrics, the recovery factor for 2P and 3P is more than 100%. After a full review of the petrophysics in early 2004, Adam Hill (Santos) performed volumetric calculations. Depth structure maps were generated from the Caladan 3D survey and phantomed to the relevant top porosity for each reservoir unit. The sand trends were based on the gross sand thickness for each interval, and were constructed in the Petrosys mapping package. Weighted average method was used for calculating porosity, shale precent and net-to-gross sand thickness. Shale percent for the VC20/VL22 was calculated using earlier wells (*before the majority of production and depletion occurred)* to negate the effects of water invasion. The volumetrics were calculated for each reservoir unit. OGIP was calculated for the VC00, VL05, VL11, VC20 and VL22 reservoir intervals and OOIP was calculated for the VC20 and VL22 oil rim. This study showed an improvement in volumetric estimation, but still the recovery factor for 2P and 3P was more than 100%. Therefore a detailed reservoir characterisation study was needed to address this issue in detail.

Apak, S. N., W. J. Stuart, et al. (1997). "Structural Evolution of the Permian-Triassic Cooper Basin, Australia: Relation to Hydrocarbon Trap Styles." American Association of Petroleum Geologists **81**(4): pp. 533-555.

Brakel, A. T. and J. M. Totterdell (1996). Palaeogeographic Atlas of Australia. Canberra, Australia, Australian Government Publishing Service.

Flottmann, T., D. J. Campagna, et al. (2004). Horizontal Microfracutres and Cores Discing in Sandstone Reservoirs, Cooper Basin, Australia. PESA Eastern Australasian Basins Symposium II, Adelaide, SA, Australia.

Hill, A. (2004). Daralingie Volumetrics, How Big Was The Prize? Adelaide, SA, Australia, Santos.

Nakanishi, T. and S. C. Lang (2002). "Towards An Efficient Exploration Frontier: Constructing A Portfolio of Stratigraphic Traps in Fluvio-Lacustrine Successions, Cooper-Eromanga Basin." APPEA Journal **42**: 131-50.

Santos (1987). Daralingie-18 P.V.T. Report. Adelaide, SA, Australia: 25.

Strong, P. C., G. R. Wood, et al. (2001). Moomba Area Patchawarra Study, Santos: 59.

Strong, P. C., G. R. Wood, et al. (2002). "High Resolution Palaeogeographic Mapping of the Fulvial-Lacustrine Patchawarra Formation in the Cooper Basin, South Australia." APPEA Journal **42**: 65-81.

Chapter 3

Daralingie Field Reservoir Characterisation

3.1 Facies Scheme

Daralingie-2, -9, -19, -22 and -23 cores were logged to identify the main facies in the reservoir. Daralingie-2 was selected because it is the only core with 100% recovery through the Patchawarra Formation in Daralingie Field. The remaining wells were selected because they have good core recovery across the reservoir interval (VC20-VC25).

The described core facies were matched to their petrophysical log signatures. This resulted in the development of a log-motif-based facies association scheme to identify facies at wells that did not have cores. The facies defined in this study were:

1. Fluvial Channels: Isolated or multistorey fine to medium-grained cross-bedded sandstones with blocky or fining-upward log motifs (Fig. 3.1). They were interpreted as either isolated or amalgamated meandering channels or distributary channels.

2. Crevasse/Splay Complex: Isolated or stacked very fine to medium-grained parallel-laminated or ripple-laminated sandstones with blocky or coarsening-upward log motifs (Fig. 3.2).

3. Peat Mire (Coal): The coals are dull and massive with thickness ranging from a few centimetres to a few metres in some sequences such as VC25-VC30 (Fig. 3.3).

4. Overbank/Marsh: Interbedded mudstone and siltstone, usually with ripple cross-lamination with occasional burrows and rootlets (Fig. 3.4).

The facies scheme for this study was consistent with the scheme that was developed by Strong et al. (2002) for the Moomba Area in the Patchawarra interval and by (Lang and Ceglar, 2000)(2000) in the Baryulah Area.

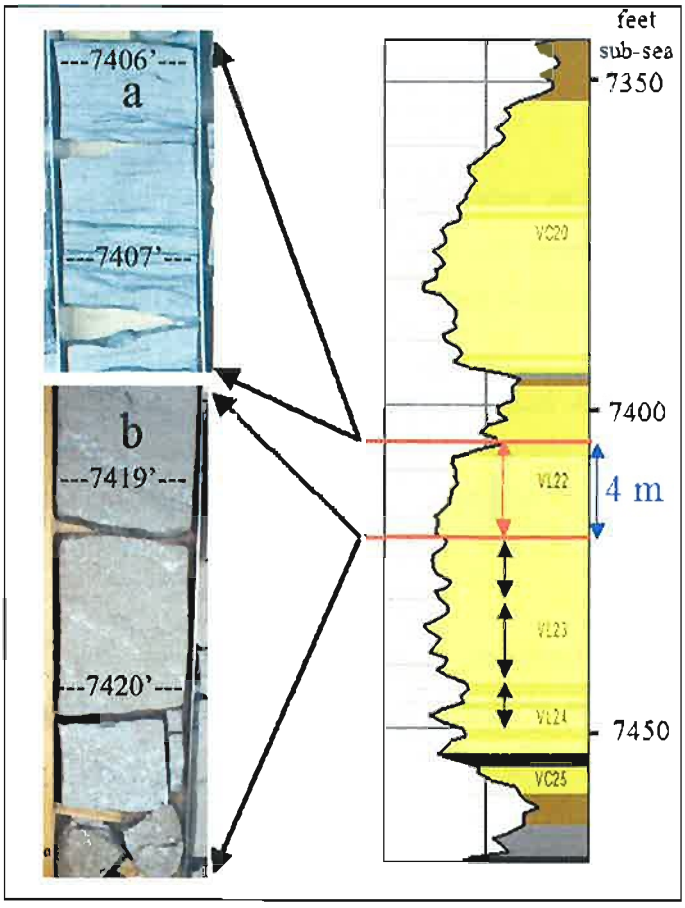

Figure 3.1: Core and log correlation for Daralingie-2. The highlighted interval shows an upward-fining sequence and (a) was interpreted as a channel top and (b) was interpreted as the channel base. The bank-full channel thickness is calculated to be 4 metres thick.

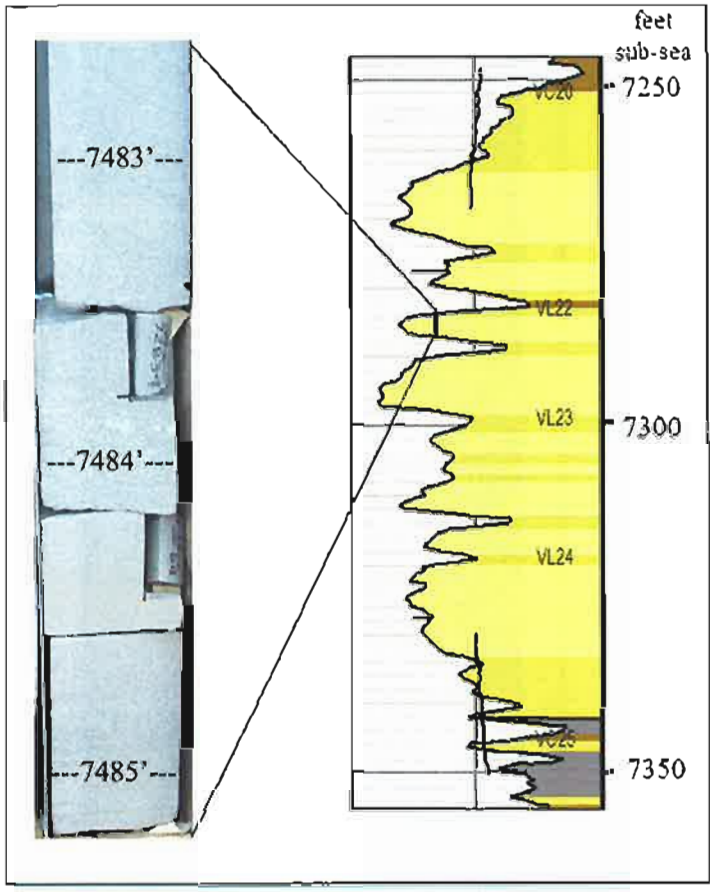

Figure 3.2: An example of the Crevasse/Splay Complex interpreted in Daralingie-9. Note the spiky log motif and massive laminated sandstone.

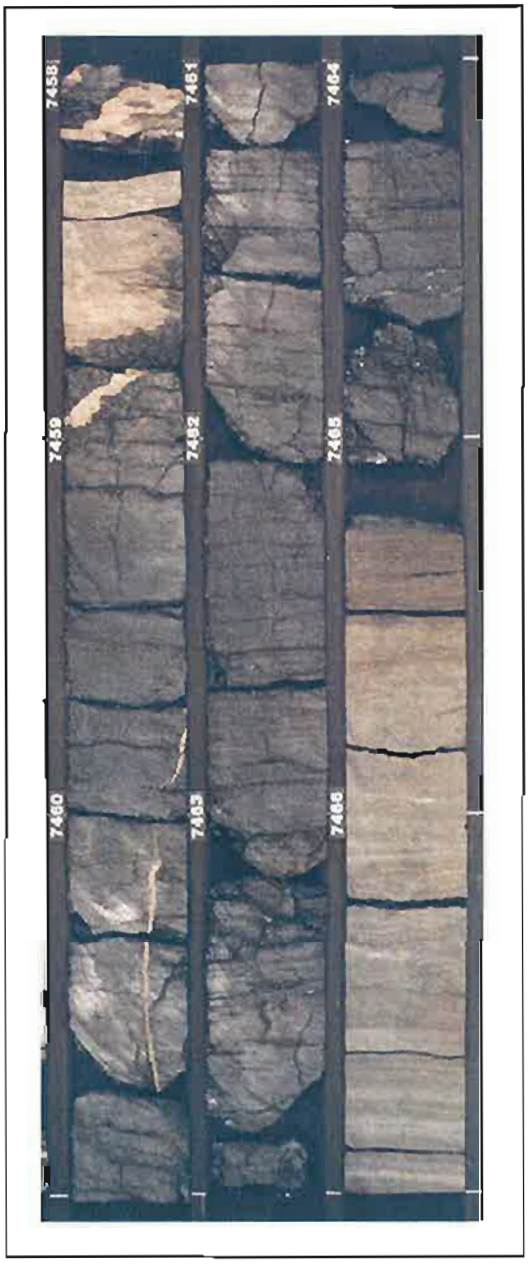

Figure 3.3: A core sample from Daralingie-23 showing massive and dull coals found in the Patchawarra Formation in Daralingie Field. Depth is in feet.

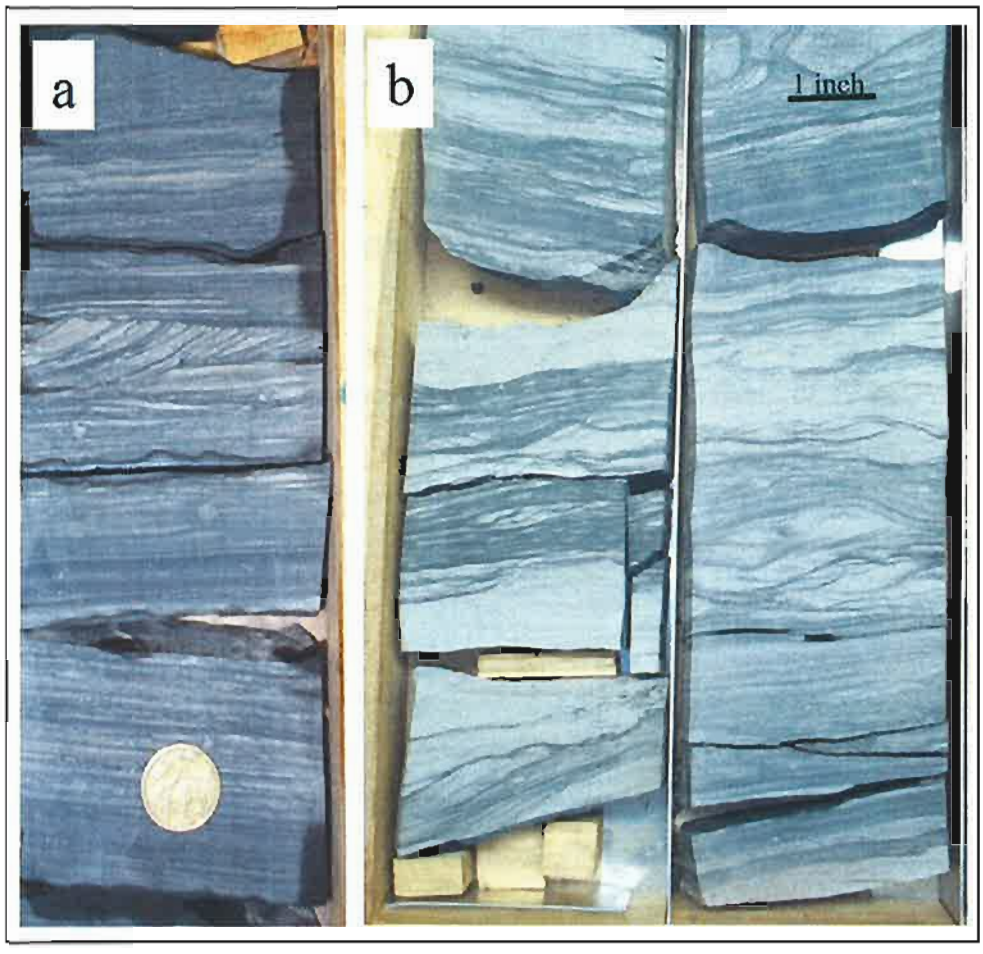

Figure 3.4: Two examples for the Overbank/Marsh facies from Daralinge-2 showing different interbedded mudstone and siltstone with ripple cross-lamination.

3.2 Sequence Stratigraphy

The study interval was interpreted using the principles of sequence stratigraphy (Posamentier and Allen, 1999). Figures 3.5 and 3.6 show cross-sections through the Daralingie Field from east to west and from north to south. A complete listing for the reservoir interval tops is shown in Appendix 1. The following is a brief sequence description for each reservoir interval (further description will follow in section 3.4):

VC30-VC35 interval: is a Lowstand Systems Tract (LST). This interval represents several cycles that were grouped together, because they show very heterolithic characteristics with stacked channels and splays, and flood plain shales. There is no evidence of hydrocarbons in this interval within the Daralingie Field.

VC25-VC30 interval: is a Transgressive Systems Tract/ Highstand Systems Tract (TST/HST) with VC30 as a flooding surface. This is a predominately shale and coal prone interval. The last of the major Patchawarra coals exist in this interval with an average of 35% of the total facies. There is no evidence of hydrocarbons in this interval within the Daralingie Field.

VL22-VC25 interval: is a Late Highstand Systems Tract/ early Lowstand Systems Tract (HST/LST). This interval shows multilateral and multistorey-stacked fluvial channels. This is the lower unit in the reservoir interval. This interval and the VL22-VC25 interval are the main reservoir interval in Daralingie Field.

VC20-VL22 interval: is a Transgressive Systems Tract (TST). As in the VL22-VC25, this interval shows multilateral and multistorey-stacked fluvial channels. There are possible incisions into the underlying interval VL22-VC25 at some wells such as D-16, which may provide communication and connectivity between the two reservoir intervals.

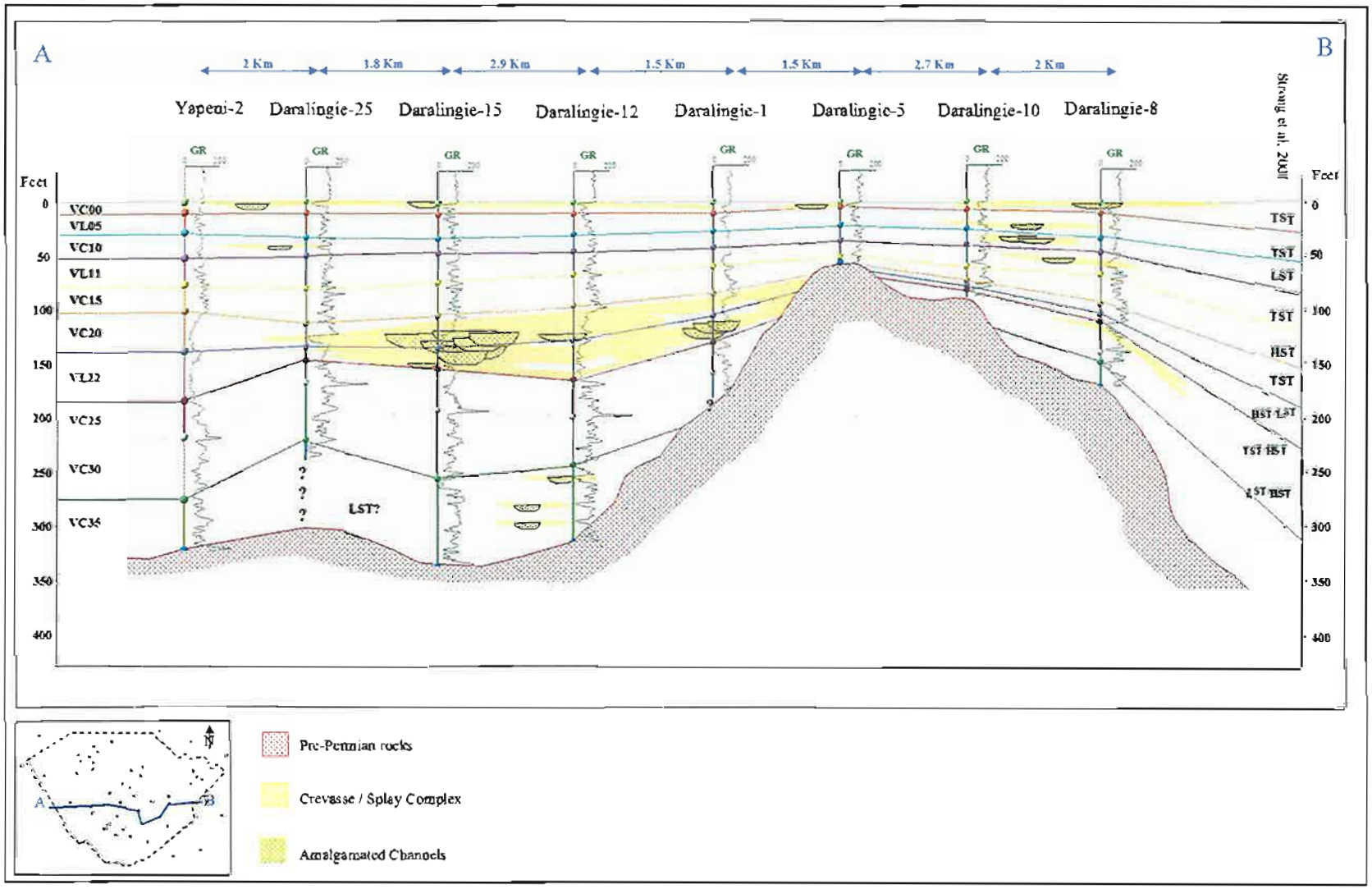

Figure 3.5: An east-west cross-section through Daralingie Field showing the mapped reservoir interval and the stacked channels with associated crevasse splays.

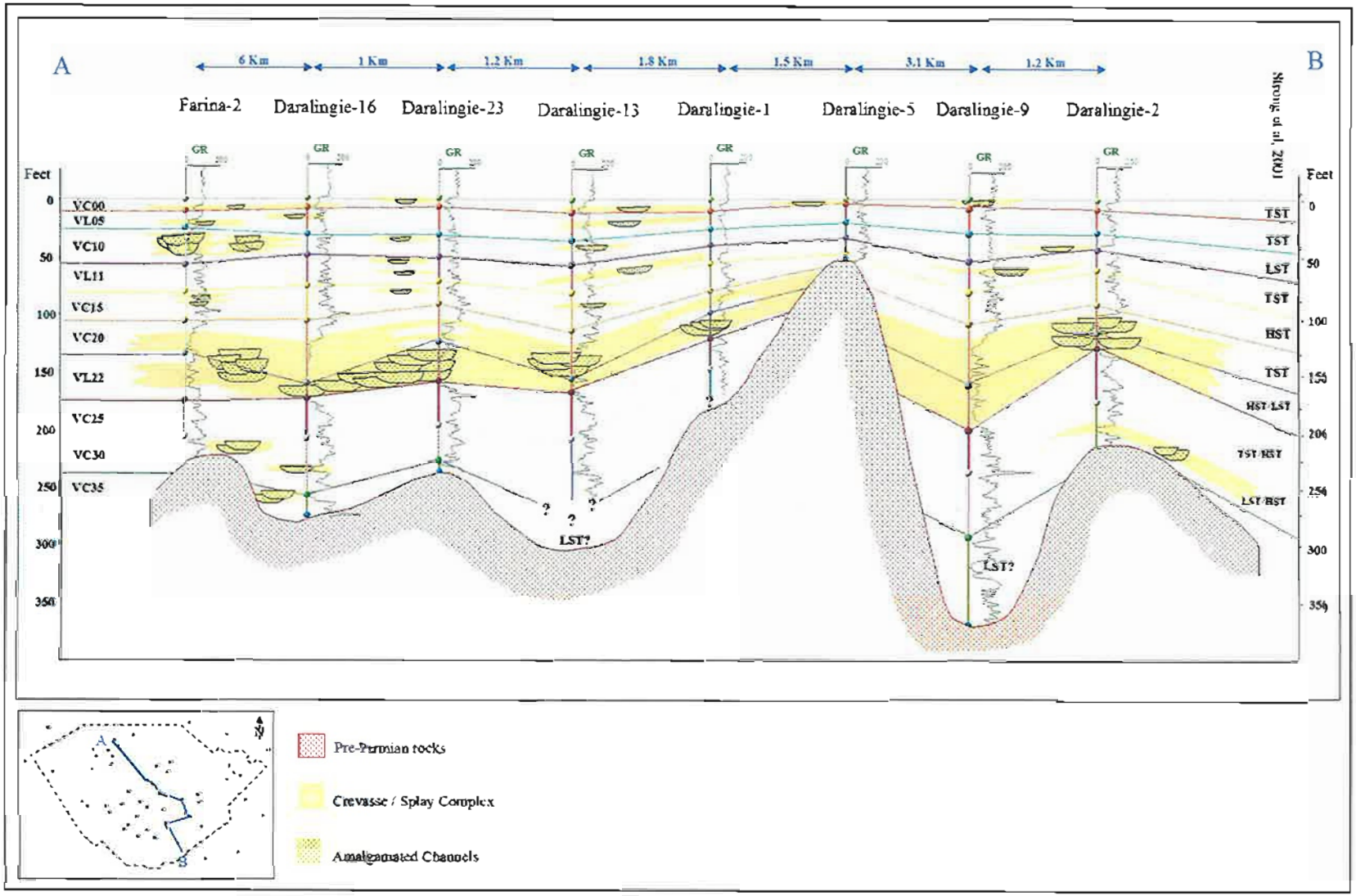

Figure 3.6: A north-south cross-section through Daralingie Field showing the mapped reservoir interval and stacked channels and associated crevasse splays.

VC15-VC20 interval: is a Highstand Systems Tract (HST). Only Cowan-2 in this interval intercepts a channel, hence the location of the channel elsewhere in the field is speculative. The log signatures show that this interval is mainly dominated by flood plain shale. The VC15 is possibly a transgressive flood surface.

VL11-VC15 interval: is a Transgressive Systems Tract (HST). This interval is predominantly shale-prone and shows isolated distributary channel belts. The palaeogeographic setting is similar to VC15-VC20.

VC10-VL11 interval: is a Lowstand Systems Tract (LST). It shows multilateral channel belts across the field area. The main non-reservoir interval lies over the palaeohigh areas, possibly with mild uplift.

VL05-VL10 interval: is a Transgressive Systems Tract (TST). It shows an isolated distributary channels. Daralingie-3 produces gas from this interval along with VC00-VL05.

VC00-VL05 interval: is a Transgressive Systems Tract (TST). Its palaeogeographic setting is similar to VC00-VL05. The VC00 represents the transgressive lacustrine shale of Murteree Shale.

3.3 Reservoir Geometry

3.3.1 Thickness-to-Width ratios

For a given chronostratigraphic interval, estimating channel belt widths from preserved channel-fills can be attempted using a methodology originally proposed by Fielding and Crane (1987). A summary of this methodology can be found in Strong et al (2002). The process requires a complete fluvial channel-fill to be identified from cores or wireline logs. The compacted thickness of the whole channel-fill (sandstone and any mudstone fill) is then converted to a minimum estimate of channel bankfull depth, which is then compared to published ranges of channel belt widths-to-thickness ratio for meandering streams (both modern and ancient). Importantly the ratio is dependent on the channels behaviour as a meandering stream. Within each reservoir interval, channel belt depths were calculated. In the main reservoir intervals (VC20-VC25), they ranged from 2.5 to 3.3 metres. As pointed out by Bridge and Tye (2001), the reliability of these estimates is dependent on careful picking of complete channel-fills, usually the last in a stack of channel sands, including both the thickness of the sand and the abandoned channel-fill.

For each study interval, a range of channel belt widths were derived from a compilation of published data (Figs. 3.7 to 3.13). The mean channel belt width was used for illustrating the facies maps; however, a range of values was used in the modeling to represent the uncertainty in channel belt width. In reservoir intervals where interpreted channels were not intercepted, such as VL11-VC15 and VC25-VC30, the channel belt width was estimated from other intervals in this reservoir with similar geological settings.

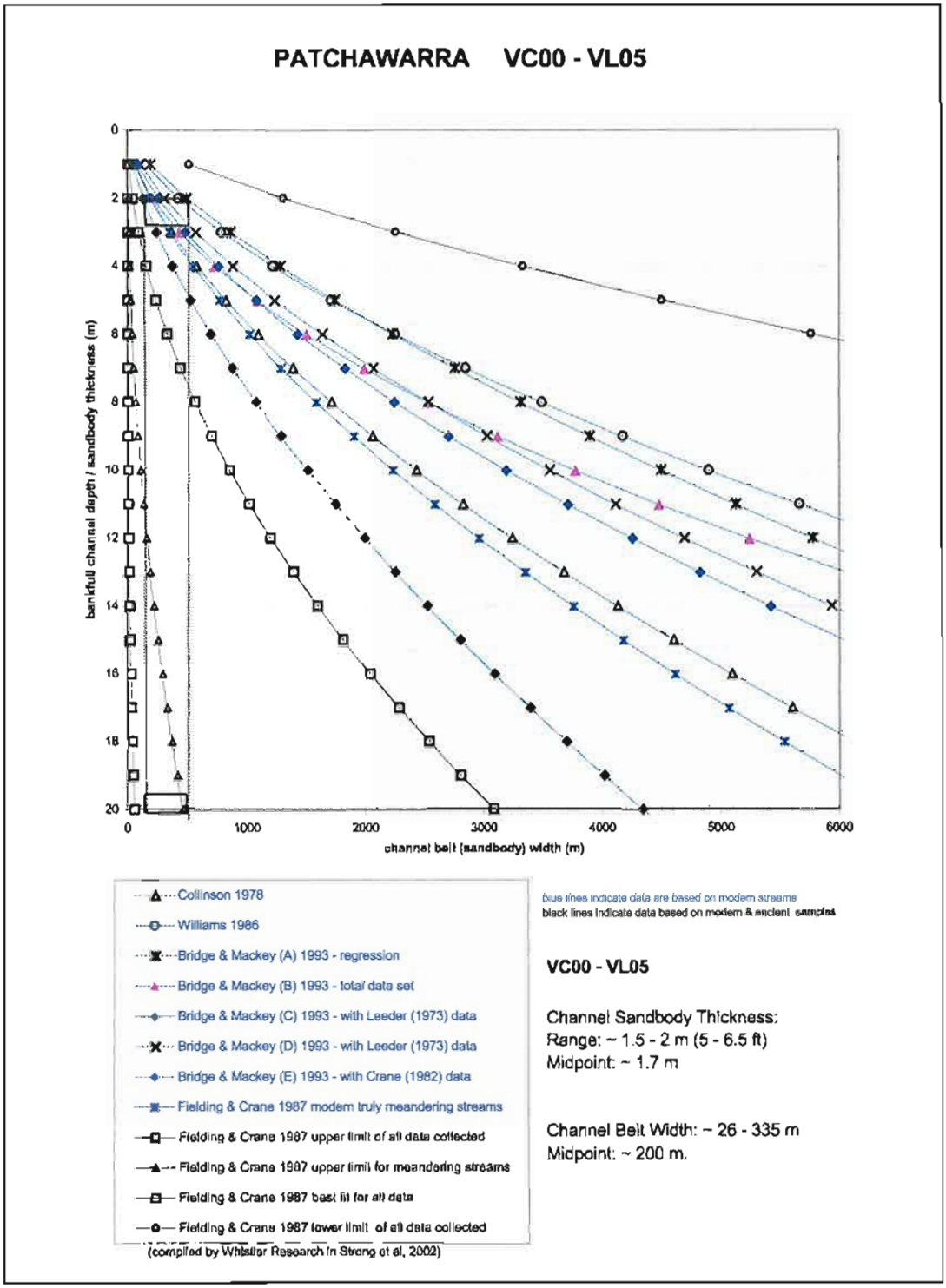

Figure 3.7: Estimated range of channel belt width for the interpreted bankfull channel depth of the VC00–VL05 interval in the Daralingie Field, Patchawarra Formation, based on published data (after Strong et al., 2002).

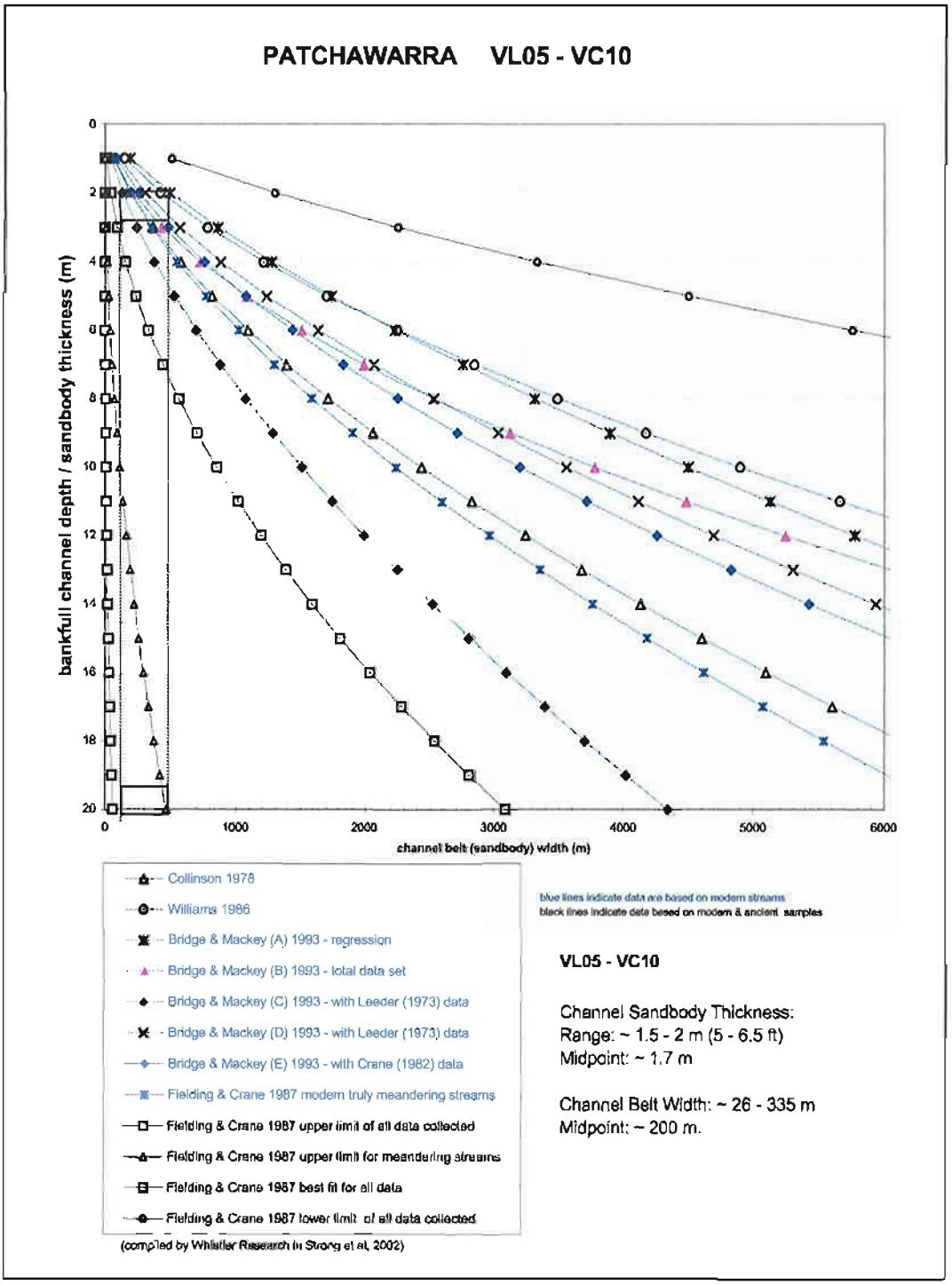

Figure 3.8: Estimated range of channel belt width for the interpreted bankfull channel depth of the VL05-VC10 interval in the Daralingie Field, Patchawarra Formation based, on published data (after Strong et al., 2002).

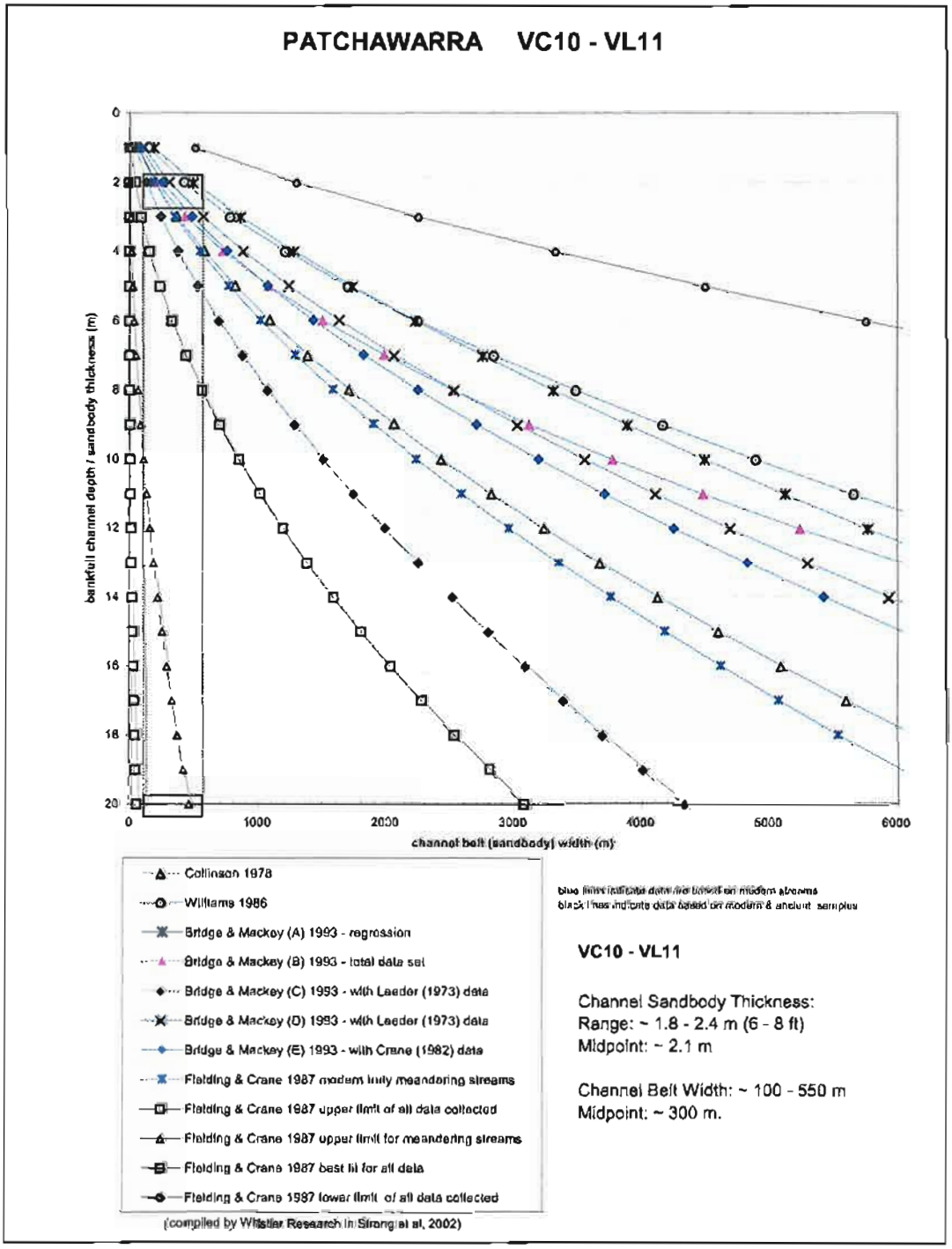

Figure 3.9: Estimated range of channel belt width for the interpreted bankfull channel depth of the VC10-VL11 interval in the Daralingie Field, Patchawarra Formation, based on published data (after Strong et al., 2002).

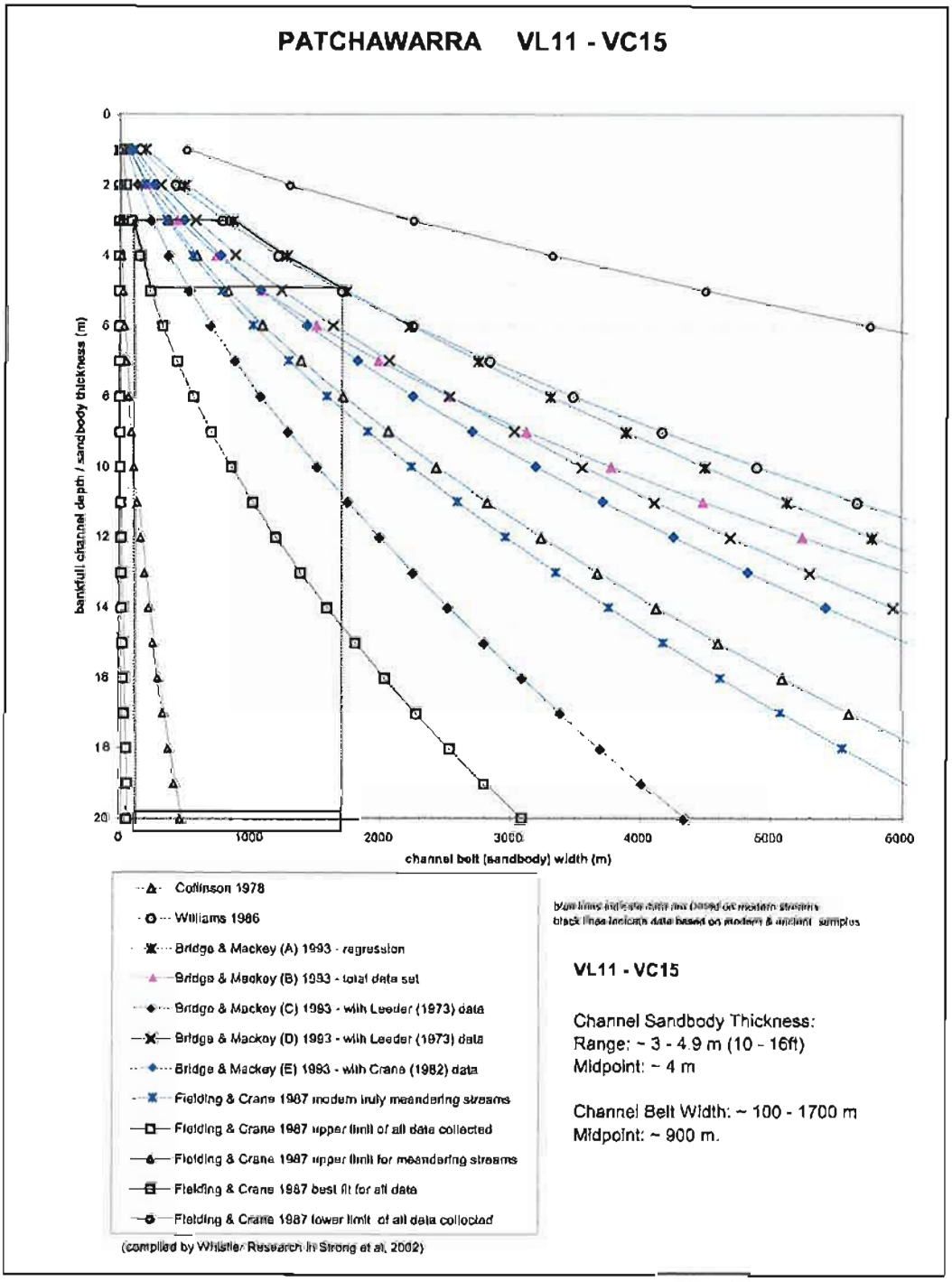

Figure 3.10: Estimated range of channel belt width for the interpreted bankfull channel depth of the VL11-VC15 interval in the Daralingie Field, Patchawarra Formation, based on published data (after Strong et al., 2002).

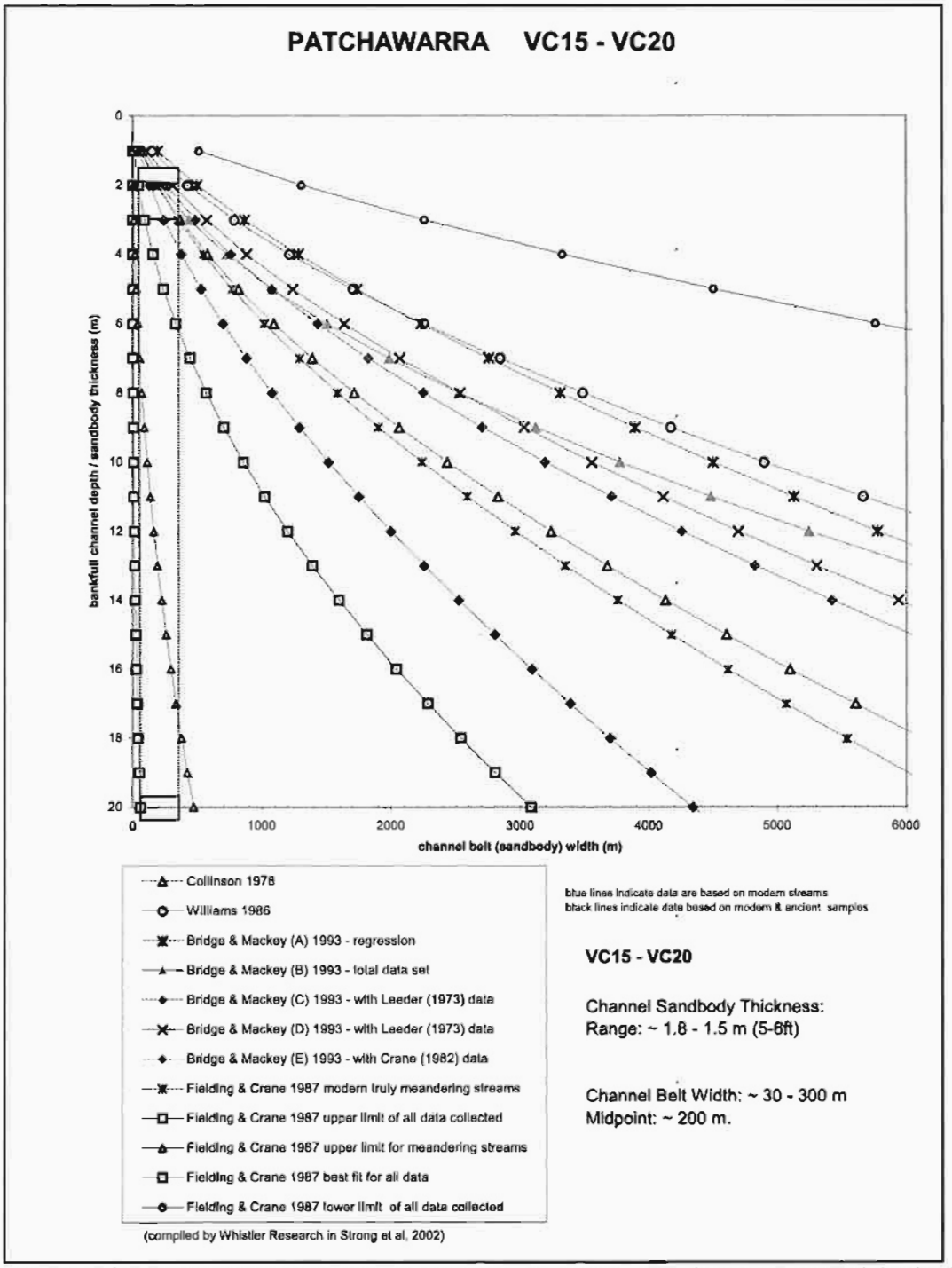

Figure 3.11: Estimated range of channel belt width for the interpreted bankfull channel depth of the VC15-VC20 interval in the Daralingie Field, Patchawarra Formation, based on published data (after Strong et al., 2002).

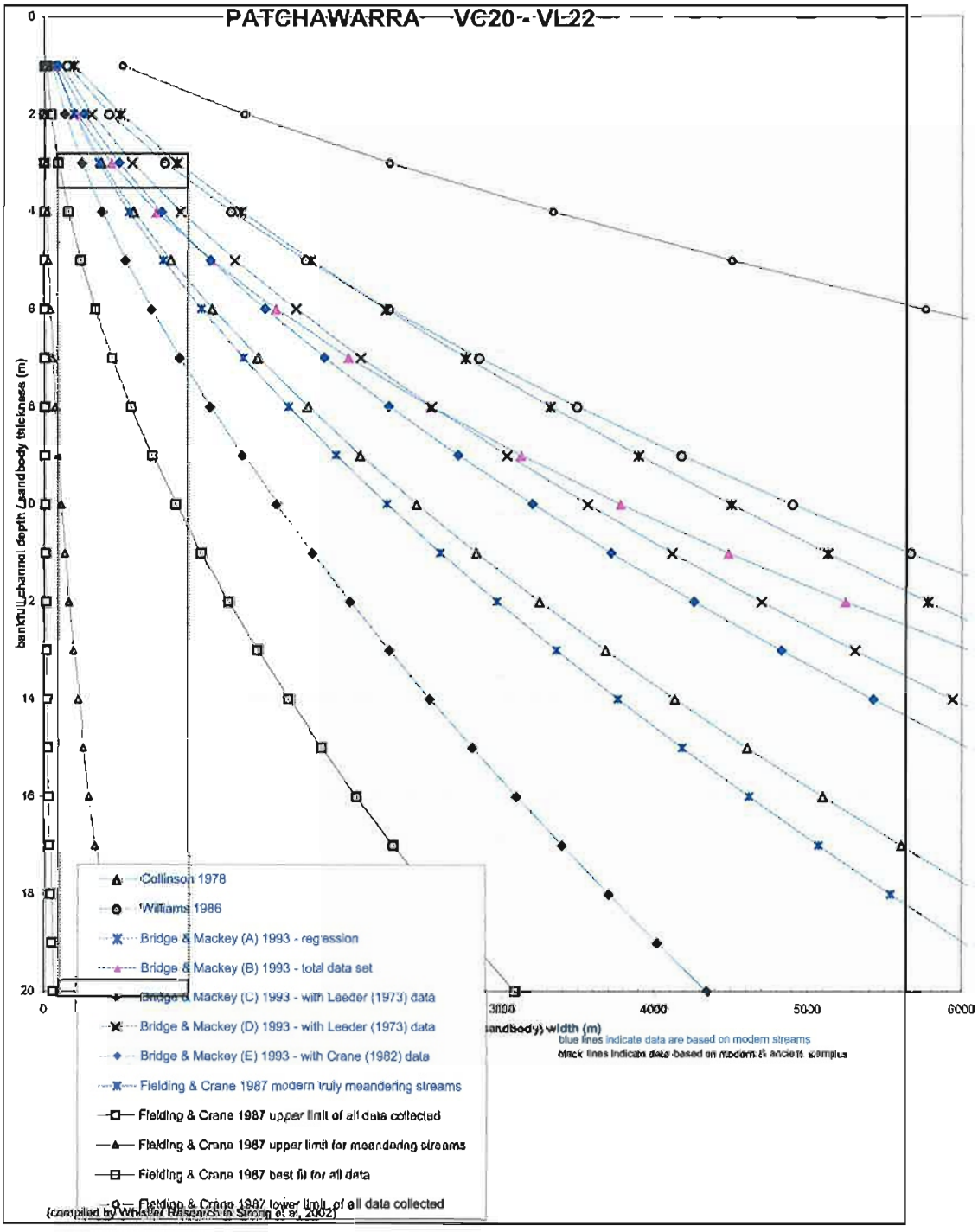

Figure 3.12: Estimated range of channel belt width for the interpreted bankfull channel depth of the VC20-VL22 interval in the Daralingie Field, Patchawarra Formation, based on published data (after Strong et al., 2002).

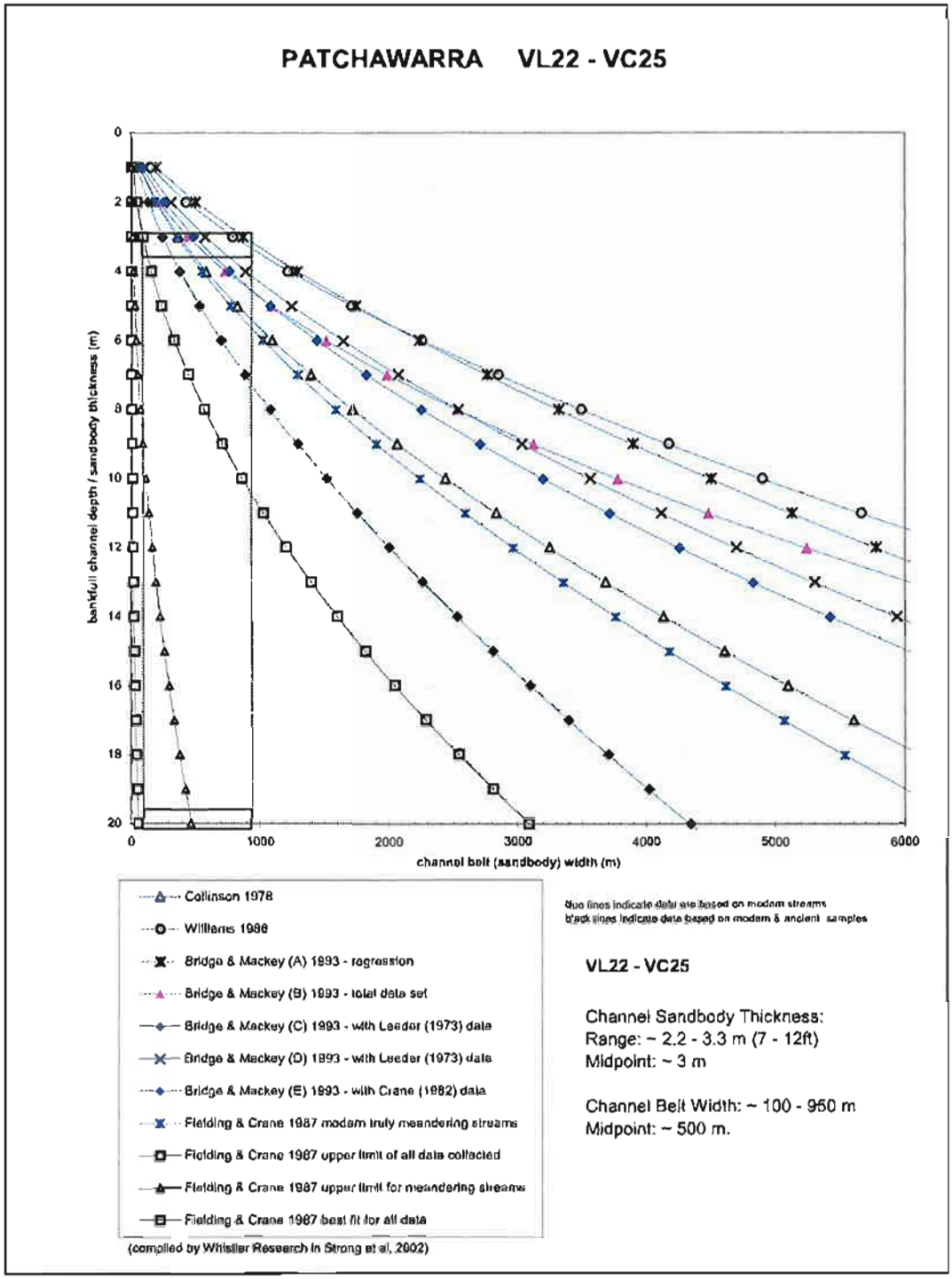

Figure 3.13: Estimated range of channel belt width for the interpreted bankfull channel depth of the VL22-VC25 interval in the Daralingie Field, Patchawarra Formation, based on published data (after Strong et al., 2002).

3.3.2 Net/Gross Plots

For each genetic reservoir interval, interval thickness versus sand percentage was plotted. These plots show that most intervals have either a weakly positive relationship (thicker intervals are more sandy), whereas others showed no particular trend (Figs. 3.14 – 3.23). VC10-11 (Fig. 3.17) had a strongly positive relationship, and this is interpreted as indicating an axial fluvial system (Lang et al., 2001), where the thicker sand was focussed over the area of higher accommodation. VC20-VL22 (Fig. 3.19) and the VL22-25 (Fig. 3.20) interval show confused trends, and this is because of the association with the Pre-Permian unconformity.

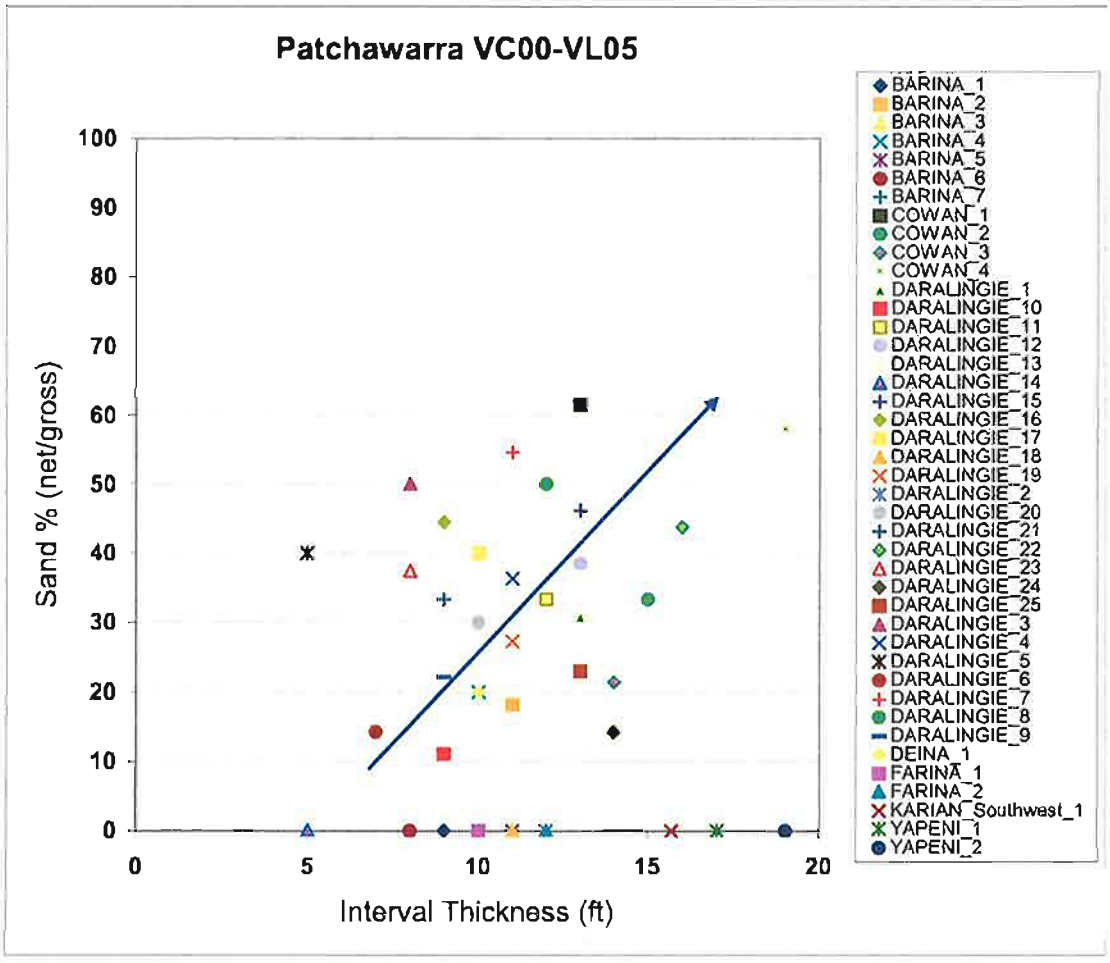

Figure 3.14: Interval thickness vs. sand percentage plot for interval VC00-VL05. A positive relationship between interval thickness and sand percentage is present, indicating the existence of high accommodation space and high sediment supply during deposition.

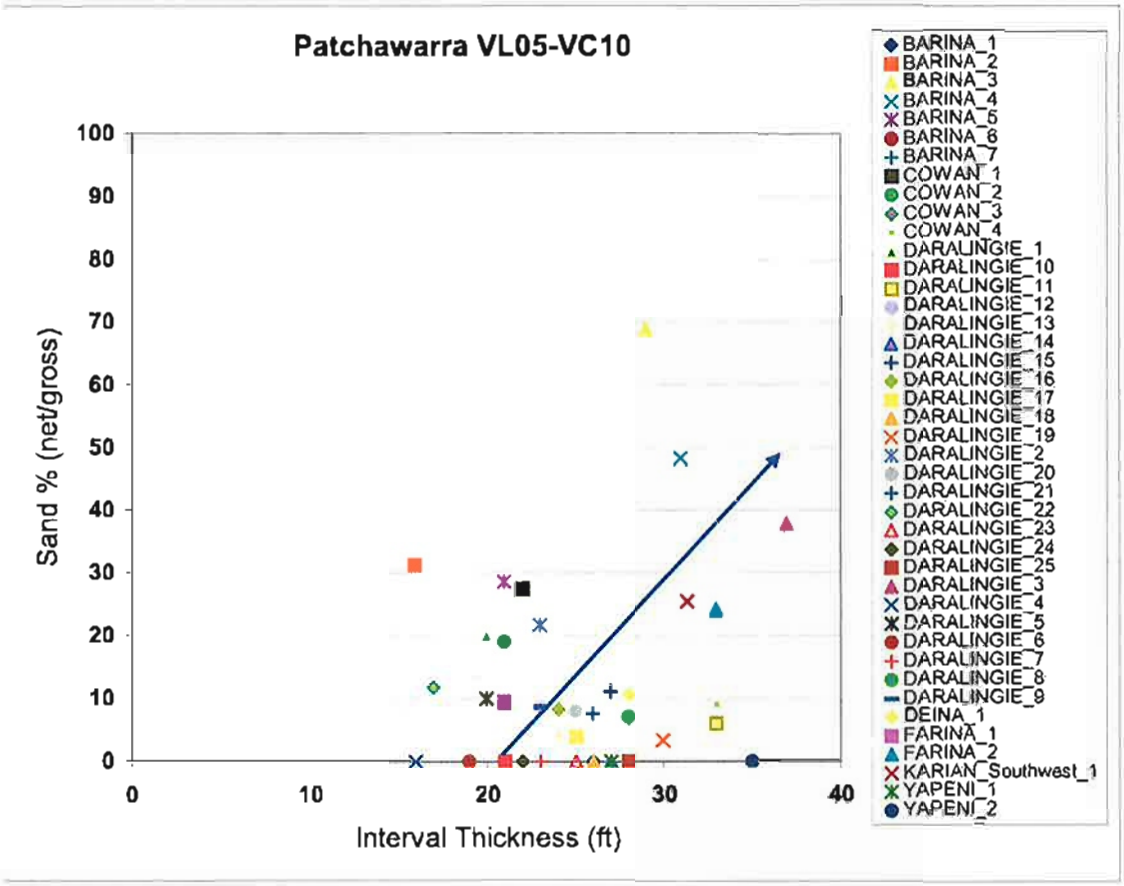

Figure 3.15: Interval thickness vs. sand percentage plot for interval VL05-VC10. A slight positive relationship between interval thickness and sand percentage indicates the existence of moderate accommodation space during deposition, but not as much as in the VC00-VL05 interval.

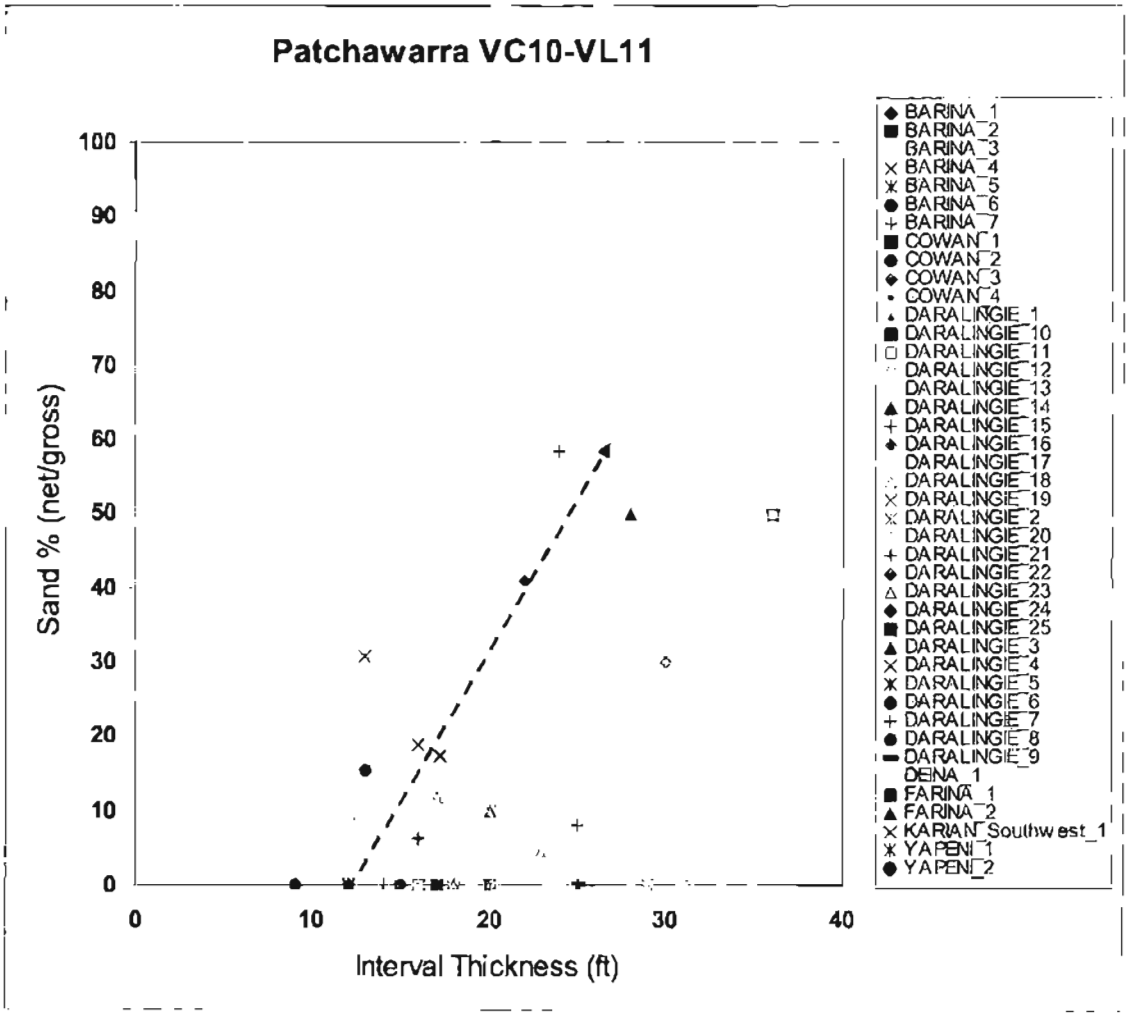

Figure 3.16: Interval thickness vs. sand percentage plot for interval VC10-VL11. A positive relationship between interval thickness and sand percentage indicates the existence of accommodation space during deposition. The accommodation space may be localised in certain areas that may explain the existence of a thicker area with very low sand percentages.

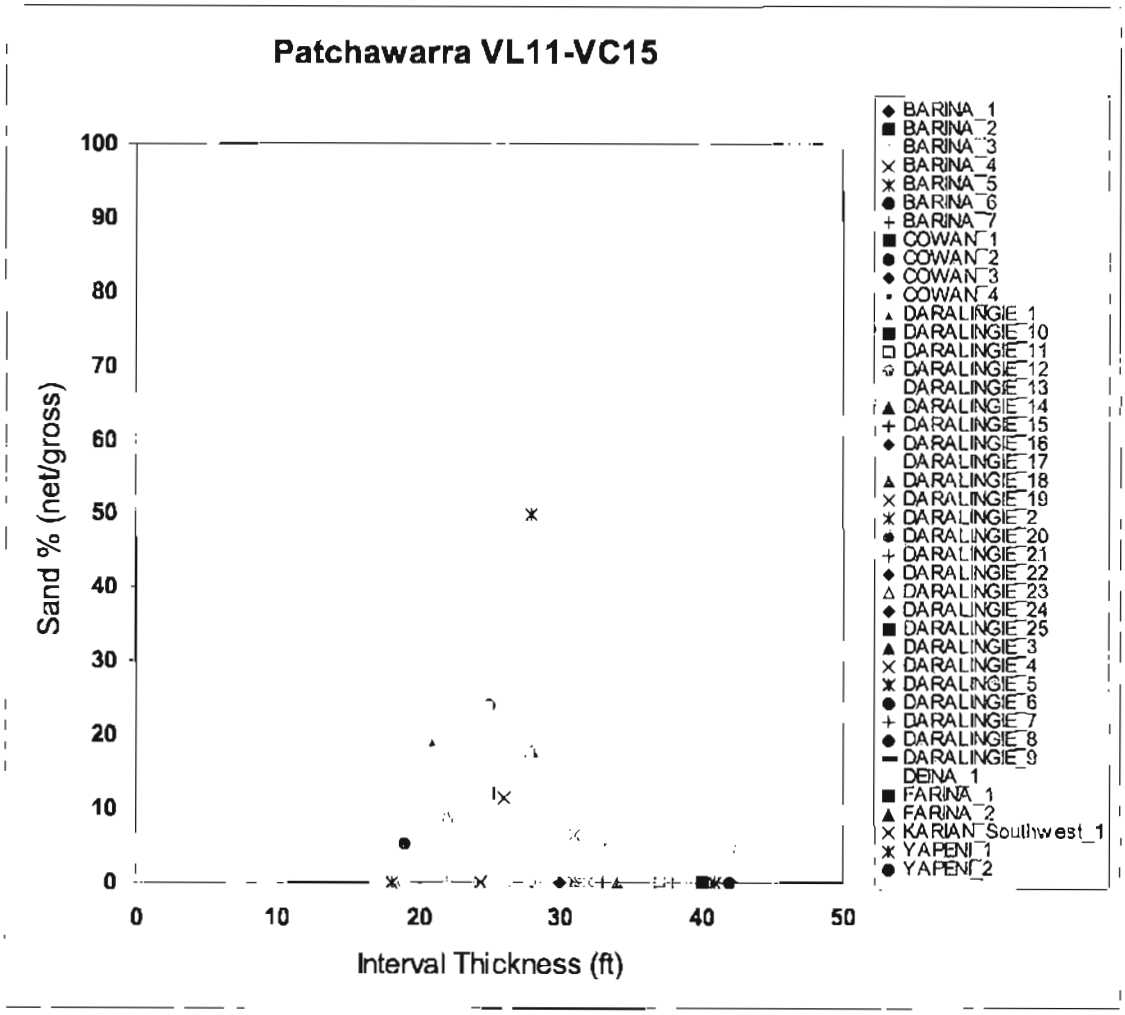

Figure 3.17: Interval thickness vs. sand percentage plot for interval VL11-VC15. There is no particular relationship between interval thickness with sand percentage indicating there was little accommodation space during deposition.

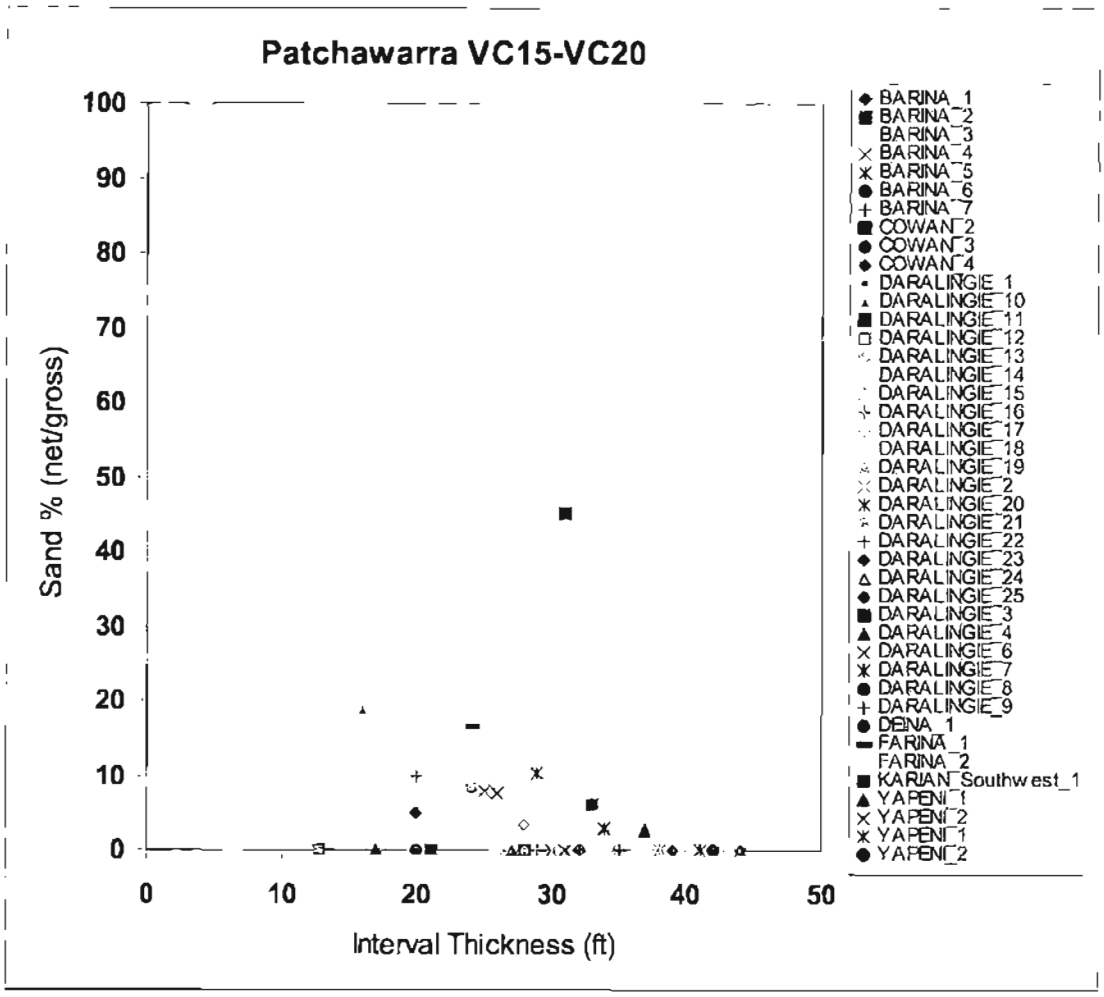

Figure 3.18: Interval thickness vs. sand percentage plot for interval VL11-VC15. This interval is very similar to VL11-VC15 as there was little accommodation space during deposition.

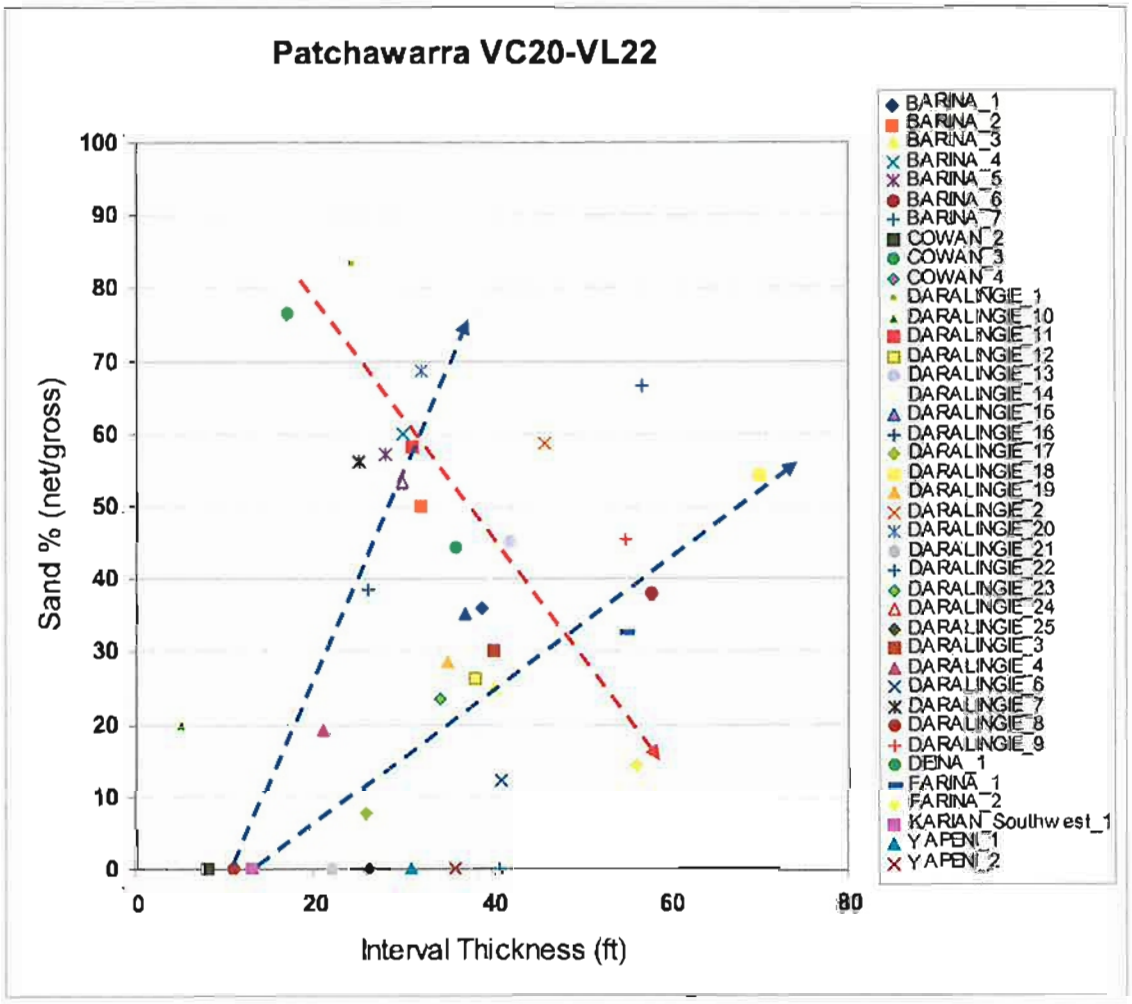

Figure 3.19: Interval thickness vs. sand percentage plot for interval VC20-VL22. This interval shows inconclusive relationships. Two positive relationships and one negative could be interpreted. This is due to the fact that VC20-VC25 overlies a regional unconformity, which makes the accommodation space highly variable. The amount of accommodation space depends on the morphology of the unconformity surface, which is very irregular.

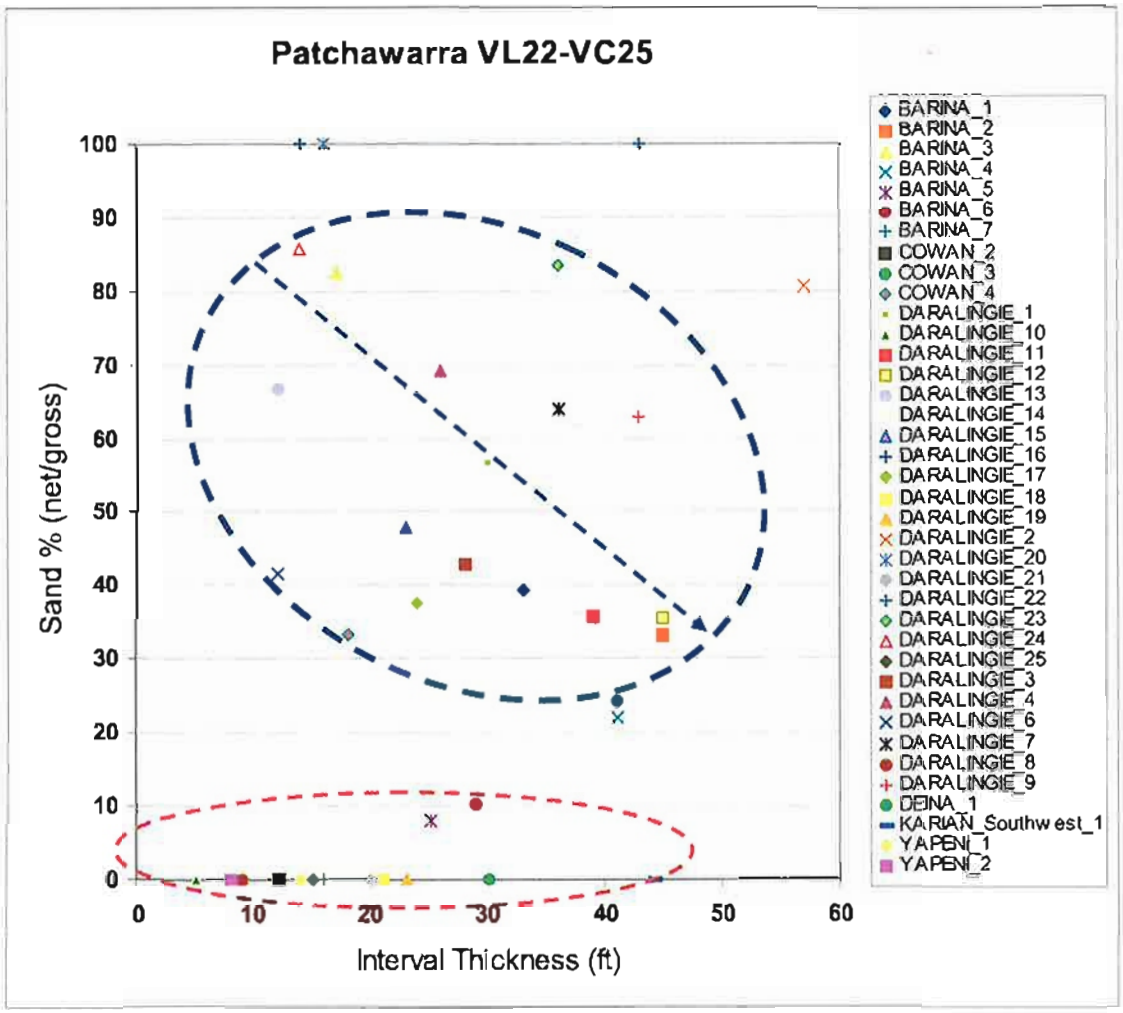

Figure 3.20: Interval thickness vs. sand percentage plot for interval VL22-VC25. This interval shows inconclusive relationships, which can be divided into two groups. The first group, highlighted in blue, shows a negative relationship. The second group, highlighted in red, does not show any relationship at all except low sand percentages. This is due to this interval overlying a regional unconformity, which makes the accommodation space highly variable similar to the VC20-VL22 interval. The amount of accommodation space depends on the morphology of the unconformity surface, which is very irregular.

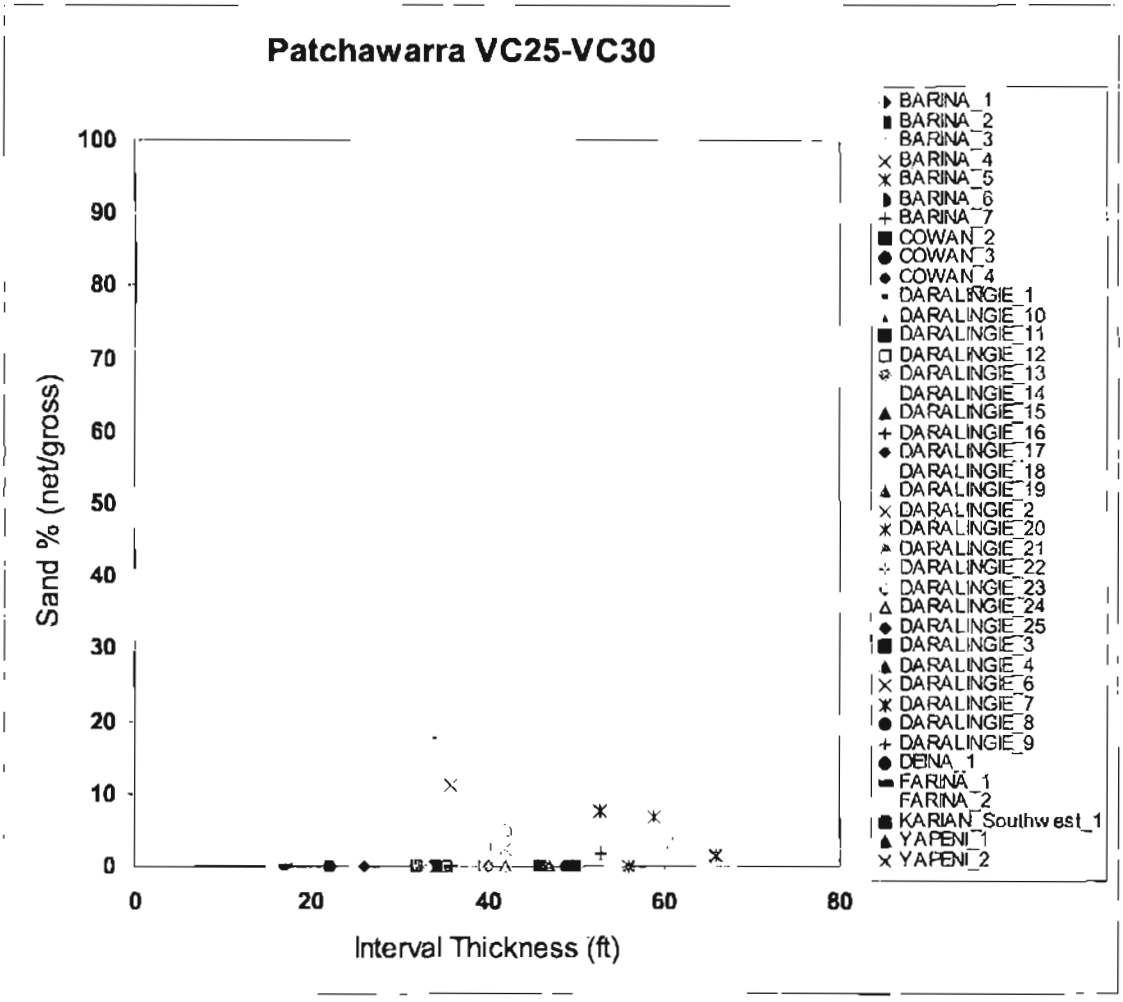

Figure 3.21: Interval thickness vs. sand percentage plot for interval VC25-VC30. There was little accommodation space during the deposition of this interval.

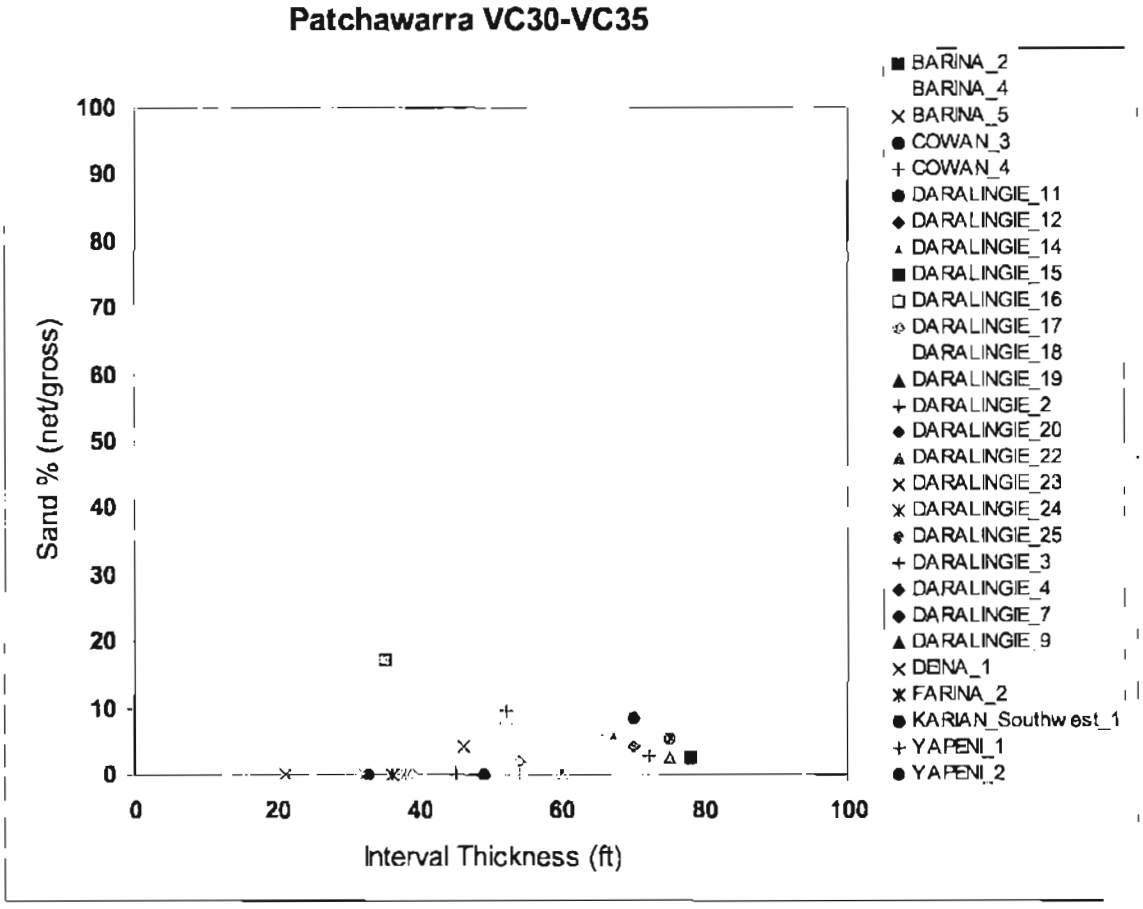

Figure 3.22: Interval thickness vs. sand percentage plot for interval VC30-VC35. There was little accommodation space during the deposition of this interval.

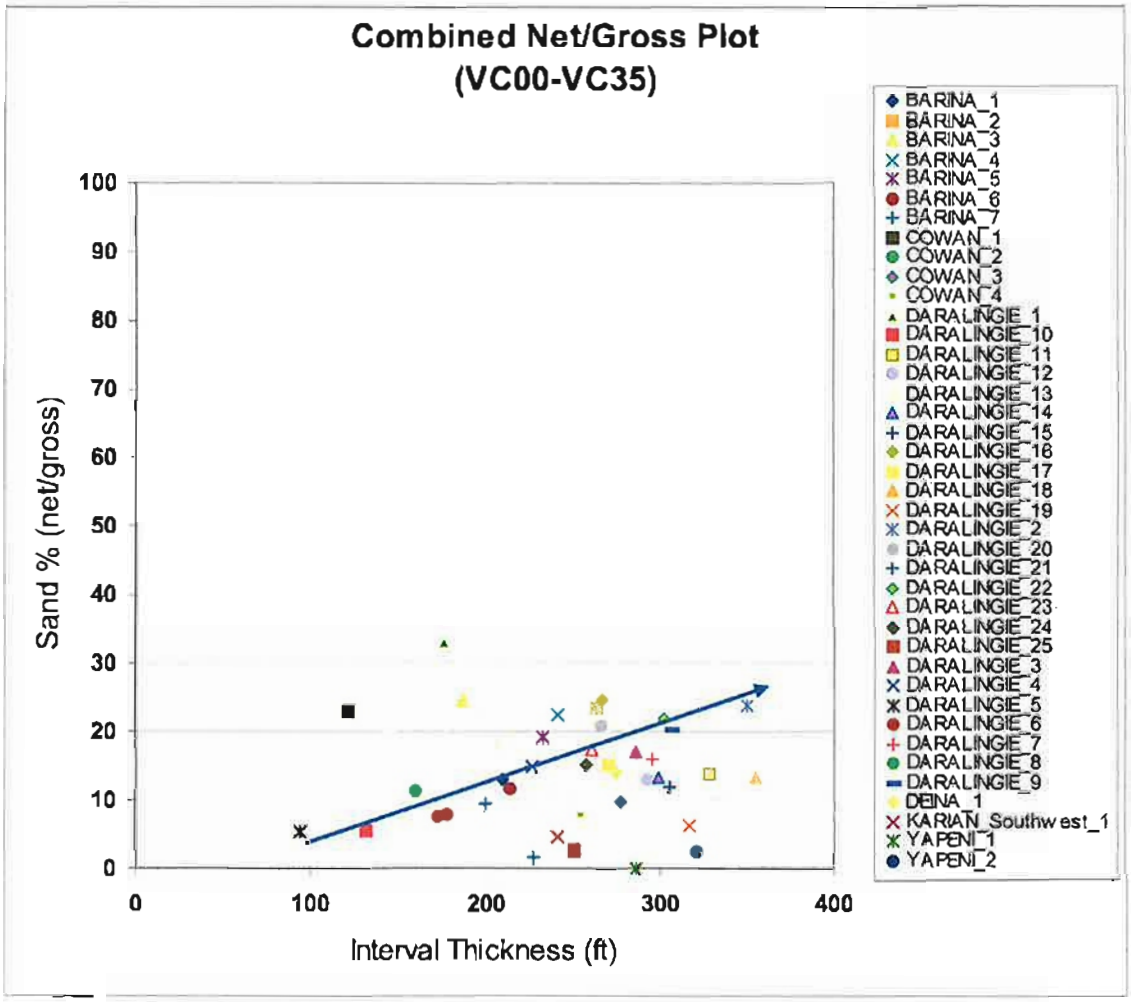

Figure 3.23: Interval thickness vs. sand percentage plot for intervals VC00-VC35 combined. A slight positive relationship exists between the interval thickness and sand percentage. However, this is not representative for every reservoir interval as shown in Figures 3.14-3.22. Therefore, each interval needs to be investigated separately to accurately reflect the geology in the reservoir model.

3.3.3 Modern and Ancient Analogues

The facies interpretation for the Daralingie Field was supported by a range of depositional analogues that can be related to wireline log motifs. Of particular use have been the modern cool-temperate, peat-forming fluvial systems of Saskatchewan and Western Siberia, and the Late Permian coal measures of the Bowen Basin described by Lang et al. (2000; 2001; 2002) and Strong et al. (2002). The rationale for selecting these modern, high-latitude, cool-temperate, peat forming fluvial systems is based mainly on similarities with the palaeolatitude and palaeoclimatic situation of the Cooper Basin in the Permian, which was part of a large peat-forming alluvial basin lying at high palaeolatitudes (Veevers, 2000). Satellite images, especially Synthetic Aperture Radar (SAR) imagery from Smith and Alsdorf (1998) of the Ob River, Siberia were particularly useful to obtain cloud- and snow-free images depicting channel belt scale, relative orientation and relationship of channels and splays to floodplain, floodbasin lakes and interfluve peat lands and *Taiga* coniferous forest.

A key facies type observed in the West Siberian plain is narrow crevasse splay distributaries surrounded by floodplains adjacent to major fluvial fairways. In Western Siberia, these splay complexes are particularly dominant in the lower reaches near the town of Salekhard, where extremely low relief, flooding, and ice jams promote abundant avulsions (Smith and Alsdorf, 1998; Lang et al, 2000). The numerous splay networks can evolve to significant river systems parallel to the major fluvial axes. Many of these narrow, slightly sinuous channels contain sand and feed splay complexes, either into floodplain lakes or over extensive marshes adjacent to raised mires (coal). Smith and Alsdorf (1998) used satellite-borne SAR images of thes splay complexes adjacent to the Ob River (Fig. 3.25) as part of an analysis of sediment delivery to the Arctic Ocean. What is clear from this image is that there can be numerous parallel small crevasse splay distributaries on the floodplain of a much larger river system, and these could be useful analogues for the narrow fluvial channel belts interpreted in Daralingie Field.

Based on studies from other analogues in Saskatchewan (Smith and Perez-Arlucea, 1994) and coal mine datasets from Permian coal measures (Avenell, 1998; Lang et al, 2000), crevasse splays are likely to form complex, lobate, distributary and anastomosing networks in the low-relief areas adjacent to the channel belts.

Palaeo-interfluve areas between the main channel belts are likely to be more coal prone, lying slightly higher and away from sediment influx where raised mires can flourish in the raised water tables, as occurs in the Vasuganye and Noyabrsk peatland systems (Vasiliev, 2001).

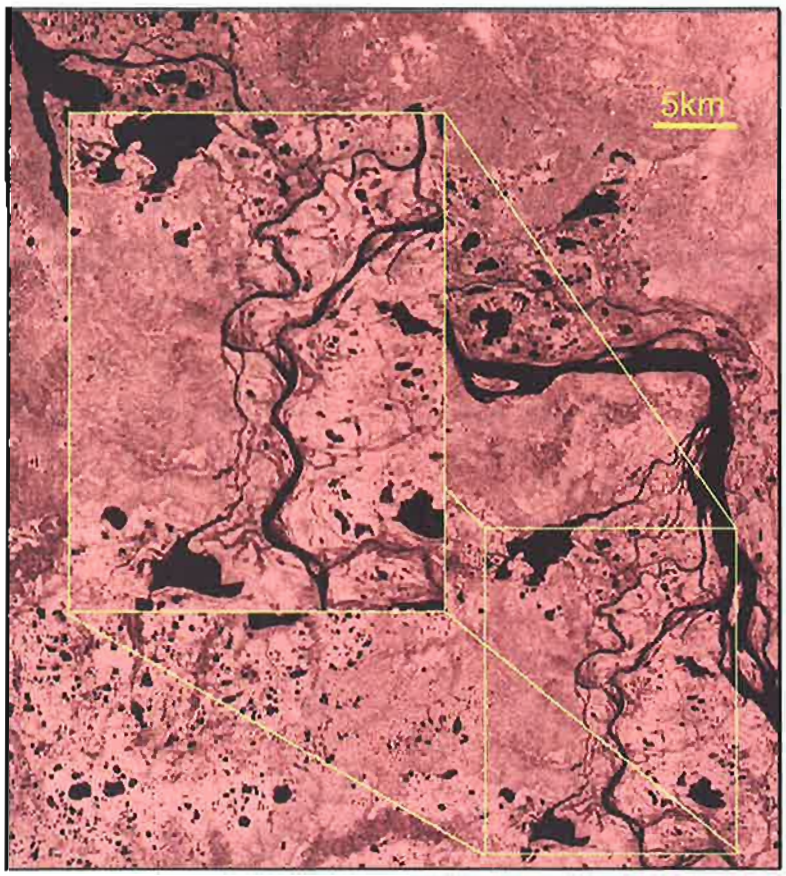

Figure 3.24: Satellite-borne SAR image of splay complexes adjacent to the Ob River. The top of water is indicated by black colors and the sediments are indicated by red colors, from Smith and Alsdorf (1998)

3.4 Palaeogeographic maps

Nine intervals were selected for facies mapping, either side of the reservoir intervals, and they include: VC00, VL05, VC10, VC15, VC20, VL22, VC25, VC30 and VC35. Facies distribution in these maps was guided by concepts from the literature (Avenell, 1998; Lang et al., 2000; Strong et al., 2002), including modern and ancient analogues of comparable fluvial systems (e.g. Ob River, Siberia). Also, the Figures 3.5 and 3.6 were used as a guide to help in the lateral interpolation between wells. These maps were compared to facies maps that were done by Strong et al. (2001) on the Moomba Area in the Patchawarra interval and they have a high genetic agreement level in facies distribution (Fig. 3.25). The facies maps are shown in Figures 3.26 – 3.34

There are several uncertainties associated with these facies maps. Although these maps indicate an active channel belt system through the mapped succession, it does not indicate that the channel is vertically continuous from reservoir interval top to bottom. These maps should be used as an indication for the existence of channels during the deposition of each systems tract or interval. Also, there are channels that exist but were not intersected by the existing wells, and hence further wells may show channels that have not been mapped and visa versa. Nevertheless, particular intervals are prone to more amalgamation of channels and therefore are more connected than other intervals (e.g. VC20-VL22 and VL22-VC25).

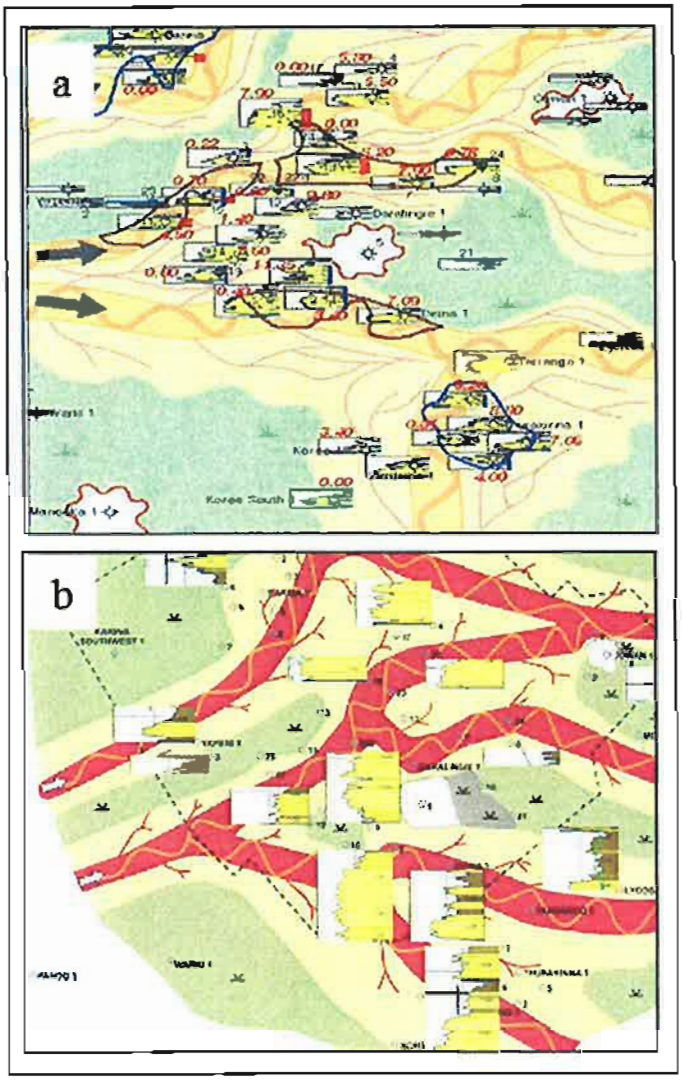

Figure 3.25: Comparison between VL22-VC25 interval facies map from Strong et al. (2001) (a) with VL22-VC25 interval facies map from this study (b) for the same study area. Note: the Strong et al. (2001) covers the Moomba area and this image is only a part of the original map.

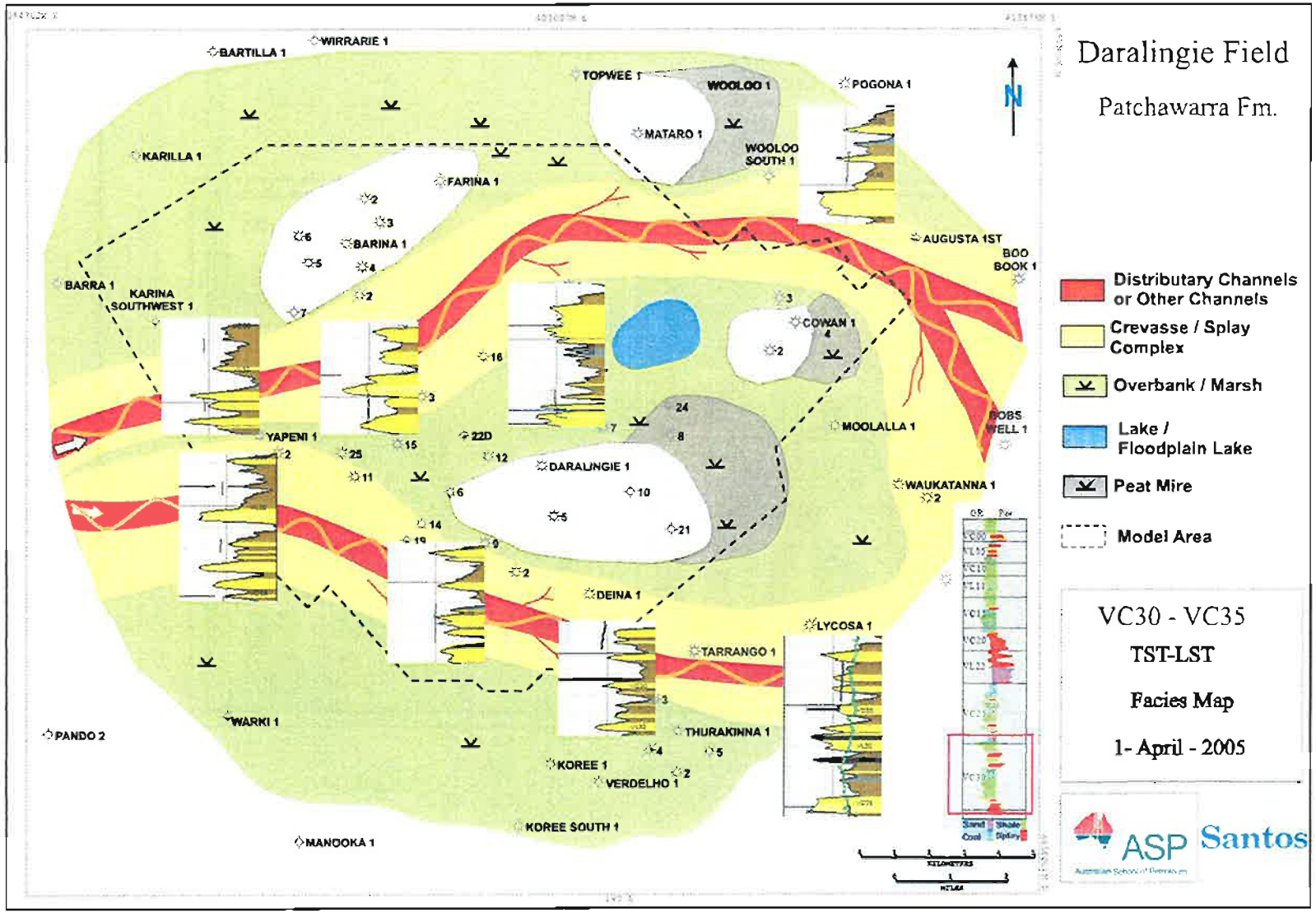

Figure 3.26: VC30-VC35 interval facies map showing a flooding surface (VC30). This interval represents several cycles that were grouped together, because they show very heterolithic characteristics with stacked channels and splays and floodplain shales. The interval thickness ranges from 6.5-24 m (21 to 78 feet) with an average of 17 m (55 feet). This interval has a very variable thickness due to the underlying unconformity. The sand percentage (net/gross) ranges from 0% to 17% with an average of 3%. There is very low sand deposition in this interval compared to the total interval thickness. As with VC25-VC30, the existence of channels is suggested by the existence of splays in some wells. Also, the channel belt width is assumed to be similar to the VL22-VC25 sequence. There is no evidence of hydrocarbons in this interval within the Daralingie Field.

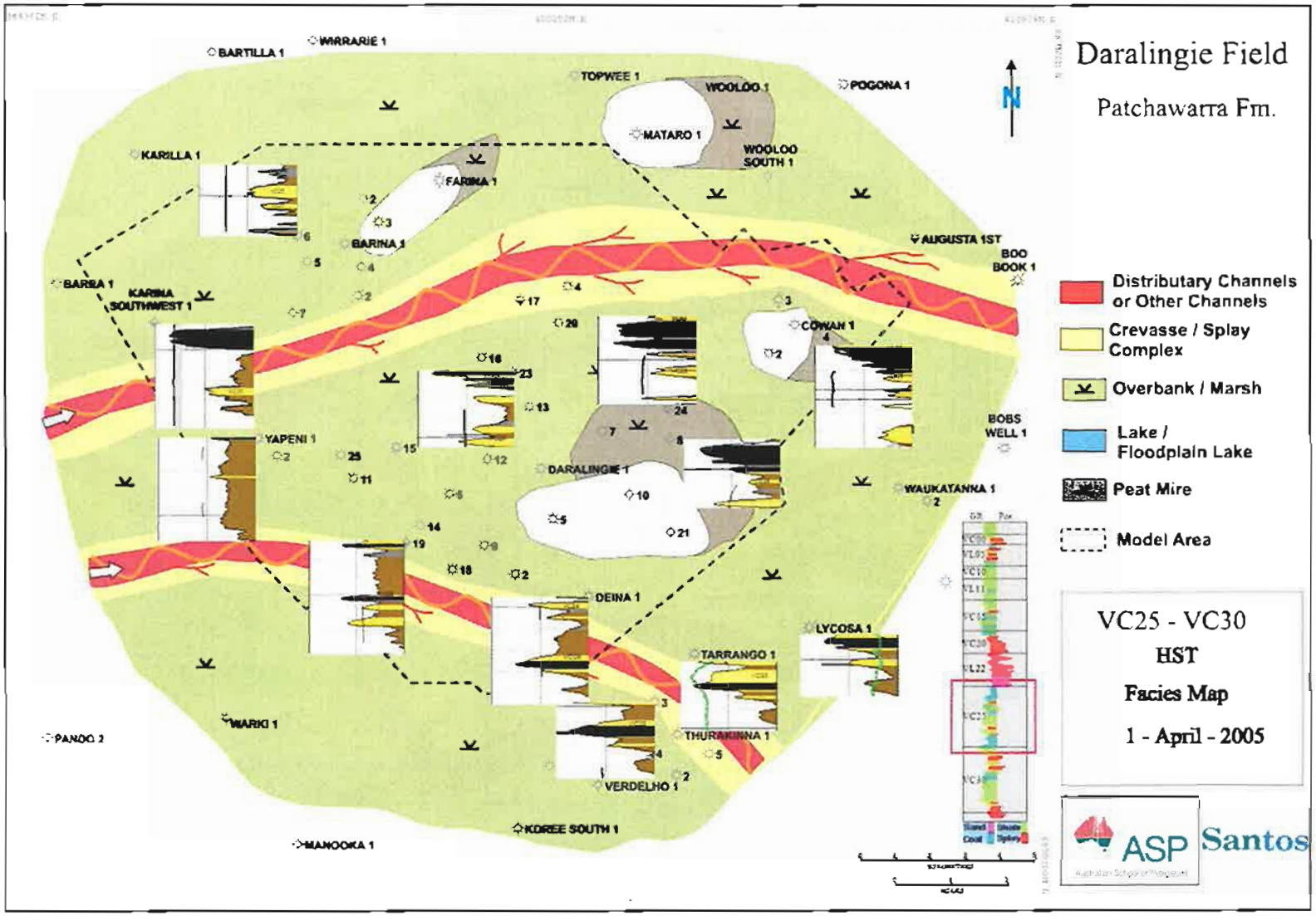

Figure 3.27: VC25-VC30 interval facies map showing a Transgressive Systems Tract/ Highstand Systems Tract (TST/HST). This interval is predominantly shale and coal prone. The last of the major Patchawarra coals exist in this interval with an average of 35% of the total facies. The interval thickness ranges from 5.3-20.5 m (17 to 67 feet) with an average of 13.5 m (43 feet.) The sand percentage (net/gross) ranges from 0% to 21% with an average of 3%. Wells in Daralingie Field have not intercepted channels in this interval, but the existence of channels is suggested by the existence of splays in some wells. The channel belt width is assumed to be similar to the VL22-VC25 sequence. Also, the channel locations are expected to be outside the structure closure because of the possibility of the existence accommodation space there. There is no evidence of hydrocarbons in this interval within the Daralingie Field.

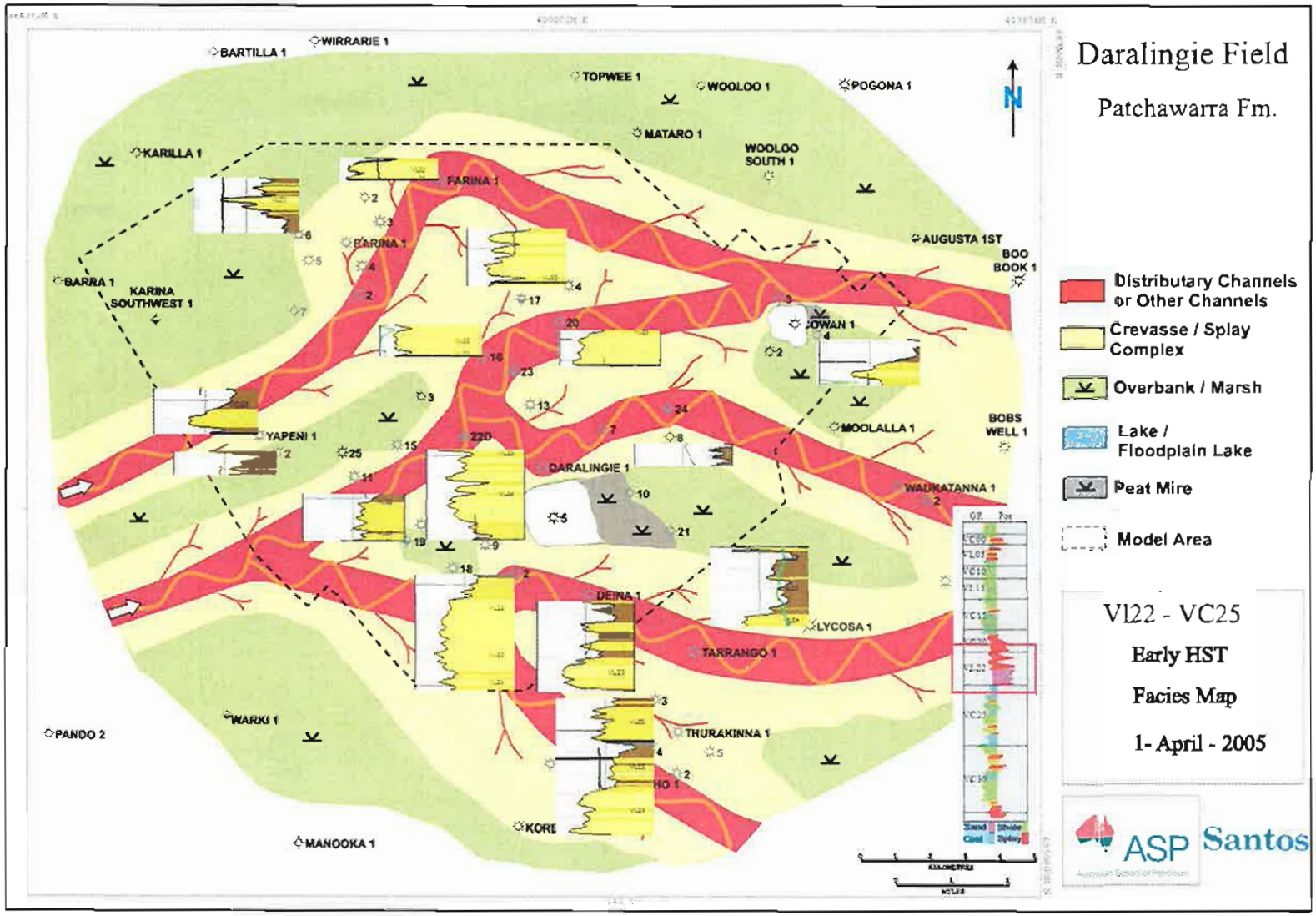

Figure 3.28: VL22-VC25 interval facies map. A Late Highstand Systems Tract/ early Lowstand Systems Tract (HST/LST), showing multilateral and multistorey-stacked fluvial channels. This is the lower unit in the reservoir interval. The interval thickness ranges from 1.5-17.5 m (5 to 57 feet) with an average of 8 m (26 feet). The sand percentage (net/gross) ranges from 0% to 100% with an average of 37%. The channel belt widths range from 100 - 950 m (330-3000 feet) to a midpoint of 500 m (1600 feet).

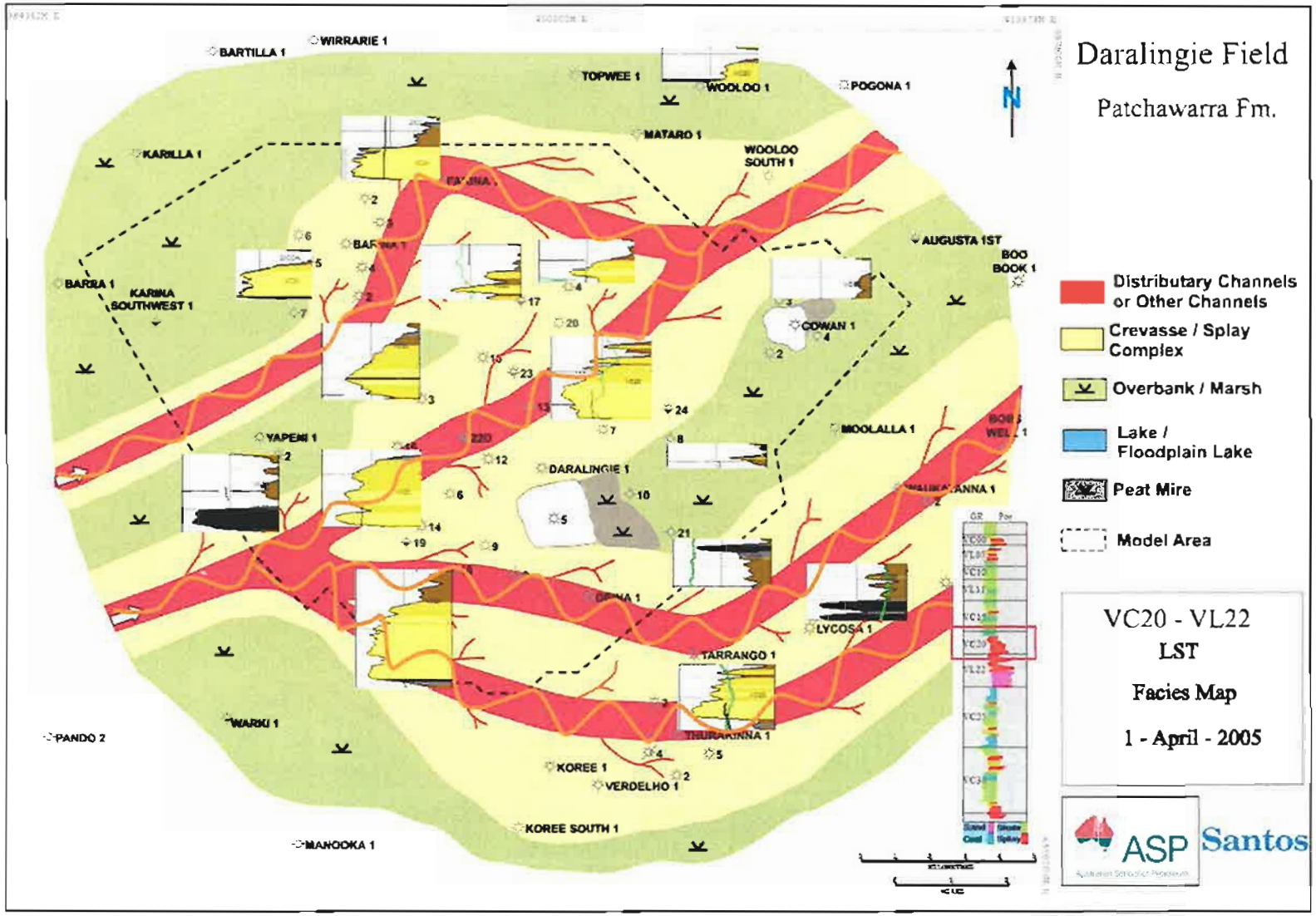

Figure 3.29: VC20-VL22 interval facies map. A Transgressive Systems Tract (TST), showing multilateral and multistorey-stacked fluvial channels. This interval and VL22-VC25 are the main reservoir intervals. The palaeohigh areas, such as around Daralinge-5, are eroded. The interval thickness ranges from 1.5-21.5 m (5-70 feet) with an average of 10.5 m (34 feet). The sand percentage (net/gross) ranges from 0% to 83% with an average of 33%. The channel belt widths ranges from 100 - 950 m (330-3000 feet) to a midpoint of 500 m (1600 feet). Some wells such as Daralinge-16 show VC20-VL22 channel sands on the top of VL22-VC25 channel sands with no shale break between. This might indicate possible incision of VC20-VL22 channels into VL22-VC25 channels.

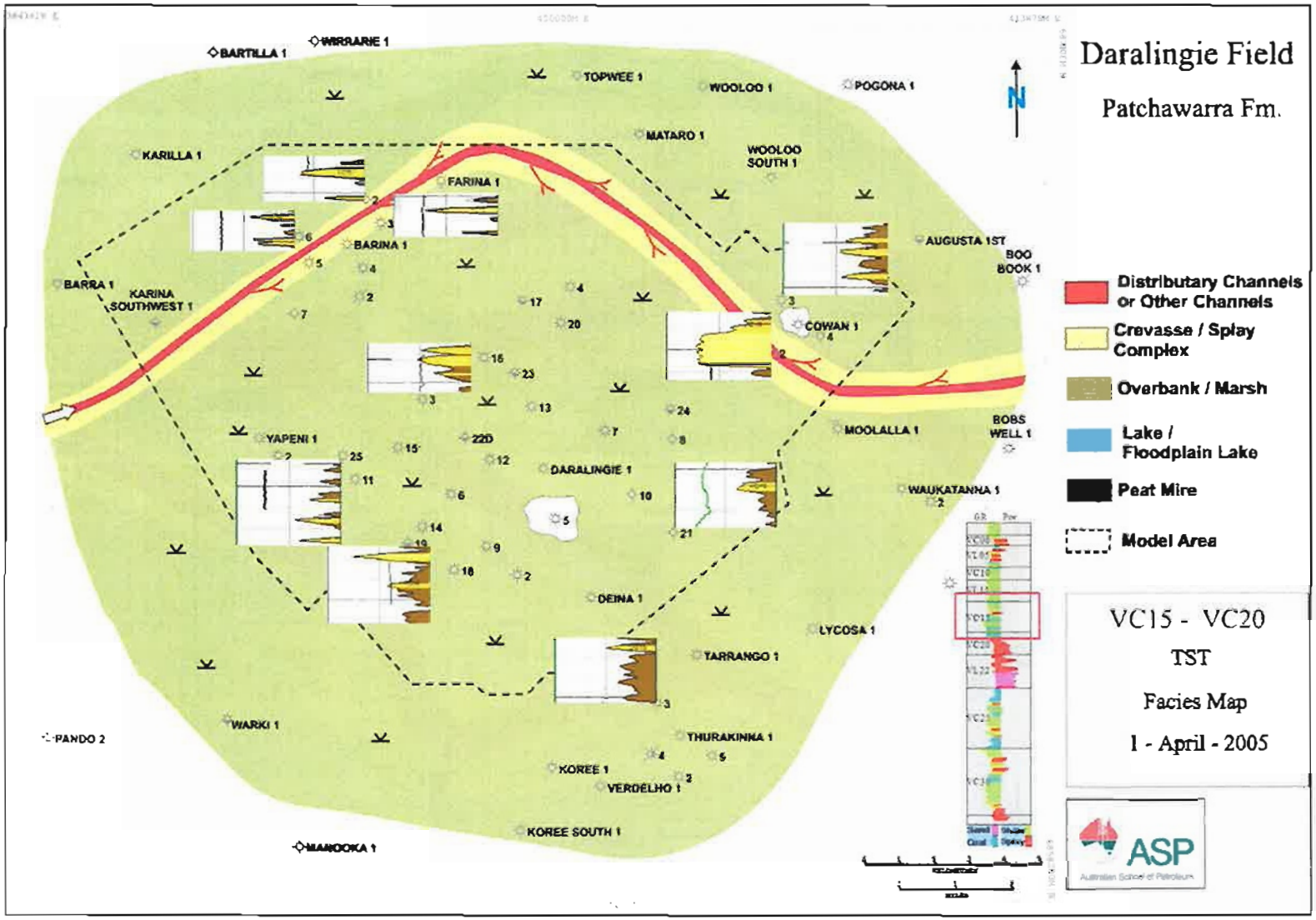

Figure 3.30: VC15-VC20 interval facies map showing a Highstand Systems Tract (HST). Palaeogeographic setting is similar to VL11-VL15. The interval thickness ranges from 4-13.5 m (13-44 feet) with an average of 9 m (30 feet.) The sand percentage (net/gross) ranges from 0% to 45% with an average of 5%. The channel belt widths range between 30-300 m (100-950 feet) with a midpoint of 200 m (650 feet). Only Cowan-2 in this interval intercepts a channel, so the location of the channel elsewhere on the field is speculative.

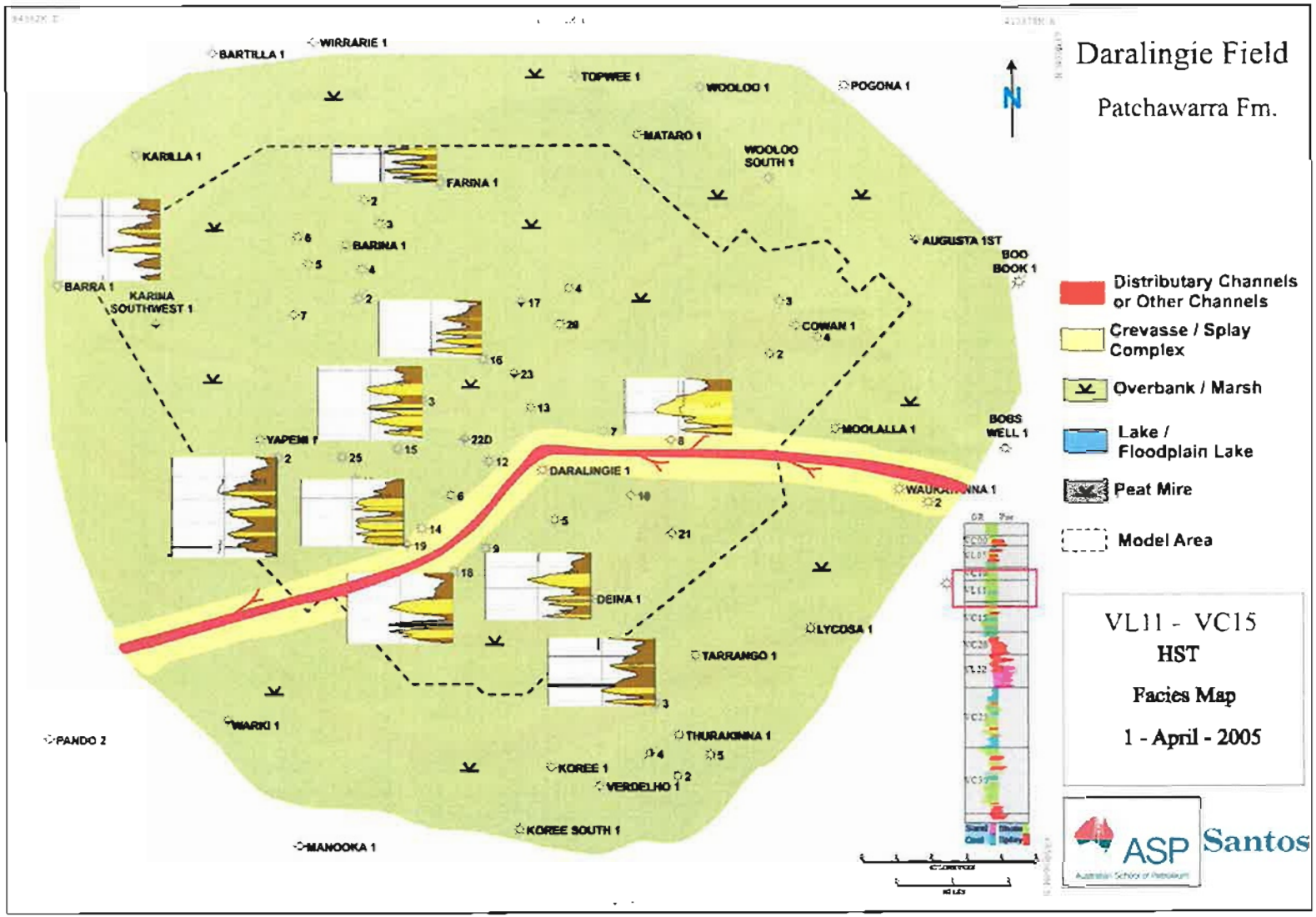

Figure 3.31: VL11-VC15 interval facies map. A Transgressive Systems Tract (TST), showing an isolated distributary channel belt. This with a predominantly shale prone interval. The interval thickness ranges from 5.5-13 m (18-42 feet) with an average of 9 m (29 feet.). The net gross sand percentage ranges from 0% to 50% with an average of 5%. Wells in Daralingie Field have not intercepted channels in this interval, but the existence of channels is suggested by the existence of splays in some wells. The channel belt width is assumed to be similar to the VC05-VC10 sequence.

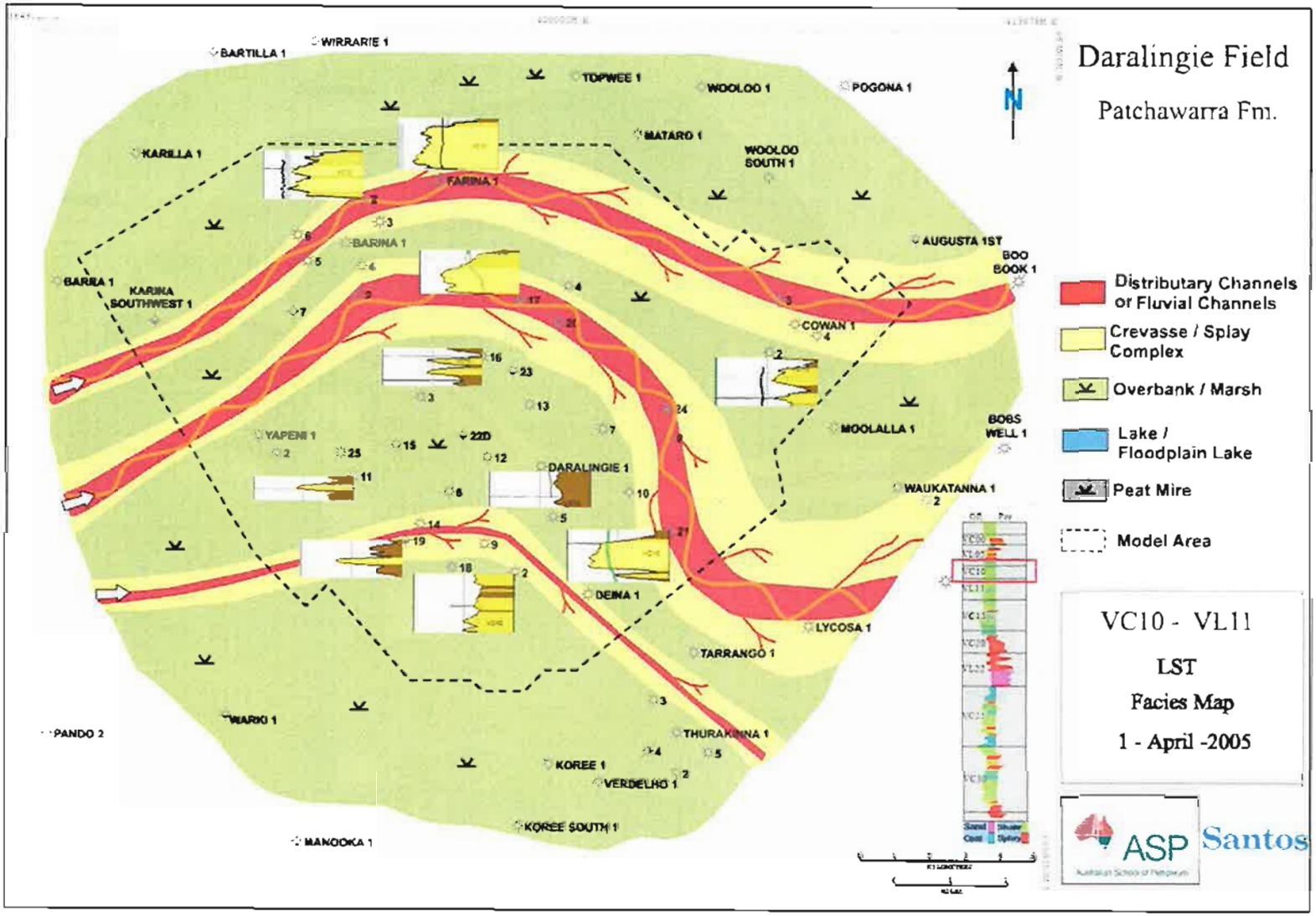

Figure 3.32: VC10-VL11 interval facies map showing a Lowstand Systems Tract (LST), with multilateral channel belts across of the field area. The main non-reservoir interval lies over the palaeohigh areas, possibly with mild uplift. The interval thickness ranges from 2.7-11 m (9-36 feet) with an average of 6 m (20 feet). The sand percentage (net/gross) ranges from 0% to 67% with an average of 11%. The channel belt widths range from 100 - 550 m (320-1770 feet) with a midpoint of 300 m (950 feet). The channel belts are wider than those estimated in VC00-VL05 and VL05-VC10 intervals.

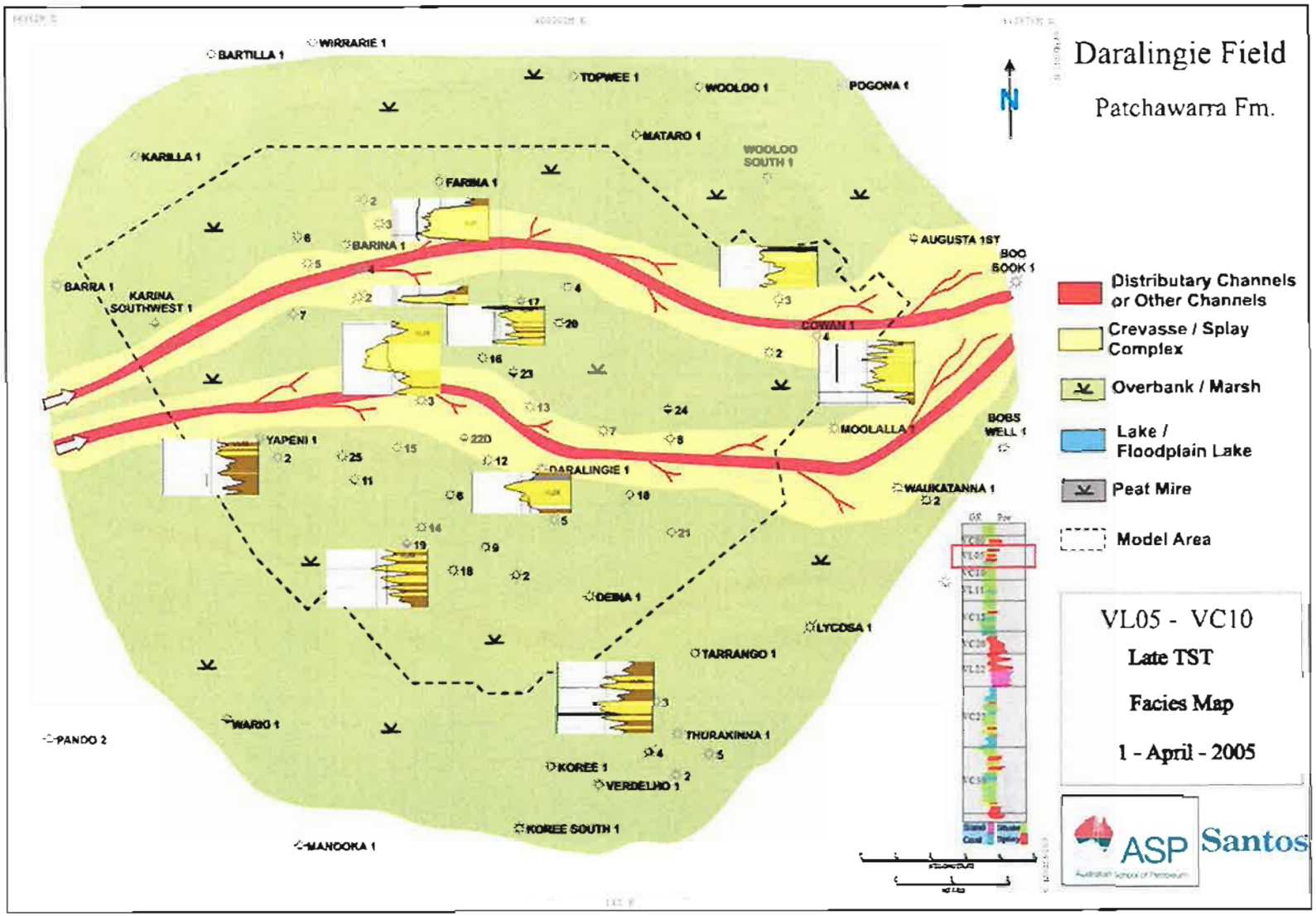

Figure 3.33: VL05-VL10 interval facies map showing Transgressive Systems Tract (TST). Its palaeogeographic setting is similar to VC00-VL05. The interval thickness ranges from 4.9-11.5 m (16-37 feet) with an average of 7.5 m (25 feet). The sand percentage (net/gross) ranges from 0% to 69% with an average of 11%. The channel belt widths range from 26-335 m (85-1080) with a midpoint of 200 m (650 feet). Daralingie-3 produces gas from this interval along with VC00-VL05.

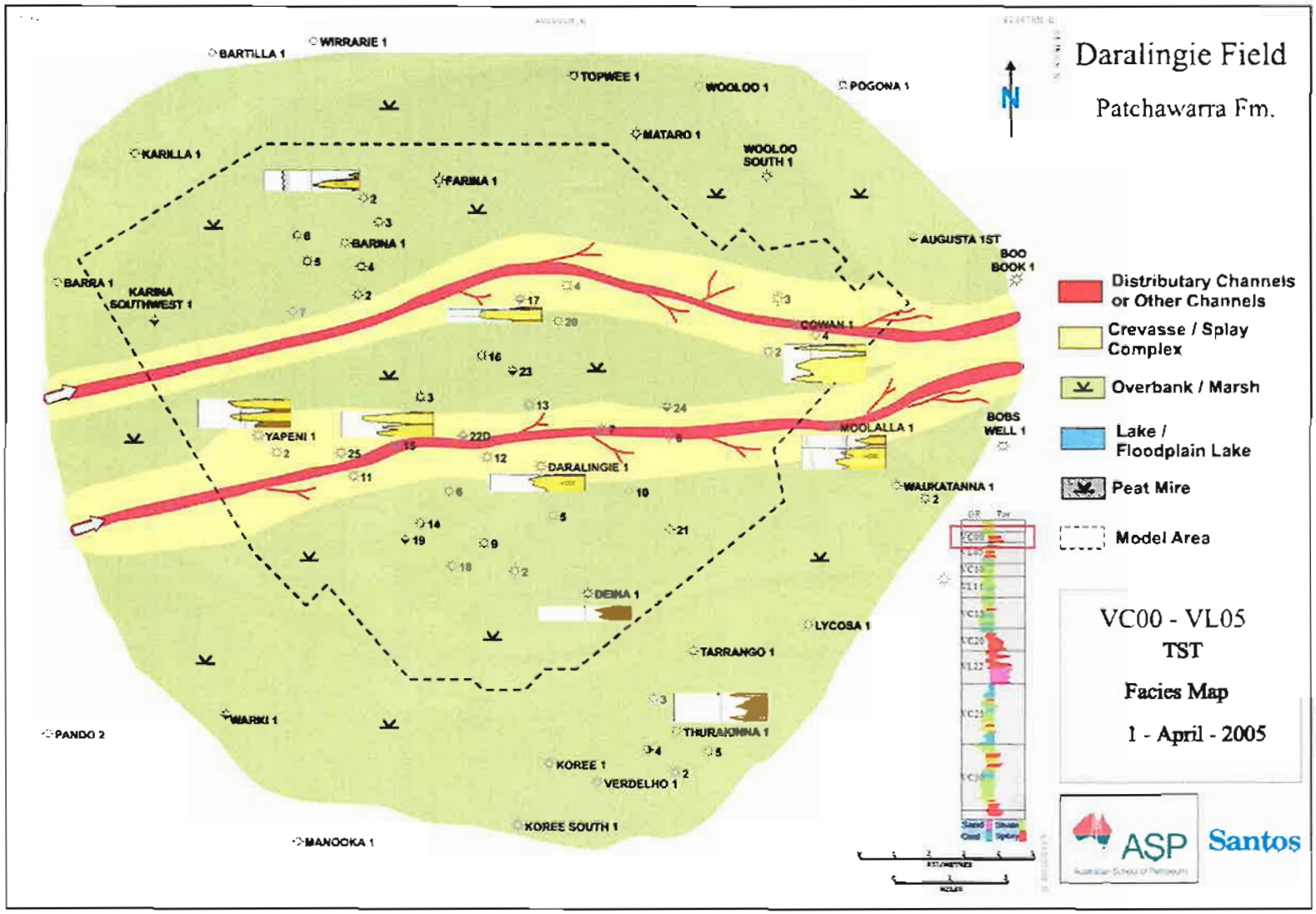

Figure 3.34: VC00-VL05 interval facies map showing a Transgressive Systems Tract (TST), with isolated distributary channels immediately under the transgressive lacustrine shale of Murteree Shale (VC00). The interval thickness ranges from 1.5 - 5.9 m (5 - 19 feet) with an average of 3.5 m (11 feet). The sand percentage (net/gross) ranges from 0% to 62% with an average of 25%. The channel belt widths range from 26 - 335 m (80 – 1000 feet) with a midpoint of 200 m (650 feet).

3.5 Uncertainty in the Depositional Facies Model

Each study has a component of risk and uncertainty in it. Risk and uncertainty in reservoir characterisation cannot be eliminated, but they can be reduced. They cannot be eliminated because the exact description of the reservoir will not be known, but using available data will help in narrowing down the possible choices. The geologist must make the best educated guess based on the currently available data.

In this study, the risk is represented by the following questions:

- What if this model is totally wrong?
- What is needed to reduce the risk of getting the wrong depositional model?

The uncertainty is represented by the following questions:

- The model is correct but what are the possible ranges of the geological objects defined in this study?
- What is the possible channel belt width range, direction and vertical thickness?

Before answering these questions, a closer look into the uncertainty of the data used to generate this model is needed (i.e. core, logs and analogues.) If one of the inputs has a high risk and a high uncertainty, this would lead to high risk and high uncertainty in the depositional model.

The first inputs into this study are the cores. Cores are the best available representation for the reservoir rocks. The risk in defining wrong rock type in the core is very low. However, the risk in defining the wrong depositional environment based on one core sample is very high. As more core data becomes available, the risk reduces. The risk here is not in the core data itself but in the interpretation. The geologist's interpretations are highly subjective because they are dependent on knowledge and experience. In this study, there was good core coverage of the reservoir and these cores were examined by a multiple geologists, a factor that reduced the risk of getting the wrong depositional

model. However, at this stage uncertainty remains high about the geometry of the geological objects (i.e. channel direction and orientation.) More samples are needed to further reduce the uncertainty about the geological objects geometry.

Well logs can provide more samples to facilitate a better understanding of the reservoir, but they are an indirect measure of the reservoir properties. For example, they cannot show if the reservoir is fluvial or deltaic system. However, they give measurements that can be correlated to some known reservoir properties. For example, gamma-ray logs in sandstone can be an indicative of grain size, high gamma-ray may mean low grain size and lower gamma-ray may mean bigger grains sizes. Hence a vertical grain profile may be constructed. This has to be confirmed with core data, because core data are the only available direct measure of the reservoir data.

In this study, the correlation between core and log signature has been established with high confidence as shown in Figures 3.1 and 3.2. The risk associated with using logs as an indicator of channels and splay is low once a fluvial depositional system is established. After examining the logs, a list of possible geological object properties such as channel thickness was generated. By using these properties and the plots that were derived from a compilation of published data (Figs. 3.7 to 3.13), possible width ranges can be estimated. These ranges help in quantifying the uncertainty of geological objects.

The third input is analogue data. The analogues can be classified as modern or ancient analogues and each has their own advantages and disadvantages. The modern analogues (also called modern depositional systems) provide excellent opportunities to study the possible aerial dimensions of the reservoir. A very low risk and very low uncertainty can be assigned to defining the geological objects in two dimensions. The only possible source of problems is human error, because all geological features can be measured directly. However, modern analogues may be in a different climate or tectonic regime than the reservoir under study. Also, they do not give a vertical exposure, although this could be solved by digging trenches or cutting cores to obtain the third dimension.

Ancient analogues (outcrops) represent excellent opportunities to study a reservoir's possible vertical heterogeneities. They are good for studying vertical grain profile and possible vertical permeability barriers. Unfortunately, they are limited to the exposure and they often do not provide an areal coverage unless associated with large open cut mines. Uncertainty in ancient analogues is dependent on the geologist's interpretations. Merging of modern and ancient analogues may significantly reduce the risk and the uncertainty of any geological study.

In this study all steps were taken to ensure the reduction of associated risk and uncertainty. Based on the currently available data at the time of this study, the defined depositional model is the best representation for the VC00-VC35 reservoir intervals of the Patchawarra in Daralingie Field.

Chapter 4

Daralingie Field Stochastic Modeling

4.1 Overview

To ensure high geological reliability of the final stochastic geological model, a modeling workflow (Fig. 4.1) was developed to check the quality of each completed modeling step.

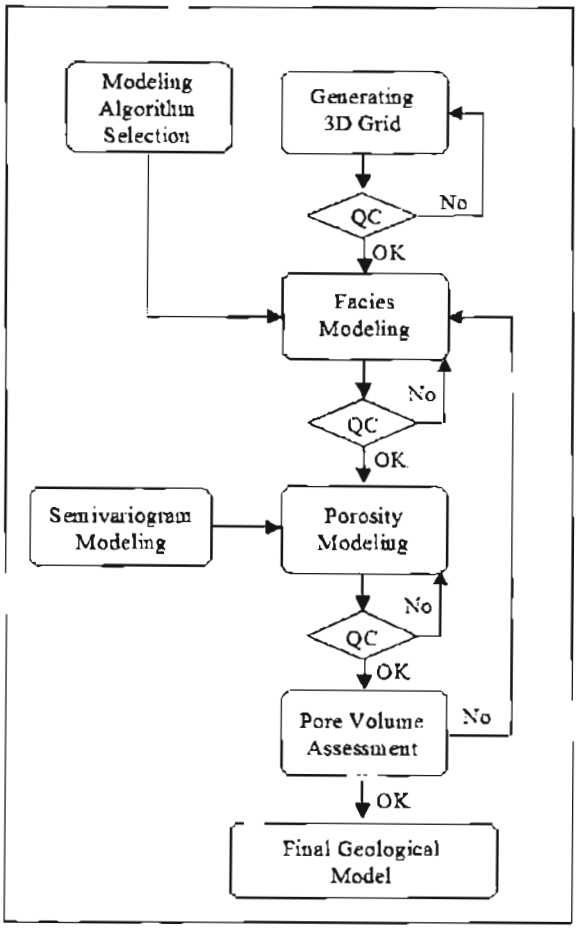

Figure 4.1: An illustration for the major steps in the stochastic modeling phase of the Daralingie Field Study.

4.2 Modeling algorithms

Geological and porosity modeling in this study were done using Roxar RMS version 7.2. The following is a brief description for each algorithm used in this study. For more information, refer to the RMS user guide.

4.2.1 Facies modeling algorithms

Two object-based modeling algorithms were selected: 'channels' and 'composite'. The channel-modeling algorithm is used for modeling a variety of channel depositional settings. This channel-modeling algorithm is designed to model straight to moderate sinuosity channels, and divides the reservoir facies into two groups:

- Channels and related facies: these include channels belts and crevasse splay facies. While modeling these facies a spatial relation is kept between them.
- Background facies: the remaining facies are grouped in this facies and modelled as one facies.

The channels and related facies are modelled based on facies logs and channel geometry, such as channel width, direction and sinuosity. After modeling is completed, the remaining model volume is filled with background facies. The channel algorithm does not model coal, therefore coal was modeled separately and merged with the channel model.

The 'composite' algorithm can be used for a wide range of depositional settings. Each facies is modeled as a geometrical object with a defined shape. As with the channel algorithm, the composite method uses facies well logs and facies geometries. The composite algorithm does not guarantee that the facies will have a spatial relationship with each other, unlike the channel-modeling algorithm. In this study, the composite algorithm was used to model coal to later merge with the channel model.

4.2.2 Semi-variogram Modeling

An important input into stochastic modeling is the semi-variogram, which is a mathematical tool that quantifies spatial correlation and continuity of a variable. It is a plot of the average squared difference in value between data points against their separation distance. It is computed as half the average squared difference between the components of every data pair:

$$\gamma(h) = \frac{1}{2N(h)} \sum_{i=1}^{N(h)} \left[z(x) - z(x+h) \right]^2$$

where $N(h)$ is the number of pairs of data locations a vector h (lag distance) apart and z is the measurement at locations x and $x+h$. The output is represented by an experimental semi-variogram.

The lag spacing defines the incremental distance at which the semi-variogram is calculated. Usually the first lag distance is at least equal to the minimum well spacing. The number of lags used usually varies from 10 to 15 and it should be restricted to the dimensions of the data coverage. On average the maximum lag distance is about half the diagonal of the data extent (Coombes, 1997).

The experimental semi-variogram must be fitted with an appropriate model semi-variogram. Several mathematical models are available that can be used for fitting purposes and are well described in the literature. Examples of such models are: spherical, exponential, gaussian, power and periodic. The rule when selecting a model is that it should fit most points near the origin. In addition, the same model should be used when calculating directional semi-variograms (Isaaks and Srivastava, 1989; Journel and Huijbregts, 1978).

4.2.3 Porosity modeling algorithm

Stochastic simulation is the process of building alternative, equiprobable, high-resolution models. Each of these models is called a realisation. Simulation is conditional if the resulting realisations use the hard data values at their locations. Either categorical or continuous variables may be conditionally simulated.

The sequential simulation procedure in determining data points is as follows: it first assigns data values to the closest grid node. After that it establishes a random path through all of the grid nodes. Then it visits each grid node in the model and finds nearby data and previously simulated grid nodes to krige a value from all available data. This value will be used to construct a conditional distribution function *(cdf)*. Then, a simulated value will be drawn randomly from the *cdf* and assigned to the grid node. This process will be repeated until all grid nodes have been simulated. All the simulated values should honor the data derived from semi-variograms and histograms (Isaaks and Srivastava, 1989)

There are two major stochastic simulation algorithms; Gaussian and indicator simulation. Gaussian simulation is used to simulate continuous values such as porosity, while indicator simulation is used mainly for categorical data such as facies. All sequential simulation algorithms honor the data points at their locations (Chambers et al., 1994).

In this study, a facies-based Gaussian simulation algorithm was used to generate the porosity models. This algorithm generates a stochastic porosity model, based on porosity logs, semi-variograms and the facies model. It simulates porosity values by utilising porosity distribution in each facies separately (Fig. 4.2). This is important because facies heterogeneity is the main control on spatial and vertical distribution of porosity in this reservoir. Therefore, a realistic level of heterogeneity in porosity is needed to reflect the large-scale facies heterogeneity observed in the facies model.

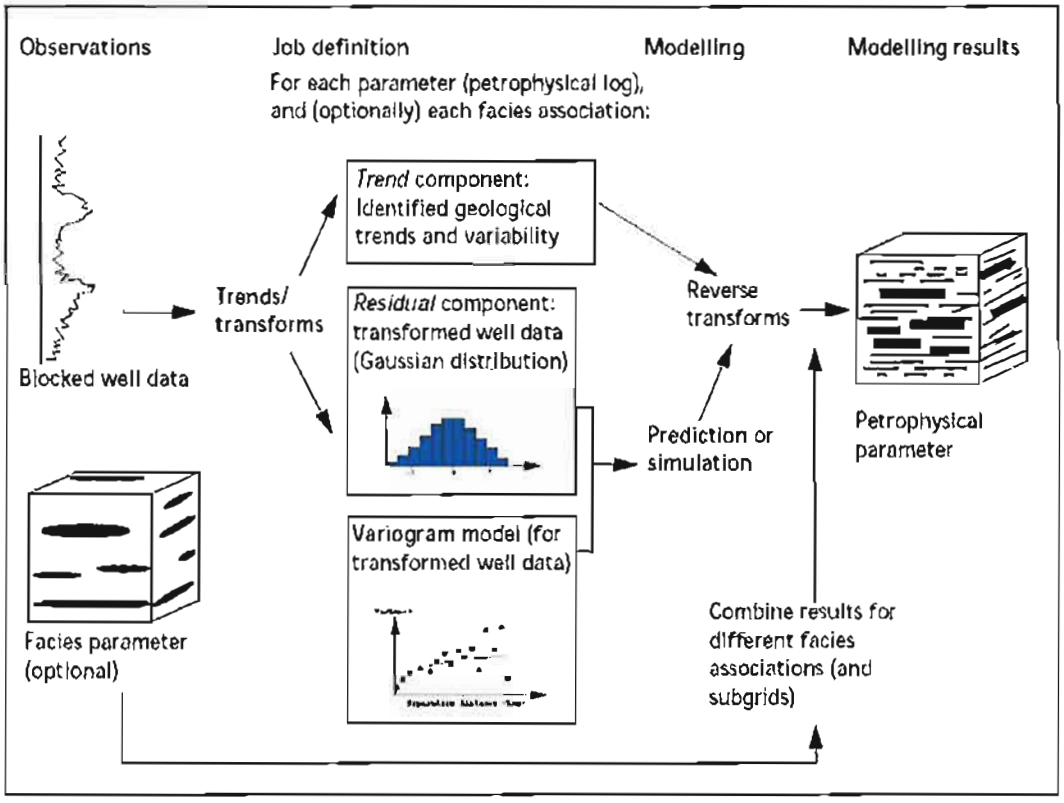

Figure 4.2: Porosity modeling methodology used in this study (from Roxar RMS 7.2 user manual).

4.3 3-D Grid Generation

After quality control of the Daralingie Field data, they were loaded into RMS. Well logs, sequence tops, fault polygons and the interpreted tops were sequentially loaded. That was followed by the creation of key surfaces for the nine reservoir intervals to be modeled in the reservoir.

In accordance with the industry practice in the Cooper Basin, the depth of the well logs and surfaces provided were in feet, while the well location and areal dimensions of the surfaces are in metres. Therefore, the modeling units will be metres for areal and feet in depth. Having set these parameters, the next step is to select optimum modeling vertical and areal limits that were sufficient to capture the reservoir intervals in Daralingie Field and surrounding fields. The top of the model is VC00 and its base is VC30. The model areal coverage is 21,900 x 17,600 metres and its dimensions in UTM coordinates system were as follows:

X min: 385,700	X max: 407,600
Y min: 6,856,700	Y max: 6,874,300

An isopach map was created for each reservoir interval. These isopach maps along with the VC25 surface were used to generate structure surfaces for VC00, VL05, VC10, VL11, VL15, VC20, VL22 and VC30. All of these surfaces were adjusted to match well tops at well locations. Furthermore, the surfaces were re-gridded to 100 x 100 metres to increase their spatial resolution.

More than 350 fault polygons were provided by Santos for the top of VC25. Since the surface grid used was 100 x 100 metres, faults of 200 metres in length or less have no impact on the 3-D grid model. Therefore a filter was applied to eliminate faults that are smaller than 200 metres. Also, faults that have a separation distance of less than 200 metres between lateral end points were connected with each other. The final number of faults used in the model was 280.

Before the start of the modeling work and the upscaling of log data for subsequent steps, it is important to review the statistical distribution of input facies data. This provides a valuable guide to quality control (QC) the upscaled facies data. Table 4.1 summarises the facies percentages in each zone. These facies were derived from the interpretation of wireline logs to a resolution of 0.5 ft.

Table 4.1: Facies statistics from logs for each modeled interval based on raw data.

Reservoir Interval	Channels %	Splay %	Coal %	Shale %
VC00-VL05	6	35	5	54
VL05-VC10	7	20	20	53
VC10-VL11	15	12	4	69
VL11-VC15	2	12	8	78
VC15-VC20	1	6	14	79
VC20-VL22	18	30	17	35
VL22-VC25	27	26	4	42
VC25-VC30	2	7	35	56

Due to the size limitation and CPU time, the raw data was upscaled before the start of stochastic modeling. The upscaling process involves the averaging of raw data that have 0.5 foot resolution into cells with coarser thickness. It is very important that the upscaling scheme keeps the facies proportions as close as possible to the raw data, and that it does not change the facies propositions, which may lead to unrealistic facies proportions in the stochastic model. The general rule followed was that the number of upscaled cells (model layers) in each of the modeled interval zones was dependent on the modeled interval thickness and reservoir quality. After trying several schemes with a different number of vertical cells, the scheme outlined in Table 4.2 was selected.

Table 4.2: Vertical layering scheme used in generating Daralingie model 3D grid.

Reservoir Interval	Number of vertical Cells
VC00-VL05	5
VL05-VC10	10
VC10-VL11	10
VL11-VC15	20
VC15-VC20	10
VC20-VL22	30
VL22-VC25	30
VC25-VC30	10

This scheme gives an almost a perfect match in facies percentages, as shown in Table 5, compared to the raw data in Table 4.3 for the original log data:

Table 4.3: Upscaled facies percentages in each reservoir interval in the Daralingie model 3D grid.

Reservoir Interval	Channels %	Splay %	Coal %	Shale %
VC00-VL05	6	37	2	55
VL05-VC10	7	19	21	53
VC10-VL11	14	12	4	70
VL11-VC15	2	11	8	79
VC15-VC20	1	4	14	81
VC20-VL22	17	30	17	36
VL22-VC25	26	26	3	45
VC25-VC30	3	7	35	55

After checking the upscaling impact on all wells, further investigation was done on a well-by-well basis. The facies upscaling impact on Daralingie-18 is illustrated in Figure 4.3. In reservoir intervals with coarse cells, such as VC25, thinly layered facies will disappear. Where the reservoir intervals have fine cells, such as VC20, thinly layered facies will be preserved. This helps in capturing the reservoir heterogeneity in the important reservoir layers.

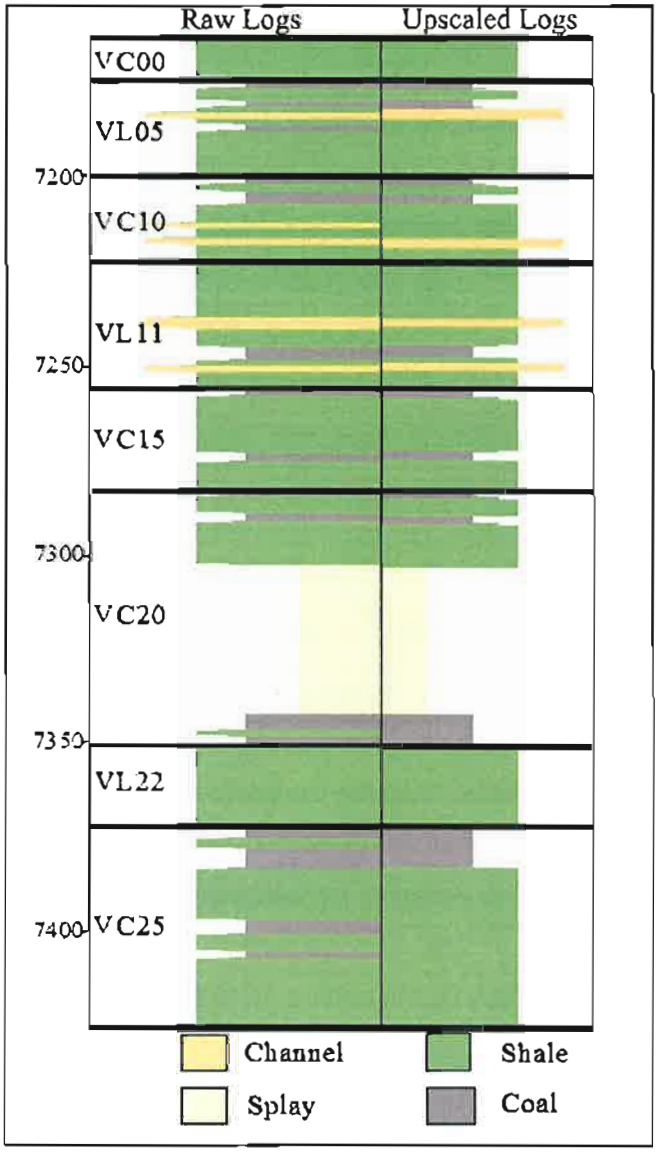

Figure 4.3: An illustration of vertical upscaling impact of the facies in Daralingie-18. Depth is in feet and sub-sea.

The next step was to add the unconformity to the 3-D grid. This was done using the top of the Permian-unconformity surface to cut the 3-D grid. All cells that fall below the unconformity were set to undefined cells. This resulted in a total number of cells of 4,818,000 with 3,121,494 defined cells and 1,696,506 undefined cells. The defined cells have facies and porosity values. The total number of columns is 219; the total number of rows is 176 with 125 layers.

4.4 Facies Modelling

As mentioned previously, two facies modeling algorithms were used in this study. The first facies model was built utilising a composite-modeling algorithm. Facies percentages used were the same as the well data with added uncertainty as shown in Table 4.4. All facies are associated with uncertainty, except shale, because it is the background facies.

Table 4.4: Facies percentages used in building the composite model.

Reservoir Interval	Channels %	Splay %	Coal %	Shale %
VC00-VL05	6 (+/-2)	36 (+/- 5)	4 (+/- 1)	54
VL05-VC10	7 (+/- 2)	20 (+/- 4)	20 (+/- 4)	54
VC10-VL11	14 (+/- 2)	12 (+/- 2)	4 (+/- 1)	70
VL11-VC15	2 (+/- 1)	10 (+/- 2)	7 (+/- 2)	81
VC15-VC20	2 (+/- 1)	5 (+/- 1)	13 (+/- 2)	80
VC20-VL22	17 (+/- 3)	30 (+/- 5)	17 (+/- 3)	36
VL22-VC25	25 (+/- 5)	26 (+/- 5)	4 (+/- 1)	45
VC25-VC30	3 (+/- 1)	7 (+/- 2)	34 (+/- 5)	56

The facies geometries used in building the composite facies model and the subsequent channel model were derived from the geological study. Tables 4.5 to 4.7 show the geometries used for each facies, excluding the background facies.

Table 4.5: Channel body geometry used in building the composite model.

Reservoir Interval	Shape	Length (metres)	Width (metres)	Vertical Thickness (ft)	Azimuth
VC00-VL05	Rectangular	7000 (+/-500)	500 (+/-100)	8 (+/-4)	90 (+/-10)
VL05-VC10	Rectangular	7000 (+/-500)	500 (+/-100)	8 (+/-4)	90 (+/-10)
VC10-VL11	Rectangular	7000 (+/-500)	500 (+/-100)	8 (+/-4)	90 (+/-10)
VL11-VC15	Rectangular	7000 (+/-500)	500 (+/-100)	8 (+/-4)	90 (+/-10)
VC15-VC20	Rectangular	7000 (+/-500)	500 (+/-100)	8 (+/-4)	90 (+/-10)
VC20-VL22	Rectangular	7000 (+/-500)	1000 (+/-200)	8 (+/-4)	90 (+/-10)
VL22-VC25	Rectangular	7000 (+/-500)	1000 (+/-200)	8 (+/-4)	90 (+/-10)
VC25-VC30	Rectangular	7000 (+/-500)	500 (+/-100)	8 (+/-4)	90 (+/-10)

Table 4.6: Splay body geometry used in building the composite model.

Reservoir Interval	Shape	Length (m)	Width (m)	Vertical Thickness (ft)	Azimuth
VC00-VL05	Rectangular	7000 (+/-500)	1000 (+/-100)	8 (+/- 4)	90 (+/- 10)
VL05-VC10	Rectangular	7000 (+/-500)	1000 (+/-100)	8 (+/- 4)	90 (+/- 10)
VC10-VL11	Rectangular	7000 (+/-500)	1000 (+/-100)	8 (+/- 4)	90 (+/- 10)
VL11-VC15	Rectangular	7000 (+/-500)	1000 (+/-100)	8 (+/- 4)	90 (+/- 10)
VC15-VC20	Rectangular	7000 (+/-500)	1000 (+/- 100)	8 (+/- 4)	90 (+/- 10)
VC20-VL22	Rectangular	7000 (+/-500)	2000 (+/- 200)	8 (+/- 4)	90 (+/- 10)
VL22-VC25	Rectangular	7000 (+/-500)	2000 (+/- 200)	8 (+/- 4)	90 (+/- 10)
VC25-VC30	Rectangular	7000 (+/-500)	1000 (+/- 100)	8 (+/- 4)	90 (+/- 10)

Table 4.7: Coal body geometry used in building the composite model

Reservoir Interval	Shape	Length (m)	Width (m)	Vertical Thickness (ft)
VC00-VC30	Circular	4000 (+/-400)	4000 (+/- 400)	8 (+/- 4)

In the first model runs, few channels were generated in areas where no channels were interpreted. Pseudo-wells (Dummy_1-_12) were added to the model to prevent the generation of these channels. The addition of pseudo-wells improved the model; however it was not geologically appealing (Fig. 4.4). It did not give a realistic channel like appearance.

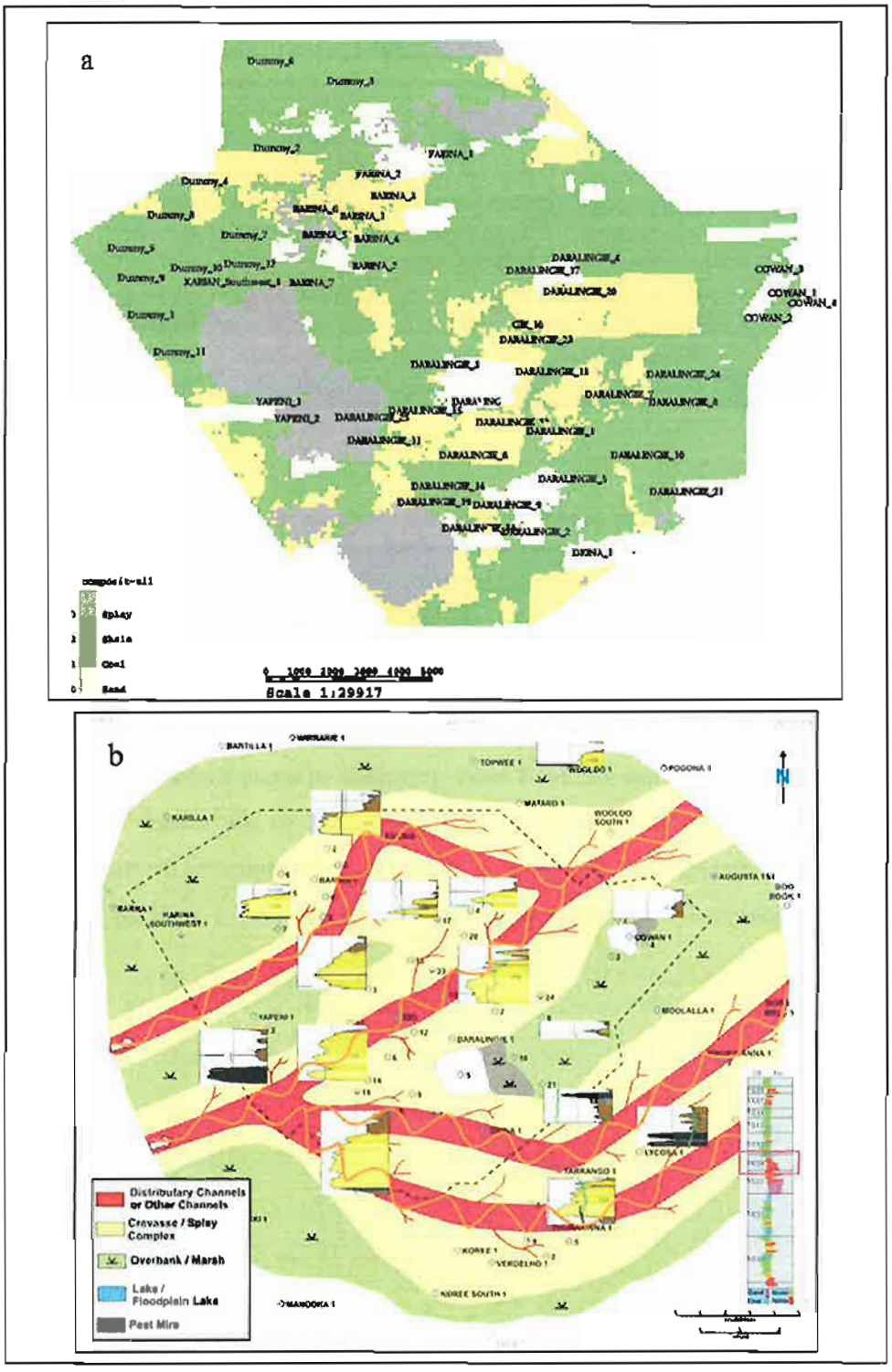

Figure 4.4: A slice in the stochastic facies composite model (a) in the VC20-VL22 reservoir interval honouring facies proportions, but showing a poor reflection of the geology compared to the depositional facies maps of the same interval (b).

The second facies model was built using the channel-modeling algorithm. The same geometrical parameters used in the composite model were used with the addition of the geometrical parameters for the channels. The geometrical parameters used are shown in Table 4.8.

Table 4.8: Modeling parameters for fluvial channels for each interval.

Reservoir Interval	Channels System %	Width (m)	Thickness (ft)	Amplitude (m)	Sinuosity	Azimuth
VC00-VL05	25 (+/-4)	500 (+/- 100)	8 (+/- 4)	2000 (+/- 200)	1.1	90° (+/- 10°)
VL05-VC10	25 (+/-4)	500 (+/- 100)	8 (+/- 4)	2000 (+/- 200)	1.1	90° (+/- 10°)
VC10-VL11	25 (+/-4)	500 (+/- 100)	8 (+/- 4)	2000 (+/- 200)	1.1	90° (+/- 10°)
VL11-VC15	10 (+/-2)	500 (+/- 100)	8 (+/- 4)	2000 (+/- 200)	1.1	90° (+/- 10°)
VC15-VC20	5 (+/-2)	500 (+/- 100)	8 (+/- 4)	2000 (+/- 200)	1.1	90° (+/- 10°)
VC20-VL22	45 (+/-4)	1000 (+/- 200)	8 (+/- 4)	2000 (+/- 200)	1.1	90° (+/- 10°)
VL22-VC25	50 (+/-4)	1000 (+/- 200)	8 (+/- 4)	2000 (+/- 200)	1.1	90° (+/- 10°)
VC25-VC30	10 (+/-2)	500 (+/- 200)	12 (+/- 4)	2000 (+/- 200)	1.1	90° (+/- 10°)

Three issues were faced in this modeling step. Firstly the channels generated in the VC20-VL22 and VL22-VC25 intervals did not appear geologically correct (Fig. 4.5.) These intervals should have more channels and splays (see Figs. 3.30 and 3.31). Secondly, modeling the channels and splays together took a very long time. Some model runs took more than 20 hrs. Thirdly, this algorithm did not model coal.

A solution for these issues was to use two different modeling algorithms and build the geological model in three modeling steps. The first was to build a channel belt model with a shale background. The second step involved building a composite model with splays and coal facies only. The final step merged the two models, letting the channels cut all other facies (Fig. 4.6). The results were very good in that they showed geologically sensible channels as shown in Figure 4.7.

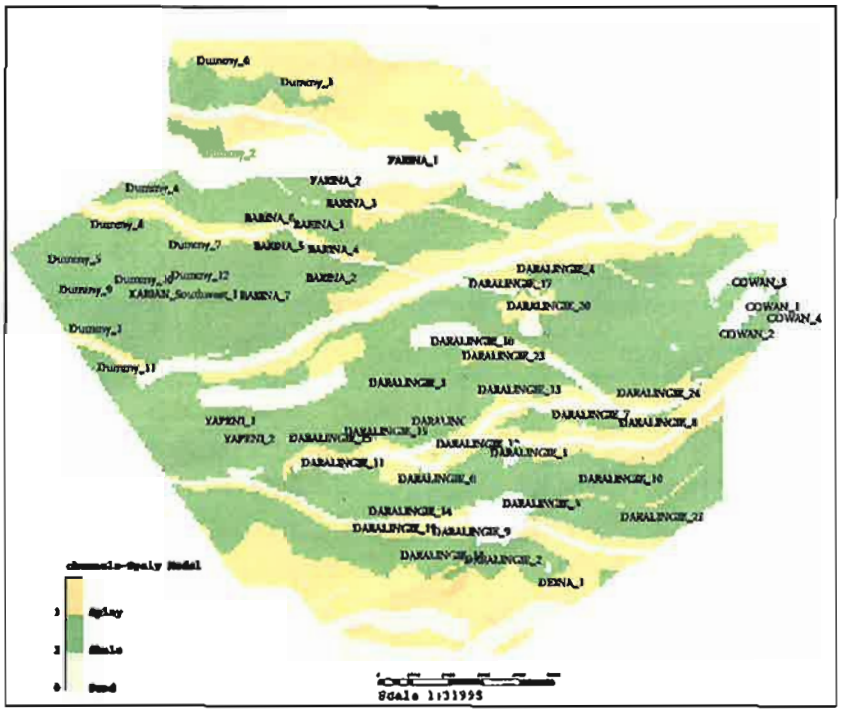

Figure 4.5: A slice in the channel system model in the VL22-VC25 reservoir interval using the channel modeling algorithm. Note the absence of coal in this slice, because this algorithm models channel and splays with a background facies only. This is the major drawback to this algorithm.

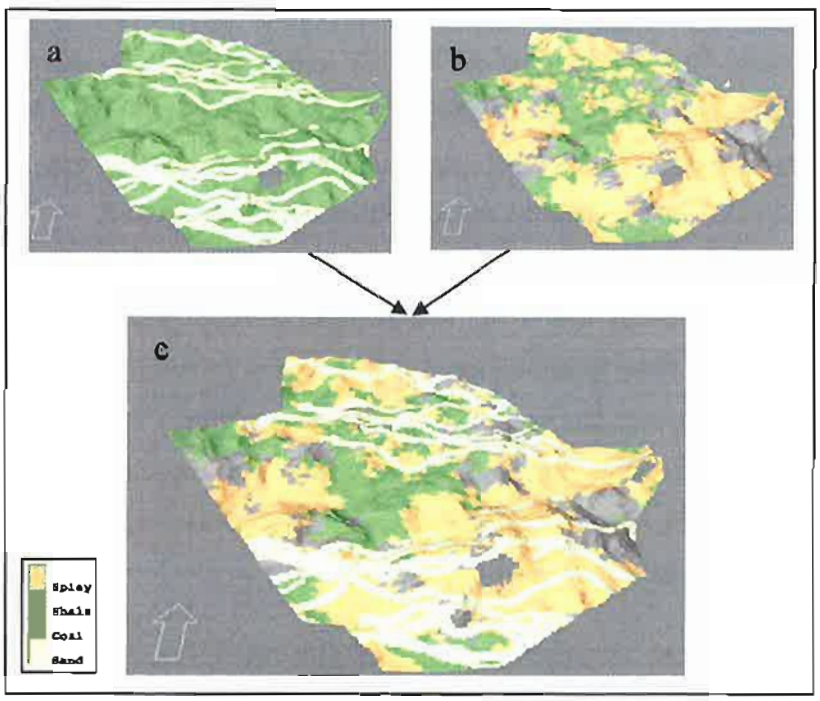

Figure 4.6: An illustration for the merging process of two stochastic facies models, a) channels and back ground facies, b) splay, coal and back ground facies, c) the final merged model.

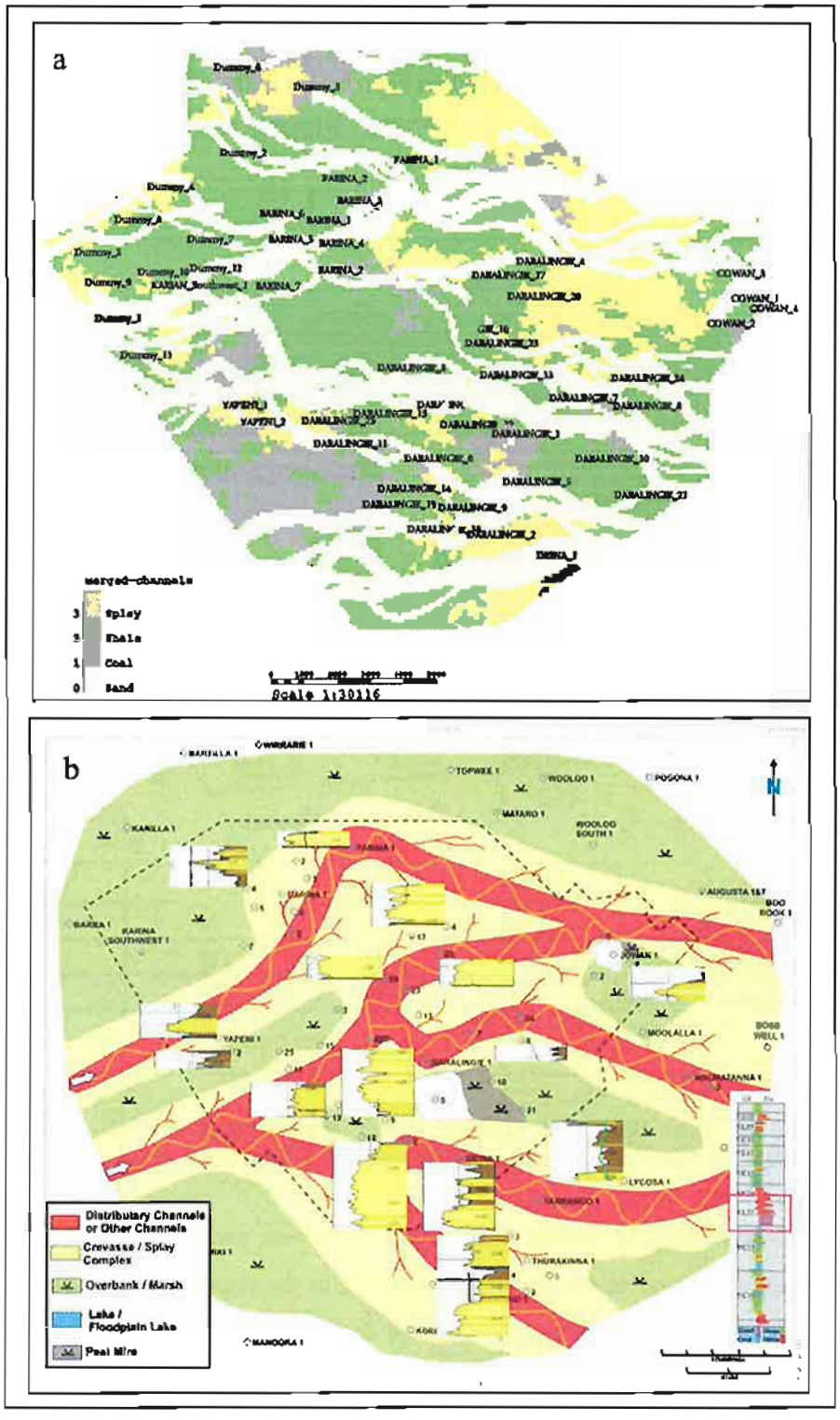

Figure 4.7: (a) A slice in the merged facies model in the VL22-VC25 reservoir interval, (b) the facies map for the VL22-VC25 interval. Note the similarity in channel direction and belt widths.

After completing the visual quality control for the facies model, a statistical quality approach was used. A comparison of facies distribution from raw log data, upscaled log data and from the merged model in the main reservoir interval (VC20-VC25) was performed (Fig. 4.8).

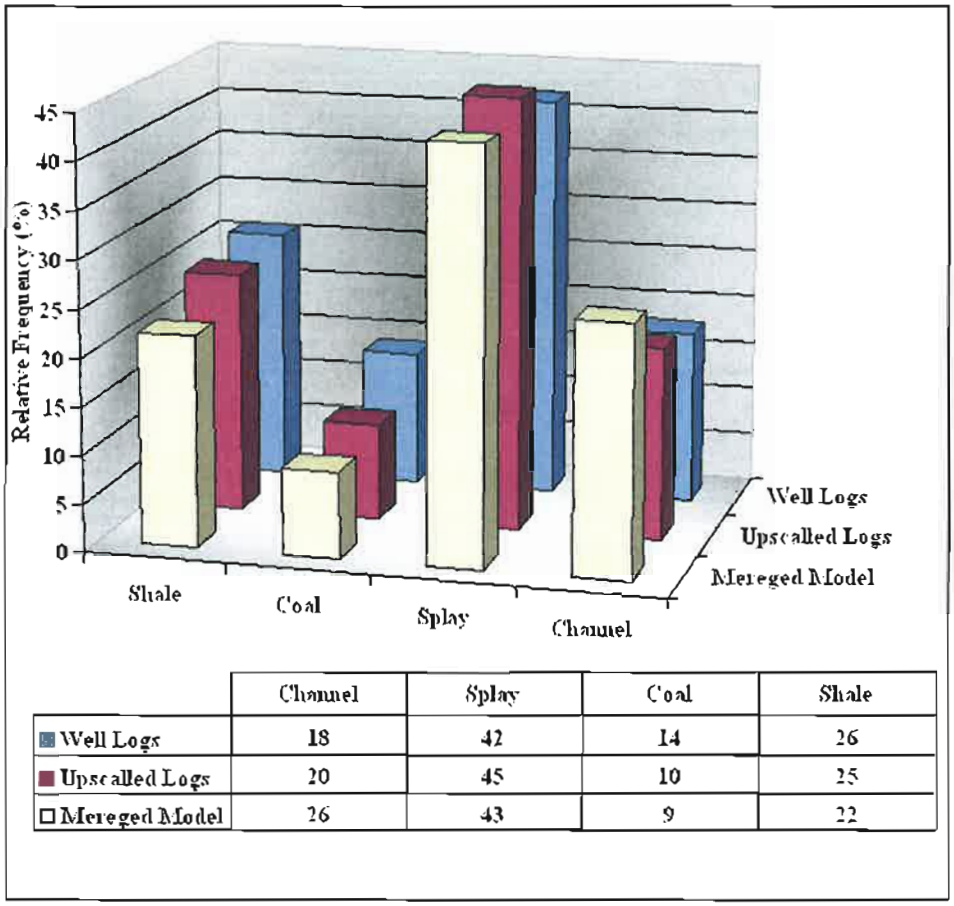

	Channel	Splay	Coal	Shale
Well Logs	18	42	14	26
Upscalled Logs	20	45	10	25
Mereged Model	26	43	9	22

Figure 4.8: Statistical distribution of facies in the main reservoir interval (VC20-VC25) in Daralingie Field, for raw well logs, upscaled logs and facies distribution in the merged model.

The results show that the overall facies distribution was preserved in every modeling step. The slight increase in the channel percentage in the merged model was due to the merging process used. When merging the two facies models, the channel objects were made to cut other existing facies. This condition was introduced to have realistic channel belt shapes as observed in nature. The result of this modeling step provides the most

realistic geological model and was used for the simulation of porosity and pore volume calculations.

4.5 Porosity Model

The porosity model was generated using effective porosity logs (PHIE) based on the merged facies model. The effective porosity statistical parameters for the modelled reservoir intervals are shown in Table 4.9.

Table 4.9: Statistical porosity values for effective porosity log in the modeled reservoir intervals.

Reservoir	Channel Sand			Splay			Coal			Shale		
Interval	Min	Max	Mean	Min	Max	Mean	Min	Max	Mean	Min	Max	Mean
VC00-VL05	0	0.14	0.08	0	0.18	0.07	0	0	0	0	0.05	0.01
VL05-VC10	0	0.16	0.06	0	0.18	0.05	0	0	0	0	0.08	0.01
VC10-VL11	0	0.16	0.06	0	0.13	0.04	0	0	0	0	0.06	0.01
VL11-VC15	0	0.13	0.06	0	0.15	0.05	0	0	0	0	0.07	0.01
VC15-VC20	0	0.05	0.02	0	0.14	0.05	0	0	0	0	0.07	0.01
VC20-VL22	0	0.20	0.11	0	0.27	0.10	0	0	0	0	0.09	0.01
VL22-VC25	0	0.21	0.10	0	0.19	0.09	0	0	0	0	0.08	0.01
VC25-VC30	0	0.12	0.04	0	0.15	0.05	0	0	0	0	0.08	0.01

After analysing the log data in conjunction with the geological study and after running five trial tests, semi-variogram parameters were selected for use in the porosity model. The rationale for deriving these numbers was as follows:

1- The azimuth direction was selected to be 90 degrees because it is the main channel direction as interpreted in the geological study.

2- A long semi-variogram radius of 5500 meters allowed the interpolation of porosity values in the channel body from any well falling in the same range.

3- The short radius was set to maximum channel width to generate the lateral extrapolation of porosity in the channels.

4- The vertical continuity of channel bodies found in cores was around 10 feet with a maximum of 14 feet. The use of this number generates the vertical continuity of modelled channels, unless they were cut by other facies.

As with the facies logs, the porosity logs were upscaled prior to modeling. The upscaling process was biased to the dominant facies type. For example, if the dominant facies was channel sand, then the upscaled porosity values were taken from the channel sand porosity only. This preserved porosity statistical parameters in each facies (Fig. 4.9). The generation of the porosity model was faster than the facies model, as it took less time to simulate than building objects for the same model size. Figure 4.10 shows a slice through a porosity model (more model slices are shown in appendix 2.) The high porosity areas are within the channel belts and splays, while the low porosity areas are in the shale and coal, as would be expected.

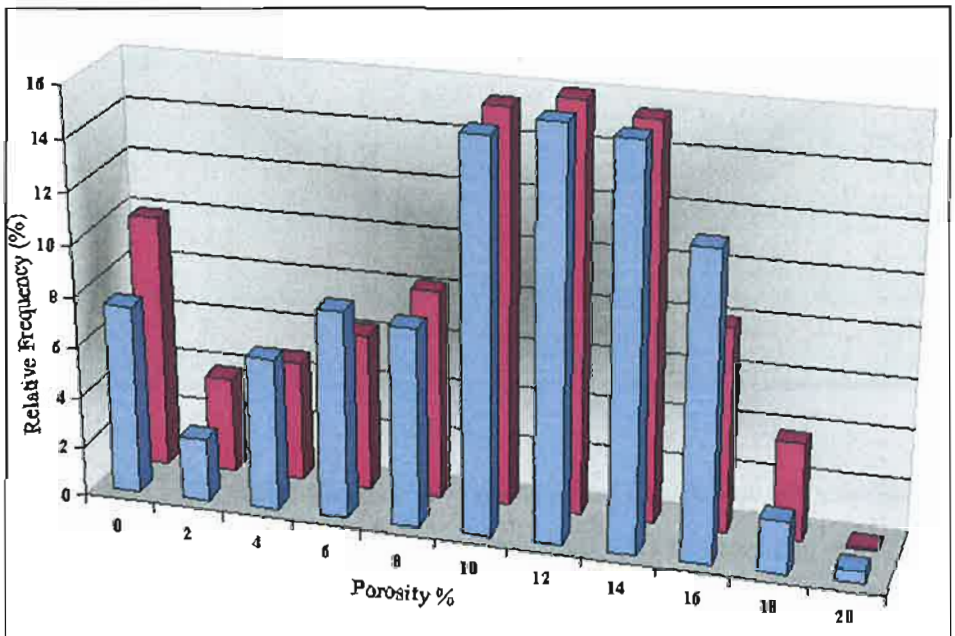

	0	2	4	6	8	10	12	14	16	18	20
Well Logs	7.5	2.5	6	8.2	7.8	15.3	16	15.6	12	2	0.5
Upscalled Logs	10	3.8	4.8	6.2	8.2	15.5	16	15.5	8	3.8	0.05

Figure 4.9: Statistical comparison between porosity raw logs and upscaled porosity logs for channel facies in VC20-VL22 reservoir interval.

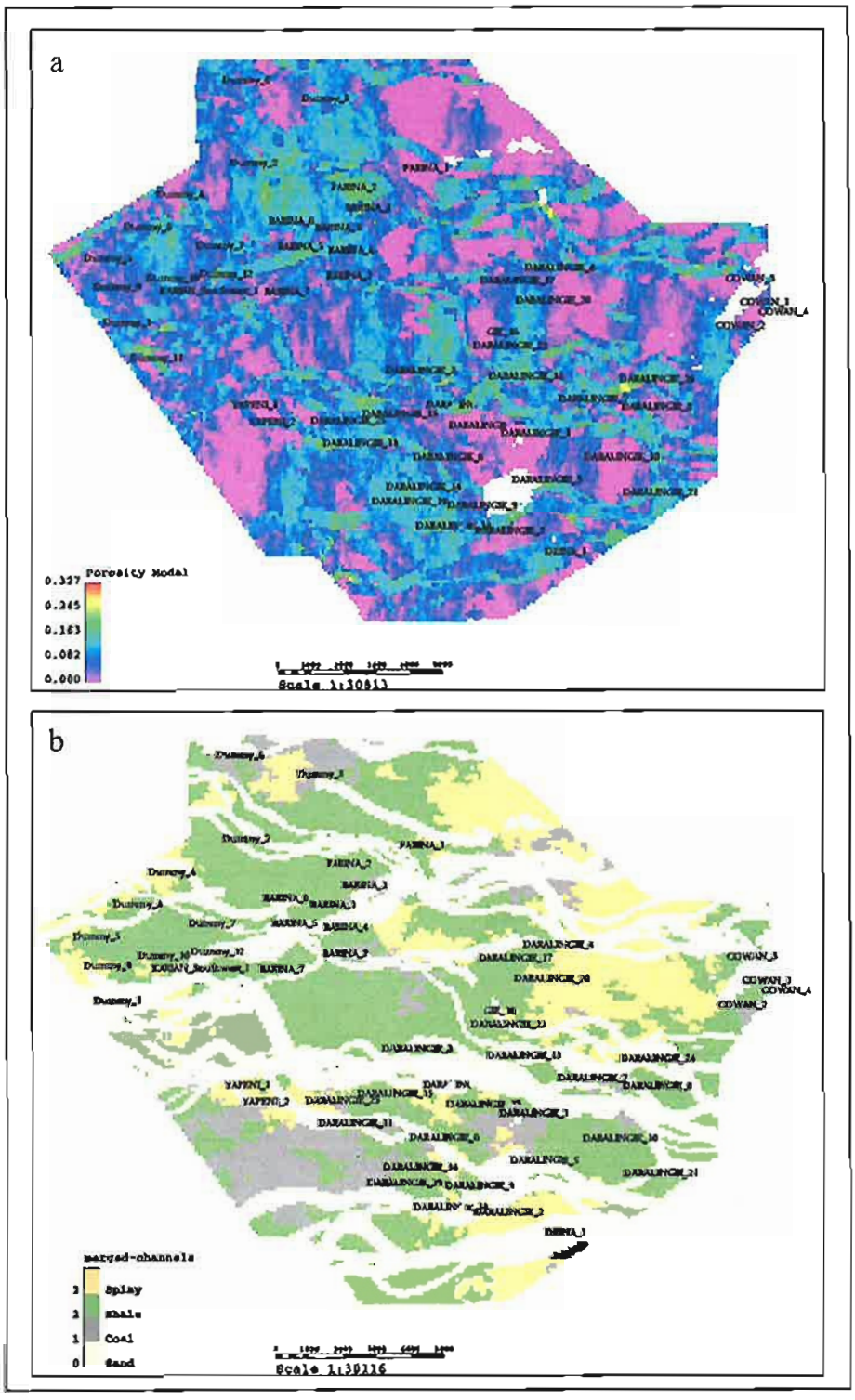

Figure 4.10: (a) A slice in the Daralingie Field porosity model, (b) facies model in the VL20-VC25 reservoir interval. Note the similarity between high porosity areas in the porosity model and the channel belt bodies in the facies model.

Chapter 5

Reserves Classification and Estimation

5.1 Reserve Classifications

The classification of reserves is associated with difficulties. This is especially the case when a field is at an early stage of development where there are few wells available and insufficient information about fluid contacts, reservoir continuity and petrophysical properties. Reserve classification therefore should incorporate the uncertainty level associated with the reserve estimates (Cronquist, 2001). Reserve classification is an evolving method and a significant development has occurred in the last decade. Several international professional organisations such as the Society of Petroleum Engineers (SPE), the World Petroleum Congress (WPC) and the American Association of Petroleum Geologists (AAPG) collaborated to produce a consistent reserve classification that can be used worldwide (Etherington and Hunt, 2004).

Reserves can be classified as either deterministic or probabilistic, based on their estimation method. Deterministic estimates are represented by a single value, while the probabilistic are represented by a range of values with an associated certainty of occurrence (Cosentino, 2001). Further discussion for each method will follow in section 5.2.

5.1.1 Need for a universal classification system

The need for one universal classification and nomenclature system for hydrocarbon reserves has long been recognised by the various technical societies, professional organizations, governmental agencies and the petroleum industry. One of the important reasons for reserve classification is to justify financial investment, especially in the early life of a field. For example, offshore fields require huge financial investments that must be made before the start of oil production (Schlagenhauf and Jaynes, 1995).

Another reason to have a universal classification system is the need for a common understanding of reserves. Deterministic estimates are represented by a single value, while the probabilistic are represented by a range of values with an associated certainty of occurrence. Deterministic estimates are calculated by using the best estimate of input variables in the reserve equation and the statistical distribution is ignored (Cronquist, 1991). Usually the probabilistic reserves are reported as proved, probable and possible (PPP).

The use of PPP to quantify reserves has different meanings in different countries. For example, the Australian Minerals and Energy Council defined 'proved' with 93% certainty and 'probable' with only 60%. In Europe, the UK proved reserves are defined as virtually certain and probable reserves have more than 50% certainty while both Austria and the Netherlands define proved as having more than 90% certainty and probable as having more than 50% certainty (Cronquist, 1991). Another example of the different interpretation of words is the work done by Behn and Vaupel (1982). They ran a survey randomly asking participants to assign probabilities to word descriptions and the results are shown in Table 5.1. The survey results indicate that people understanding of abstract terms such as "probable" and "possible" may vary dualistically.

Table 5.1: Range understanding of probability related to statements (from Behn and Vaupel, 1982)

Statement	Range
It is probable that...	20-98%
There is a possibility that...	52-92%
There is a chance that...	1-70%
It is very improbable that	1-80%

Adding more complexity, oil companies listing and trading in stock exchanges are required to report hydrocarbon reserves according to specific regulations, which may be different than the accepted oil industry classifications. For example, oil companies trading in US stock markets must adhere to the Security and Exchange Commission (SEC) reserve reporting regulations. To establish a new exploration discovery, SEC requires a demonstration of productivity through a well test that flows at commercial

rates. Whereas in the SPE classification, a flowing well test is enough and in certain cases proved reserves may be booked based on log or core analysis. It is clear that SEC regulations will result in very conservative reserve estimates, which may not be adequate for oil companies internal budget and financial planning (Etherington and Hunt, 2004).

In spite of the need for standardisation of definitions and concepts, differences in definitions continue to cloud the exact meaning of reserve definitions published by technical societies and regulatory bodies. The societies have established study groups to recommend a classification system; however, a universal system acceptable to all estimators and users has not yet been agreed upon as of December 2005.

5.1.2 Reserves/Resources classification development

Reserve classification has a long history in the literature. Most of the current classification systems used worldwide are based on concepts first proposed by the U.S. Geological Survey (USGS), which later were known as the "McKelvey box", shown in Figure 5.1. This system was first proposed in 1972 for the classification of hard minerals such as coal and later was adopted in the oil industry. This system classifies mineral resources using two attributes: degree of geological assurance and feasibility of commercial extraction. Reserves may be classified as probable because the subsurface geologic data are considered insufficient to classify them as proved, or reserves may be classified as probable because of uncertainties in the efficiency of the reservoir drive mechanism. The McKelvey classifications gave direction to subsequent classification efforts (Cronquist, 1991; Ahlbrandt et al., 2004).

The term proved reserves was based on a lexicon developed by the American Petroleum Institute (API). Between 1936 and 1979, the API published a series of annual reports of proved domestic reserves of crude oil, natural gas liquids and natural gas (Cronquist, 1991). In 1980, a study group consisting of representatives of oil producing countries recommended a set of definitions and classifications. The year after, a joint committee of SPE, AAPG and API developed a set of definitions and a glossary of terms (Garb, 1985).

Since that date, several classifications have been published. SPE, WPC and AAPG all have published their own definitions of reserves. As expected, these definitions needed consistent revisions. For example, the 1987 SPE reserve definitions did not provide guidelines for classifying reserves that resulted from using probabilistic methods. Furthermore, the criterion of classifying reserves as proved is that recovery be "reasonably certain" with regard to the probability of recovery, which makes it highly subjective (Cronquist, 2001).

In 1997 the SPE and the WPC published a joint resource classification and a reserve definition to help in standardising the terminology. Three years later, SPE, WPC and AAPG published the resource classification of 2000 (Fig. 5.2). This new system builds on the 1997 SPE/WPC system and the reserve and resources definition did not change. The new system includes the project maturity and the range of uncertainty that is a major expansion on the 1997 SPE/WPC classification (Ross, 2001). More details about the 1997 SPE/WPC and the 2000 SPE/WPC/AAPG Classification systems are attached in Appendix 3 and 4 respectively.

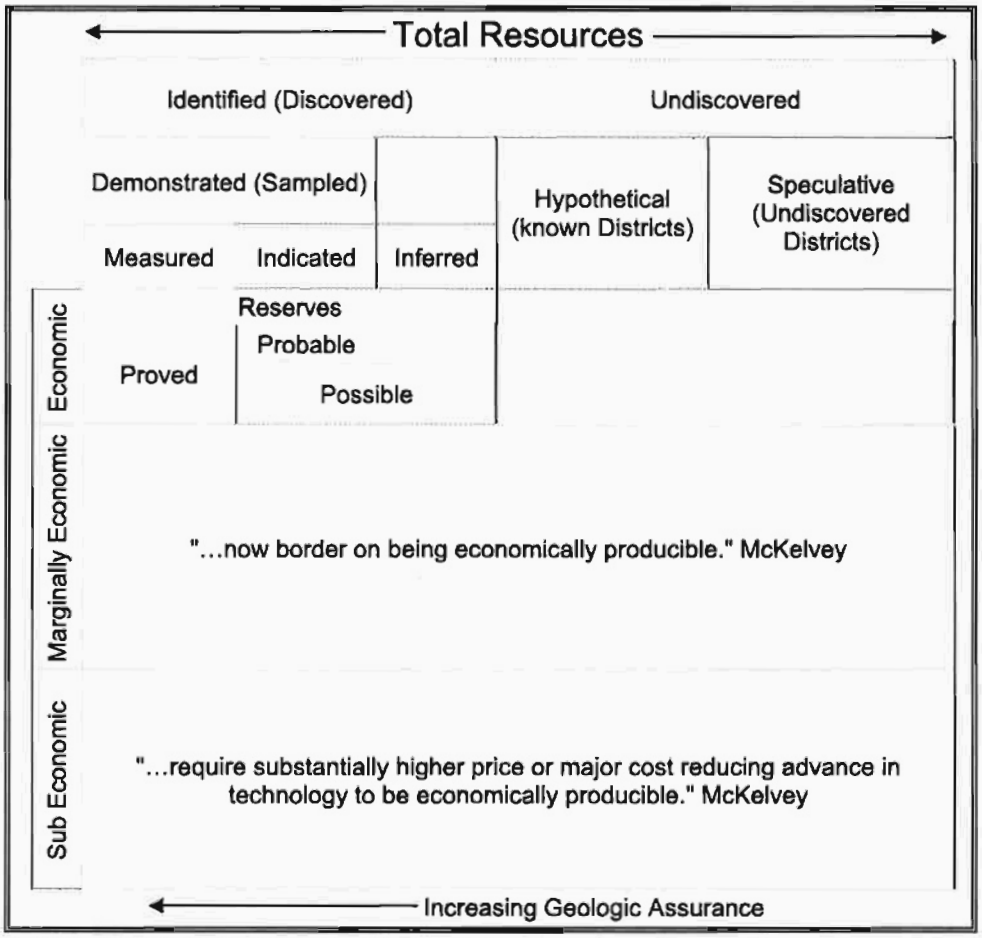

Figure 5.1: McKelvey box illustrating USGS system of classifying mineral resources (From Cronquist, 1991).

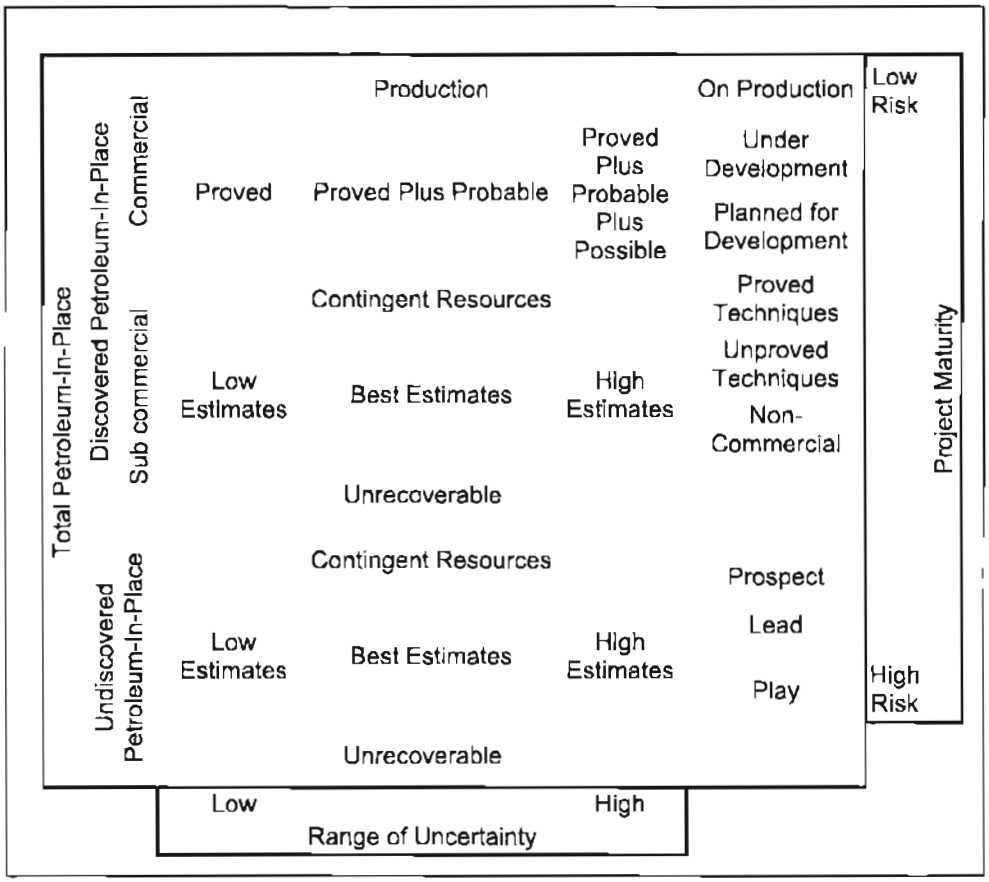

Figure 5.2: The 2000 SPE/WPC/AAPG resources classification system showing possible Resource Status Categories (From Cosentino, 2001).

In 2003 the United Nation (UN) proposed a new three dimensional classification system called the United Nations Framework Classification for Reserves and Resources (UNFC) (Fig. 5.3.) The aim of this step is to have a worldwide classification that works for hard and liquid resources (Ahlbrandt et al., 2004). A comparison between the 2000 SPE/WPC/AAPG reserves definition and the UNFC definitions is attached in Appendix 5. The rationale for this classification is that the reserves and resources are classified according to the following three factors:

1- The level of geological knowledge
2- Project status and feasibility
3- Economic and commercial viability.

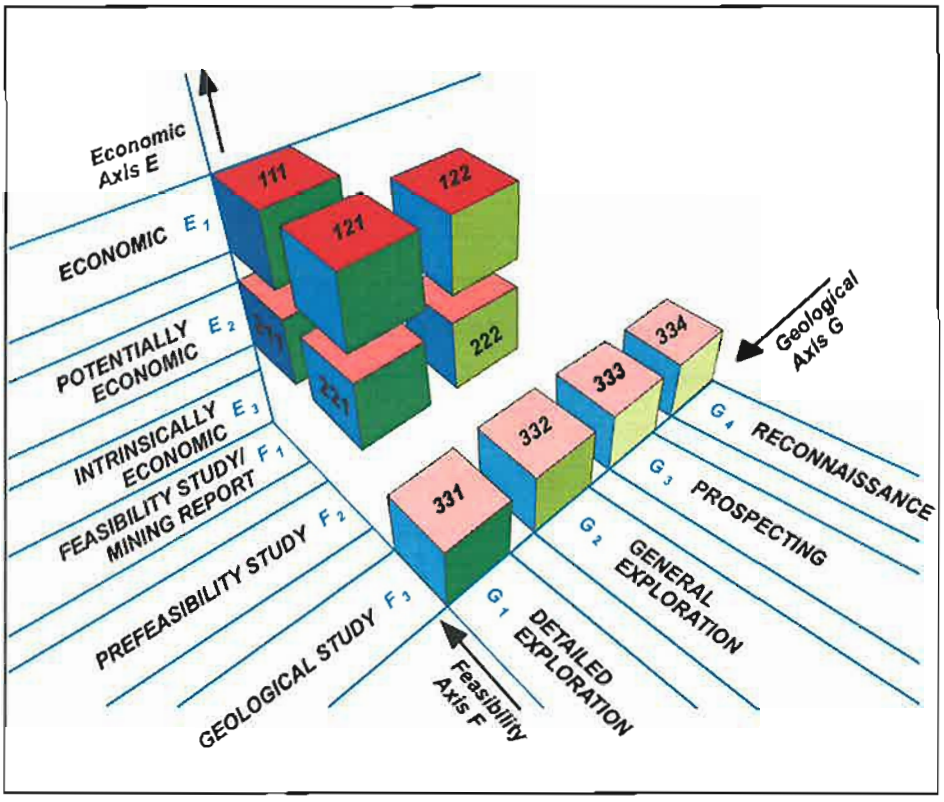

Figure 5.3: The United Nations Framework Classification for reserves/resources of solid fuels and minerals commodities (From Ahlbrandt et al., 2004).

The classification is made easy to use by using simple conventions. The main categories are called E for economic, F for field project status and G of the level of geological knowledge. These categories are always quoted in the alphabetical sequence (i.e. EFG.) Also, numbers are used for each category with the usual understanding that lower numbers are better than higher numbers. For example, category E1F1G1 is the best category representing reserves with the best economical conditions, best feasibility conditions and best geological certainty knowledge. Furthermore, the classification allows the use of numbers without the letters, for example E1F1G1 can be referred to as 111 (Ahlbrandt et al., 2004).

One of the advantages of the UNFC is its ability to integrate existing classifications. For example the SPE/WPC/AAPG 2000 classification can be easily integrated with UNFC. The F-axis in the UNFC classification represents the project status that corresponds with the project maturity in the SPE/WPC/AAPG 2000 classification. The G-axis in the UNFC corresponds with the range of uncertainty in the SPE/WPC/AAPG 2000 classification. The use of this classification worldwide will help develop a common understanding and better management of reserves and resources (Ahlbrandt et al., 2004).

The adoption of UNFC by the oil industry would be a major step to achieve a high level of consistency in the classification and description of reserves and resources worldwide. The benefits of this system, such as ease of use and the ability to be integrated with existing resources classification, would make it very attractive to the different parties in the oil industry. It is understandable that some oil companies may resist its use because changing reserves and resources classification systems may require manpower and time. However, through globalisation the need for a universal classification systems will increase. The use of classification system cannot be forced, but it can be well-presented and well advertised. There should be collaboration between the professional organisations, the oil industry and academia to promote the use of this classification system.

5.2 Reserve Estimation Methods

Reserve estimation methods can be divided into two categories: deterministic and probabilistic methods. The deterministic methods estimate single numbers without associated uncertainty, while the probabilistic reserve estimation methods give a range of possible numbers and an associated uncertainty level. Estimation methods can be further classified into analogue, volumetric and performance and are applied depending on the field maturity as shown in Figure 5.4.

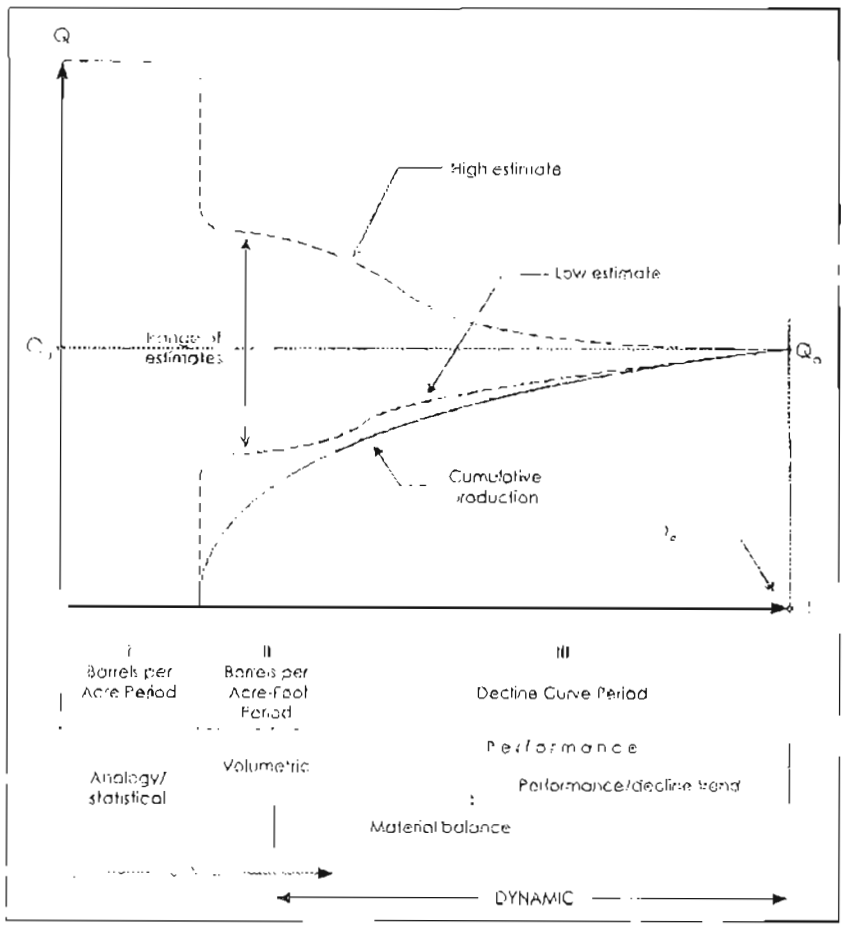

Figure 5.4: Periods in estimating ultimate recovery (Q) and reserves, illustrating how reserves estimating methodology and range of recovery estimates depend on the maturity of the reservoir (From Cronquist, 2001).

Dynamic estimate methods use production data, unlike static methods. Often more than one method is used to estimate reserves and results from one method are used to validate results from the other. The following sections cover the main reserve estimation methods catagorised as analogues, volumetrics, dynamic and probabilistic methods.

5.2.1 Analogue Methods

The simplest volumetric equation to estimate **O**riginal **H**ydrocarbon **I**n **P**lace at reservoir conditions is as follows (Cosentino, 2001):

$$OHIP = V * N/G * \phi * (1-S_w) * FVF$$

Where:

V	Reservoir Volume
N/G	Net-to-gross ratio
ϕ	Porosity, fraction
S_w	Water Saturation, fraction
FVF	Formation Volume Factor

The outcome of this equation is multiplied by a recovery factor and the reserve number is obtained. This is a very simple approach to estimating reserves and it is rarely used in mature fields. This equation uses reservoir average porosity, average water saturation and average net-to-gross ratio, which assumes a homogeneous reservoir. Because this is an unlikely scenario, the use of this equation will lead to either under estimating or over estimating reserves (OHIP).

Analogy methods are usually used to estimate reserves in undrilled prospects. Also analogue methods can be used to validate reserves estimated by other methods. Analogue methods are divided into two main categories: analytical and statistical. The analytical method estimates values of the input parameters in the above equation from a mature reservoir or from published reservoir data that are in geological and engineering comparable conditions.

The statistical analogue methods include using values per-well from analogous wells in the same geological and engineering producing regions. If this method is chosen, then special care has to be given to well completion types, production methods and production rates. Needless to say, the analogue method estimates carry a high degree of uncertainty that results in a high degree of risk. However, in some scenarios such as exploration in a new basin, this may be the only possible method to give reserves quantification.

5.2.2 Volumetric Methods

The simplest way to estimate OHIP by the volumetric method is to use average reservoir properties in the volumetric equation mentioned in Section 5.2.1. This is similar to the analogue method, but the input parameter values such as gross rock volume and porosity are taken from the actual reservoir instead of from an analogue. Also, the equation can be applied per-well by using the expected drainage volume of the well. The estimates from this method will have less uncertainty than the analogue method, but using average values will result in eliminating the effects of reservoir heterogeneities.

Hand Contouring Method

A popular volumetric method is hand contouring, and although these days most of the mapping is done by computers, the name remains the same. It uses the same basic equation, but calculation is done on a well-by-well basis. The OHIP value at each well is plotted and contoured. The sum of the map area represents the reservoir OHIP, which can be multiplied by a recovery factor to obtain the reserves. This method considers the reservoir heterogeneity, which will give a better estimation. However, it assumes that the OHIP is a variable than can be mapped from one well to another, which is often not the case. The solution to this problem is to generate three isopach maps: net-to-gross thickness, porosity and saturation. These three maps multiplied and the sum of the newly generated map area gives a better representation for OHIP (Harrell et al., 2004).

Stochastic Geological Models Method

A relatively new approach in volumetric reserve estimation is the use of stochastic geological models. Stochastic modeling methods have the ability to create many equi-probable realisations from the same geological data. Unlike other reserve estimation methods, the use of this method shows the impact of geological interpretation on reserves estimation. Different values for important geological features, such as channel belt percentage, width and thickness, can be used to understand their impact on reserve estimates. This method can be applied to reservoirs in different geological settings and maturity stages. It will work well in a mature field with a long history of production, as well as in a newly discovered field (Ates et al., 2003).

The OHIP calculations are done on a cell-by-cell basis utilising the 3-D porosity and facies models. Cell sizes vary from one model to another. The cell size used in the reservoir intervals in the Daralingie model is 100 x 100 metres aerially and 0.7 metres vertically on average. Furthermore, conditions can be set so that OHIP calculations are performed on selected facies only, which eliminates the use of gross net ratios. This gives a representative OHIP estimate for the reservoir. This method was used to calculate the Daralingie Field volumetrics using the stochastic models generated in Chapter 4.

5.2.3 Dynamic Methods

Dynamic methods are used after a reservoir has been on production for a sufficient period to give a representative production trend or a fluid volume that can be analysed mathematically. The analysis could include curve fitting, material balance equations and reservoir fluid flow simulations. Theoretically these methods should give better estimates than the previous methods because they include information coming from production data, however this is not always the case (Cronquist, 2001). There are some pitfalls in each method as will be discussed below.

Pressure Decline Curve Method

A very common deterministic method is the decline curve. The theory behind decline curve analysis is that plotting of production data versus time would establish a trend. Usually plots are made in logarithmic scale and a trend is established by using any of several curve-fitting techniques such as exponential, hyperbolic or harmonic. Then the trend is extrapolated into the future until production falls below economical limits or reaches zero production (Thompson et al., 1987; Towler, 2002; Harrell et al., 2004).

The advantage of this method is that it takes into consideration the status of field production data. Also, it can give a reserve estimate without any geological bias since no geological parameters are used. However, it cannot be used in newly discovered fields or fields with a short production history. Another disadvantage is the highly subjective nature of this method, as the use of the curve fitting technique will influence the final results. There are no thumb rules on which technique to use, it will depend on the knowledge and experience on the interpreter (Towler, 2002; Harrell et al., 2004).

Thompson et al. (1987) carried out an experiment in which about 80 students estimated reserves by the curve decline method. They used actual filed data, which had four wells and 12 years of production history. Moreover, the Filed was depleted and total field production was known. This study results showed that there was large variation in the students reserve estimates. This indicated that more production data did not improve the estimation accuracy. Moreover, some of the fitting methods used resulted in an unreasonable estimate, which illustrates the subjectivity of this method. Therefore, the assumption that this method gives better estimates as more production data are available, is inaccurate, and may, in fact, lead to unreasonable estimates (Thompson et al., 1987).

Material Balance Equations

The material balance equations express the law of material conservation applied to petroleum reservoirs. They relate the net reservoir porosity due to production to the expansion of reservoir fluids. The input parameters needed for this method are independent from the input parameters used in the volumetric equation. This means that the results from this method can be used to validate results from the volumetric equation (Cosentino, 2001).

The data requirements for this method are pressure-volume-temperature (PVT) fluid analysis, accurate static bottom hole pressure history and accurate monthly production for all produced fluids from the reservoir. Hence any error in these will result in wrong hydrocarbon estimates. Also, the reservoir drive mechanism type has a strong influence on the results. For example, in the case of strong water drive or large initial gas cap the reservoir pressure decline will be very small to result in representative hydrocarbon estimates (Cronquist, 2001).

Reservoir Fluid Flow Simulators Method

With advances in computing power in the last decade, reserve estimation is increasingly done by reservoir simulation. The rationale for this is the use of technology to mimic reservoir conditions to get an estimation of production. Such runs are either done on geological models or on tank models (Palke and Rietz, 2001). A tank model is a simplistic representation of the reservoir that assumes constant reservoir properties. The reliability of the results depends on the accuracy of the geological model. Consequently these methods can result in erroneous hydrocarbon estimates.

5.2.4 Probabilistic methods

In recent years probabilistic reserve estimation methods have been used to increase the confidence in reserve estimates. Probabilistic methods take into account uncertainties related to each input of the OHIP equation. Instead of using one number in the OHIP equation, a distribution of variables are used which results in a range of values for OHIP with probability of occurrence (Cronquist, 2001). The most common approach is the simple Monte Carlo Simulation method. Monto Carlo is a statistics based analysis tool that yields probability values for the compilation of several parameters (Fig. 5.5.) It has the advantage of being easy to use and takes a very short time to simulate. However, it is like a black box and the user does not have much control on the output. Furthermore, there is no geological component in this method. For example, different facies types and geometries have no impact on the outcome of such a simulation (Cosentino, 2001). This method was used to estimate Daralingie Field hydrocarbons, as will be discussed further in Chapter 7.

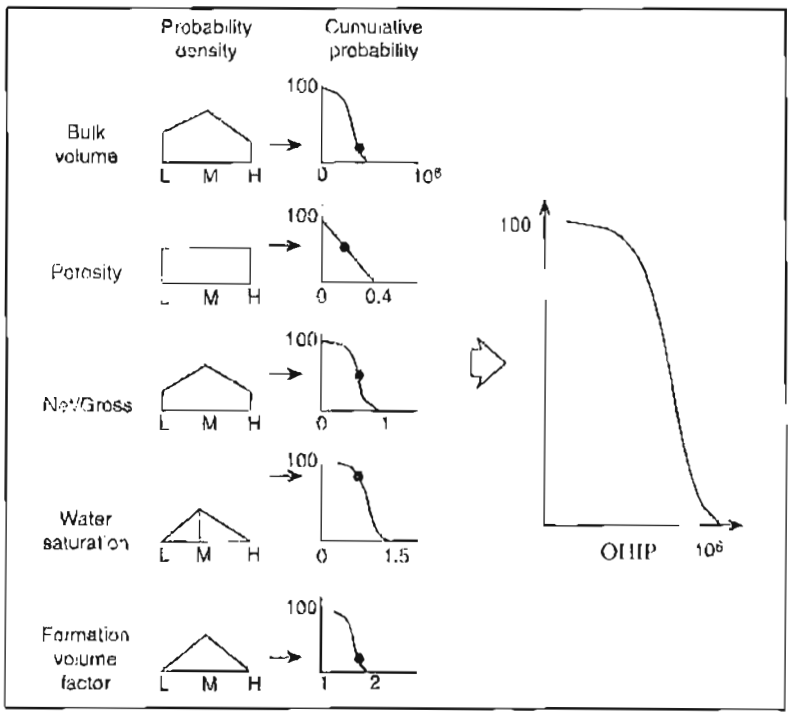

Figure 5.5: Monte Carlo technique for probabilistic OHIP estimation (from Cosentino, 2001).

Chapter 6
Daralingie Field Volumetric Estimation

6.1 Overview

In this chapter, hydrocarbon estimates were calculated in two different ways. First, the hydrocarbon estimates were done for a facies-based porosity model. Three porosity models were built for every facies proportion to investigate the impact of depositional facies proportions on hydrocarbon estimates. The facies proportions were categroised into minimum, mean and maximum, which related to the uncertainty in the estimation of the depositional facies proportions in the Daralingie Field, as explained in Section 3.5. After the completion of this task, hydrocarbon estimates were done, based on a stochastic model that was built based on well logs only. The results were compared with the results from the facies-based porosity model estimates. Possible explanations for the difference in the two estimates are presented.

6.2 Porosity Facies Based Model

This study uses the same fluid contacts and petrophysical logs as Hill (2004) used in his Daralingie Field volumetric study as described in Section 2.2.6. The calculations here were performed using the facies and porosity stochastic models created in Chapter 4. All hydrocarbon calculations were performed in Roxar RMS 7.2 for every reservoir interval and every reservoir area. Results were exported as ASCII file and entered manually in an excel sheet for subsequent analysis. Three volumetrics calculations were done with different facies proportions (Model-A, B and C). In all facies model runs the same facies geometry was used. The aim of this was to see the impact of facies proportions on volumetrics. Also, cumulative productions were used to validate hydrocarbon estimates for each model. Expected recovery factors were calculated for the cumulative production and the proposed ultimate development scenarios (1P, 2P and 3P) that were done by

Santos. These development scenarios were based on the pressure decline study of Daralingie Field.

6.2.1 Minimum Facies Proportions (Model-A)

This was the first facies model built. The facies proportions were derived from raw logs and were used as an initial guide for generating the facies model (Table 6.1). After building the stochastic facies model, a facies-based porosity model was created as explained in Section 4.2. The hydrocarbon estimates were done based on the porosity model and the results are shown in Tables 6.2 to 6.7. The hydrocarbon estimates validations and the expected recovery factors for stochastic facies porosity model-A are shown in Tables 6.8 and 6.9.

Table 6.1: Facies proportions used in creating stochastic facies model-A.

Reservoir Interval	Channels %	Splay %	Coal %	Shale %
VC00-VL05	10	30	5	55
VL05-VC10	10	20	20	50
VC10-VL11	15	10	5	70
VL11-VC15	5	10	8	77
VC15-VC20	5	5	15	75
VC20-VL22	20	30	15	35
VL22-VC25	25	25	5	45
VC25-VC30	5	5	35	55

Table 6.2: The 1P original gas in place (OGIP) for the stochastic facies based porosity model-A.

	OGIP - 1P						
	VC00	VL05	VL11	VC20	VL22	VC20-VL22	Total 1P
Dara Main	8.4 Bcf	7.7 Bcf	3.6 Bcf	43.1 Bcf	32.4 Bcf	75.5 Bcf	95.2 Bcf
Dara #16	2.5 Bcf	0.0 Bcf	0.0 Bcf	2.6 Bcf	6.7 Bcf	9.3 Bcf	11.8 Bcf
Dara #3	0.6 Bcf	0.9 Bcf	0.1 Bcf	5.0 Bcf	4.7 Bcf	9.7 Bcf	11.4 Bcf
Dara #4/20	0.1 Bcf	0.0 Bcf	0.0 Bcf	4.6 Bcf	2.5 Bcf	7.1 Bcf	7.2 Bcf
Dara #11/25	1.5 Bcf	2.0 Bcf	0.4 Bcf	6.9 Bcf	5.7 Bcf	12.6 Bcf	16.4 Bcf
Yapeni	0.8 Bcf	1.5 Bcf	0.4 Bcf	4.8 Bcf	4.9 Bcf	9.7 Bcf	12.4 Bcf
Total	13.9 Bcf	12.1 Bcf	4.5 Bcf	67.0 Bcf	56.9 Bcf	123.9 Bcf	154.4 Bcf

Table 6.3: The 1P Original oil in place (OOIP) for stochastic facies-based porosity model-A.

	OOIP - 1P		
	VC20	VL22	VC20-VL22
Dara Main	8.1 Mbbl	9.3 Mbbl	17.4 Mbbl
Dara #16	2.6 Mbbl	13.6 Mbbl	16.2 Mbbl
Dara #3	1.1 Mbbl	3.6 Mbbl	4.7 Mbbl
Dara #4/20	1.6 Mbbl	2.1 Mbbl	3.7 Mbbl
Dara #11/25	3.8 Mbbl	5.1 Mbbl	8.9 Mbbl
Yapeni	2.6 Mbbl	1.9 Mbbl	4.5 Mbbl
Total	19.8 Mbbl	35.6 Mbbl	55.4 Mbbl

Table 6.4: The 2P OGIP with associated gas liberated from the oil rim for stochastic facies-based porosity model-A.

	OGIP - 2P						
	VC00	VL05	VL11	VC20	VL22	VC20-VL22	Total 2P
Dara Main	8.4 Bcf	9.3 Bcf	4.3 Bcf	43.1 Bcf	32.4 Bcf	75.5 Bcf	97.5 Bcf
Dara #16	2.6 Bcf	2.4 Bcf	0.2 Bcf	2.6 Bcf	6.7 Bcf	9.3 Bcf	14.5 Bcf
Dara #3	0.6 Bcf	3.3 Bcf	0.3 Bcf	5.0 Bcf	4.7 Bcf	9.7 Bcf	13.9 Bcf
Dara #4/20	0.2 Bcf	0.1 Bcf	0.1 Bcf	5.8 Bcf	3.9 Bcf	9.7 Bcf	10.1 Bcf
Dara #11/25	1.5 Bcf	3.7 Bcf	0.8 Bcf	6.9 Bcf	5.7 Bcf	12.6 Bcf	18.6 Bcf
Yapeni	0.9 Bcf	2.8 Bcf	0.8 Bcf	4.8 Bcf	4.9 Bcf	9.7 Bcf	14.2 Bcf
Total	14.1 Bcf	21.6 Bcf	6.5 Bcf	68.2 Bcf	58.3 Bcf	126.6 Bcf	168.7 Bcf

Table 6.5: The 2P OOIP with associated gas liberated from the oil rim for stochastic facies-based porosity model-A.

	OOIP - 2P			Associated Gas Bcf		
	VC20	VL22	VC20-VL22	VC20	VL22	VC20-VL22
Dara Main	8.1 Mbbl	9.3 Mbbl	17.4 Mbbl	5.1 Bcf	5.8 Bcf	10.9 Bcf
Dara #16	2.6 Mbbl	13.6 Mbbl	16.2 Mbbl	1.6 Bcf	8.5 Bcf	10.1 Bcf
Dara #3	1.1 Mbbl	3.6 Mbbl	4.7 Mbbl	0.7 Bcf	2.2 Bcf	2.9 Bcf
Dara #4/20	0.3 Mbbl	0.6 Mbbl	0.9 Mbbl	0.2 Bcf	0.4 Bcf	0.6 Bcf
Dara #11/25	3.8 Mbbl	5.1 Mbbl	8.9 Mbbl	2.4 Bcf	3.2 Bcf	5.6 Bcf
Yapeni	2.6 Mbbl	1.9 Mbbl	4.5 Mbbl	1.6 Bcf	1.2 Bcf	2.8 Bcf
Total	18.5 Mbbl	34.1 Mbbl	52.6 Mbbl	11.6 Bcf	21.3 Bcf	32.9 Bcf

Table 6.6: 3P OGIP with associated gas liberated from the oil rim for the stochastic facies-based porosity model-A.

	OGIP - 3P						
	VC00	VL05	VL11	VC20	VL22	VC20-VL22	Total 2P
Dara Main	8.4 Bcf	9.6 Bcf	4.6 Bcf	43.1 Bcf	32.4 Bcf	75.5 Bcf	98.1 Bcf
Dara #16	2.6 Bcf	2.8 Bcf	0.5 Bcf	2.6 Bcf	6.7 Bcf	9.3 Bcf	15.1 Bcf
Dara #3	0.6 Bcf	3.6 Bcf	0.5 Bcf	5.0 Bcf	4.7 Bcf	9.7 Bcf	14.4 Bcf
Dara #4/20	0.2 Bcf	0.2 Bcf	0.1 Bcf	6.3 Bcf	4.6 Bcf	10.9 Bcf	11.4 Bcf
Dara #11/25	1.5 Bcf	3.9 Bcf	1.1 Bcf	6.9 Bcf	5.7 Bcf	12.6 Bcf	19.1 Bcf
Yapeni	0.9 Bcf	2.9 Bcf	1.0 Bcf	4.8 Bcf	4.9 Bcf	9.7 Bcf	14.5 Bcf
Total	14.1 Bcf	22.9 Bcf	7.8 Bcf	68.7 Bcf	59.0 Bcf	127.7 Bcf	172.6 Bcf

Table 6.7: 3P OOIP with associated gas liberated from the oil rim for the stochastic facies-based porosity model-A.

	OOIP - 3P			Associated Gas Bcf		
	VC20	VL22	VC20-VL22	VC20	VL22	VC20-VL22
Dara Main	8.1 Mbbl	9.3 Mbbl	17.4 Mbbl	6.1 Bcf	7.0 Bcf	13.1 Bcf
Dara #16	2.6 Mbbl	13.6 Mbbl	16.2 Mbbl	2.0 Bcf	10.2 Bcf	12.2 Bcf
Dara #3	1.1 Mbbl	3.6 Mbbl	4.7 Mbbl	0.8 Bcf	2.7 Bcf	3.5 Bcf
Dara #4/20	0.0 Mbbl	0.0 Mbbl	0.0 Mbbl	0.0 Bcf	0.0 Bcf	0.0 Bcf
Dara #11/25	3.8 Mbbl	5.1 Mbbl	8.9 Mbbl	2.9 Bcf	3.8 Bcf	6.7 Bcf
Yapeni	2.6 Mbbl	1.9 Mbbl	4.5 Mbbl	2.0 Bcf	1.4 Bcf	3.4 Bcf
Total	18.2 Mbbl	33.5 Mbbl	51.7 Mbbl	13.7 Bcf	25.1 Bcf	38.8 Bcf

Table 6.8: Validation for hydrocarbon estimates calculated from stochastic facies-based porosity model-A in the VC20-VC25 reservoir interval in the DARA Main and DARA 3 areas.

Recover factors		Model Volumetric		
		1P	2P	3P
		94.5 Bcf	118.5 Bcf	123.2 Bcf
Cumulative	152.6	161.4%	128.8%	123.8%
1P Dev	168	177.7%	141.8%	136.3%
2P Dev	177	187.3%	149.4%	143.6%
3P Dev	186	196.8%	157.0%	150.9%

Table 6.9: Validation for hydrocarbon estimates calculated from the stochastic facies-based porosity model-A in the reservoir interval VC20-VC25 in the DARA 4/20 area.

Recover factors		Model Volumetric		
		1P	2P	3P
		7.1 Bcf	10.3 Bcf	10.9 Bcf
Cumulative	15.9 Bcf	224.3%	154.3%	145.9%
1P Dev	16.6 Bcf	234.1%	161.1%	152.3%
2P Dev	16.7 Bcf	235.5%	162.1%	153.2%
3P Dev	17.0 Bcf	239.8%	165.0%	156.0%

It is clear from the Table 6.9 that the use of facies proportions derived from well logs is not enough to match the cumulative production from DARA Main and DARA 3 areas. Cumulative production to 2003-year end is 161.4% more than the OGIP calculated from the model. Therefore, this model cannot be used for fluid flow simulation, because the volume it has estimated is much less than produced. It will be impossible to get a history match with this model.

6.2.2 Mean Facies Proportions (Model-B)

Model-A was generated using facies proportions derived from well logs and it was not sufficient to match the produced gas volumes. In Model-B the channel and the splay facies proportions were estimated from the facies map generated in Chapter 3. The rationale for this is that in Daralingie Field, porosity distribution is highly controlled by facies. Hence, if the facies proportions increased than porosity would increase and improve the volumetrics. Furthermore, the results would show if estimating the facies proportions from facies maps is better then estimating them from wells. Table 6.10 shows the new proportions for every reservoir interval. The hydrocarbon estimates were done based on the porosity model generated afterwards and the results are shown in Tables 6.11 to 6.16. The hydrocarbon estimates validations and the expected recovery factors for stochastic facies porosity model-A are shown in Tables 6.17 and 6.18.

Table 6.10: Facies proportions estimated from facies maps and used in creating stochastic facies model-B.

Reservoir Interval	Channels %	Splay %	Coal %	Shale %
VC00-VL05	15	35	5	45
VL05-VC10	10	30	20	50
VC10-VL11	15	10	5	70
VL11-VC15	5	10	8	77
VC15-VC20	5	5	15	75
VC20-VL22	25	40	15	20
VL22-VC25	30	35	5	30
VC25-VC30	5	5	35	55

Table 6.11: The 1P OGIP for the stochastic facies-based porosity model-B.

	OGIP - 1P						
	VC00	VL05	VL11	VC20	VL22	VC20-VL22	Total 1P
Dara Main	11.7 Bcf	8.9 Bcf	3.6 Bcf	52.2 Bcf	35.4 Bcf	87.6 Bcf	111.8 Bcf
Dara #16	2.8 Bcf	0.1 Bcf	0.0 Bcf	3.6 Bcf	6.1 Bcf	9.7 Bcf	12.6 Bcf
Dara #3	1.7 Bcf	0.6 Bcf	0.1 Bcf	5.3 Bcf	4.5 Bcf	9.8 Bcf	12.2 Bcf
Dara #4/20	0.1 Bcf	0.0 Bcf	0.0 Bcf	5.6 Bcf	3.2 Bcf	8.8 Bcf	8.9 Bcf
Dara #11/25	3.9 Bcf	2.0 Bcf	0.4 Bcf	7.4 Bcf	5.8 Bcf	13.2 Bcf	19.5 Bcf
Yapeni	1.3 Bcf	1.5 Bcf	0.4 Bcf	4.9 Bcf	4.9 Bcf	9.9 Bcf	13.1 Bcf
Total	21.5 Bcf	13.1 Bcf	4.5 Bcf	79.1 Bcf	59.9 Bcf	139.0 Bcf	178.1 Bcf

Table 6.12: The 1P OOIP for the stochastic facies-based porosity model-B.

	OOIP - 1P		
	VC20	VL22	VC20-VL22
Dara Main	9.4 Mbbl	9.8 Mbbl	19.2 Mbbl
Dara #16	3.3 Mbbl	13.5 Mbbl	16.8 Mbbl
Dara #3	1.4 Mbbl	3.5 Mbbl	4.9 Mbbl
Dara #4/20	2.5 Mbbl	2.1 Mbbl	4.6 Mbbl
Dara #11/25	4.5 Mbbl	5.0 Mbbl	9.5 Mbbl
Yapeni	2.7 Mbbl	2.0 Mbbl	4.6 Mbbl
Total	23.7 Mbbl	35.8 Mbbl	59.5 Mbbl

Table 6.13: 2P OGIP with associated gas liberated from the oil rim for the stochastic facies-based porosity model-B.

	OGIP - 2P						
	VC00	VL05	VL11	VC20	VL22	VC20-VL22	Total 2P
Dara Main	11.8 Bcf	11.2 Bcf	4.3 Bcf	52.2 Bcf	35.4 Bcf	87.6 Bcf	115.0 Bcf
Dara #16	2.8 Bcf	2.3 Bcf	0.2 Bcf	3.6 Bcf	6.1 Bcf	9.7 Bcf	15.1 Bcf
Dara #3	1.7 Bcf	2.7 Bcf	0.3 Bcf	5.3 Bcf	4.5 Bcf	9.8 Bcf	14.5 Bcf
Dara #4/20	0.1 Bcf	0.1 Bcf	0.1 Bcf	7.4 Bcf	4.7 Bcf	12.2 Bcf	12.5 Bcf
Dara #11/25	4.0 Bcf	3.8 Bcf	0.8 Bcf	7.4 Bcf	5.8 Bcf	13.2 Bcf	21.8 Bcf
Yapeni	1.4 Bcf	2.6 Bcf	0.8 Bcf	4.9 Bcf	4.9 Bcf	9.9 Bcf	14.6 Bcf
Total	21.8 Bcf	22.7 Bcf	6.5 Bcf	80.9 Bcf	61.4 Bcf	142.4 Bcf	193.4 Bcf

Table 6.14: The 2P OOIP with associated gas liberated from the oil rim for the stochastic facies-based porosity model-B.

	OOIP - 2P			Associated Gas Bcf		
	VC20	VL22	VC20-VL22	VC20	VL22	VC20-VL22
Dara Main	9.4 Mbbl	9.8 Mbbl	19.2 Mbbl	5.9 Bcf	6.1 Bcf	12.0 Bcf
Dara #16	3.3 Mbbl	13.5 Mbbl	16.8 Mbbl	2.1 Bcf	8.5 Bcf	10.5 Bcf
Dara #3	1.4 Mbbl	3.5 Mbbl	4.9 Mbbl	0.8 Bcf	2.2 Bcf	3.0 Bcf
Dara #4/20	0.6 Mbbl	0.6 Mbbl	1.1 Mbbl	0.4 Bcf	0.4 Bcf	0.7 Bcf
Dara #11/25	4.5 Mbbl	5.0 Mbbl	9.5 Mbbl	2.8 Bcf	3.1 Bcf	5.9 Bcf
Yapeni	2.7 Mbbl	2.0 Mbbl	4.6 Mbbl	1.7 Bcf	1.2 Bcf	2.9 Bcf
Total	21.8 Mbbl	34.3 Mbbl	56.1 Mbbl	13.6 Bcf	21.5 Bcf	35.1 Bcf

Table 6.15: The 3P OGIP with associated gas liberated from the oil rim for the stochastic facies-based porosity model-B.

	OGIP - 3P						
	VC00	VL05	VL11	VC20	VL22	VC20-VL22	Total 2P
Dara Main	11.8 Bcf	11.5 Bcf	4.6 Bcf	52.2 Bcf	35.4 Bcf	87.6 Bcf	115.5 Bcf
Dara #16	2.8 Bcf	2.7 Bcf	0.5 Bcf	3.6 Bcf	6.1 Bcf	9.7 Bcf	15.7 Bcf
Dara #3	1.7 Bcf	2.8 Bcf	0.5 Bcf	5.3 Bcf	4.5 Bcf	9.8 Bcf	14.8 Bcf
Dara #4/20	0.1 Bcf	0.2 Bcf	0.1 Bcf	8.9 Bcf	5.4 Bcf	14.3 Bcf	14.7 Bcf
Dara #11/25	4.0 Bcf	4.0 Bcf	1.1 Bcf	7.4 Bcf	5.8 Bcf	13.2 Bcf	22.3 Bcf
Yapeni	1.4 Bcf	2.7 Bcf	1.0 Bcf	4.9 Bcf	4.9 Bcf	9.9 Bcf	14.9 Bcf
Total	21.8 Bcf	23.9 Bcf	7.8 Bcf	82.4 Bcf	62.1 Bcf	144.5 Bcf	198.0 Bcf

Table 6.16: The 3P OOIP with associated gas liberated from the oil rim for the stochastic facies-based porosity model-B.

	OOIP - 3P			Associated Gas Bcf		
	VC20	VL22	VC20-VL22	VC20	VL22	VC20-VL22
Dara Main	9.4 Mbbl	9.8 Mbbl	19.2 Mbbl	7.1 Bcf	7.3 Bcf	14.4 Bcf
Dara #16	3.3 Mbbl	13.5 Mbbl	16.8 Mbbl	2.5 Bcf	10.1 Bcf	12.6 Bcf
Dara #3	1.4 Mbbl	3.5 Mbbl	4.9 Mbbl	1.0 Bcf	2.6 Bcf	3.6 Bcf
Dara #4/20	0.0 Mbbl	0.0 Mbbl	0.0 Mbbl	0.0 Bcf	0.0 Bcf	0.0 Bcf
Dara #11/25	4.5 Mbbl	5.0 Mbbl	9.5 Mbbl	3.4 Bcf	3.8 Bcf	7.1 Bcf
Yapeni	2.7 Mbbl	2.0 Mbbl	4.6 Mbbl	2.0 Bcf	1.5 Bcf	3.5 Bcf
Total	21.2 Mbbl	33.7 Mbbl	54.9 Mbbl	15.9 Bcf	25.3 Bcf	41.2 Bcf

Table 6.17: Validation for hydrocarbon estimates calculated from the stochastic facies based-porosity Model-B in the VC20-VC25 reservoir interval in the DARA Main and DARA 3 Areas.

Recover factors		Mapped		
		1P	2P	3P
		107.1 Bcf	132.7 Bcf	137.8 Bcf
Cumulative	152.6	142.4%	115.0%	110.8%
1P Dev	168	156.8%	126.6%	121.9%
2P Dev	177	165.2%	133.4%	128.5%
3P Dev	186	173.6%	140.2%	135.0%

Table 6.18: Validation for hydrocarbon estimates calculated from the stochastic facies based porosity Model-B in the VC20-VC25 reservoir interval in the DARA 4/20 Area.

Recover factors		Mapped		
		1P	2P	3P
		8.8 Bcf	12.9 Bcf	14.3 Bcf
Cumulative	15.9 Bcf	180.1%	123.4%	111.2%
1P Dev	16.6 Bcf	188.0%	128.8%	116.1%
2P Dev	16.7 Bcf	189.1%	129.6%	116.8%
3P Dev	17.0 Bcf	192.5%	132.0%	118.9%

As expected, the volumetrics numbers have improved over Model-A by using the channel and the splay facies proportions estimated from the facies maps (Table 6.17). However, the improvement was not enough to match the cumulative production to date (year-end

2003) as shown in Table 6.17 and 6.18. Therefore, this model cannot be used for fluid flow simulation, because its volume is again much less than gas produced.

6.2.3 Maximum Facies Proportions (Model-C)

In Model-C the channel and the splay facies proportions have been increased to the maximum geological limit as shown in Table 6.19. For example, in reservoir interval VC20-VL22 a 5% of shale was used whereas the wells showed the shale to be 35%. Model-C uses the maximum facies proportions possible while honoring the geology. The hydrocarbon estimates were done based on the porosity model generated afterwards and the results are shown in Tables 6.20 to 6.25. The hydrocarbon estimates validations and the expected recovery factors for stochastic facies porosity model-C are shown in Tables 6.26 and 6.27.

Table 6.19: Facies proportions used in creating stochastic facies model-C.

Zone	Channels %	Splay %	Coal %	Shale %
VC00-VL05	20	40	5	35
VL05-VC10	15	40	20	25
VC10-VL11	15	10	5	70
VL11-VC15	5	10	8	77
VC15-VC20	5	5	15	75
VC20-VL22	30	50	15	5
VL22-VC25	35	45	5	15
VC25-VC30	5	5	35	55

Table 6.20: The 1P OGIP estimates for the stochastic facies-based porosity model-C.

	OGIP - 1P						
	VC00	VL05	VL11	VC20	VL22	VC20-VL22	Total 1P
Dara Main	15.4 Bcf	9.9 Bcf	3.6 Bcf	71.0 Bcf	50.2 Bcf	121.2 Bcf	150.1 Bcf
Dara #16	3.4 Bcf	0.1 Bcf	0.0 Bcf	3.9 Bcf	5.2 Bcf	9.1 Bcf	12.6 Bcf
Dara #3	2.5 Bcf	1.0 Bcf	0.1 Bcf	4.6 Bcf	5.5 Bcf	10.2 Bcf	13.8 Bcf
Dara #4/20	0.1 Bcf	0.0 Bcf	0.0 Bcf	5.0 Bcf	4.0 Bcf	8.9 Bcf	9.0 Bcf
Dara #11/25	4.1 Bcf	2.6 Bcf	0.4 Bcf	7.9 Bcf	3.9 Bcf	11.8 Bcf	18.8 Bcf
Yapeni	4.3 Bcf	1.5 Bcf	0.4 Bcf	2.9 Bcf	1.0 Bcf	3.9 Bcf	10.1 Bcf
Total	29.8 Bcf	15.1 Bcf	4.5 Bcf	95.4 Bcf	69.7 Bcf	165.1 Bcf	214.4 Bcf

Table 6.21: The 1P OOIP for the stochastic facies-based porosity model-C.

	OOIP - 1P		
	VC20	VL22	VC20-VL22
Dara Main	15.3 Mbbl	11.9 Mbbl	27.3 Mbbl
Dara #16	3.5 Mbbl	9.8 Mbbl	13.3 Mbbl
Dara #3	1.6 Mbbl	2.9 Mbbl	4.5 Mbbl
Dara #4/20	2.1 Mbbl	2.9 Mbbl	4.9 Mbbl
Dara #11/25	9.0 Mbbl	4.7 Mbbl	13.7 Mbbl
Yapeni	2.3 Mbbl	1.1 Mbbl	3.4 Mbbl
Total	33.8 Mbbl	33.3 Mbbl	67.0 Mbbl

Table 6.22: The 2P OGIP with associated gas liberated from the oil rim for the stochastic facies-based porosity model-C.

	OGIP - 2P						
	VC00	VL05	VL11	VC20	VL22	VC20-VL22	Total 2P
Dara Main	15.5 Bcf	13.4 Bcf	4.3 Bcf	71.0 Bcf	50.2 Bcf	121.2 Bcf	154.4 Bcf
Dara #16	3.5 Bcf	2.4 Bcf	0.2 Bcf	3.9 Bcf	5.2 Bcf	9.1 Bcf	15.2 Bcf
Dara #3	2.6 Bcf	3.1 Bcf	0.3 Bcf	4.6 Bcf	5.5 Bcf	10.2 Bcf	16.2 Bcf
Dara #4/20	0.1 Bcf	0.3 Bcf	0.1 Bcf	4.6 Bcf	6.0 Bcf	10.6 Bcf	11.1 Bcf
Dara #11/25	4.2 Bcf	5.5 Bcf	0.8 Bcf	6.3 Bcf	3.9 Bcf	10.2 Bcf	20.7 Bcf
Yapeni	4.4 Bcf	2.6 Bcf	0.8 Bcf	2.9 Bcf	1.0 Bcf	3.9 Bcf	11.7 Bcf
Total	30.3 Bcf	27.3 Bcf	6.5 Bcf	93.4 Bcf	71.8 Bcf	165.2 Bcf	229.2 Bcf

Table 6.23: The 2P OOIP with associated gas liberated from the oil rim for the stochastic facies-based porosity model-C.

	OOIP - 2P			Associated Gas Bcf		
	VC20	VL22	VC20-VL22	VC20	VL22	VC20-VL22
Dara Main	15.3 Mbbl	11.9 Mbbl	27.3 Mbbl	9.6 Bcf	7.5 Bcf	17.1 Bcf
Dara #16	3.5 Mbbl	9.8 Mbbl	13.3 Mbbl	2.2 Bcf	6.1 Bcf	8.3 Bcf
Dara #3	1.6 Mbbl	2.9 Mbbl	4.5 Mbbl	1.0 Bcf	1.8 Bcf	2.8 Bcf
Dara #4/20	0.5 Mbbl	0.8 Mbbl	1.3 Mbbl	0.3 Bcf	0.5 Bcf	0.8 Bcf
Dara #11/25	9.0 Mbbl	4.7 Mbbl	13.7 Mbbl	5.6 Bcf	2.9 Bcf	8.6 Bcf
Yapeni	2.3 Mbbl	1.1 Mbbl	3.4 Mbbl	1.4 Bcf	0.7 Bcf	2.1 Bcf
Total	32.2 Mbbl	31.2 Mbbl	63.4 Mbbl	20.2 Bcf	19.5 Bcf	39.7 Bcf

Table 6.24: The 3P OGIP with associated gas liberated from the oil rim for the stochastic facies-based porosity model-C.

	OGIP - 3P						
	VC00	VL05	VL11	VC20	VL22	VC20-VL22	Total 2P
Dara Main	15.5 Bcf	14.0 Bcf	4.6 Bcf	71.0 Bcf	50.2 Bcf	121.2 Bcf	155.3 Bcf
Dara #16	3.5 Bcf	2.7 Bcf	0.5 Bcf	3.9 Bcf	5.2 Bcf	9.1 Bcf	15.8 Bcf
Dara #3	2.6 Bcf	3.4 Bcf	0.5 Bcf	4.6 Bcf	5.5 Bcf	10.2 Bcf	16.7 Bcf
Dara #4/20	0.1 Bcf	0.5 Bcf	0.1 Bcf	7.0 Bcf	2.3 Bcf	9.3 Bcf	10.0 Bcf
Dara #11/25	4.2 Bcf	6.1 Bcf	1.1 Bcf	7.9 Bcf	6.9 Bcf	14.8 Bcf	26.2 Bcf
Yapeni	4.4 Bcf	2.8 Bcf	1.0 Bcf	2.9 Bcf	1.0 Bcf	3.9 Bcf	12.1 Bcf
Total	30.3 Bcf	29.4 Bcf	7.8 Bcf	97.4 Bcf	71.1 Bcf	168.5 Bcf	236.0 Bcf

Table 6.25: The 3P OOIP with associated gas liberated from the oil rim for the stochastic facies-based porosity model-C.

	OOIP - 3P			Associated Gas Bcf		
	VC20	VL22	VC20-VL22	VC20	VL22	VC20-VL22
Dara Main	15.3 Mbbl	11.9 Mbbl	27.3 Mbbl	11.5 Bcf	9.0 Bcf	20.5 Bcf
Dara #16	3.5 Mbbl	9.8 Mbbl	13.3 Mbbl	2.6 Bcf	7.4 Bcf	10.0 Bcf
Dara #3	1.6 Mbbl	2.9 Mbbl	4.5 Mbbl	1.2 Bcf	2.2 Bcf	3.4 Bcf
Dara #4/20	0.0 Mbbl	0.0 Mbbl	0.0 Mbbl	0.0 Bcf	0.0 Bcf	0.0 Bcf
Dara #11/25	9.0 Mbbl	4.7 Mbbl	13.7 Mbbl	6.8 Bcf	3.5 Bcf	10.2 Bcf
Yapeni	2.3 Mbbl	1.1 Mbbl	3.4 Mbbl	1.7 Bcf	0.8 Bcf	2.5 Bcf
Total	31.7 Mbbl	30.4 Mbbl	62.1 Mbbl	23.8 Bcf	22.8 Bcf	46.6 Bcf

Table 6.26: Validation for hydrocarbon estimate calculated from the stochastic facies-based porosity Model-C in the VC20-VC25 reservoir interval in the DARA Main and DARA 3 areas.

Recover factors		Model Volumetric		
		1P	2P	3P
		140.5 Bcf	168.7 Bcf	174.3 Bcf
Cumulative	152.6	108.6%	90.5%	87.6%
1P Dev	168	119.6%	99.6%	96.4%
2P Dev	177	126.0%	104.9%	101.6%
3P Dev	186	132.4%	110.3%	106.7%

Table 6.26: Validation for hydrocarbon estimates calculated from the stochastic facies based-porosity Model-C in the VC20-VC25 reservoir interval in the DARA 4/20 area.

Recover factors		Model Volumetric		
		1P	2P	3P
		8.9 Bcf	11.4 Bcf	13.3 Bcf
Cumulative	15.9 Bcf	178.7%	139.7%	171.2%
1P Dev	16.6 Bcf	186.5%	145.8%	178.7%
2P Dev	16.7 Bcf	187.6%	146.7%	179.8%
3P Dev	17.0 Bcf	191.0%	149.3%	183.0%

Using Model-C, Table 6.25 shows that hydrocarbon estimates for the VC20-VC25 reservoir interval in DARA Main are compatible with existing cumulative production if situation 2P and 3P are correct. However, it is impossible to get the cumulative production from DARA 4/20 in any situation (Table 6.26).

6.3 Impact of Using Facies on Hydrocarbon Estimates

Does the use of geological models improve hydrocarbon estimates? The creation of an adequate geological model requires an understanding of the geology, which cannot be achieved without a proper reservoir characterisation study. However, these studies require the allocation of manpower and technical resources, and cost money. In some cases due to limited resources, the reservoir characterisation step may be bypassed and the project moves on estimating hydrocarbons directly. The argument for this is that the absence of geology will not significantly impact the volumetrics. The following is a case study done to address such issues and cast more light on the importance of using facies models in estimating hydrocarbons. The workflow involved the generation of a porosity model using porosity logs without any influence of geological data. Then hydrocarbons were calculated based on these data and the results were compared to those generated from the facies-based models.

6.3.1 Wells Only Porosity Model

The porosity model was built using effective porosity logs (PHIE) and the effective porosity statistical parameters for the modeled reservoir intervals are shown in Table 6.27.

Table 6.27: Statistical porosity values for effective porosity logs used to build a wells only porosity model.

Reservoir Interval	Porosity Min	Mean	Max
VC00-VL05	0	0.04	0.18
VL05-VC10	0	0.03	0.18
VC10-VL11	0	0.028	0.16
VL11-VC15	0	0.03	0.15
VC15-VC20	0	0.02	0.14
VC20-VL22	0	0.055	0.27
VL22-VC25	0	0.05	0.2
VC25-VC30	0	0.025	0.15

The same semi-variogram used to generate the facies-based porosity model was used in the log-porosity model. The semi-variogram azimuth direction was 90 degrees with the long semi-variogram radius value of 5500 metres and the short radius value of 200 metres. A Gaussian sequential simulation algorithm was used to build the porosity model and a slice through the model is shown in Figure 6.1. Because no geological knowledge was used in building this porosity model, there is no visual evidence of any channel or splay features as compared to Figure 4.9. This is expected because the simulation of porosity will depend on the values of surrounding wells only.

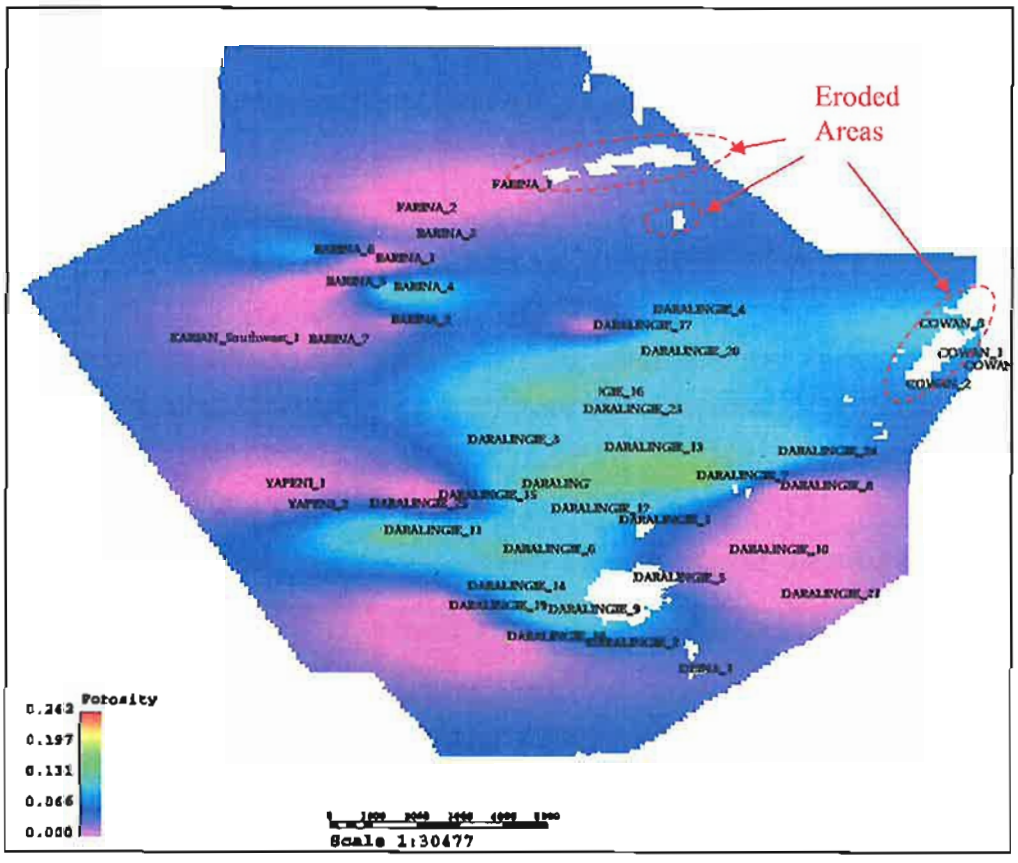

Figure 6.1: Slice through the porosity model. Note that no geological features are visible in this model.

6.3.2 Hydrocarbon Estimates and Results Analysis

For practical reasons, the hydrocarbon estimates were done for the VC20-VC25 reservoir interval in the Main Dara area only. The objective of this part of the case study was to compare the two approaches, using the Main Dara area as an example only. The hydrocarbon estimation was done in RMS as in the previous section. Since there were no facies used in this model, net-gross ratios (N/G) were used. Table 6.27 shows the Interval thickness, sand thickness and N/G for wells in the Main Daralingie area. Since there were variations in the N/G, three values were selected that represent the minimum, mean and maximum N/G as shown in Table 6.28. The hydrocarbon estimate for the 1P, 2P and 3P are shown in Table 6.29. A comparison between the Main Dara area oil and gas volume estimates from the wells-only porosity model and the facies-based porosity model is shown in Figures 6.2 and 6.3.

Table 6.27: Interval thickness, sand thickness and net gross ratios for wells in the Main Daralingie area.

Well Name	Interval Thickness (ft)	Sand Thickness (ft)	N/G %
1	54	37	68.5
5		Eroded	
6	53	10	18.9
7	61	37	60.7
8	20	0	0.0
9	98	52	53.1
12	83	26	31.3
13	54	27	50.0
14	79	28	35.4
18	91	38	41.8
19	58	10	17.2
22	69	53	76.8
23	70	38	54.3
24	44	28	63.6

Table 6.28: The three net gross ratios used to estimate hydrocarbons volumes of the wells only porosity model

N/G %	Low	Mean	High
	17.20	47.60	76.80

Table 6.29: Volumetrics results from the porosity model generated from the wells-only model.

Hydrocarbon Type		N/G %		
		17.2 (Low)	47.6 (Mean)	76.8 (High)
Oil (Mbbl)		2.46	6.81	10.99
Gas (Bcf)	1P	24.28	67.20	108.42
	2P	25.82	71.46	115.30
	3P	26.13	72.31	116.66

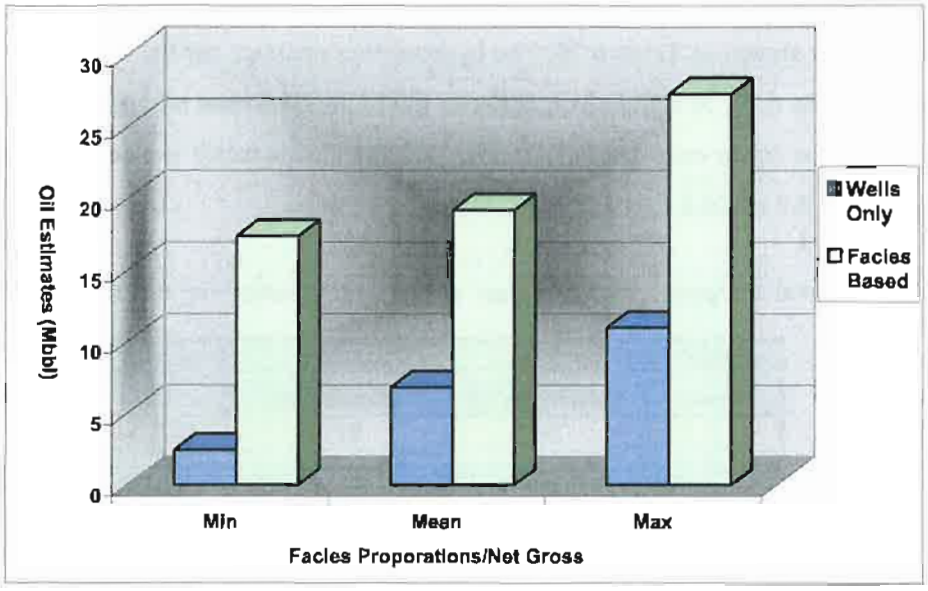

Figure 6.2: Comparison between OOIP estimated from the porosity wells-only model and the facies based porosity model for the Main Dara area. The facies based porosity model gave much better estimates because it included geological knowledge, hence modeled porosity in areas interpreted where no well coverage exists.

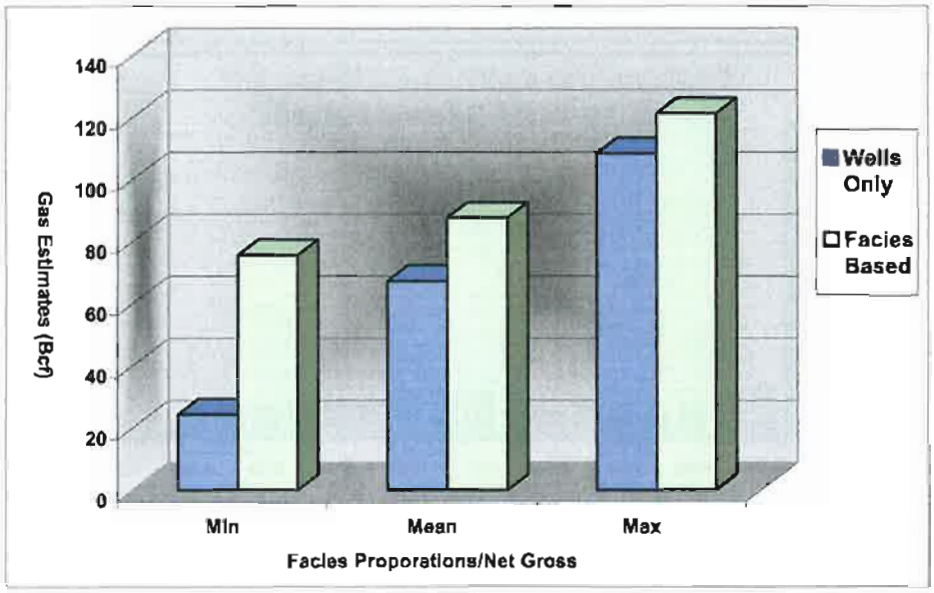

Figure 6.3: Comparison between OGIP estimated from the porosity wells-only model and the facies based porosity model. The facies based porosity model gave better estimates because it used geological knowledge, hence the modeled porosity is highly influenced by facies types.

The results showed that the use of facies data gave higher oil and gas estimates, due to the mechanism of the porosity simulation based on geological data (Fig. 6.2, 6.3). The porosity was simulated independently in each facies object in each reservoir interval. As explained earlier in Section 4.2.1, the use of a porosity histogram within the specific facies increases the probability of selecting the correct value. However, in the absence of a facies model, a single histogram could be used for the whole reservoir interval, combining porosity from channel, splay, coal and shale (Fig. 6.4).

Another point to consider is continuity of porosity. Without the facies objects, porosity continuity will be dependent on semi-variograms and values at wells. In the absence of any well data, the continuity will be estimated for the semi-variogram parameters, namely range and direction. The use of facies bodies influences porosity continuity, even in the absence of wells, because it is derived from geological understanding of the facies rather than semi-variograms. The modeling algorithm in Roxar RMS tends to connect porosity in the same facies body by using semi-variograms as a guide. For these reasons, the use of facies models is very important and improves hydrocarbon estimates, as illustrated by this case study.

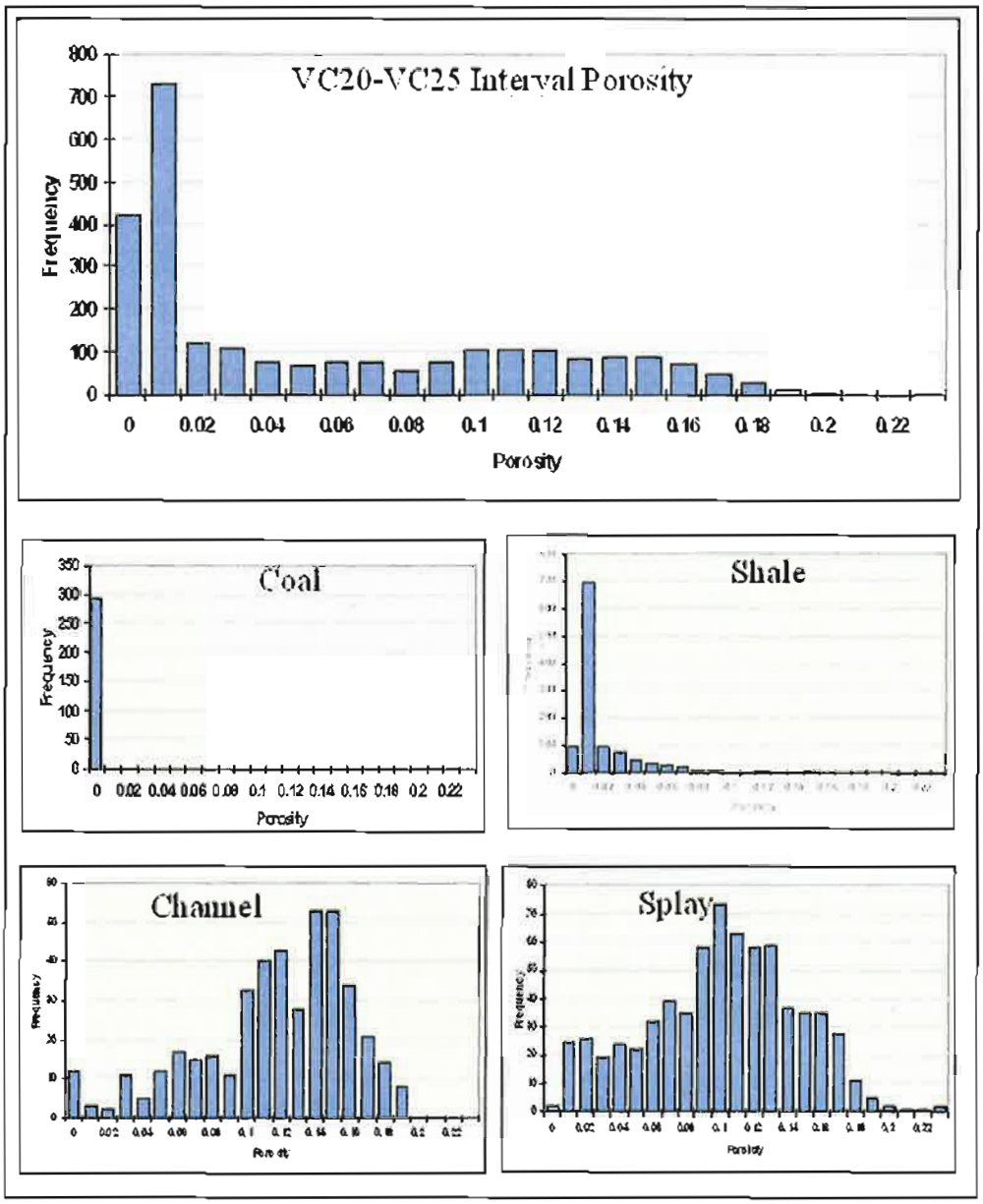

Figure 6.4: Porosity histograms for VC20-VC25 interval; the total interval porosity does not have any signatures of the facies that exist in the interval. The use of one composite histogram will lead to porosity spatial and vertical simulation that is not related to the geological features.

Chapter 7

Uncertainty Assessment of Hydrocarbon Estimates

7.1 Introduction

Uncertainty assessment is a crucial step in any volumetric study. Uncertainty exists in all variables used to estimate OHIP. The estimates calculated in Chapter 6 were highly dependent on facies proportions; therefore uncertainty in facies proportions as well as other input parameters are studied in great detail here.

The assessment of uncertainty in hydrocarbon estimates, derived from facies proportions, can be accomplished through running hundreds of stochastic facies models and estimating their hydrocarbon volumes. The end results would be a distribution of hydrocarbon estimates that can be related to the variation in facies proportions. By analysing this distribution, the impact of facies proportions on the hydrocarbon estimate can be evaluated. This is a very time-consuming process. For example, in the case of Daralingie Field, building a single stochastic porosity and facies model, followed by calculating hydrocarbon estimates, would take on average one day to complete. Another faster alternative is the use of Monte Carlo simulation methods to get the desired results without running many models (Cosentino, 2001; Garb, 1988). However, the conventional Monte Carlo simulation method does not take into account the facies proportions as mentioned in Section 5.2.1. A novel method is developed here to overcome this issue. The basic principle of this method is to use facies volumes extracted from the three different stochastic facies models as input into the Monte Carol simulation algorithm. This method is covered in more detail in Section 7.3.

In the following sections a conventional Monte Carlo approach is used to assess uncertainty, as practiced in the oil industry. Following this, a newly developed method that combines stochastic facies modeling and Monte Carlo simulation is used to assess

uncertainty related to facies proportions in hydrocarbon estimates. The two main reservoir intervals, VC20-VL22 and VL22-VC25, within the Main Dara area were selected for this part of the study (Fig. 7.1). These two reservoir intervals within the Main Dara area have sufficient reservoir heterogeneity to represent the whole reservoir complexity found in throughout the Daralingie Field.

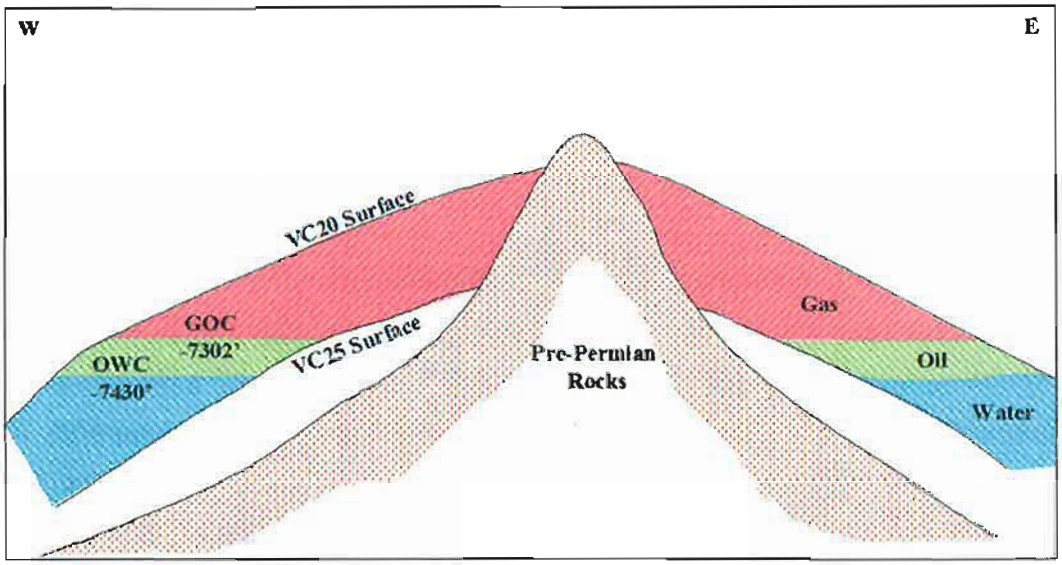

Figure 7.1: A simplistic east-west cross-section through the Main Dara showing the different fluid contacts and the missing section in the VC20-VC25 reservoir interval.

The Monte Carlo simulations were run by using @Risk version 4.5, which is a Microsoft Excel spreadsheet add-in. The results from the Monte Carlo simulations were compared with hydrocarbon estimates from the three stochastic facies models shown in Table 7.1.

Table 7.1: Stochastic facies model OHIP estimates for different facies proportions (Chapter 4).

Hydrocarbon Type		Facies Proportions		
		Minimum	Mean	Maximum
Oil (BBL)		17.4 MMbbl	19.2 MMbbl	27.3 MMbbl
Gas (SCF)	1P	75.5 Bcf	87.6 Bcf	121.2 Bcf
	2P	86.4 Bcf	99.6 Bcf	138.3 Bcf
	3P	88.6 Bcf	102.0 Bcf	141.7 Bcf

7.2 Monte Carlo Simulation

The process of Monte Carlo simulation consists of several steps. The first step, and the most important step, is experimental design. In this step, the key input variables, the sequences of the study and the results analysis methods are defined. This is followed by the selection of an appropriate distribution for each input parameter and running the simulation process. The final step is the analysis of the simulation results.

7.2.1 Experimental Design

In any experimental design there is a need for an elaborated design to ensure the coverage of most, if not all, possibilities of alternative relationships. Furthermore, the experiment design should help in the search for relationships as opposed to simply describing the results. If a specific condition has changed in the experiment between inputs, then results are expected to reflect this effect. Therefore, in designing a Monte Carlo simulation plan, several important points need to be addressed carefully. These points are discussed individually in the following parts.

Random Number Selections and Number of Iterations

The success of any experiment depends on the repeatability of results with a certain degree of error and this is what Monte Carlo Simulation can achieve. Since Monte Carlo simulation is an iterative process and dependent on the generation of a random number, then the quality of the results depend on the number of iterations and random numbers selected. To avoid selecting a different random number in each simulation, a constant random number value of one was used throughout this study.

To optimise the number of iterations, several simulations were run with different iteration numbers. The results of each simulation were analysed for changes in the distribution shape and changes in the P10, the P50 and the P90 hydrocarbon estimates.

Input Distribution Shape

One of the many advantages of using Monte Carlo Simulation is its ability to use a range of values instead of a single value. Each input variable has a range of values with an appropriate probability of occurrence. There are three main sources of distributions: fundamental principles, expert opinions and historical data. The fundamental principles help in expecting the distribution shape for an input variable. For example, the oil or gas field size which is a product of net gross, field area and recovery factor, is expected to be log normal as a consequence of the Central Limit Theorem (CLT) (Murtha, 1994). The CLT in statistics states that multiplication of several distributions will result in a lognormal distribution and the addition of several distributions will result in a normal distribution (Murtha, 2002).

Expert opinion is another source for input distribution. However, this method is subjective because it depends on experience. A geoscientist accustomed to working in sandstone reservoirs that have a normal distribution may tend to use the same background knowledge in a newly discovered carbonate reservoir. Therefore, alternative distributions should be used only when expert opinion is available. Historical data is a very important and a powerful type of distribution if data quantity and quality are good. There are several sources for historical data such as corporate databases and published literature (Montgomery and Morgan, 1998; Murtha, 1994). In this part of the study different distribution types for input variables were used based on expert opinion, published literature and historical data.

Sampling Method

There are several methods to randomly pick data from distributions. In this study the Latin Hypercube method was selected. Latin hypercube sampling is a recent development in sampling technology designed to accurately recreate the input distribution through sampling in fewer iterations when compared with the conventional Monte Carlo sampling method (@Risk, 2004). The key to Latin hypercube sampling is stratification of the input probability distributions. Stratification divides the cumulative curve into equal intervals

on the cumulative probability scale (0 to 1.0). A sample is then randomly taken from each interval of the input distribution. Once a sample is taken from a particular stratification, it will not be sampled from again. Therefore, sampling is forced to represent values in each interval and accurately reflects the distribution of the input values. Latin Hypercube offers great benefits in terms of increased sampling efficiency and faster runtimes (Startzman and Wattenbarger, 1985).

Source of Input Data

The main input variables in Monte Carlo simulation are porosity, water saturation, formation volume factor, net-gross ratio (N/G) and gross rock volume (GRV). Some of the input variables, such as porosity and water saturation, were taken from the upscaled well logs used in building the porosity stochastic model (Chapter 4). This was necessary for comparison of hydrocarbon estimates from Monte Carlo Simulation with those estimates from the stochastic model. As explained in Section 4.3, the raw porosity logs were upscaled for use in porosity modeling. The upscaled logs were biased to the dominant facies type and they were very close to the raw logs. If raw logs were used instead of upscaled logs, an unmeasurable bias may be introduced in the results and stochastic model hydrocarbon estimates cannot be correlated to Monte Carlo estimates.

The oil and gas formation volume factors were provided and used as a single value in the previous estimates. Three error factors of $\pm$10%, $\pm$20% and $\pm$30% were used to investigate their uncertainty on the final hydrocarbon estimates. Due to the complex nature of the reservoir as the result of erosion and faulting, the GRV was calculated in RMS. Two GRV values were calculated within the Main Dara, one for the gas zone and the other for the oil zone (Fig. 7.1). The GRV of the gas zone is bounded by the following surfaces: top VC20, base VC25, gas oil contact and the top Pre-Permian unconformity. The GRV of the oil zone is bounded by top VC20, base VC25, gas oil contact, oil water contact and the top Pre-Permian unconformity.

Dependency Between Input Parameters

The outcome of the Monte Carlo Simulation is highly dependent on input parameters and their dependency, and ignoring this fact may lead to erroneous hydrocarbon estimates (Cronquist, 2001; Garb, 1988; Murtha, 1994). The dependency between the input parameters could range from 100% positive dependency to 100% negative dependency. The determination of dependency can be done by cross-plotting the two parameters on a graph and analysing the trend in the plot (Fig. 7.2). Dependent variables have a strong trend whereas independent variables result in a scatter (Garb, 1988). If a relationship exists, then the correlation between them should be calculated and used in the Monte Carlo simulator.

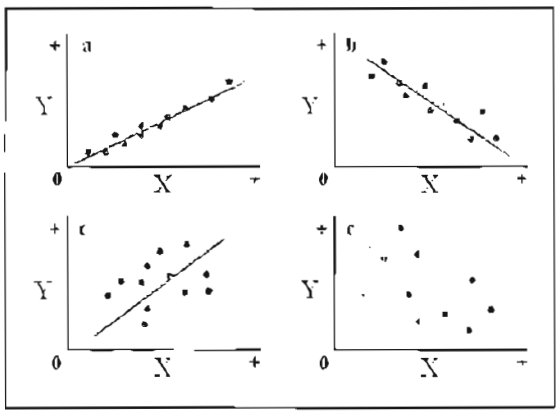

Figure 7.2: Four different types of possible dependency between variables X and Y- a) strong positive, b) strong negative, c) moderate positive, and d) no dependency.

Dependency may exist between three pairs: net pay and area; recovery factor and net pay; and porosity and water saturation (Cronquist, 2001). In some cases dependency between input parameters may change totally from one field to another. For example, net pay and porosity display a positive correlation in one reservoir and negative correlation in another reservoir (Garb, 1988). Therefore, the dependency between input parameters should be approached with an open mind without presumptions.

Results Presentation and Ranking

The Monte Carlo simulation generated a histogram distribution for each case built in this study. The histograms were transferred into cumulative density function curves that were converted to hydrocarbon expectation curves (Fig. 7.3). This was done to follow the oil industry practice of reporting the probabilistic estimates with the appropriate confidence taken from expectancy curves (Behrenbruch, 2005). For each case, the P10, P50 and P90 are reported in a tabular form. The P90 means that there is 90% confidence that there will be this hydrocarbon amount or more, and the same for P50 and P10. In some classification systems P90 is equivalent to P1 and in other systems P90 is equivalent to approved. The issue of different definitions has been addressed in Section 5.1. This study follows the SPE/WPC/AAPG 2000 reserve and resources classifications (Cronquist, 2001).

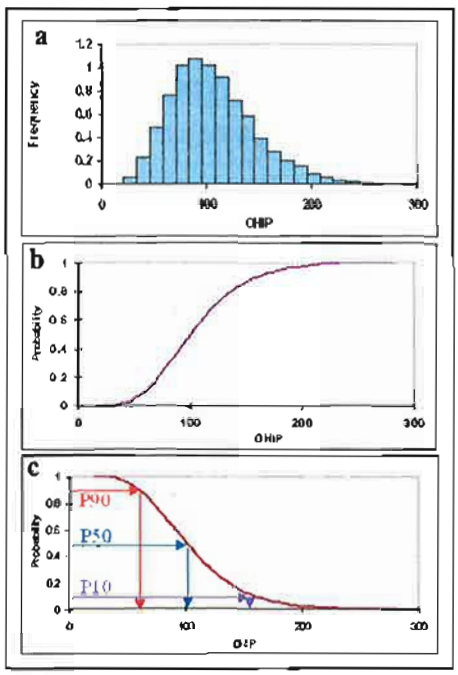

Figure 7.3: Hydrocarbon estimates graphical presentation. a) frequency distribution of the OHIP estimates, b) cumulative probabilities of the OHIP estimates, c) expectancy OHIP estimate curve from which the P10, P50 and P90 are taken.

The industry practice ranks probabilistic reserves by using a (P10-P90)/P50 formula. Estimates with low ratios are expected to have less uncertainty than estimates with higher ratios. However, the accuracy of this result depends on the shape of the distribution. A better measure would be to use the Coefficient Of Variance (COV), which is a ratio between the standard deviation value and the mean value (Macary et al., 1999). It is useful to review the formulas for the mean, standard deviation and COV.

Mean (μ) = $\frac{1}{n}\sum_{i=1}^{n} x_i$, where n is the number of samples

Standard Deviation (δ) = $\sqrt{\frac{\sum x_i^2 - n\mu^2}{n}}$, where μ is the mean

COV = $\frac{\delta}{\mu}$

The COV is very useful in comparing the variability of several distributions. Basically, a low COV implies lower variability and lower uncertainty (Kazmier, 1996). In this study both ranking methods were used and compared for their effectiveness as a ranking tool.

7.2.2 Input Parameters

The simplest equation to estimate original hydrocarbon in place is as follow (Cosentino, 2001):

OHIP = GRV * N/G * ϕ * (1-Sw)/FVF, where:

GRV	Gross Rock Volume
N/G	Net gross ratio, fraction
ϕ	Porosity, fraction
Sw	Water Saturation, fraction
FVF	Formation Volume Factor, fraction

In typical Monte Carlo simulation, the needed parameters are estimated from well data and fitted with an appropriate distribution. In this study, N/G, porosity and water saturation were taken from the upscaled well logs in the Dara Main area as shown in Table 7.2. The GRV was calculated in RMS software as described in the previous section

and the results are shown in Table 7.3. The values of FVF for oil (Bo) and for gas (Bg) were 0.00558 and 1.675 respectively.

Table 7.2: Summary of petrophysical properties for all wells in the Main Dara area.

Well	Interval	Sand	N/G	Porosity			Water Saturation		
Name	Thickness (ft)	Thickness (ft)	%	Low	Mean	High	Low	Mean	High
1	54	37	68.5	No Logs					
5			Eroded						
6	53	10	18.9	0.033	0.098	0.146	0.21	0.51	0.81
7	61	37	60.7	0.042	0.091	0.183	0.11	0.46	0.80
8*	20	0	0.0	Non Pay Interval					
9	98	52	53.1	0.066	0.164	0.262	0.10	0.41	0.72
12	83	26	31.3	0.055	0.117	0.180	0.12	0.43	0.74
13	54	27	50.0	0.070	0.130	0.190	0.12	0.35	0.58
14	79	28	35.4	0.056	0.124	0.191	0.14	0.37	0.60
18	91	38	41.8	0.065	0.120	0.175	0.19	0.42	0.64
19	58	10	17.2	0.040	0.088	0.135	0.58	0.76	0.93
22	69	53	76.8	0.033	0.102	0.172	0.44	0.60	0.75
23	70	38	54.3	0.020	0.098	0.177	0.27	0.57	0.87
24	44	28	63.6	0.073	0.102	0.131	0.27	0.54	0.80

* N/G value of Daralingie-8 was not used in this study because the reservoir is eroded

Table 7.3: Gross rock volume for rocks containing gas and oil in the Main Dara Area in the Daralingie Field.

	Gross Rock Volume (m^3)
Gas	483,242,157
Oil	101,810,834

Having gathered the input data, the next step is to investigate the dependency between the input parameters. This is done by cross plotting the following pairs: porosity with water saturation, N/G with mean porosity, and N/G with mean water saturation (Figs. 7.4 to 7.6). The correlation coefficient was calculated by using the following equations:

Correlation Coefficient (cc) = $\frac{COV(X,Y)}{\delta_x * \delta_y}$, where COV is the coefficient of variance between array X and array Y, δ_x is the standard deviation for array X and δ_y the standard deviation for array X.

COV (X, Y) = $\frac{1}{n}\sum_{i=1}^{n}(x_i - \mu_x)(y_i - \mu_y)$, where n is the number of samples in array X and Y, μ_x is the mean of array X and μ_y is the mean of array Y.

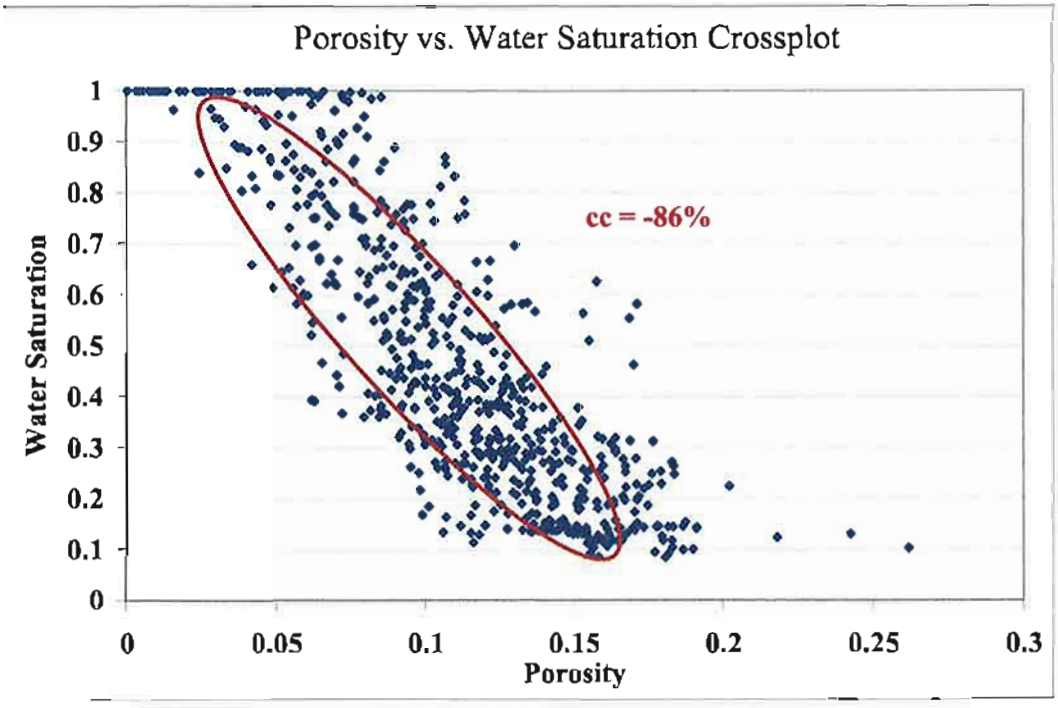

Figure 7.4: Crossplot between porosity and water saturation for wells in the Main Dara area in the VC20-VC25 reservoir interval showing a strongly negative correlation.

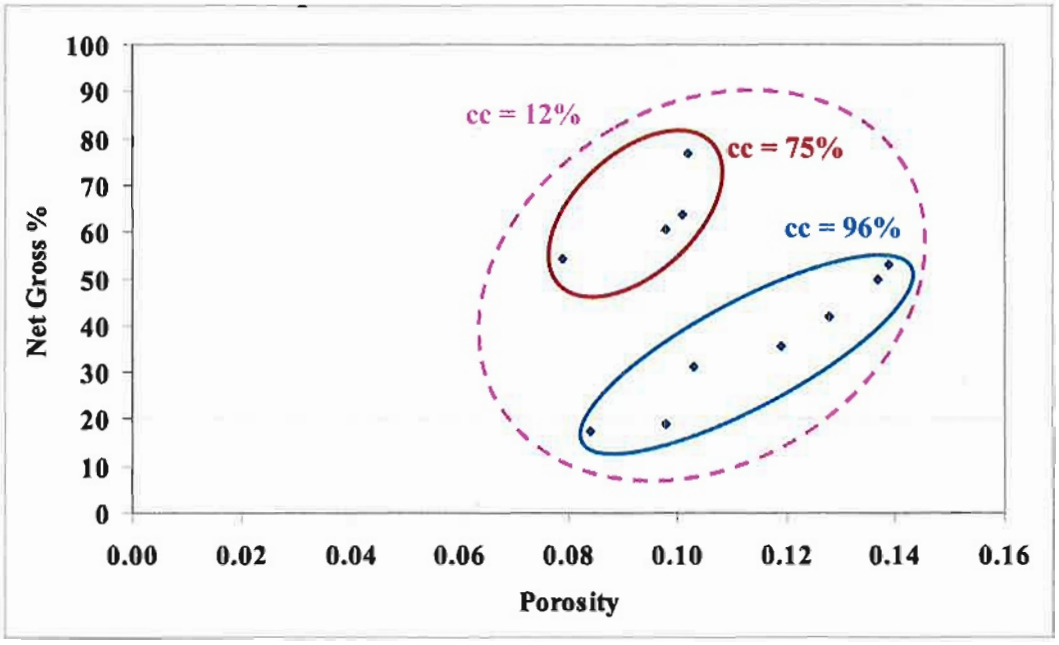

Figure 7.5: Crossplot between mean porosity value and N/G per well; the correlation coefficient for all points is equal to 12%, but it can be divided into two trends with cc of 75% and 96%.

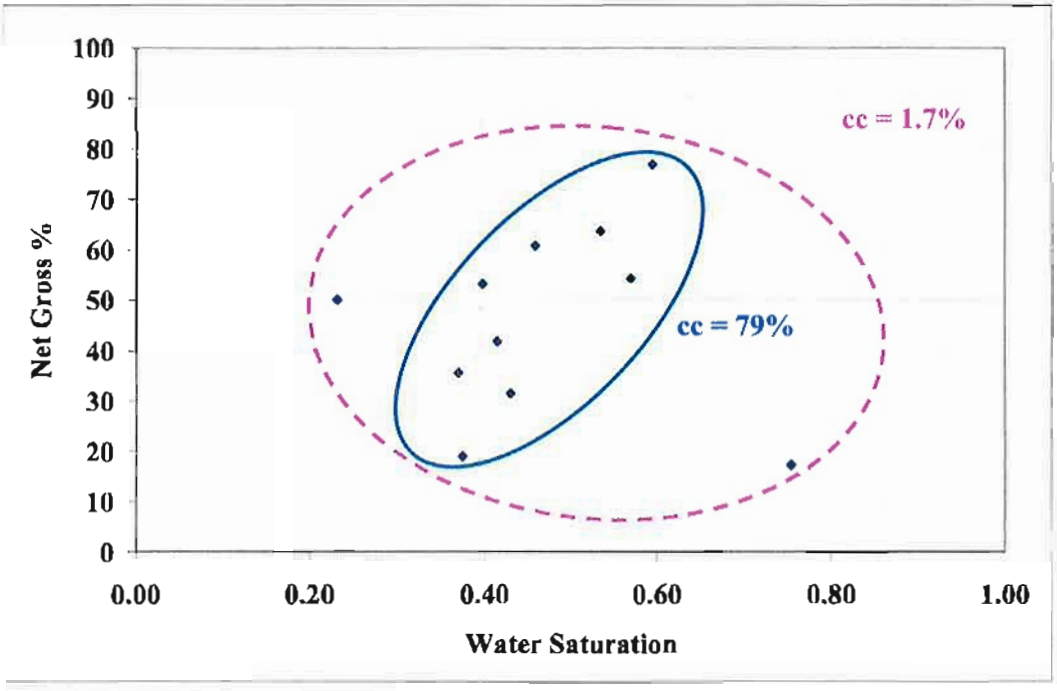

Figure 7.6: Crossplot between mean water saturation value and N/G per well showing a very low correlation coefficient of 1.7%; however if the outlier is excluded the correlation coefficient rises to 79%

In Figure 7.4 the porosity and water saturation crossplot shows a strong negative correlation of -86%. This is the result of the capillary pressure effect. Lower porosity values mean small pore throat that leads to high capillary pressures that hold the water. Geologically speaking, low porosity may result from poorly sorted grains or high compactions. In Daralingie Field there is no evidence of very high compaction, therefore the low porosity is the result of poorly sorted grains. In channel systems, poorly sorted grains occur at the top of the channel fills, which explains the high water saturation streaks in the upper parts of the channels.

The second crossplot between mean porosity value and N/G (Fig. 7.5) shows that the overall correlation coefficient for all points are very low, but the crossplot show two clear and almost parallel trends. The upper trend has a correlation coefficient of 75% and the lower has 96%. The correlation coefficient measures the overall trend of the data, but if the data has two different trends, the correlation coefficient equation will not give a representative value as illustrated by this case. The geological reason for these two trends is that each trend may represent different facies types such as splays verse channels. It could also reflect the geological nature of two different channels. Both of the trends show that there is an increase in porosity as the N/G increases which is a very useful relationship. In Monte Carlo simulation only one correlation coefficient can be used, therefore an average of the two will be used, which is 86%.

The crossplot between mean water saturation value and N/G (Fig. 7.6) shows a very low correlation coefficient of 1.7% throughout. However, if the outliers were excluded, then the correlation coefficient rises to 79%. Both crossplots of porosity versus net gross and water saturation versus net-gross, show that relaying of the correlation coefficient number estimates without visually investigating the plots may be misleading. Hence the visual examination of the cross-plots is necessary.

The porosity versus water saturation plot (Fig. 7.4) has higher density compared to the other two plots (Figs. 7.5; 7.6) due to plotting the upscaled log values for all wells. In Figures 7.5 and 7.6 there is only one net-gross value per well that was plotted against the

mean values of porosity and water saturation, which limit the number of data points to the number of wells in the Main Dara area.

There are different methods to select distribution shape and value ranges for the input parameters. In this study, several methods were used: triangle, normal, lognormal and fitted; which resulted in twelve different cases. Table 4 show the different cases, which were simulated in this study.

Table 7.4: Different cases that were simulated in this study.

Case	N/G %				Porosity %				Water Saturation %				Dependency
Number	L	M	H	Distribution	L	M	H	Distribution	L	M	H	Distribution	
1	17.2	44	76	Triangle	5	10.8	17.6	Triangle	30	30	30	Discrete	No
2	17.2	44	76	Triangle	5	10.8	17.6	Triangle	23.2	46.7	75	Triangle	No
3	17.2	44	76	Log Normal	5	10.8	17.6	Log Normal	23.2	46.7	75	Log Normal	No
4	17.2	44	76	Normal	5	10.8	17.6	Normal	23.2	46.7	75	Normal	No
5	17.2	44	76	Triangle	2	10.8	26.2	Triangle	10	46.7	93	Triangle	No
6	17.2	44	76	Log Normal	2	10.8	26.2	Log Normal	10	46.7	93	Log Normal	No
7	17.2	44	76	Normal	2	10.8	26.2	Normal	10	46.7	93	Normal	No
8	17.2	44	76	Triangle	5	10.8	17.6	Triangle	23.2	46.7	75	Triangle	Yes
9	17.2	44	76	Log Normal	5	10.8	17.6	Log Normal	23.2	46.7	75	Log Normal	Yes
10	17.2	44	76	Normal	5	10.8	17.6	Normal	23.2	46.7	75	Normal	Yes
11	17.2	44	76	Triangle	8.8	12.6	16.4	Fitted	37	56.5	76	Fitted	No
12	17.2	44	76	Triangle	8.8	12.6	16.4	Fitted	37	56.5	76	Fitted	Yes

The low, mean and high values are enough to fit the triangle distribution, but the normal and lognormal distributions need to have mean (μ) values and a standard deviation (δ). The μ and the δ were approximated using the following equations taken from (Murtha, 2002):

$$\mu = \frac{L + M + H}{3}$$

$$\text{Variance } (\delta^2) = \frac{(L^2 + M^2 + H^2 - LM - LH - MH)}{18}$$

$$\delta = \sqrt{\delta^2}$$

In the first case triangle distribution was used for N/G and porosity and a single value used for water saturation, which was 30%. This case is designed to mimic the hydrocarbon estimates by the stochastic model. When selecting values to fit a distribution, such as for porosity, the mean of low values can be taken as the low estimate. Alternatively, the lowest value can be taken as the low estimate. The same applies to the high value, in which case either the mean or the highest value can be taken. Therefore cases 2 to 4 and cases 5 to 7 were designed to test the impact of selecting extreme values versus mean values.

The input data can be modeled by using different distribution shapes, such as normal, lognormal and triangle. The statistical distribution parameters for the normal, the lognormal and the triangle can be found in Appendix 6. Cases 2 to 4 were designed with the same input parameter ranges but with different distribution types. Cases 8 to 10 are designed to investigate the effect of dependency between the input parameters as compared to cases 2 to 4 which do not have dependency. It is expected that the negative dependency between porosity and water saturation would help in increasing the mean and decreasing the standard deviation of the estimates. This should lead to a decrease in the uncertainty of the hydrocarbon estimates.

Cases 11 and 12 have a special design. The distribution shape is fitted according to the data distribution and the range is estimated by using the mean value. This is accomplished by plotting a histogram showing the distribution of the input variables, such as porosity or water saturation, and plotting the mean value of each well. Next this distribution is fitted with an appropriate distribution using an @RISK fitting algorithm (Figs. 7.7; 7.8). The range of the newly generated distributions is cut from both ends based on the minimum and maximum mean well values. The water saturation is fitted to a lognormal distribution and the porosity is fitted with a logistic distribution (full statistical details for this distribution is attached in Appendix 6.) This addresses the question of what is the chance of having one of the extreme values of a distribution everywhere in the reservoir. The rationale for this is that extreme values do not represent the reservoir.

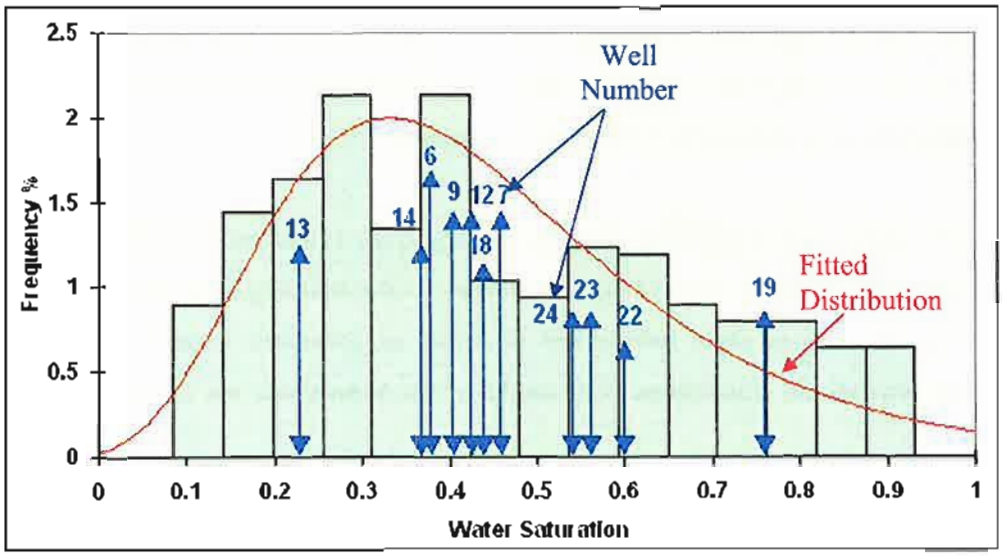

Figure 7.7: Distribution of water saturation values in the Main Dara area with the mean value at each well overlaid. The red line represents the newly fitted distribution using @RISK.

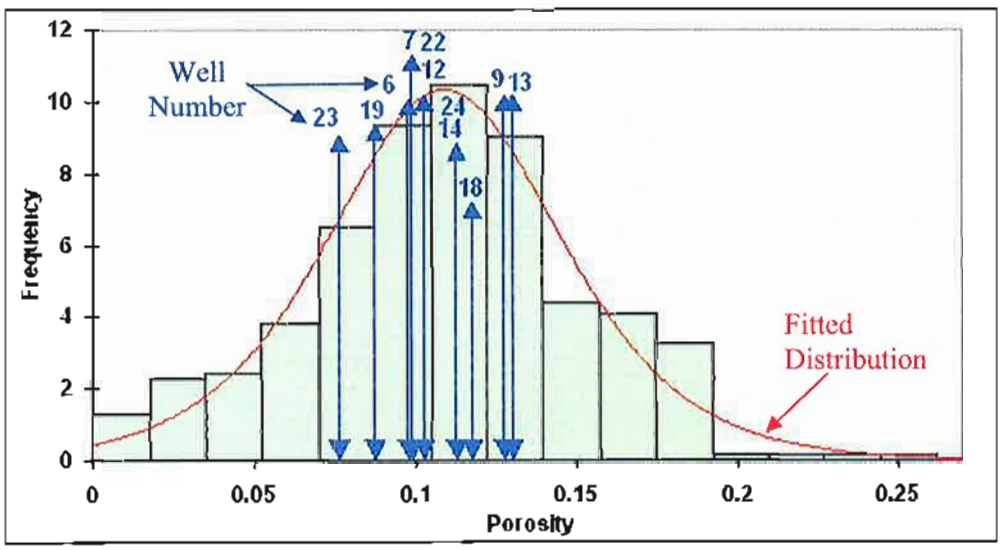

Figure 7.8: Distribution of porosity values in the Main Dara area with the mean value at each well overlaid. The red line represents the newly fitted distribution using @RISK.

Will the porosity be 26.2% porosity everywhere in the reservoir? The answer is no because there are recorded values above or below both extreme ends of the distribution. These numbers should not be used in Monte Carlo simulation, because they will result in the generation of an impossible hydrocarbon estimate.

Case 11 and 12 were designed to test dependency. Case 11 has no dependency between the input parameter while case 12 has dependency. After building these twelve cases, the next step was to run some simulations to select an optimised iteration number and afterward run all the simulations. The results of the simulations are covered in section 7.2.3.

Units and Conversion Factors

The units and conversion factors used in this Monte Carlo simulation study are as follows:

Reservoir Volume is calculated in meters cubed (m^3)
One-meter = 3.28 feet (ft)
One-meter cube (m^3) = 6.28 standard oil barrel (bbl)
One-meter cube (m^3) = 35.28 standard cubic feet (cf)
Mbbl = one million standard oil barrels
Bcf = One billion standard cubic feet

7.2.3 Simulation Results

The first step in the simulation was to optimise the iterations number. This task was accomplished by simulating case 2 with different iteration numbers. Figure 7.9 shows the distribution for each number of iterations. At 5,000 iterations and above the shape of the distribution remains constant. The visual investigation suggests that 5,000 iterations are sufficient to sample the entire range of the input parameters. It is significant that although all of the input parameters in case 2 have triangle distribution, the outcome is a lognormal distribution. This illustrates the Cental Limit Theorem (CLT) principle that the product of distributions will approach a lognormal distribution (Murtha, 2002).

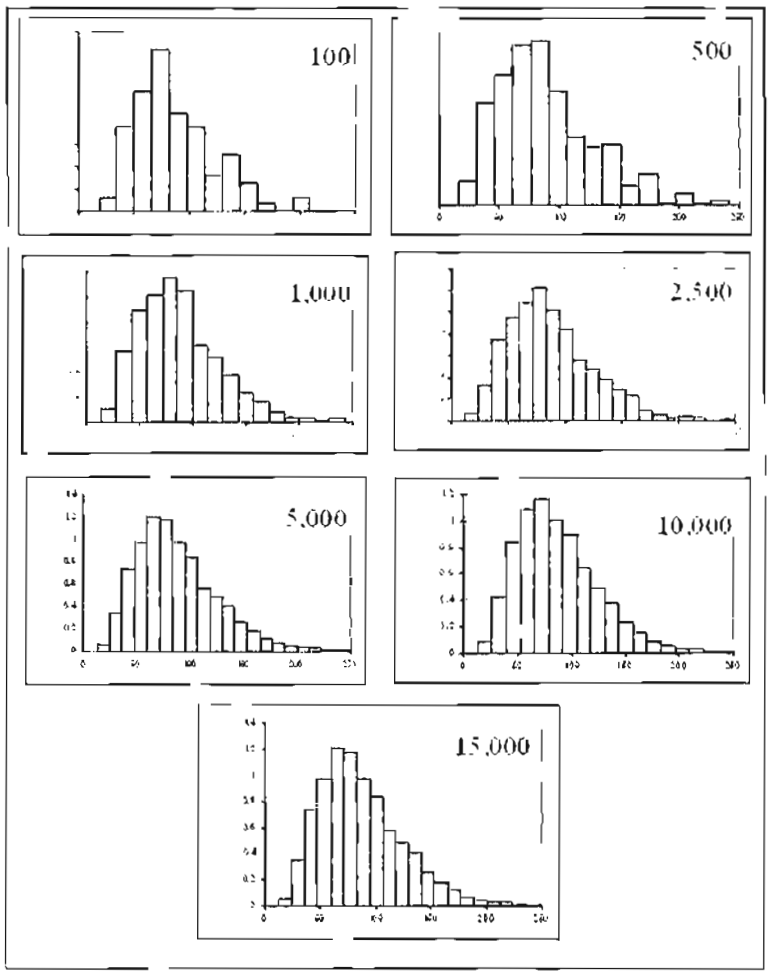

Figure 7.9: Monte Carlo simulation of case-2 using different iteration numbers. After 5,000 iterations the distribution shape does not change.

To confirm that the 5,000 iterations were suitable, the P90, the P50 and the P10 from each simulation were plotted to investigate their stability (Fig. 7.10). In all iterations the P90 and the P50 remained almost constant, but the P10 fluctuated and stabilised after 5,000 iterations. Based on the visual and the statistical investigation, 5,000 iterations were considered adequate to sample the entire input range and produce reliable results. Therefore, the 5,000 iterations number was used in the remaining part of this study.

The next step was to investigate the uncertainty in oil and gas formation volume factor (Bo and Bg). In the early part of this study, single values were provided respectively with no measure of uncertainty. The Bo and Bg were simulated with an error factor of ±10%, ±20% and ±30% using a triangle distribution. The results for each simulation run were analysed by a tornado chart to investigate their uncertainty impact on the results (Fig. 7.11). The Bg is ranked the least input affecting the uncertainty of the gas estimates. Figure 12 shows the impact of different error ranges on gas volume estimates for case 2. Minor changes are observed in the P10 and the P50, however the P90 slightly increased as the error range increased. The same analysis was performed on Bo and the results are shown in Figures 7.13 and 7.14. The Bo impact on the oil volume estimation is very similar to Bg. The tornado charts show that Bo is the least input affecting the oil volume uncertainty and results in only minor changes in the P10, the P50 and the P90 estimates.

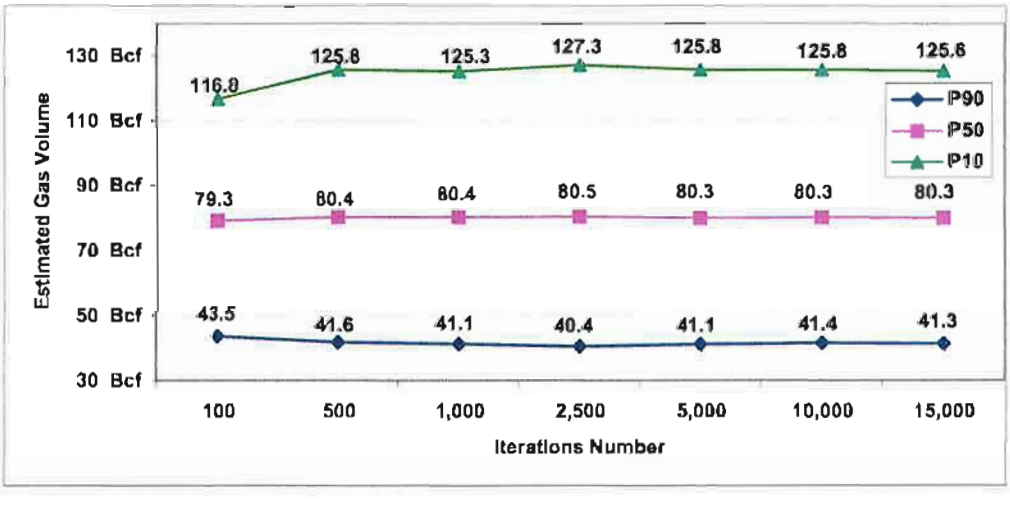

Figure 7.10: Plot of the P10, the P50 and the P90 values with their corresponding iteration number. After the 5,000 iterations all estimates almost remain constant.

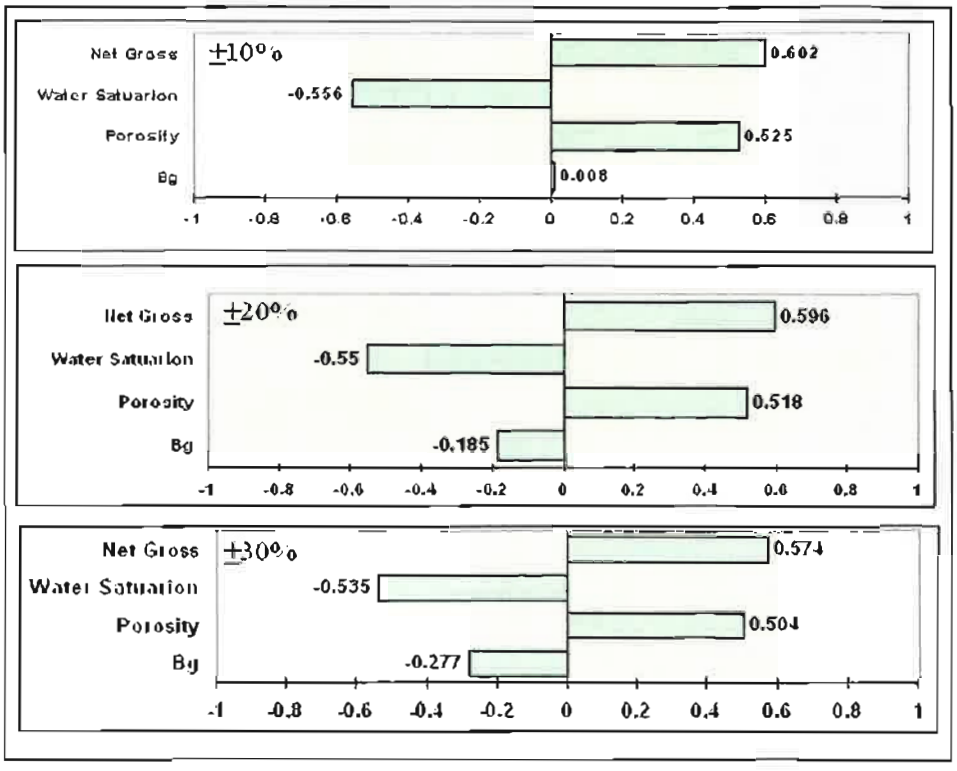

Figure 7.11: Sensitivity analysis for different error ranges in Bg. At ±10% there is very low impact on the gas volume estimates and a higher impact is noticed at level ±30%.

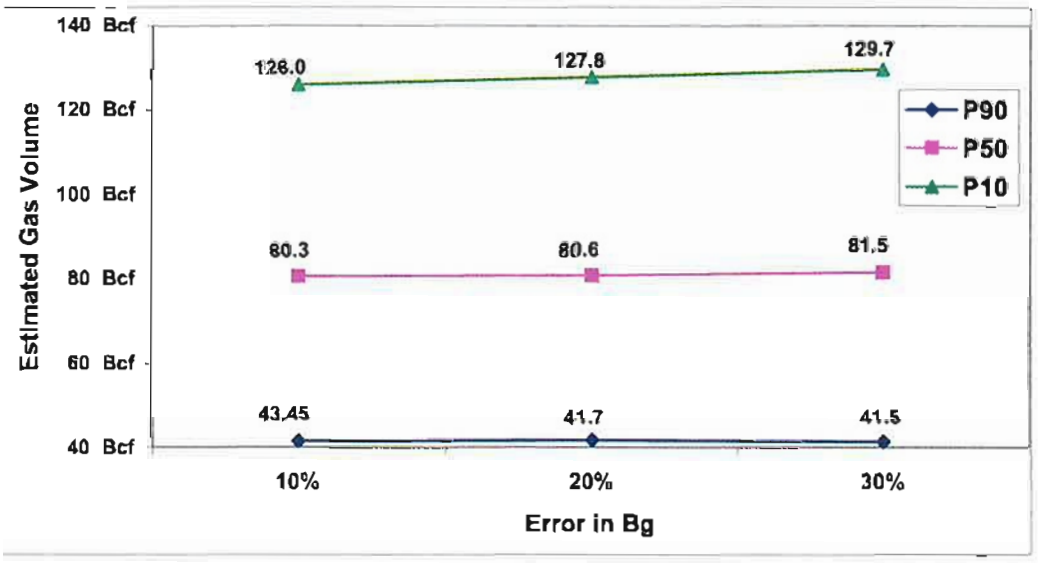

Figure 7.12: The impact of error range in Bg on gas volume estimates for case 2 generated using the Monte Carlo simulation method. There is minor change in the P10 and the P50, however the P90 has slightly increased as the error range increased.

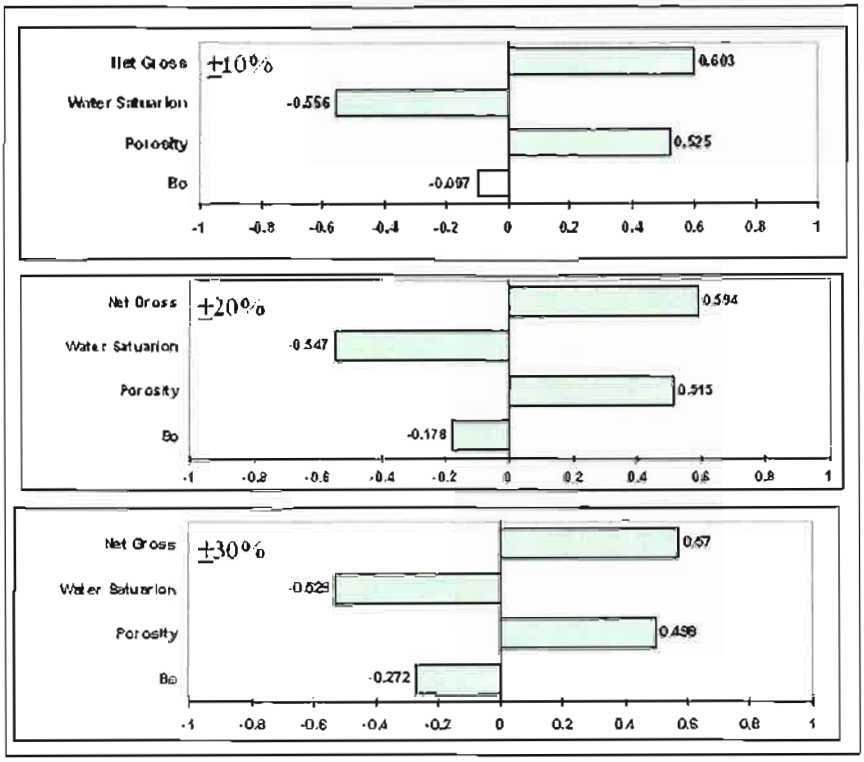

Figure 7.13: Sensitivity analysis for different error ranges in Bo. At ±10% there is a very low impact on the oil volume estimates and higher impact is noticed at level ±30%.

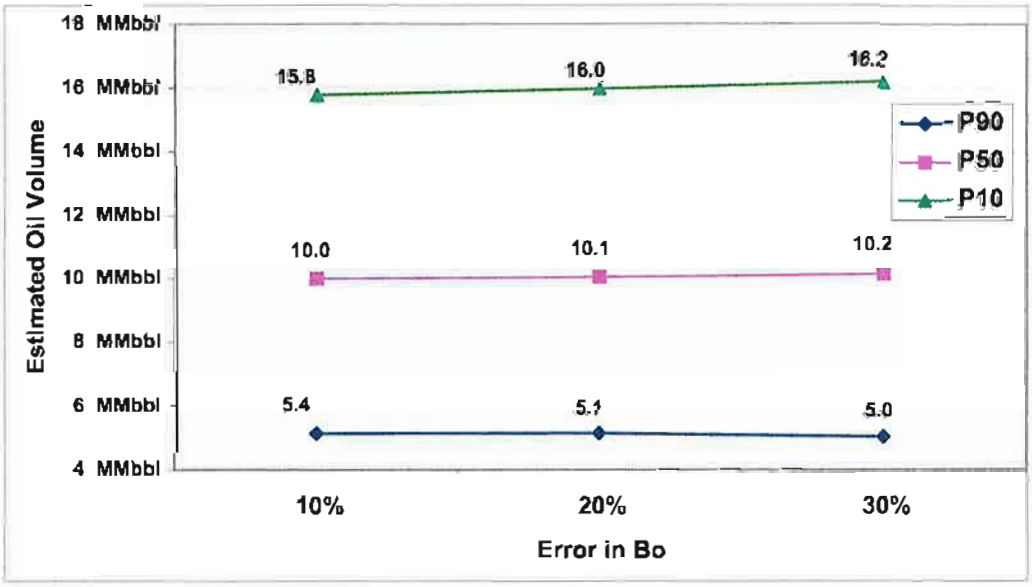

Figure 7.14: The impact of error range in Bo on oil volume estimates for case-2 generated using the Monte Carlo simulation method. There is minor change in the P10, the P50 and the P90 as the error range increases.

An error range of +10% FVF has no effect on the hydrocarbon estimates and it is highly unlikely that the error range in volume factor would be higher than that. Also they were ranked as the lowest input affecting the uncertainty of the hydrocarbon estimates. It is a good practice in any uncertainty analysis study to isolate the variables with least uncertainty. For practical reasons, a single value for Bo and Bg is used in simulating the twelve cases designed in Section 7.2. The simulated hydrocarbon estimates are shown in Tables 7.5 and 7.6. All the results are plotted with estimates from the stochastic model method overlaid for visual comparison in Figures 7.15 to 7.16.

Table 7.5: Initial gas in place estimates, generated using the Monte Carlo simulation method, for the twelve cases listed in Table 4.

Case		Estimates (Bcf)		Ranking	
Number	P90	P50	P10	(P10-P90)/P50	COV
1	61.57	104.72	161.47	0.95	0.359
2	41.34	75.46	126.87	1.13	0.422
3	41.78	71.73	117.15	1.05	0.398
4	43.08	76.81	123.55	1.05	0.395
5	31.06	79.68	166.73	1.70	0.607
6	29.40	66.09	135.70	1.61	0.598
7	29.29	72.64	149.90	1.66	0.592
8	41.83	75.32	126.00	1.12	0.415
9	42.37	71.68	116.43	1.03	0.394
10	42.89	76.67	122.70	1.04	0.396
11	55.85	93.83	147.56	0.98	0.367
12	56.12	94.32	147.15	0.97	0.361

Table 7.6: Initial oil in place estimates for the twelve cases listed in Table 4.

Case		**Estimates (MMbbl)**		**Ranking**	
Number	P90	P50	P10	(P10-P90)/P50	COV
1	7.69	13.08	20.17	0.95	0.359
2	5.16	9.43	15.85	1.13	0.422
3	5.22	8.96	14.63	1.05	0.398
4	5.38	9.59	15.43	1.05	0.395
5	3.88	9.95	20.83	1.70	0.607
6	3.67	8.26	16.95	1.61	0.598
7	3.66	9.07	18.72	1.66	0.592
8	5.23	9.45	15.64	1.10	0.416
9	5.29	8.95	14.54	1.03	0.394
10	5.36	9.58	15.33	1.04	0.396
11	6.98	11.72	18.43	0.98	0.367
12	7.01	11.78	18.38	0.97	0.361

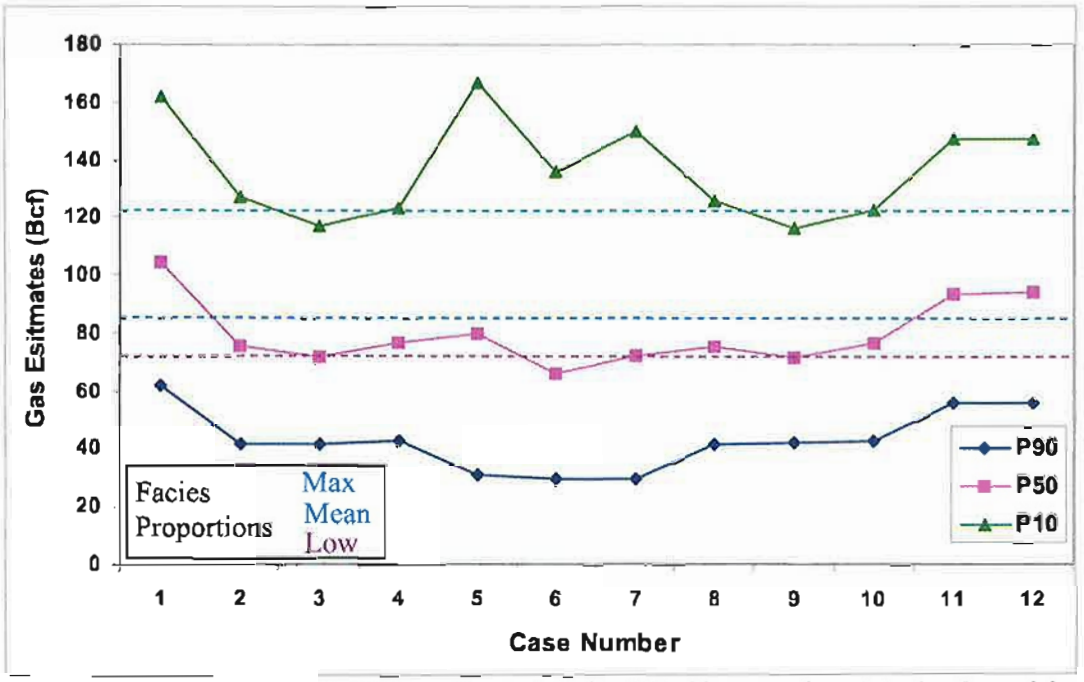

Figure 7.15: Plot of gas estimates for each case in Table 7.4 with an overlay of stochastic model estimates. The range of the gas estimates of the stochastic model method is narrower than the range of the gas estimates of the Monte Carlo simulation method.

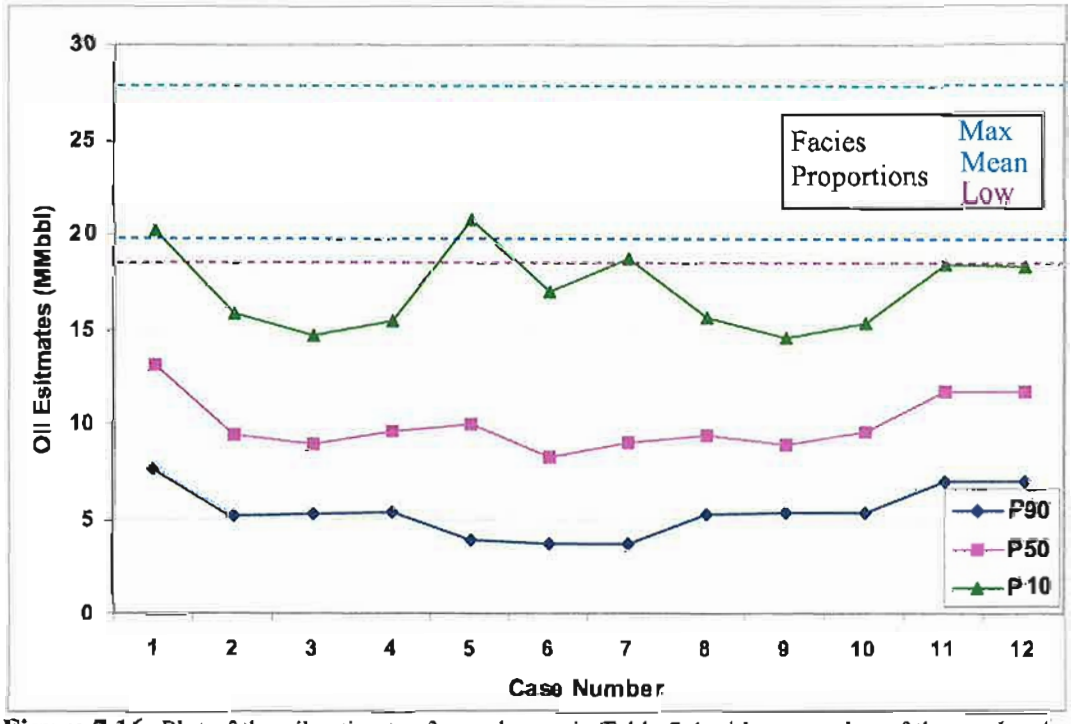

Figure 7.16: Plot of the oil estimates for each case in Table 7.4 with an overlay of the stochastic model estimates. The range of the oil estimates of the stochastic model method is similar to the range of the gas estimates of the Monte Carlo simulation method.

Some points need to be addressed before analysing the Monte Carlo simulation results. First, Figures 7.15 and 7.16 show a clear consistency between gas and oil estimates. For example, if the P90 gas estimate in case-x is higher than case-y, then the same is true for the oil estimate. The uncertainty rank for the estimated gas is identical to those of the oil estimates. This was expected, because both estimates were done using the same random number and the same number of iterations. For practical reasons and to avoid repeating the same information, the analysis was made on gas, but the conclusions derived from this analysis are true for the oil estimates too. Finally, both ranking methods gave an identical measure of uncertainty as shown in Figure 7.17. Therefore, the use of any one of them would be sufficient to rank the probabilistic hydrocarbon estimates.

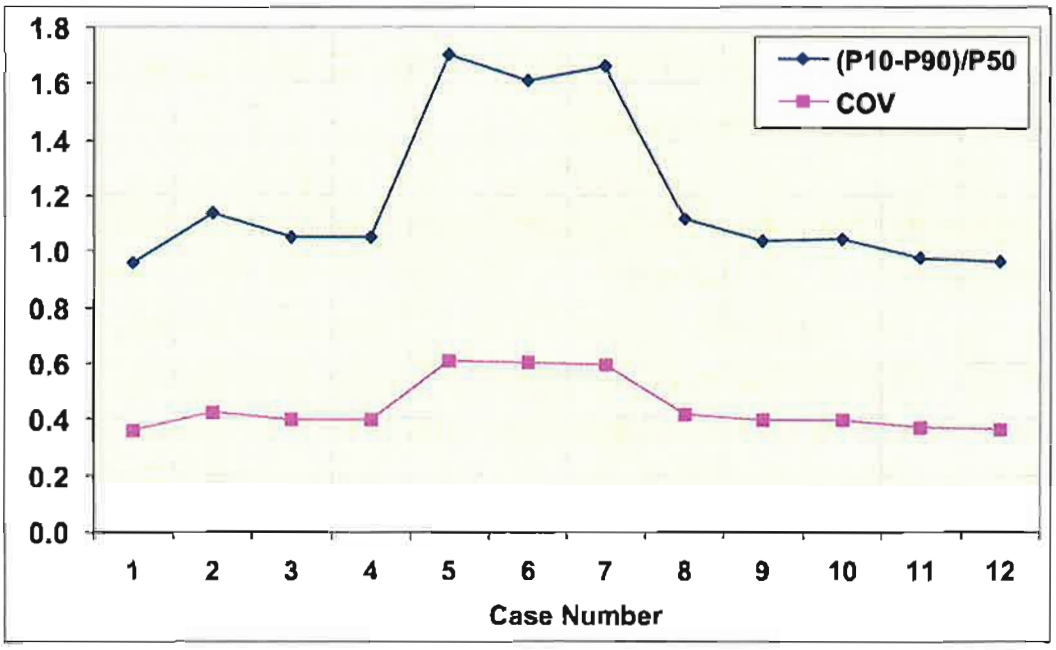

Figure 7.17: Comparison between the two different ranking methods used in the study. The (P10-P90)/P50 ratio gives similar results as the coefficient of variance (COV). Case 5, 6 and 7 have higher uncertainty compared to other cases because of the use of extreme values in the input distribution.

Case Study Results

Case 1 gave higher gas estimates for the P10, the P50 and the P90 compared to other cases and has lower uncertainties. The higher estimates are due to the use of a single value for water saturation that is lower than the mean estimates for all wells. Moreover, the uncertainty in these estimates is a function of porosity and net gross, whereas in the other cases it is a function of net-gross, porosity and water saturation. Therefore, a comparison of case 1 estimates uncertainty with the others is invalid.

Case 2 to case 4 were designed by using mean values for low, mean and high input with three different distribution shapes, which were triangle, lognormal and normal. Case 2 gave a higher P10 estimate and a longer P10-P90 range, which resulted in a higher uncertainty compared to case 3 and case 4. Case 3 estimates were conservative compared to the other two cases. Case 4 estimates are more realistic and it is safe to say that for this reservoir normal distribution is suitable.

Case-5 to case 7 were designed to investigate the use of extreme input values in Monte Carlo simulation as described earlier. The first impact of using extreme values is the increase in uncertainty values as shown in Figure 17. Depending on the ranking method used, the uncertainty has increased by 40% to 60% compared to all other cases. The increase in uncertainty is directly related to the increase in the P10-P90 range. Also, as in case 3, the triangle distribution increases uncertainty. It is safe to conclude that the use of extreme distribution data will result in the increase of uncertainty regardless of the distribution model used.

Case 8 to case 10 were designed like case 2 to case 4, with a difference in dependency. In cases 8 to case 10, dependencies between porosity, water saturation and net-gross were used. The correlation coefficient has been obtained from cross-plots as described in the previous section. The uncertainty in cases 8 to 10 has decreased slightly compared to cases 2 to 4, due to the use of dependency. The P10-P90 range has decreased slightly. As

in case 2 to 4, normal distribution gave better estimates although here it is slightly higher than the lognormal.

The last two cases, case 11 and 12, had a special design where the input distributions were fitted to the wells mean log values as explained earlier. Also, case 12 had dependency between porosity, water saturation and net gross while case 11 did not. The differences in these estimates compared to others are very clear. The P90 and the P50 are higher and their uncertainties are lower than cases-2 to -10. As explained earlier case-1 will not be used in comparison because it does not represent uncertainty in water saturation. The results from case 11 and case 12 showed that truncating the distributions based on the mean of the properties is a very good approach to reduce the uncertainty of the estimates. Case 12 gave reasonable initial in-place oil and gas estimates.

Case Study Discussion

The hydrocarbon estimates from the stochastic model method did not correlate well with the hydrocarbon probabilistic estimates as shown in Figures 7.15 and 7.16. For the gas estimates the maximum facies proportions approaches the P10 value, while the minimum and the low facies proportions estimates fall around P50. The results are totally different for the oil estimates. The minimum and the low facies proportions oil estimates fall around the P10 and the maximum facies proportions estimate is much higher. The possible geological explanation is that in the oil intervals, there are channel or splay facies, which result in the increase of porosity in that interval and hence higher fluid saturation.

Liberated Gas Estimation

The volume of liberated gas needs to be estimated and combined with the case 12 estimate. As mentioned in Chapter 2, the P1 development scenario is zero gas-liberated from the oil rim. The P2 development scenario is the liberation of 626 cf/bbl and the P3 scenario is the liberation of 750 cf/bbl. There are two ways to do this task,

deterministically or probabilistically. A deterministic approach is to multiply the gas-liberated ratio by the oil estimate for each estimate (i.e. P10, P50 and P90) and add it to the corresponding gas estimates (i.e. P10, P50 and P90). This will result in several numbers and may lead to confusion.

Three cases are presented for liberated gas, (low 0, mean 626 cf/bbl and high 750 cf/bbl) and there is not an exact time frame for when the process of gas liberation actually started. There are uncertainties associated with the gas liberation process and it will be very useful to incorporate this uncertainty with the gas estimates. A suitable distribution for the gas/oil liberation ratio can be generated and multiplied with the oil estimate distribution and the results added to the gas estimates distribution. The final results would be a probabilistic estimate that combines all the uncertainty factors.

Three distribution shapes (i.e. triangle, normal and lognormal) were evaluated. The normal distribution gave the best results (Fig. 7.18). The criterion of selection was to determine which distribution has a P50 closer to 626 cf/bbl, which was used as the mean. The triangle P50 was 484 cf/bbl, the normal P50 was 579 cf/bbl and the lognormal P50 was 566 cf/bbl. The normal distribution was very close to the mean estimate. Also, the normal distribution curve rises gradually and covers lower ratios unlike the lognormal. In actual reservoir conditions the gas liberation ratio did not start at 626 cf/bbl, in fact it started at a much lower ratio and continued rising (Fig. 7.18). This uncertainty should be reflected in the gas estimates. The final Monte Carlo simulation gas estimates are shown in Table 7.7. Figure 7.19 shows the oil and gas expected volume curves and Figure 7.20 shows sensitivity analysis for the key input parameter in the Monte Carlo simulation.

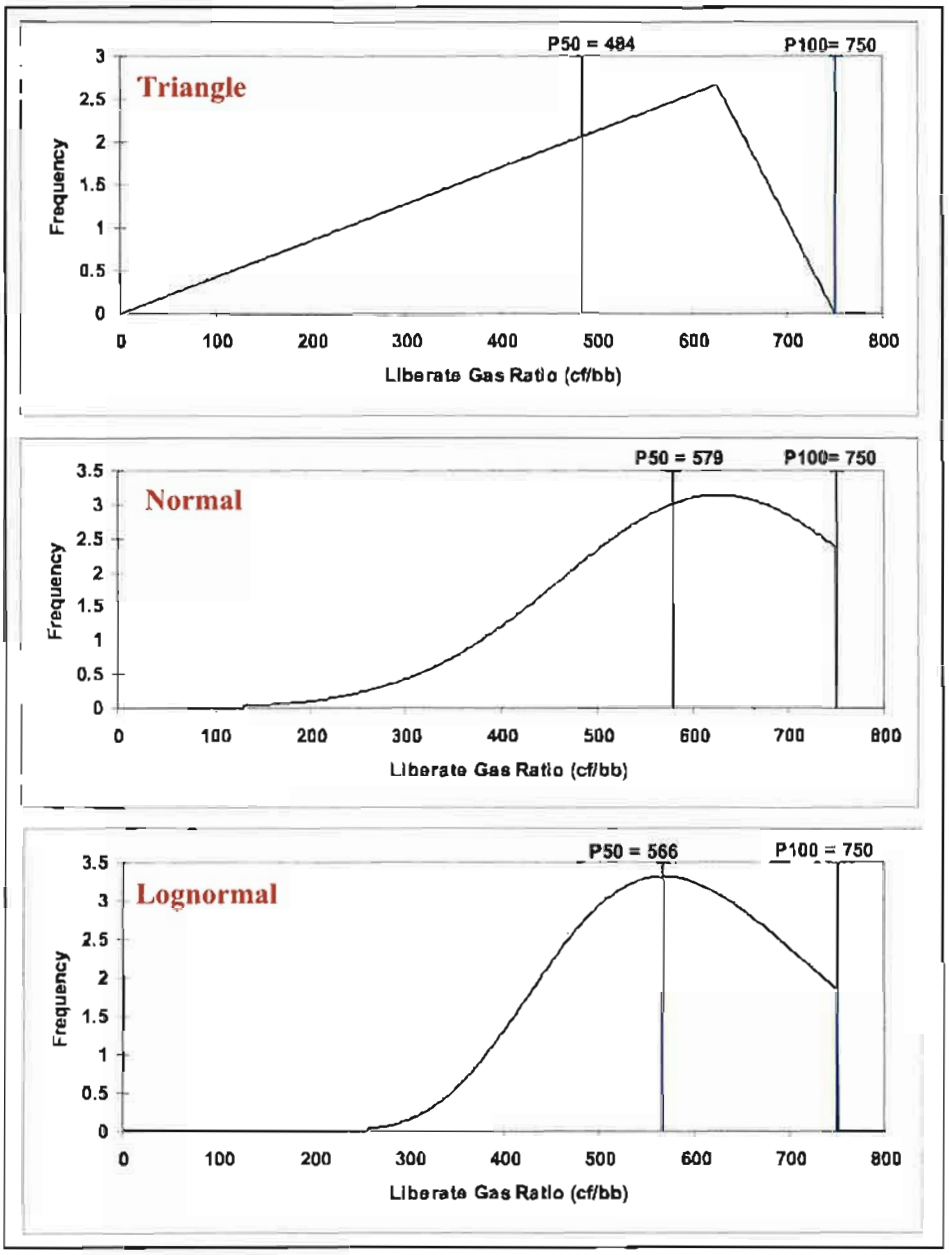

Figure 7.18: Three different distributions used to fit the liberation gas ratio. The P50 in normal distribution gave the closest estimate to the mean and hence it was selected.

Table 7.7: Hydrocarbon estimates, generated using the Monte Carlo simulation method, for case-12 considering the liberated gas from the oil rim.

Estimates	P90	P50	P10	(P10-P90)/P50	COV
Gas (Bcf)	58.99	100.61	156.72	0.97	0.361
Oil (MMbbl)	7.01	11.78	18.38	0.97	0.361

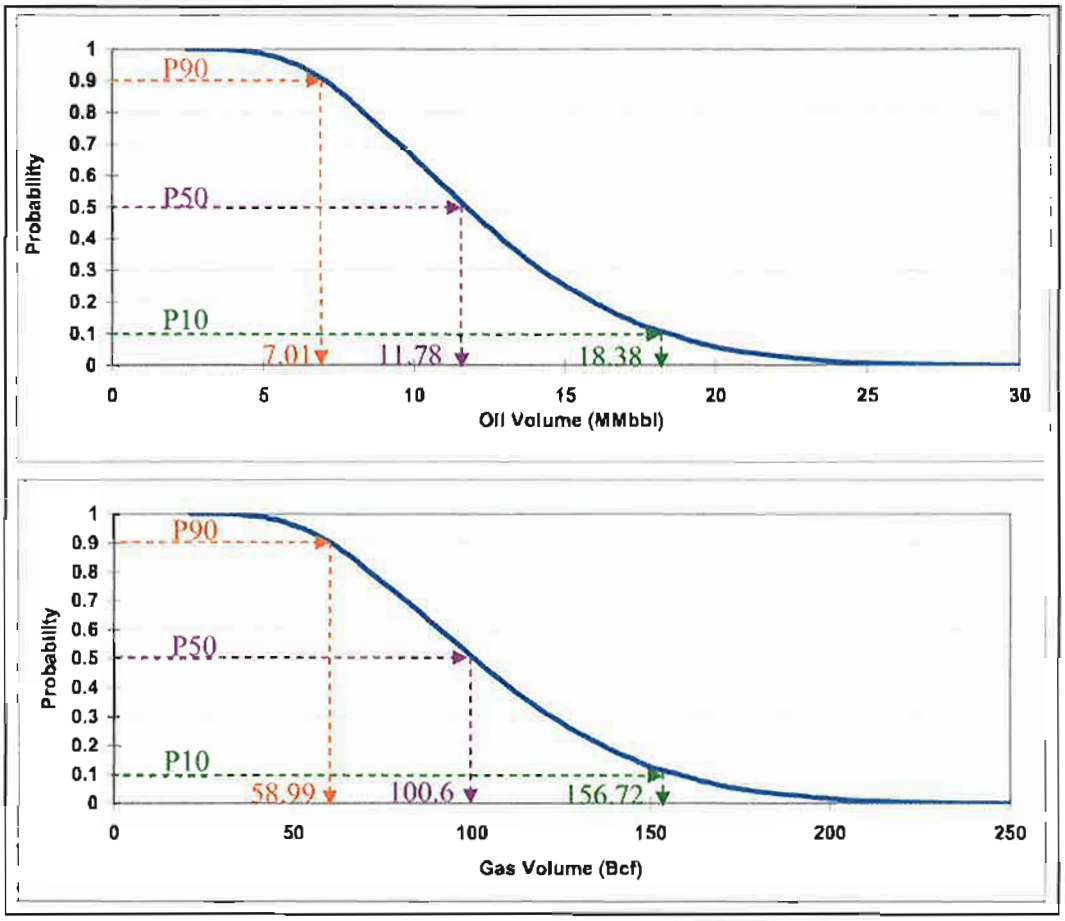

Figure 7.19: Oil and gas expected volume curves, generated using the Monte Carlo simulation method, with the P90, the P50 and the P10 estimates values plotted.

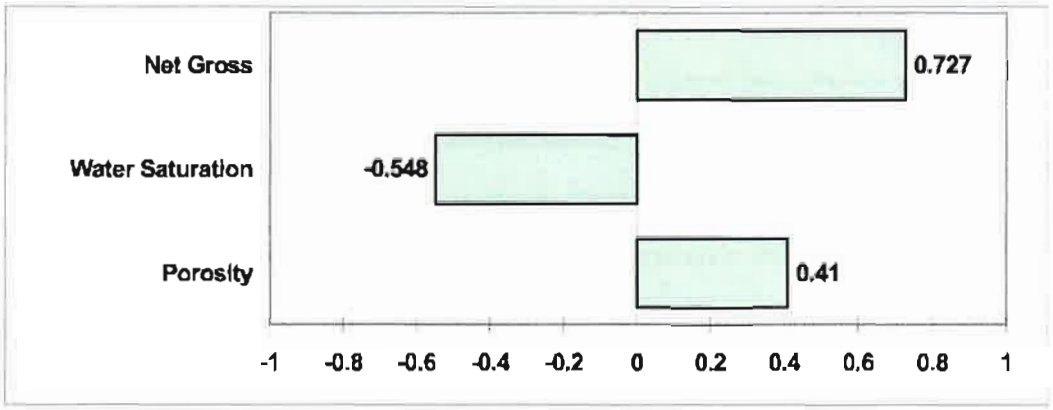

Figure 7.20: Sensitivity analysis for the key input parameters used in simulating case-12 hydrocarbon estimates. Net gross is the key uncertainty in this study.

7.3 Geologically Driven Volumetrics

The sensitivity analysis showed that the N/G is ranked as the highest source of uncertainty compared to water saturation and porosity (Fig. 7.20). One of the reasons for this high uncertainty is the limited data available for the N/G ratio. The porosity and water saturation distribution were derived based on log data, while net-gross values are limited to one value per well. If the available geological knowledge was incorporated into Monte Carlo simulation, it should reduce the N/G ratio uncertainty. However, the current Monte Carlo simulation method does not have any input for this critical and important knowledge. In the following section a technique was developed that combines the Monte Carlo simulation process with the stochastic facies model to overcome this problem.

7.3.1 Rationale

Monte Carlo simulation is a powerful tool in measuring uncertainty in hydrocarbon estimates. Monte Carlo models can be easily built and run fast. The output results can be examined visually as well as statistically. However, its main drawback is the absence of any geological knowledge in the simulation process. The geological knowledge comes from different sources such as drilled cores, wireline well logs, facies maps and modern and ancient analogues. This knowledge is currently employed in the stochastic modeling process.

The stochastic facies model is built based on facies proportions. Theoretically there could be an infinite number of facies proportion combinations as long as their sum equals to one and no single facies proportion is less than zero or greater than 1. However, there must be two facies or more, otherwise there would not be any need for a stochastic geological model. If all possible facies proportions can be accounted for, then there would be a better understanding of uncertainty. If facies proportions can be used in Monte Carlo simulation, then uncertainty in them can be related to hydrocarbon estimates. In the following section theoretical derivation of this relationship is presented.

7.3.2 Theoretical Derivation

All stochastic models are made up of cells. The volume of a single cell (V_c) in the stochastic model can be calculated by the following equation:

$V_c = dx \cdot dy \cdot dz$, where *dx*, *dy* and *dx* are the length of the cell in the x, y and z direction respectively.

Therefore the total volume of a 3-D stochastic model (V_t) is equal to

$V_t = \sum_{i=1}^{n} (dx \cdot dy \cdot dz)_i = \sum_{i=1}^{n} (V_c)_i$, Where *n* is the total number of cells in the stochastic model.

Assuming that in a stochastic facies model there is a facies called (*f*), the facies volume (V_f) is directly related to the facies proportions (f_p) as expressed by the following equation:

$V_f = V_t \cdot f_p$

The facies volume of facies (*f*) in the stochastic model can be calculated by the equation:

$V_f = \sum_{i=1}^{n} (V_{cf})_i$, where (V_{cf}) is the volume of the cells that contains facies (*f*).

The part of the facies volume (V_f) that is above a fluid contact (a) can be named as (V_a) and calculated by applying the following filter on the stochastic model:

$$V_a = \begin{cases} \text{If } z > a, \text{ then } \sum_{i=1}^{n} (V_f)_i \\ \text{Else } V_i = 0 \end{cases}$$, where z is the cell centre depth.

The above filter can be modified to calculate a facies volume (V_β) that is bounded between two fluid contacts (a) and (b) as follows

$$V_\beta = \begin{cases} \text{If } z > a \text{ and } z<b, \text{ then } \sum_{i=1}^{n} (V_f)_i \\ \text{Else } V_i = 0 \end{cases}$$

The above filter can be modified further to calculate a facies volume ($V\gamma$) that is bounded

between the two fluid contacts (*a*) and (*b*) and located in the stochastic model interval (*r*)

$$V_y = \begin{cases} \text{If interval = r and z > a and z<b and, then } \sum_{i=1}^{n}(V_f)_i \\ \text{Else } V_i = 0 \end{cases}$$

The original hydrocarbon in place in facies V_y can be estimated by the Monte Carlo method with the following equation:

$OHIP_{Vy} = V_y * \phi * (1\text{-Sw}) / FVF$, Where:

V_y	Facies volume extracted from the stochastic model
ϕ_f	Porosity distribution in the *f* facies
S_{wf}	Water saturation distribution in the *f* facies
FVF	Formation volume factor

If there were (n) number of stochastic models generated by varying the facies proportions, then there would be (n) number of facies volumes for facies (*f*). These volumes can be used to generate a facies volume distribution that can be used in the above equation instead of the single value. By this approach, the need to use N/G ratio has been eliminated. Furthermore, geological knowledge has been included as an input into the Monte Carlo simulation by using the facies volumes that are directly related to facies proportions. Hence uncertainty in the facies proportions can be related to hydrocarbon estimates. This concept is here named geologically driven volumetrics (GDV), because the final estimates are highly dependent on the geological knowledge. The final step would be to calculate the total hydrocarbons ($OHIP_t$) in the reservoir interval as follow:

$OHIP_t = \sum_{i=1}^{k}(OHIP_{vy})_i$, where k is the number of facies defined in the stochastic model and contains hydrocarbons.

7.3.3 Application

The Main Dara area is very suitable to test the applicability of the GDV concept. Figure 7.21 shows the two hydrocarbon bearing facies, which are channels and splays.

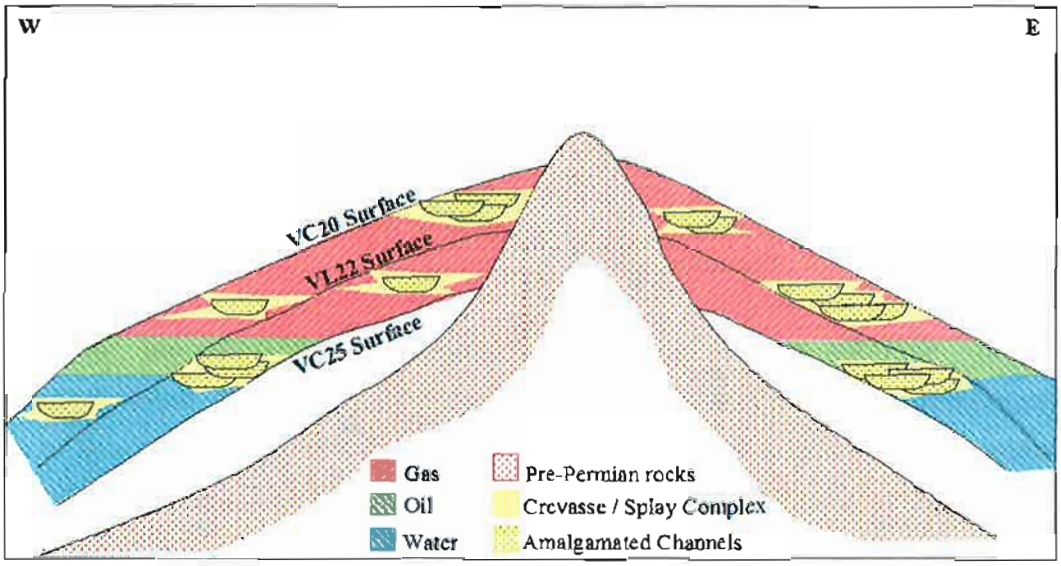

Figure 7.21: Different fluid contacts, the eroded section and the two reservoir facies in the VC20-VC25 reservoir interval.

Input Data Selection and Distribution Fitting

The calculations were done for each reservoir interval (i.e. VC20-VL22 and VL22-VC25). Three stochastic facies models were built representing low, mean and high facies proportions (Chapter 6). For every reservoir interval there are three volumes for each facies in the gas zone and another three volumes in the oil zone. The facies volumes were calculated in cubic metres and were fitted into a suitable probability distribution (Table 7.8.)

Table 7.8: Summary of facies volumes and distributions used to fit them.

Reservoir Interval	Facies	Volume in Gas Zone (m^3)				Volume in Oil Zone (m^3)			
		L	M	H	Distribution	L	M	H	Distribution
VC20	Channel	5.51E+07	7.44E+07	1.08E+08	Normal	1.26E+07	1.84E+07	2.50E+07	Triangle
	Splay	7.64E+07	8.72E+07	9.39E+07	Lognormal	1.24E+07	1.81E+07	2.91E+07	Triangle
VL22	Channel	4.86E+07	6.95E+07	9.02E+07	Lognormal	2.04E+07	2.49E+07	2.76E+07	Triangle
	Splay	3.46E+07	3.82E+07	4.21E+07	Triangle	6.15E+06	7.49E+06	8.29E+06	Lognormal

The porosity and water saturation distributions were calculated using the same approach as for case 12. A mean value was calculated for each well in the Main Dara area to truncate the distribution of the fitted data. Table 7.9 shows the distribution of petrophsycial properties for each facies in each reservoir zone in the Main Dara area. There were very strong negative correlations between porosity and water saturation in each reservoir interval as shown in Figure 7.22. This relation was used in the Monte Carlo simulation. The channels had a relatively strong negative correlation compared the splays. The Bg and Bo values were 0.00558 and 1.675 respectively; the same values were used in the previous Monte Carlo simulation. The same liberated gas distribution used in the previous simulation was used in this case to account for the different liberated gas ratios.

Table 7.9: Statistical distribution of facies petrophysical properties used in the Monte Carlo simulation for each facies in each reservoir zone in the Main Dara area.

Reservoir Interval	Facies	Porosity %				Water Saturation %			
		L	M	H	Distribution	L	M	H	Distribution
VC20	Channel	6.3	11.1	14.3	Logistic	24.5	43.7	80.7	Inverse gaussian
	Splay	6.7	10.5	15.6	Logistic	19.6	49.9	78.7	Lognormal
VL22	Channel	9.4	11.6	15.0	Normal	15.0	55.0	80.9	Logistic
	Splay	8.5	10.7	13.5	Normal	21.9	48.4	82.1	Logistic

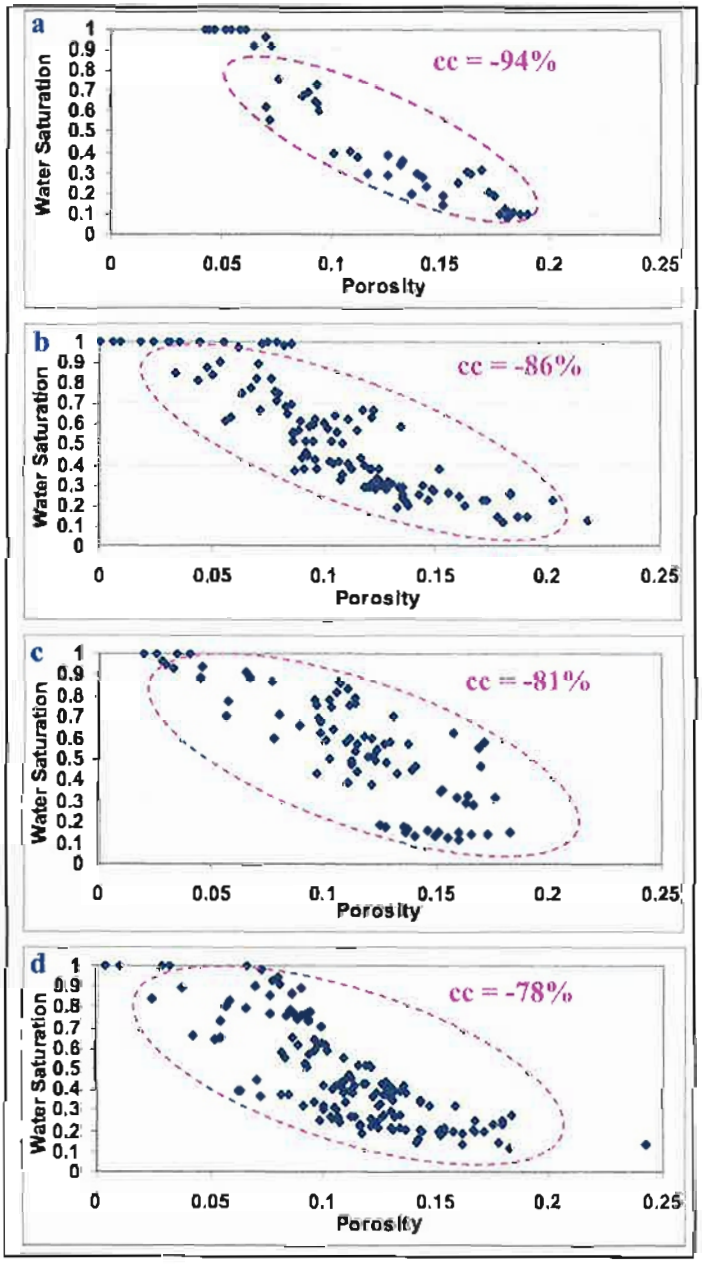

Figure 7.22: Cross-plots between porosity and water saturation from well logs for channels and splays in the Main Dara area. a) channels in the VC20 interval, b) splays in the VC20 interval, c) channels in the VL22 interval and d) splays in the VL22 interval.

Probabilistic Hydrocarbon Addition

The hydrocarbon calculations were made for every facies, zone by zone. This resulted in four probabilistic gas estimates and four probabilistic oil estimates. There are two different methods to add two or more probabilistic reserve distributions: arithmetic addition or random addition. The arithmetic method simply adds the reserve of the same probability from each distribution; for example adding the value of the P10 from all distributions. The random addition is done by picking values randomly from all available reserve distributions to generate a new distribution. Then values, such as the new P10, the P50 and the P90, are taken from this new distribution (Etherington et al., 2001).

The Central Limit Theorem (CLT) helps in understanding these points. There are *n* number of distributions that can be of different distribution shapes that need to be added. The CLT states that the sum of *n* distributions is approximately a normal distribution. Secondly, the mean of the new distribution is equal to the sum of means of all distributions. The standard deviation of the new distribution is equal to the sum of all distributions standard deviation times the square root of n (Murtha, 2002)

The method of reserves addition will have different results depending on shape of the distribution and the dependencies. According the CLT the mean will not be affected by either method since the mean of the new distribution will be the sum of all means. Also, the shape of the outcome will approximate a normal distribution regardless of the method used. However, there will be a strong impact on the range of the distribution. In the case of totally independent reserve distributions, such as the two different reservoirs in different basins, the arithmetic addition would underestimate the P10 and would overestimate the P90. On the other hand, if there is a strong dependency such as in different areas of the same reservoir, the arithmetic approach will give better representations than the random. Because the two reservoir intervals in this study are geologically related, the hydrocarbon estimates will be added with high dependency.

Simulation Results

The GDV simulation results showed an overall increase in the oil and gas estimates and a substantial decrease in uncertainty compared to case 12 (Table 7.10.) Figure 7.23 shows the oil and gas expected volume curves. Sensitivity analysis results for the Main Dara area hydrocarbon estimates showed that the key uncertainties were the porosity of the channel facies in the VC20 reservoir interval and the water saturation in the VC20 reservoir interval (Fig. 7.24.) Figures 7.25 and 7.26 display a comparison between the GDV, the case-12 and the stochastic model for the gas and the oil estimates.

Table 7.10: Hydrocarbon estimates for the Main Dara area using the GDV method.

Estimates	P90	P50	P10	(P10-P90)/P50	COV
Oil (MMbbl)	11.40	16.62	22.82	0.69	0.262
Gas (Bcf)	82.61	119.85	163.65	0.68	0.257

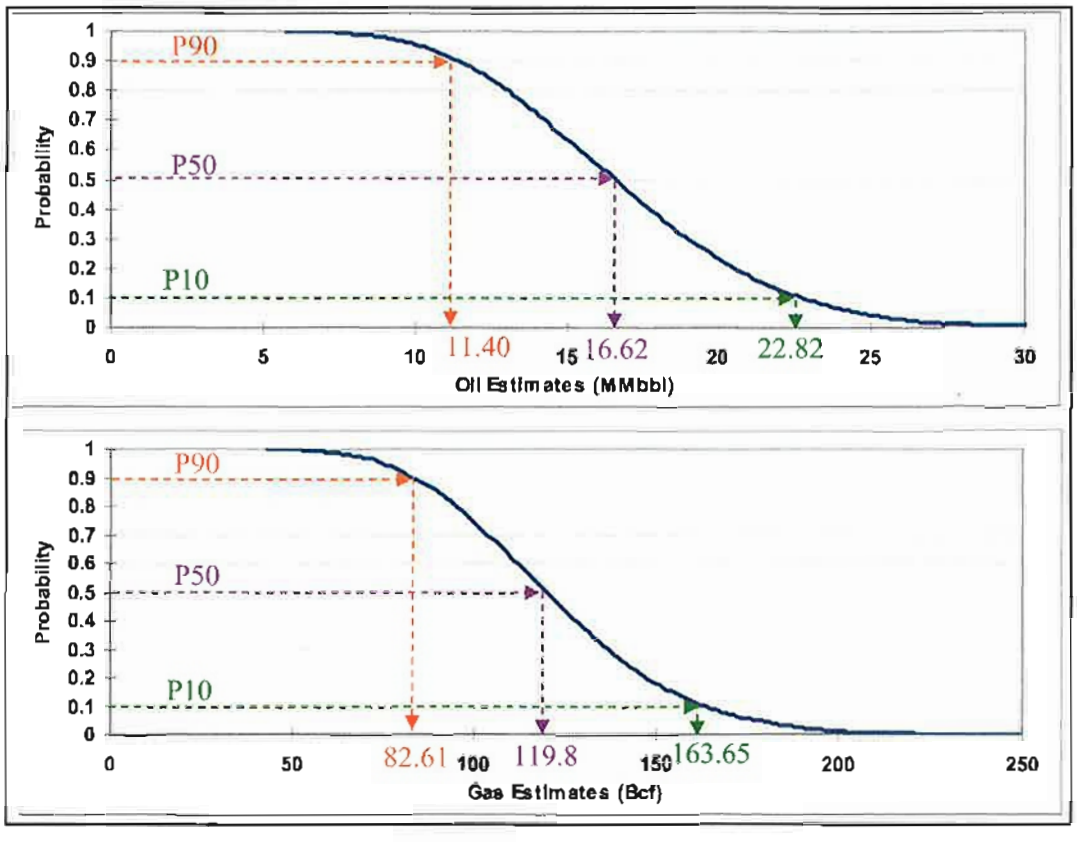

Figure 7.23: Oil and gas expected, generated using the GDV method, volume curves with the P90, the P50 and the P10 estimated values plotted.

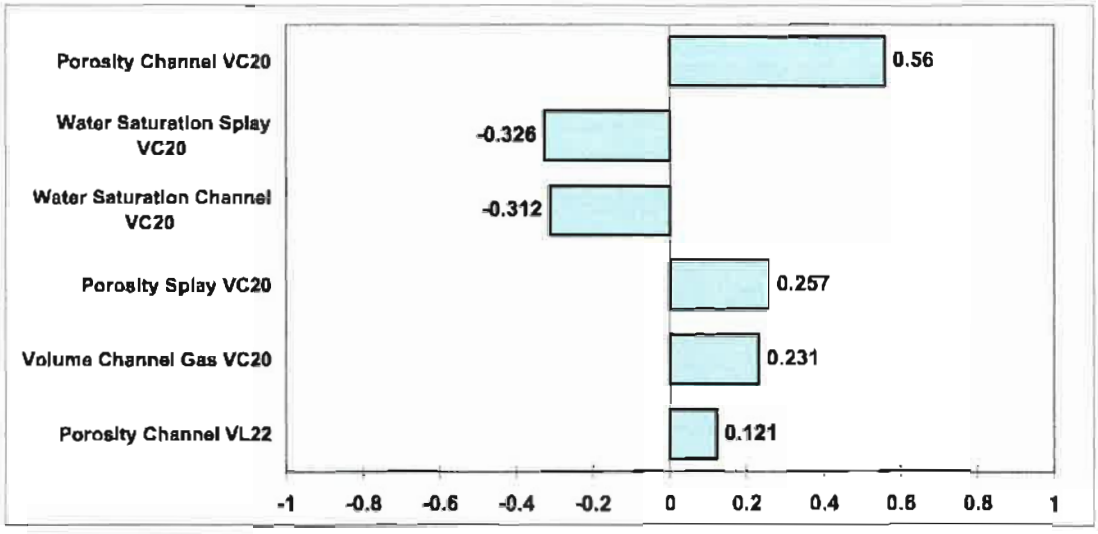

Figure 7.24: Sensitivity analysis results for the Main Dara area gas estimates by using the GDV method. The key uncertainties are the porosity of the channel facies in the VC20 reservoir interval and the water saturation in the VC20 reservoir interval.

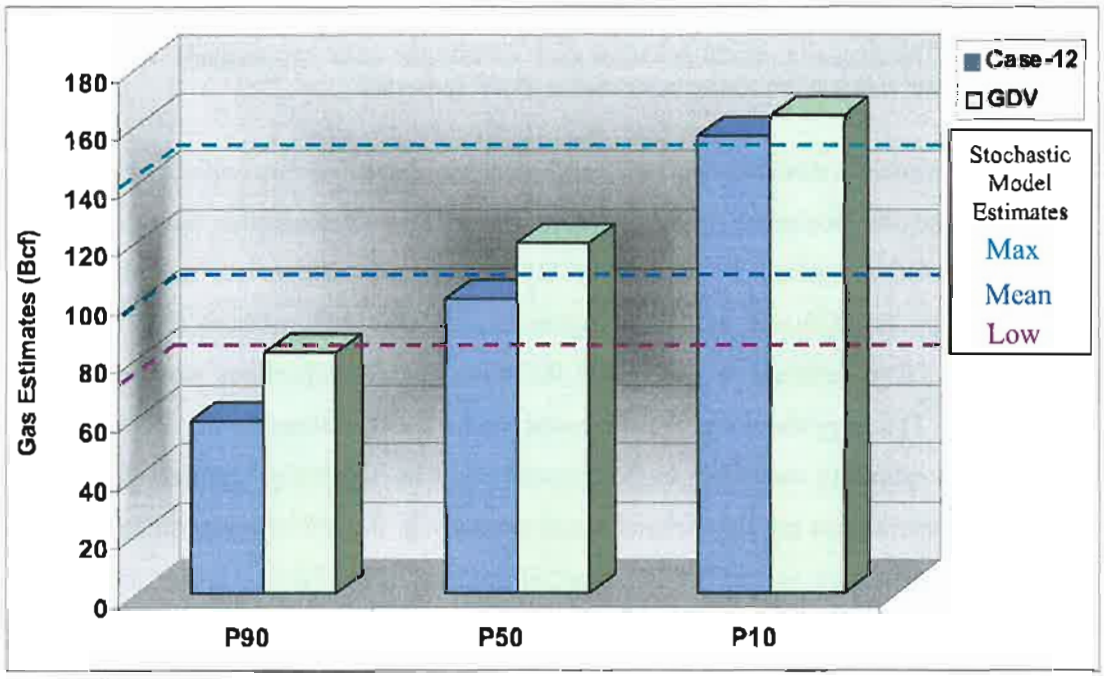

Figure 7.25: Comparison between gas estimates calculated by different methods for the Main Dara area. The GDV method gave the better estimates with lower uncertainty.

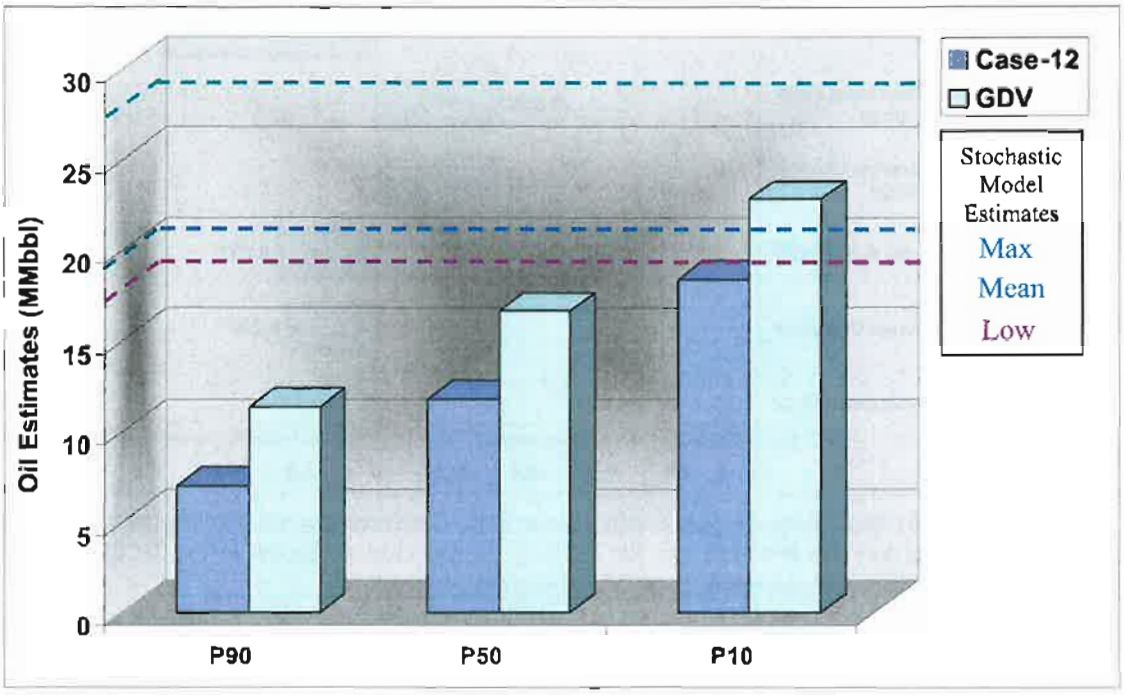

Figure 7.26: Comparison between oil estimates calculated by different methods for the Main Dara area. The stochastic model predicted more oil than the other two methods. The maximum GDV estimate is just above the mean stochastic model estimates.

The gas volumes estimated by GDV are higher and have less uncertainty compared to case 12 and the stochastic model method. This clearly demonstrates the advantage of using the GDV method in decreasing the uncertainties. However, the oil volumes estimated by the stochastic model are higher than the other two methods (Fig. 7.26). The maximum GDV estimate is just above the mean facies proportions stochastic model estimates. This may show that the stochastic model is overestimating the oil volume and these high estimates may have higher uncertainty. The sensitivity analysis showed that the key uncertainties are the channel facies porosity in the VC20 reservoir interval and the water saturation in the VC20 reservoir interval (Fig. 7.24). Unlike the case 12 sensitivity analysis (Fig. 7.20), which showed that the highest uncertainty was the net-gross ratio. It can be safely concluded that the GDV method has achieved the objective of quantifying and reducing the uncertainty of hydrocarbon estimation compared to conventional Monte Carlo simulation and stochastic model methods.

Cosentino, L., 2001, Integrated Reservoir Studies: Institue Francais Du Petrole Publications: Paris, Editions TECHNIP, 310 p.

Cronquist, C., 2001, Estimation and Classification of Reserves of Crude Oil, Natural Gas and Condensate: SPE Books: Richardson, Texas, USA, SPE, pp.416 p.

Etherington, J. R., E. J. Hunt, and A. Adewusi, 2001, Aggregating Reserves and Resources for Portfolio Management: SPE 71424, SPE Annual Technical Conference and Exhibition.

Garb, F. A., 1988, Assessing Risk in Estimating Hydrocarbon Reserves and in Evaluating Hydrocarbon-Producing Properties: Journal of Petroleum Technology, v. June 1988, p. pp. 765-778.

Kazmier, L. J., 1996, Theory and Problems of Business Statistics: Scham's Outline Series: New York, USA, McGraw Hill, pp.410 p.

Macary, S. M., A. Hassan, and E. Ragaee, 1999, Better Understanding of Reservoir Statistics is the Key for Reliable Monte Carlo Simulation: SPE 53264, SPE Middle East Oil Show.

Montgomery, S. L., and C. D. Morgan, 1998, Bluebell Field, Unita Basin: Reservoir Characterization for Imporved Well Completion and Oil Recovery: American Association of Petroleum Geologists, v. 82, p. 1113-1132.

Murtha, J. A., 1994, Incorporating Historical Data Into Monte Carlo Simulation: SPE Computer Application, p. pp.11-17.

Murtha, J. A., 2002, Sums and Products of Distributions: Rules of Thumb and Applications: SPE 77422, SPE Annual Technical Conference and Exhibition.

Startzman, R. A., and R. A. Wattenbarger, 1985, An Improved Computation Procedure for Risk Analysis Problems With Unusual Probability Functions: SPE 13722, SPE Hydrocarbon Economics and Evaluation Symposium.

Chapter 8

Volumetrics Re-Estimation: A New Perspective

8.1 Introduction

In Chapter 6 hydrocarbon estimations were calculated for the Main Dara, Dara-3 and Dara-16 areas using the stochastic modeling method and the results were compared to the cumulative production and different development scenarios (Table 1). The hydrocarbon estimates showed that in most cases the gas volume produced from the Daralingie Field is much more than what was estimated as in place gas volumes. The only possible scenario which would produce this much gas is to have maximum pay facies proportions (i.e. channels and splay) with a high amount of liberated gas from the oil rim. Even in that case the recovery is very high, as shown in Table 8.1.

Table 8.1: Hydrocarbon estimates from the stochastic modeling method with possible recovery factors considering cumulative production and different development scenarios.

Pay Facies Proportions	Model Estimates (Bcf)		Cumulative Production 152.6 (Bcf)	1P Dev 168 (Bcf)	2P Dev 177 (Bcf)	3P Dev 186 (Bcf)
Minimum	1P	94.5	161	178	187	197
	2P	118.5	129	142	149	157
	3P	123.2	124	136	144	151
Mean	1P	107.1	142	157	165	174
	2P	132.7	115	127	133	140
	3P	137.8	111	122	128	135
Maximum	1P	140.5	109	120	126	132
	2P	168.7	90	100	105	110
	3P	174.3	88	96	102	107

In the following sections the hydrocarbon estimates were calculated using the GDV method to validate the results from the stochastic model. Also, an investigation into the possible recovery factors affecting these results was done. The first step was to design the Monte Carlo simulation for this part of the study. The simulation results are presented, followed by a discussion about the expected recoveries and the possible causes of the high recovery factors observed.

8.2 Input Data

The hydrocarbon re-estimation for the Main Dara, Dara-3 and Dara-16 areas was done by using the GDV methods. Total GRV for oil and gas are shown in Table 8.2. The basic petrophysical properties of wells in these areas are listed in Table 8.3. The facies volumes for channels and splays were calculated from the three stochastic facies models and were fitted with a suitable distribution (Table 8.4). The petrophysical properties for each facies body and the distribution used to fit them are shown in Table 8.5. All other parameters needed to run the Monte Carlo simulation, such as fluid properties, liberated gas, iteration number and seed number, were the same as those used in section 7.3.

Table 8.2: GRV for oil and gas in the Main Dara, Dara-3 and Dara-16 areas.

Fluid Type	Mapped Gross Rock Volume (m^3)			
	Main Dara	Dara-3	Dara-16	Total
Gas	483,242,157	47,979,664	64,296,726	595,518,548
Oil	101,810,834	26,753,934	70,392,830	198,957,597

Table 8.3: Basic petrophysical properties of wells in the Main Dara, Dara-3 and Dara-16 areas.

Well	Interval	Sand	N/G	Porosity			Water Saturation		
Name	Thickness (ft)	Thickness (ft)	%	Low	Mean	High	Low	Mean	High
1	54	37	68.5	No Logs					
3	68	24	35.2	0.020	0.075	0.171	0.28	0.52	0.92
5				Eroded					
6	53	10	18.9	0.033	0.098	0.146	0.21	0.38	0.85
7	61	37	60.7	0.042	0.098	0.183	0.12	0.46	0.80
8	20	0	0.0	Non Pay Interval					
9	98	52	53.1	0.066	0.139	0.262	0.10	0.40	0.72
12	83	26	31.3	0.055	0.103	0.180	0.12	0.43	0.74
13	54	27	50.0	0.070	0.137	0.190	0.12	0.23	0.58
14	79	28	35.4	0.056	0.119	0.191	0.14	0.37	0.60
16	71	52	73.2	0.042	0.140	0.170	0.12	0.19	0.46
18	91	38	41.8	0.065	0.128	0.175	0.19	0.42	0.64
19	58	10	17.2	0.040	0.084	0.135	0.58	0.76	0.93
22	69	53	76.8	0.033	0.102	0.172	0.44	0.60	0.75
23	70	38	54.3	0.020	0.079	0.177	0.27	0.57	0.87
24	44	28	63.6	0.073	0.101	0.131	0.27	0.54	0.80

Table 8.4: Volumes for pay facies in each zone with the distribution type used to fit them.

Reservoir Interval	Facies	Volume in Gas Zone (m3)				Volume in Oil Zone (m3)			
		L	M	H	Distribution	L	M	H	Distribution
VC20	Channel	7.19E+07	9.30E+07	1.30E+08	Lognormal	2.07E+07	2.60E+07	3.10E+07	Normal
	Splay	7.94E+07	9.75E+07	1.14E+08	Triangle	1.61E+07	2.21E+07	2.72E+07	Triangle
VL22	Channel	6.89E+07	9.18E+07	1.16E+08	Triangle	4.78E+07	5.29E+07	5.71E+07	Triangle
	Splay	4.00E+07	4.38E+07	4.79E+07	Triangle	1.06E+07	1.28E+07	1.70E+07	Triangle

Table 8.5: The petrophysical properties for each facies body and their distribution.

Reservoir Interval	Facies	Porosity %				Water Saturation %			
		L	M	H	Distribution	L	M	H	Distribution
VC20	Channel	6.3	11.1	14.3	Logistic	24.5	43.7	80.7	Inverse gaussian
	Splay	6.7	10.1	15.6	Logistic	19.6	49.5	87.7	Weibull
VL22	Channel	9.4	12.1	15.0	Logistic	15.0	47.1	80.9	Logistic
	Splay	7.2	10.9	15.6	Logistic	11.6	43.8	82.1	Inverse gaussian

8.3 Simulation Results

The initial in-place oil and gas estimates with their associated uncertainties are listed in Table 8.6 and the expected volume curves are shown in figure 8.1. Figure 8.2 shows the sensitivity analysis for the key input parameters in this GDV Monte Carlo simulation. An expected remaining reserve curve was generated as a result of subtracting the cumulative production volume from the expected gas volume curve (Fig. 8.3).

One of the advantages of using the GDV method was the consolidation of the hydrocarbon estimates into one single curve, from which the P90, P50 and P10 could be taken (Table 8.6) as compared to three different estimates from each stochastic facies model (Table 8.1). Also, this method gives a measure of uncertainty, which helps build confidence in the estimates. The sensitivity analysis showed that water saturation was the main source of uncertainty in these hydrocarbon estimates. The next step was to compare the estimated gas volumes with the cumulative production along with the three different development scenarios, which are detailed in the next section.

Table 8.6: Initial in-place oil and gas in place estimates, generated using the GDV method, for the Main Dara, Dara-3 and Dara-16 areas.

Estimates	P90	P50	P10	(P10-P90)/P50	COV
Oil (MMbbl)	18.57	25.42	32.75	0.56	0.213
Gas (Bcf)	97.88	132.46	169.00	0.54	0.206

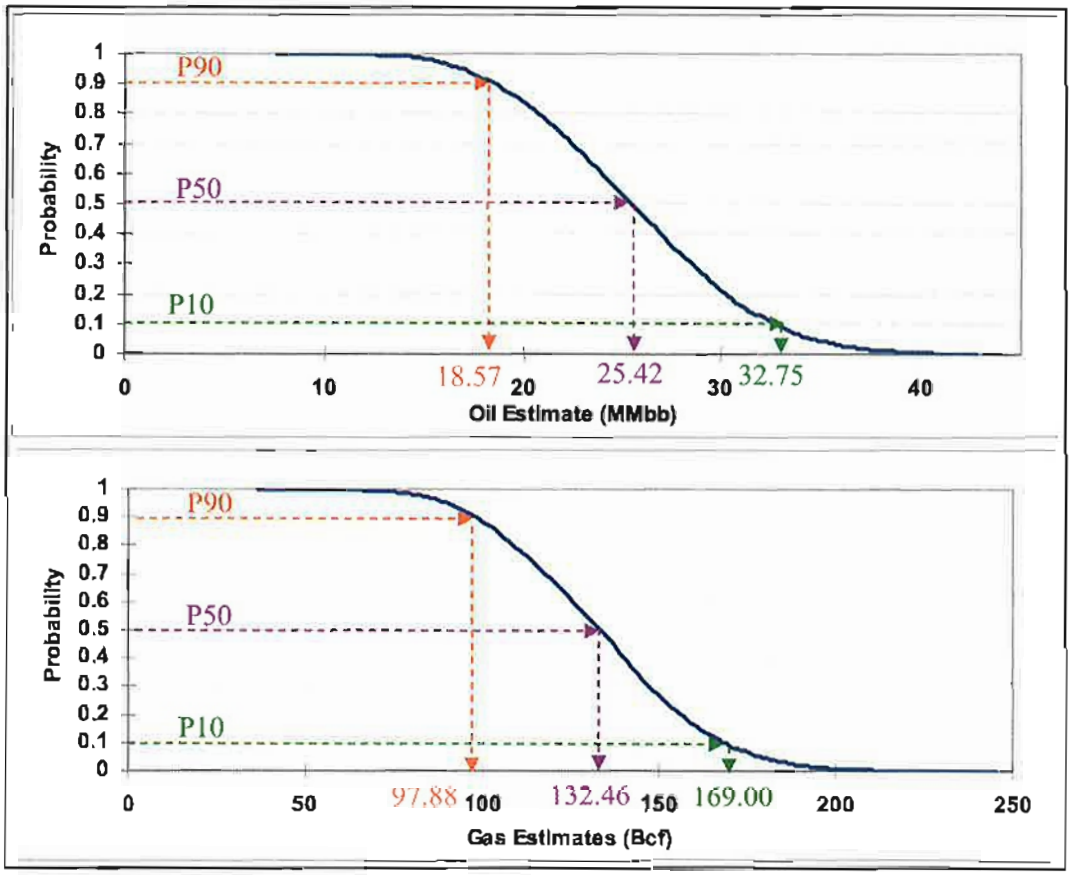

Figure 8.1: Oil and gas expected volume curves, generated using the GDV method, with P90, P50 and P10 estimated values plotted.

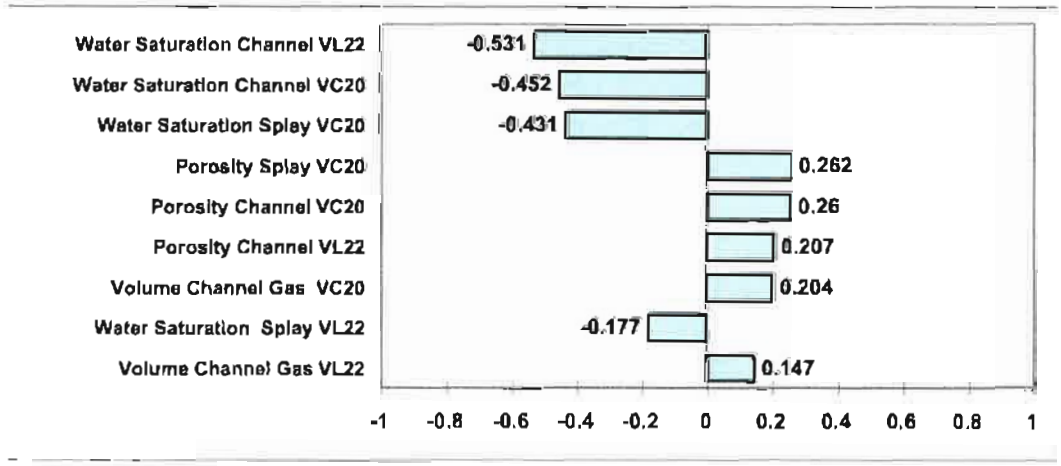

Figure 8.2: Sensitivity analysis results for the Main Dara area gas estimates. The key uncertainties is the water saturation in the channels.

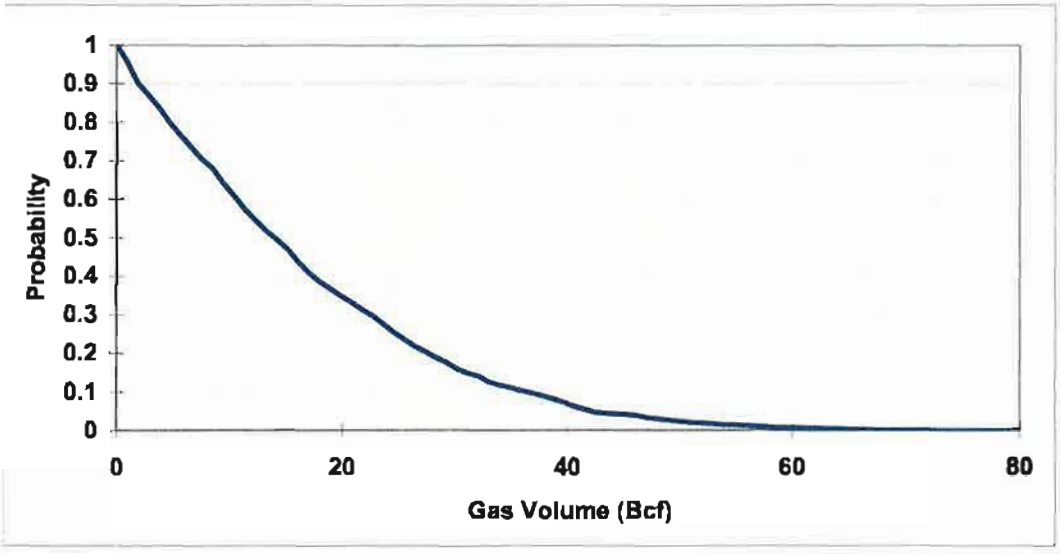

Figure 8.3: Expected remaining gas reserves, generated using the GDV method, for the Main Dara, Dara-3 and Dara-16 areas.

8.4 Expected Recovery

Part of the hydrocarbon validation process is to compare the estimates with the produced volumes to evaluate the expected recovery. Expected recovery factors can be calculated by dividing the reserve in each scenario with different gas estimates (Table 8.8). The GDV estimates were very similar to those of the stochastic model method (Tables 6.8, 6.9, 6.17, 6.18, 6.26 and 6.27) in that produced gas volume gave a very high recovery factor. The cumulative production with the P10 gave a recovery factor of 90%, which is a very high recovery factor.

Table 8.8: Expected recovery factors, generated using the GDV method, for cumulative production and different development scenarios.

Scenario	Reserves (Bcf)	Recovery %		
		P90	P50	P10
Cumulative	152.6	156	115	90
1P Dev	168.0	171	127	99
2P Dev	177.0	-	134	105
3P Dev	186.0	-	-	110

Investigation in the high recovery factors was done in Chapter 6 and 7 using two methods: stochastic modeling and GDV. The results showed that the amount of gas produced was possible when using high pay facies proportions with a high gas liberation ratio and a very high recovery factor.

8.5 Uncertainty in Recovery

The main sources of uncertainty in the recovery factor are GRV, petrophysical properties, N/G and production rates (Behrenbruch, 2005). This leads to the following questions:

- With known N/G ratio, porosity and water saturation values, what is the GRV needed to produce this amount of gas?
- With the currently used GRV, what are the N/G, porosity and water saturation values needed to get this amount of gas?

To answer these questions, if one single value is used, then one answer will be generated. However, there is no unique solution to this problem. A better strategy is to use a wide range of possible inputs to get a range of possible answers. The Monte Carlo simulation method is used here, because it is a very suitable tool to solve such problems. The solution will consider to two scenarios: without liberated gas and with liberated gas.

8.5.1 Without Gas Liberation

The cumulative gas production for the Main Dara, Dara-3 and Dara-16 areas is 152.6 Bcf. In Daralingie Field the aquifer support is very weak and gas production is due to depletion drive (Santos, 2003). The recovery factor for the depletion drive in fair to poor reservoir quality rocks ranges between 50 - 70%. The depletion drive in good reservoir quality rocks, the range is between 70 to 85% (Behrenbruch, 2005). Therefore a 70% recovery factor is a reasonable assumption for Daralingie Field.

The recoverable reserves is defined by the following equating:

Reserves = Recovery Factor * OHIP

In the above equation, the reserves part of the equation can be substituted by the cumulative production and the assumed recovery factor can be substituted by the assumed 70%. Then the equation becomes as follow

152.6 Bcf = 0.70 * OGIP = 0.70 * (GRV_{gas} * N/G * ϕ / FVF_{gas}* (1-S_w)), Where:

GRV_{gas}	Gross Rock Volume
N/G	Net to gross ratio, fraction
ϕ	Porosity, fraction
S_w	Water Saturation, fraction
FVF_{gas}	Formation Volume Factor

In the uncertainty analysis in Section 7.2, it was concluded that uncertainty in the formation volume factor does not have a significant impact on the hydrocarbon estimates. Therefore, there are four key parameters that need to be analysed, which are gross rock volume, N/G, porosity and water saturation. What are the needed values for each one of the four parameters to have a recovery of 152.6 Bcf with a recovery factor of 70%?

Gross Rock Volume

The above equation can be written as

$$GRV_{gas} = \frac{152.6Bcf}{0.70 * N/G * \phi * (1/FVF_{gas}) * (1 - S_w)}$$

Table 8.3 gives the petrophysical properties for all wells in the Main Dara, Dara-3 and Dara-16 areas. The data in Table 8.3 provides the information to build a distribution of net-gross, porosity and water saturation (Fig. 8.4). These distributions were substituted in the above equation and the results were a distribution of gross rock volume needed to get the 152.6 Bcf. Table 8.9 shows the mean values of input parameters needed produce 152.6 Bcf and Figure 8.5 shows the distribution of possible values of GRV_{gas}. To get the 152.6 Bcf with the mean properties listed in the Table 8.3 the reservoir size has to be increased by a factor of 153% over what is currently mapped.

Table 8.9: Comparison between the mapped GRV and the mean simulated gas GRV and needed to produce 152.6 Bcf with a recovery factor of 70%.

Mean Values %			GRV (m3)		Difference %
N/G	Porosity	Sw	Simulated	Mapped	
47.47	10.73	46.04	1,505,002,000	595,518,548	153

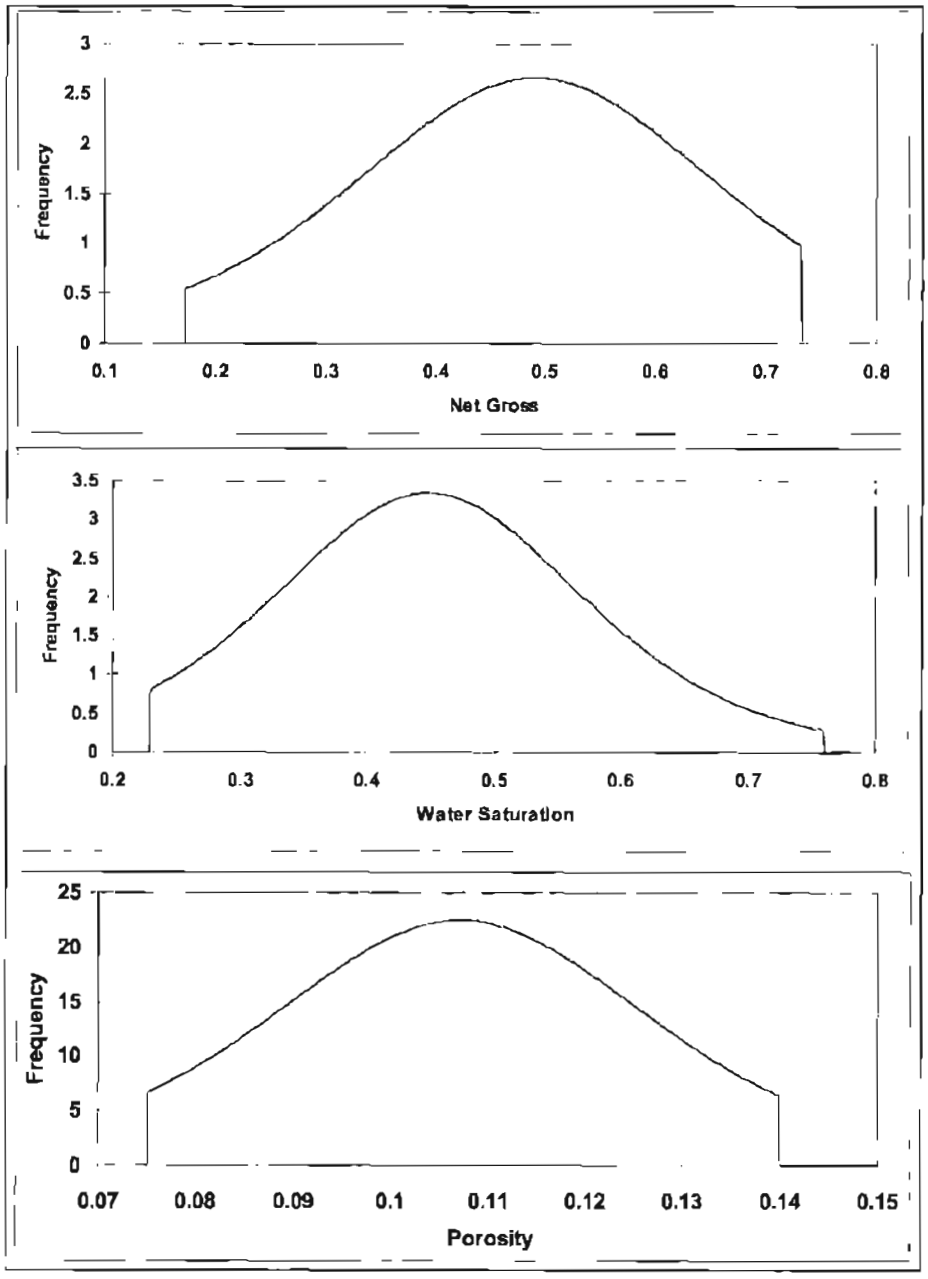

Figure 8.4: N/G ratio, porosity, water saturation distributions used to solve the volumetric equation.

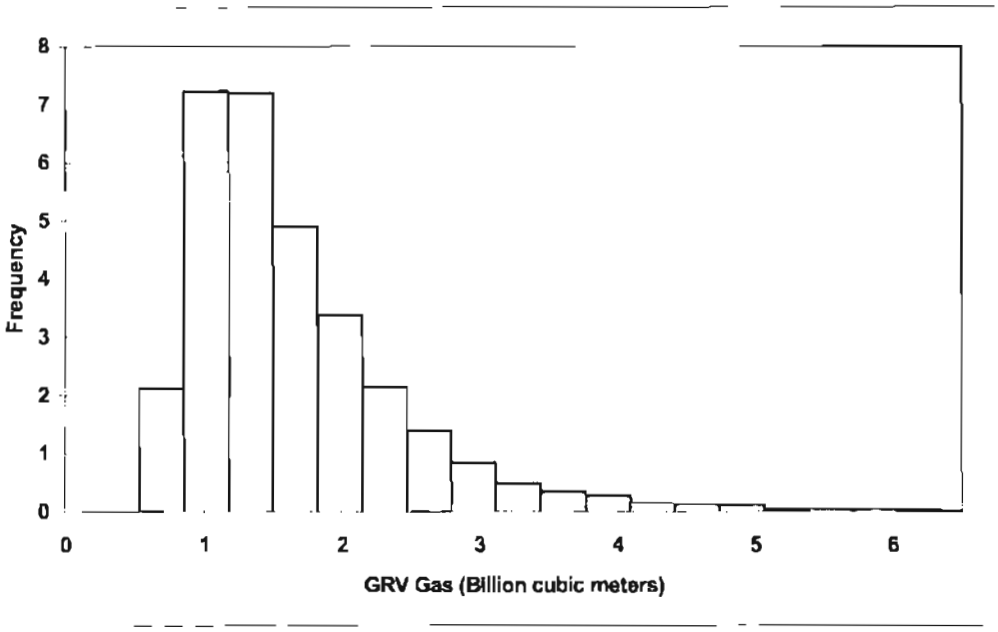

Figure 8.5: Distribution of possible GRV needed to produce 152.6 Bcf with mean well data values of N/G, porosity, water saturation and a recovery factor of 70%.

Net-Gross Ratio

The mapped GRV_{gas} and the distribution of porosity and water saturation were used to solve the equation for possible net-gross distribution. The equation is modified to simulate the net gross to

$$N/G = \frac{152.6Bcf}{0.70 * GRV_{gas} * \phi * (1/FVF_{gas}) * (1 - S_w)}$$

Table 8.10 shows the mean simulation value for net-gross and Figure 8.6 shows the distribution of possible N/G. The results indicated that with the currently mapped GRV in the gas zone with mean values of porosity and water saturation, the N/G has to be 100.8%. In other words the mean net gross has to increase by 112%, which is clearly an impossible case.

Table 8.10: Comparison between the mean N/G estimated from well data and the mean simulated N/G needed to produce 152.6 Bcf with a recovery factor of 70%.

GRV (m3)	Mean Values		Mean Net Gross %		Difference %
	Porosity %	Sw %	Simulated	Well Data	
595,518,547.76	10.73	46.04	100.8	47.47	112.34

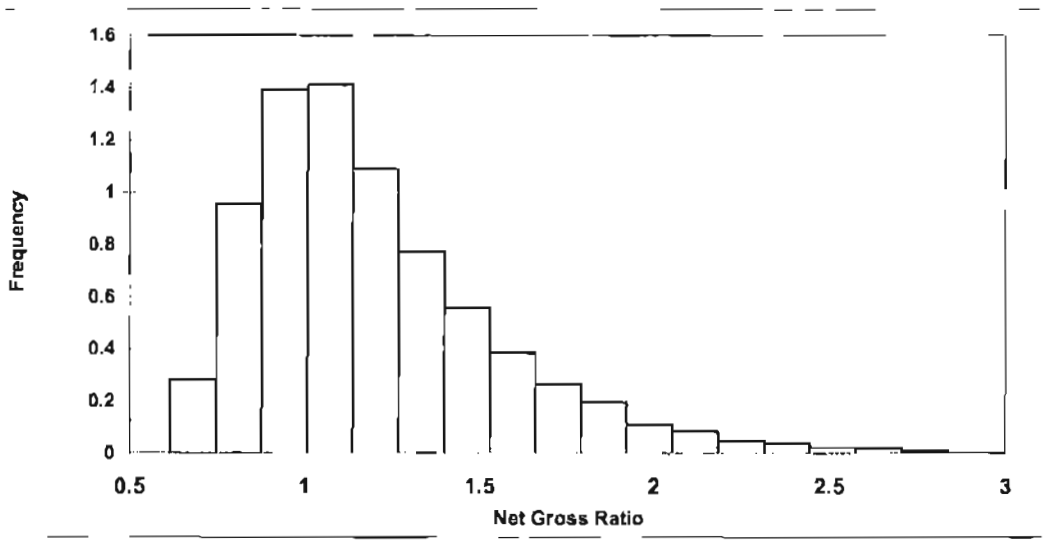

Figure 8.6: Distribution of possible N/G needed to produce 152.6 Bcf with mapped GRV in the gas zone, mean well data values of porosity, water saturation and a recovery factor of 70%.

Porosity

The mapped GRV_{gas} and the distribution of net gross and water saturation were used to solve the equation for possible porosity distribution. The equation is modified to simulate the porosity as follows:

$$\phi = \frac{152.6Bcf}{0.70 * N/G * GRV_{gas} * (1/FVF_{gas}) * (1 - S_w)}$$

Table 8.11 shows the mean simulation value for porosity and Figure 8.7 shows the distribution of possible porosity values. The results indicated that with the mapped GRV

in the gas zone with mean values of N/G and water saturation, the mean porosity has to increase to about 112%.

Table 8.11: Comparison between the mean porosity estimated from well data and the mean simulated porosity needed to produce 152.6 Bcf with a recovery factor of 70%.

Mapped GRV (m^3)	Mean Values %		Mean Porosity Values %		Difference %
	Net Gross	Sw	Simulated	Well Data	
595,518,547.76	47.47	46.04	22.78	10.73	112.30

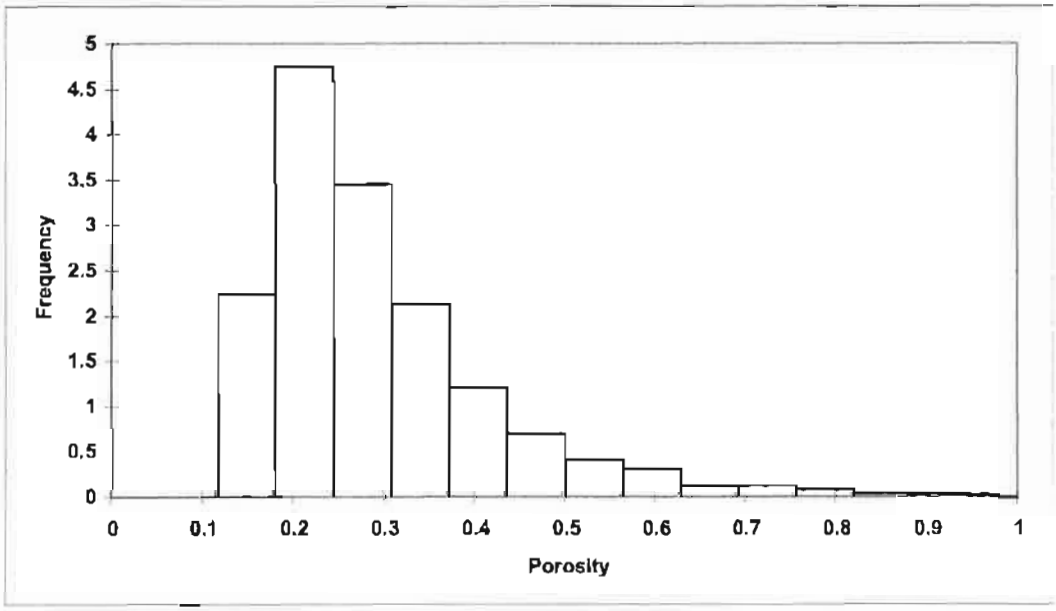

Figure 8.7: Distribution of possible porosity values needed to produce 152.6 Bcf with mapped GRV in the gas zone, mean well data values of net gross ratio, water saturation and a recovery factor of 70%.

Water Saturation

The mapped GRV_{gas} and the distribution of net gross and porosity were used to solve the equation for possible porosity distribution. The equation is modified to simulate the porosity as follows:

$$S_w = 1 - \left(\frac{152.6Bcf}{0.70 * N/G * \phi * (1/FVF_{gas}) * GRV_{gas}}\right)$$

Table 8.12 shows the mean simulation value for porosity and Figure 8.8 shows the distribution of possible porosity values. The results indicated that with the mapped GRV in the gas zone with mean values of N/G and porosity, the mean water saturation has to decrease to about 131%, which is impossible.

Table 8.12: Comparison between the mean water saturation estimated from well data and the mean simulated water saturation needed to produce 152.6 Bcf with a recovery factor of 70%.

GRV (m3)	Mean Values %		Mean Sw Values %		Difference %
	Net Gross	Porosity	Simulated	Well Data	
595,518,547.76	47.47	10.73	-14.56	46.04	- 131.62

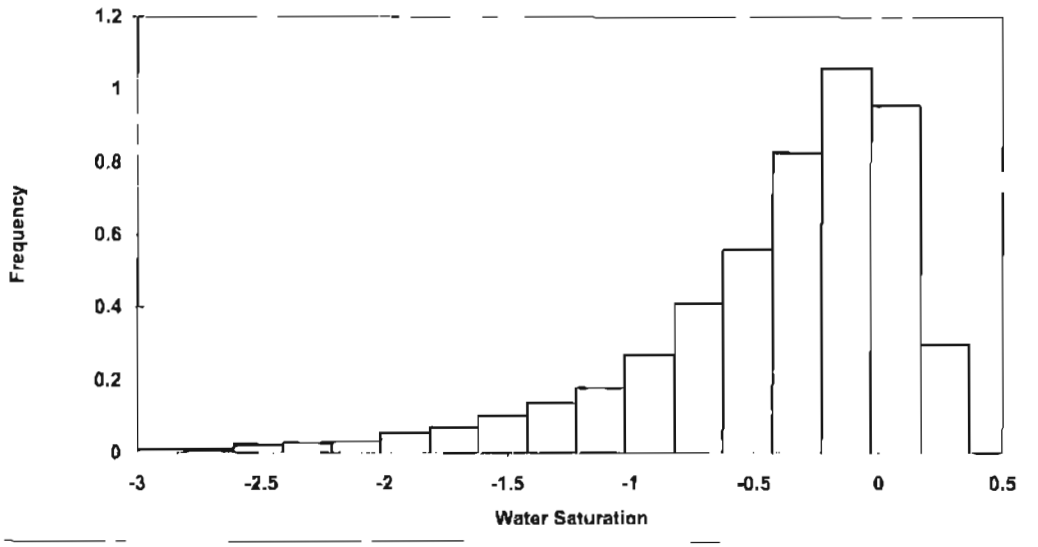

Figure 8: Distribution of possible N/G ratio needed to produce 152.6 Bcf with mapped GRV in gas zone, mean well data values of net gross ratio, porosity and a recovery factor of 70%.

8.5.2 With Gas Liberation

To account for liberated gas, the equation is as follows:

152.6 Bcf = 0.70 * OGIP + 626 cf/bbl * OOIP

152.6 Bcf = 0.70 (GRV_{gas} * N/G * ϕ * (1/FVF_{gas})* (1-S_w)) + 626 cf/bbl * (GRV_{oil} * N/G * ϕ * (1/FVF_{oil})* (1-S_w))

To simplify solving this equation, it will be assume that the N/G, the porosity and the water saturation distribution are the same for the oil and the gas. As was done for the calculation of cumulative production without gas liberation, each input will be solved separately.

Gross Rock Volume

For GRV_{gas}, the equation will be:

$$GRV_{gas} = \frac{(152.6Bcf - 626cf/bbl * (GRV_{oil} * N/G * \phi * FVF_{oil} * (1 - S_w))}{0.70 * N/G * \phi * FVF_{gas} * (1 - S_w)}$$

Table 8.13 shows the mean values of input parameters needed to produce 152.6 Bcf with a liberated gas ration of 626cf/bbl with mean well values and the mean simulated GRV_{gas}. To get the 152.6 Bcf, the reservoir size has to increase by a factor of 135% than what is mapped currently.

Table 8.13: Comparison between the mapped GRV in the gas zone and the mean simulated GRV needed to produce 152.6 Bcf with a recovery factor of 70% and accounting for the liberated gas from the oil rim ratio.

Mean Values %			GRV (m^3)			Difference %
Net Gross	Porosity	Sw	Mapped Oil	Simulated Gas	Mapped Gas	
47.47	10.73	46.04	198,957,597	1,400,965,000	595,518,548	135

For the GRV_{oil} the equation becomes

$$GRV_{oil} = \frac{152.6Bcf - 0.70 * N/G * \phi * (1/FVF_{gas}) * (1 - S_w)}{626cf/bbl * N/G * \phi * (1/FVF_{oil}) * (1 - S_w)}$$

Table 8.14 shows the mean values of input parameters needed to produce 152.6 Bcf with a liberated gas ratio of 626cf/bbl with mean well values and the mean simulated GRV_{oil}. To get the 152.6 Bcf, the reservoir size has to increase by a factor of 151,538% to what is currently mapped, which is totally impossible.

Table 8.14: Comparison between the mapped GRV in the gas zone and the mean simulated GRV needed to produce 152.6 Bcf with a recovery factor of 70% and accounting for the liberated gas from the oil rim.

Mean Values %			GRV (m^3)			Difference %
Net Gross	Porosity	Sw	Gas	Simulated Gas	Actual Oil	
47.47	10.73	46.04	595,518,548	301,695,200,000	198,957,597	151,538

Net Gross Ratio

$$N/G = \frac{152Bcf}{((0.70 * GRV_{gas} * \phi * (1/FVF_{gas}) * (1 - S_w)) + (626cf/bbl * GRV_{gas} * \phi * (1/FVF_{oil}) * (1 - S_w))}$$

Table 8.15 shows the mean values of input parameters needed produce 152.6 Bcf with a liberated gas ratio of 626cf/bbl with mean well values and the mean simulated net-gross. To get the 152.6 Bcf, the reservoir size has to increase by a factor of 94.27% to what is calculated from well data.

Table 8.15: Comparison between the mapped GRV in the gas zone and the mean simulated GRV and needed to produce 152.6 Bcf with a recovery factor of 70% and accounting for the liberated gas.

Mapped GRV (m^3)		Mean Values		Mean Net/Gross %		Difference %
Oil	Gas	Porosity %	Sw %	Simulated	Well Data	
198,957,597	595,518,547.76	10.73	46.04	92.22	47.47	94.27

Porosity

$$\phi = \frac{152Bcf}{((0.70*GRV_{gas}*N/G*(1/FVF_{gas})*(1-S_w))+(626cf/bbl*GRV_{gas}*N/G*(1/FVF_{oil})*(1-S_w))}$$

Table 8.16 show the mean values of input parameters needed produce 152.6 Bcf with liberated gas ratio of 626cf/bbl with mean well values and the mean simulated porosity. To get the 152.6 Bcf the reservoir size has to increase by a factor of 110% to what it is calculated from well data.

Table 8.16: Comparison between the mapped GRV in the gas zone and the mean simulated GRV needed to produce 152.6 Bcf with a recovery factor of 70% and accounting for the liberated gas from the oil rim.

Mapped GRV (m3)		Mean Values %		Mean Porosity Values %		Difference %
Oil	Gas	Net Gross	Sw	Simulated	Well Data	
198,957,597	595,518,547.76	47.47	46.04	22.54	10.73	110.07

Water Saturation

$$S_w = 1 - \frac{152Bcf}{(0.70*GRV_{gas}*N/G*(1/FVF_{gas})*\phi)+(626cf/bbl*GRV_{gas}*N/G*(1/FVF_{oil})*\phi)}$$

Table 8.17 shows the mean values of input parameters needed produce 152.6 Bcf with a liberated gas ratio of 626cf/bbl with mean well values and mean simulated water saturation. To obtain the 152.6 Bcf, the water saturation has to decrease by a factor of 121% to what is calculated from well data.

Table 8.17: Comparison between the mapped GRV in the gas zone and the mean simulated GRV needed to produce 152.6 Bcf with a recovery factor of 70% and accounting for the liberated gas from the oil rim.

Mapped GRV (m^3)		Mean Values %		Mean Sw Values %		Difference %
Oil	Gas	Net Gross	Porosity	Simulated	Well Data	
198,957,597	595,518,547.76	47.47	10.73	-9.72	46.04	- 121.11

Even if using higher ratios for the liberated gas, there would not be much difference in the results. So far all evidence strongly agrees that the currently mapped reservoir volume and the existing petrophysical well properties with an assumed recovery factor of 70% cannot match the cumulative production. All evidence shows that the currently mapped GRV for oil and gas is not enough to account for the cumulative production.

This study confirms that the currently mapped GRV for Daralingie Field is not enough to account for the cumulative production. As an increase in mapped GRV is impossible, this study strongly indicates that there is a gas influx into the reservoir from sources outside the mapped GRV. There are known gas fields in the Patchawarra Formation such Cowan, Barina and Farina that fall within close proximity to the Daralingie Field. Furthermore, there is evidence that indicates the existence of potential gas reserves in the weathered and deep fractured Pre-Permian rocks (Flottmann et al., 2004). The Cooper Basin is very rich with gas and these gas reservoirs could provide gas influx into the Daralingie Field, however the mechanism of this gas influx is highly speculative.

Current seismic data show that the Daralingie Field is highly faulted and some of the faults are very extensive and cut through several fields (Adam Hill, Santos, personal communication 2005.) The impact of faulting on hydrocarbon flow in reservoirs is well known and well documented in the literature (Ellevset et al., 1998; Kani and Knipe, 1998). The faults could be either conductive or sealing. Conductive faults could provide a fluid flow path that allows communication between reservoirs. The sealing faults may cause the reservoir to be compartmentalised. There is evidence that the Daralingie Field is compartmentalised due to sealing faults, for example the variability in the fluid contacts. Where the North Dara area has a different GOC to the Dara Main area. The gas accumulation in the North Dara is isolated from the other gas accumulation in the Daralingie Field, but the OWC is the same as other areas of the field. This indicates that some of the faults are sealing, which prevented GOC homogeneity, but there could be some conductive faults that allow the homogeneity of OWC. If such faults exist and were

long enough to reach the surrounding reservoir, they would allow gas influx into the reservoir.

In the literature there are a few published papers that suggest hydrocarbon mixing from different rock sources has occurred in the Eromanga Basin. The geochemistry analysis of oil samples taken from the Moorari Field indicated that it came from Jurassic-Cretaceous and Permian sources (Arouri et al., 2004; Arouri and McKirdy, 2005). There is also indication that further mixing with source rocks from Pre-Permian has occurred (David McKirdy, The University of Adelaide, personal communication, 2005.) This indicates that communication between source rocks of different ages and reservoir has occurred. The evidence refers to hydrocarbon migration paths, but supports the theory that there is current fluid communication between different reservoirs through a network of conductive faults.

It can be safely stated that there are possible sources for the gas influx into the Daralingie Field through conductive faults. The gas could be coming laterally from surrounding reservoirs or coming from deeper source rocks. The phenomenon of the very high gas recovery factor is currently observed in the Daralingie Field, but it may be discovered in other fields as they reach a maturity stage similar to Daralingie Field. The use of rock mechanics to differentiate sealing faults from conductive faults is beyond the scope of this study, but would be a significant focus for future research.

Chapter 9
Concluding Summary

9.1 Daralingie Study

An integrated reservoir characterisation study for the Daralingie Field has integrated all available data for the VC00-VC35 reservoir interval in the Patchawarra Formation. The aim of this case study was to investigate the high unexpected gas production recovery factor. This study was carried out in four phases: reservoir characterisation, stochastic geological modeling, hydrocarbon estimation and uncertainty assessment. The key conclusion of this study is that the developed reservoir model, even at the maximum geological limit, cannot account for the cumulative gas production and there must be gas influx coming from sources outside the mapped reservoir. The source of the gas influx could be coming from the Pre-Permian weathered rocks or gas influx could be coming from surrounding fields laterally through faults. Furthermore, some gas influx is coming from the oil rim that exists in the Daralingie Field.

In the reservoir characterisation phase of this study an integrated reservoir study utilising all available data from the Daralingie Field and surrounding area was conducted. It started with the geological description of the facies in the reservoir interval in the Daralingie Field based on core analysis. These facies were matched to their petrophysical log signatures, so facies could be defined based on logs in uncored wells. Extensive work was performed to estimate reservoir geometry by using thickness-to-width ratios plots, net-gross ratio plots, and modern and ancient analogues. Based on this work, nine facies maps representing the Daralingie Field depositional model were produced. The outcome of this phase was the building of a new conceptual geological model for Daralingie Field that contained all available data at the time of the study. The conceptual model was the basis for building stochastic facies and porosity models in the stochastic modeling phase.

In the stochastic modeling phase, different stochastic modeling algorithms were used to generate a range of petrophysical properties. Object-based modeling algorithms were used to generate facies-based models based on specific conceptual geological models and compared to pixel-based modeling methods. The porosity models were generated using a facies-based geostatistical algorithm. Several stochastic models constrained by well logs and facies maps were produced. These were the first stochastic models built for Daralingie Field.

In the third phase, hydrocarbon estimates were calculated using the stochastic porosity models generated in the stochastic modeling phase. These porosity models were generated using different facies percentages while keeping the same facies geometry. Cumulative production data were also used to validate volumetric calculations for each model. The final outcome of this phase showed that hydrocarbon estimates for the VC20-VC25 reservoir interval in the Dara Main area that were estimated using maximum facies proportions could be matched with the existing cumulative production if situation 2P and 3P development scenarios were true. However, it is impossible to get the cumulative production from Dara 4/20 for any development scenario.

During the course of this work, a geologically driven volumetric (GDV) method was developed to produce probabilistic hydrocarbon estimates. This method integrates the stochastic modeling method with Monte Carlo simulation to generate hydrocarbon estimates. The GDV method was applied to Daralingie Field and demonstrated advantages over Monte Carlo simulation. The GDV is geologically dependent with lower uncertainty, unlike Monte Carlo estimates that are geologically independent and have higher uncertainty. The GDV is an effective and powerful method to estimate probabilistic hydrocarbons.

In the final step uncertainty assessment was undertaken to define and quantify the key uncertainties in hydrocarbon estimates using newly developed techniques in Monte Carlo simulation. The results involved the development of a geologically driven volumetrics method that estimates reserves through the emphasis of geological knowledge. The final

part of this study was the uncertainty analysis of the high recovery factor observed in Daralingie, and a possible explanation for it.

9.2 Study Implications

There are several conclusions derived from this research that are of significance for similar studies. These are discussed below under four categories: reservoir characterisation, stochastic modeling, reserves estimation and uncertainty assessments.

9.2.1 Reservoir Characterisation

Integrated reservoir characterisation is an essential process in any geological study. It requires a multi-disciplinary approach integrating all available geological, geophysical and dynamic data. Such integration will lead to better understanding of reservoir geometry, internal structures and heterogeneities, which impact the fluid flow behaviour of the reservoir. This process should be continued through all phases of any field. As new data becomes available a review of the current understanding of the reservoir should be performed. When this process is done effectively, it reduces the geological risk and uncertainty in field development and leads to maximising field returns.

Reservoir characterisation should be the first step in any field geological study. The first stage of reservoir characterisation is data quality control. This study shows that this was essential in building up an accurate geological understanding of the reservoir. As the geological understanding of the depositional model increases, the risk of getting the wrong model decreases. Uncertainty in the depositional model can be quantified by integrating the different available data such as cores, well logs and analogues. Cores are the best available direct representation of the reservoir; unfortunately they are often limited to a few wells. Well logs are more abundant than cores, but they cannot give reliable information without calibration with core data. Ancient and modern analogues provide significant information. Combining all of these input parameters together reduces the risk and uncertainty of the depositional model, which is the basic building block in

successful reservoir development and management. To achieve a reliable geological model, the following steps are highly recommended:

- Determine and describe the geological depositional setting and important facies types through geological analysis and high-resolution sequence stratigraphy.
- Identify and map possible facies types, distribution and geometry for every reservoir sequence. This requires the examination of all available static and dynamic data and the use of modern and ancient depositional setting analogues.

9.2.2 Stochastic Modeling

The ultimate aim of stochastic modeling is to generate a 3-D petrophysical property model that can represent the reservoir, so it can be used to simulate the reservoir fluid flow behavior. Stochastic models play a significant role in field development because they are a digital representation of the reservoir. The petrophysical properties include porosity, permeability and water saturation. Therefore these models should reflect the geological knowledge obtained through the reservoir characterisation step. The best way to accomplish this objective is to build stochastic models based on the conceptual geological model. The stochastic modeling phase should be done after an adequate reservoir characterisation phase. The newly built Daralingie Field conceptual geological model resulted in petrophysical stochastic models that realistically represent the conceptual geological model.

Current stochastic modeling techniques and algorithms provide the flexibility needed to mimic the conceptual geological model. In this study, a combination of techniques was used to match the geological nature of the reservoir. In the Daralingie Field, several modeling algorithms were used to match the geological conceptual model. Also, the stochastic model must be quality-controlled visually and statistically to guarantee its adequacy. Quality controls are essential feedback loops in the model building process. It is very important to optimise an upscaling scheme that minimises the stochastic model size while preserving the main vertical reservoir heterogeneities. There are no direct methods to achieve this and it has to be done through trial and error. The upscalling scheme should also be quality controlled visually and statistically. No compromises can

be taken in the quality control step, because all results that are generated based on this model will be dependent on its accuracy.

9.2.3 Reserve Estimation

What is the best method to estimate hydrocarbon? This is not a simple question and it tends to generate more questions such as what are the available data and what will the results be used for? Should the hydrocarbon estimates be conservative with the potential to increase in the future? Should they be deterministic estimates or probabilistic estimates with an associated range of uncertainty?

The selection of the reserve estimation method depends on the data availability. Usually the end user of the estimates is not the person who made the estimates. This is the case in most oil companies, where the technical staff generates hydrocarbon estimates and reports them to senior management to make decisions. The decision could range from approving a plan to drill more wells to a multi-billion dollars development plan. Probabilistic reserve estimation methods give an objective estimate with a measure of uncertainty, unlike the other methods. Hence the decision maker may be considering possible options based on the estimate uncertainty range. The GDV method provides probabilistic estimates that represent geological data as well as petrophsycial data. It is suitable for all field types with different stages of maturity.

9.2.4 Uncertainty Assessments

Understanding and managing uncertainty is central to the oil and gas industry. The in-place hydrocarbon estimates are the life support for the industry and uncertainty in these estimates means uncertainty in the industry future. Uncertainty cannot be eliminated and ignoring it may bear undesirable consequences. Therefore it should be an essential and an integral part of any reservoir characterisation and hydrocarbon estimation study. Uncertainty assessments should be carried out after the completion of each major project step.

This study has shown that the depositional facies proportions controls the volumes of in place hydrocarbons. Therefore the ability to generate multiple possible depositional facies scenarios will allow better understanding of uncertainty, since the true geological scenario may never be known. There should be at least three basic scenarios representing minimum, mean and maximum geologically reasonable facies proportions, which will cover a large possibility range. Probabilistic hydrocarbon estimation methods such as GDV generate hydrocarbon estimates with their associated uncertainties, and are highly recommended for use in any study.

9.3 Recommendations

Further investigations for the sources of gas influx in Daralingie Field are needed. Gas composition comparison between Daralingie Field, surrounding fields and possibly deeper reservoirs are required to locate the gas influx. Also, it is highly recommended to increase the study area to include surrounding gas fields, which might be in lateral communication with Daralingie Field.

In this study, constant water saturation values were used due to the lack of J-functions. J-functions are used to generate water saturation models based on facies and porosity and hence give better estimates of water saturation in the reservoir. It is highly recommended that hydrocarbon estimation using stochastic modeling methods are based on saturation models, instead of a constant value.

The channel belt orientations could be improved by using impedance maps. These maps could be generated from the 3D seismic survey available. The orientation of the channel belts is not expected to change, but it would provide more confidence in the facies maps.

In this study, faults were provided as polygons without data on fault throws. The fault throws were calculated by Roxar RMS based on the structure maps provided by Santos. It

is highly recommended that a more detailed structure model with fault throws be incorporated in future modeling efforts.

9.4 Concluding Statement

Uncertainty is a fact of life and it is always there. But does it mater? In this study the uncertainty assessment and quantification of the Daralingie Field hydrocarbon in-place has been accomplished. The next action regarding the results of this study is in the hands of the decision maker. There are three possible actions to take, which are live with it, reduce it or exploit it. Living with the uncertainty means keeping everything as it is and no extra financial expenditure is needed. This option may seem to be attractive, but it may result in losing any upside potential. The second option is to reduce the uncertainty by acquiring more data such as those mentioned in the recommendations. This option will require manpower and expenditure, but has the upside potential of increasing the reserves. The third option is to exploit the uncertainty, for example drilling more wells, which is the riskiest option, but also has the potential to be the most rewarding financially. Whatever decision will be made, surely uncertainty will influence it.

References

Ahlbrandt, T. S., J. R. Blasic, P. Blystad, and D. Kelter, 2004, Updated United Nations Framework Classification for Reserves and Resources of Extractive Industries: SPE 90839, SPE Annual Technical Conference and Exhibition.

Aminian, K., B. Thomas, and H. I. Bilgesu, 2002, A New Approach for Reservoir Characterization: SPE 78710, SPE Eastern Regional Meeting.

Apak, S. N., W. J. Stuart, N. M. Lemon, and G. R. Wood, 1997, Structural Evolution of the Permian-Triassic Cooper Basin, Australia: Relation to Hydrocarbon Trap Styles: American Association of Petroleum Geologists, v. 81, p. pp. 533-555.

Arouri, K. R., and D. M. McKirdy, 2005, The behavior of aromatic hydrocarbons in artificial mixtures of Permian and Jurassic end-member oils: application to in-reservoir mixing in the Eromanga Basin, Australia: Organic Geochemistry, v. 36, p. 105-115.

Arouri, K. R., D. M. McKirdy, L. Schwark, D. Leythaeuser, and P. J. Boult, 2004, Accumulation and mixing of hydrocarbons in oil fields along the Murteree Ridge, Eromanga Basin, South Australia: Organic Geochemistry, v. 35, p. 1597-1618.

Ates, H., M. Kelkar, and A. Datta-Gupta, 2003, The Description of Reservoir Properties by Integrating Geological, Geophysical and Engineering Data, The University of Tulsa and Texas A&M University, Joint Industry Project, pp. 3-16.

Avenell, L. C., 1998, The South Blackwater Reservoir Analogue Project: Honours Thesis, unpublished thesis, Queensland University of Technology, Brisbane, Australia.

Azim, S. A., S. M. Abdullah, H. Al-Zaabi, W. Al-Awadi, H. M. Najeh, W. B. Bryant, R. Aldred, and M. Steel, 2005, Resistively Anisotropy and its Impact of Reserves Estimates and Technology Applications in North Kuwait Reservoirs: SPE 93503, 14th SPE Middle East Oil and Gas Show and Conference.

Behn, R. D., and J. W. Vaupel, 1982, Quick Analysis for Busy Decision Makers: New York, USA, Basic Books.

Behrenbruch, P., 2005, Short Course Notes, Oil and Gas Resources and Reserves, The Australian School of Petroleum, The University of Adelaide, Adelaide, SA, Australia.

Beliveau, D., and R. Baker, 2003, Reserves Growth: Enigma, Expectation or Fact?: SPE 84144, SPE Annual Technical Conference and Exhibition.

Brakel, A. T., and J. M. Totterdell, 1996, Palaeogeographic Atlas of Australia, v. 6: Canberra, Australia, Australian Government Publishing Service, 39 p.

Bridge, J. S., and R. S. Tye, 2001, Interpreting the Dimensions of Ancient Fluvial Channel Bars, Channels, and Channel Belts from Wireline-Logs and Cores: American Association of Petroleum Geologists, v. 84, p. 1205-28.

Chambers, R. L., M. A. Zinger, and M. C. Kelly, 1994, Constraining Geostatistical Reservoir Descriptions with 3-D Seismic Data to Reduce Uncertainty, AAPG Computer Application Geology, No. 3., p. pp. 143-57.

Coombes, J., 1997, Handy Hints for Varography: AusIMM Iron making Resources and Reserves Conference, p. pp. 127-130.

Cosentino, L., 2001, Integrated Reservoir Studies: Institue Francais Du Petrole Publications: Paris, Editions TECHNIP, 310 p.

Cronquist, C., 1991, Reserves and Probabilities - Synergism or Anachronism?: Journal of Petroleum Technology, p. pp. 1258 - 1264.

Cronquist, C., 2001, Estimation and Classification of Reserves of Crude Oil, Natural Gas and Condensate: SPE Books: Richardson, Texas, USA, SPE, pp.416 p.

Ellevset, S., R. J. Knipe, T. Olsen, Q. J. Fisher, and G. Jones, 1998, Fault Controlled Communication in the Sleipner Vest Field, Norwegian Continental Shelf; Detailed, Quantitative Input for Reservoir Simulation and Well Planning: Faulting, *in* G. Jones, Q. J. Fisher, and R. J. Knipe, eds., Fault Sealing and Fluid Flow in Hydrocarbon Reservoirs, v. 47: London, UK, Geological Society, p. 283-297.

Etherington, J. R., and E. J. Hunt, 2004, Can You Have Probable Without Proved Reserves?: SPE 90241, SPE Annual Technical Conference and Exhibition.

Fielding, C. R., and R. C. Crane, 1987, An Application of Statistical Modeling to the Prediction of Hydrocarbon Recovery Factors in Fluvial Reservoir Sequences., *in* F. G. Ethridge, R. M. Flores, and A. D. Harvery, eds., SEPM Special Publication 39, p. 321-27.

Flottmann, T., D. J. Campagna, R. Hillis, and D. Warner, 2004, Horizontal Microfracutres and Cores Discing in Sandstone Reservoirs, Cooper Basin, Australia: PESA Eastern Australasian Basins Symposium II.

Garb, F. A., 1985, Oil and Gas Reserves Classification, Estimation and Evaluation: Journal of Petroleum Technology, p. pp. 373-390.

Garb, F. A., 1988, Assessing Risk in Estimating Hydrocarbon Reserves and in Evaluating Hydrocarbon-Producing Properties: Journal of Petroleum Technology, v. June 1988, p. pp. 765-778.

Gilman, J. R., H.-Z. Meng, M. J. Uland, P. J. Dzurman, and S. Cosic, 2002, Statistical Ranking of Stochastic Geomodels Using Streamline Simulation: A Field Application: SPE 77374, SPE Annual Technical Conference and Exhibition.

Harrell, D. R., J. E. Hodgin, and T. Wagenhofer, 2004, Oil and Gas Reserves Estimates: Recurring Mistakes and Errors: SPE 91069, SPE Annual Technical Conference and Exhibition.

Hill, A., 2004, Daralingie Volumetrics, How Big Was The Prize?, Adelaide, SA, Australia, Santos.

Isaaks, E. H., and R. M. Srivastava, 1989, An Introduction to Applied Geostatistics: New York, USA, Oxford University Press, 561 p.

Jian, F. X., D. K. Laruc, A. Castellini, and J. Toldi, 2002, Reservoir Modeling Methods and Characterization Parameters for A Shoreface Reservoir: What is Important for Fluid Flow Performance?: SPE 77428, SPE Annual Technical Conference and Exhibition.

Journal, A. G., and C. J. Huijbregts, 1978, Mining Geostatistics: San Diego, CA, USA, Academic Press, p.600 p.

Kazmier, L. J., 1996, Theory and Problems of Business Statistics: Scham's Outline Series: New York, USA, McGraw Hill, pp.410 p.

Knai, T. A., and R. J. Knipe, 1998, The Impact of Faults on Fluid Flow in the Heidrun Field, *in* G. Jones, Q. J. Fisher, and R. J. Knipe, eds., Faulting, Fault Sealing and

Fluid Flow in Hydrocarbon Reservoirs, v. 47: London, UK, Geological Society, p. 269-282.

Laherrer, J. H., 2000, Learn Strengths, Weaknesses to Understand Hubbert Curve: Oil and Gas Journal, 17 April 2000, p. 63-75.

Laherrer, J. H., 1999, Reserve Growth: Technological Progress, or Bad Reporting and Bad Arithmetic?: Geopolitics of Energy, v. 4, p. PP. 7-16.

Landa, J. L., R. N. Horne, M. M. Kamal, and C. D. Jenkins, 2000, Reservoir Characterization Constrained to Well-Test Data: A Field Example: SPE Reservoir Evaluation and Engineering, v. 4, p. 325-334.

Lang, S. C., and N. Ceglar, 2000, Baryulah Analogues Project, Adelaide, SA, Australia, Australian School of Petroleum, p. 42.

Lang, S. C., N. Ceglar, S. Forder, G. Spencer, and J. Kassan, 2002, High Resolution Sequence Stratigraphy, Reservoir Analogues, and 3D Seismic Interpretation-Application to Exploration and Reservoir Development in The Baryulah Complex, Cooper Basin, Southwest Queensland: APPEA Journal, v. 42, p. 512-521.

Lang, S. C., P. Grech, R. Root, A. Hill, and D. Harrison, 2001, The Application of Sequence Stratigraphy to Exploration and Reservoir Development in the Cooper-Eromanga-Bowen-Surat Basin System: APPEA Journal, v. 41, p. pp. 223-250.

Lang, S. C., J. Kassan, J. M. Benson, C. A. Grasso, and L. C. Avenell, 2000, Applications of Modern and Ancient Geological Analogues in Characterisation of Fluvial and Fluvial-Lacustrine Deltaic Reservoirs in the Cooper Basin: APPEA Journal, v. 40, p. pp. 393-416.

Ligero, E. L., C. Maschio, and D. J. Schiozer, 2003, Quantifying the Impact of Grid Size, Upscaling and Streamline Simulation in the Risk Analysis Applied to Petroleum Field Development: SPE 79677, SPE Reservoir Simulation Symposium.

Macary, S. M., A. Hassan, and E. Ragaee, 1999, Better Understanding of Reservoir Statistics is the Key for Reliable Monte Carlo Simulation: SPE 53264, SPE Middle East Oil Show.

Marquez, L. J., M. Gonzalez, S. Gamble, E. Gomez, H. A. Vivas, H. M. Bressler, L. S. Jones, S. M. Ali, and G. S. Forrest, 2001, Improved Reservoir Characterization of a Mature Field Through an Integrated Multi-Disciplinary Approach. LL-04 Reservoir, Tia Juana Field, Venezuela: SPE 71355, SPE Annual Technical Conference and Exhibition.

Massonnat, G. J., 2000, Can We Sample the Complete Geological Uncertainty Space in Reservoir-Modeling Uncertainty Estimates?: SPE Journal, v. 5, p. 46-59.

McGilvray, W. G., and R. M. Shuck, 1998, Classification of Reserves: Guidelines and Uncertainty: SPE 39821. SPE International Petroleum Conference and Exhibition.

Meng, H. Z., K. S. Godbey, J. R. Gilman, and M. J. Uland, 2002, Integrated Reservoir Characterization and Simulation for Reservoir Management using a Web-Based Collaborative Technical Workflow Manager: SPE 77673, SPE Annual Technical Conference and Exhibition.

Montgomery, S. L., and C. D. Morgan, 1998, Bluebell Field, Unita Basin: Reservoir Characterization for Improved Well Completion and Oil Recovery: American Association of Petroleum Geologists, v. 82, p. 1113-1132.

Murtha, J. A., 1994, Incorporating Historical Data Into Monte Carlo Simulation: SPE Computer Application, p. pp.11-17.

Murtha, J. A., 2002, Sums and Products of Distributions: Rules of Thumb and Applications: SPE 77422, SPE Annual Technical Conference and Exhibition.

Nakanishi, T., and S. C. Lang, 2002, Towards An Efficient Exploration Frontier: Constructing A Portfolio of Stratigraphic Traps in Fluvio-Lacustrine Successions, Cooper-Eromanga Basin.: APPEA Journal, v. 42, p. 131-50.

Nakanishi, T., S. C. Lang, and A. B. Mitchell, 2003, Visualization of a Fluvial Channel Reservoir Analogue from The Birkhead Formation, Merrimelai, Meranji and Pelican Fields, Eromanga Basin: APPEA Journal, v. 43, p. 453-70.

Palke, M. R., and D. C. Rietz, 2001, The Adoption of Reservoir Simulation Models for Use in Reserve Certification Under Regulatory Guidelines or Reserves Definitions: SPE 71430, SPE Annual Technical Conference and Exhibition.

Posamentier, H. W., and G. P. Allen, 1999, Siliciclastic Sequence Stratigraphy-Concepts and Application: SEPM Concepts in Sedimentology and Palaeontology #7.

Qassab, H. M. A., J. Fitzmaurice, Z. A. Al-Ali, M. A. Al-Khalifa, G. A. Aktas, and P. W. Glover, 2000, Cross-Discipline Integration in Reservoir Modeling: The Impact on Fluid Flow Simulation and Reservoir Management: SPE 62902, SPE Annual Technical Conference and Exhibition.

Ross, J. G., 2001, SPE/WPC/AAPG Resource Definitions as a Basis for Portfolio Management: SPE 68573, SPE Hydrocarbon Economics and Evaluation Symposium.

Santos, 1987, Daralingie-18 P.V.T. Report., Adelaide, SA, Australia, 25 p.

Santos, 2003, 2003 CGT Reserves Review, unpublished report, Adelaide, SA, Australia, 5 p.

Schlagenhauf, M., and E. Jaynes, 1995, Geophysical Reserves Classification Proved, Probable, and Possible: SPE 30039, SPE Hydrocarbon Economics and Evaluation Symposium.

Smith, L. C., and D. E. Alsdorf, 1998, A Control on Sediment and Organic Carbon Delivery to the Arctic Ocean Revealed with Satellite SAR: Ob' River, Siberia: Geology, v. 26, p. pp. 395-98.

Smith, N. D., and M. Perez-Arlucea, 1994, Fine-grained Splay Deposition in the Avulsion Belt of the Lower Saskatchewan River, Canada: Journal of Sedimentary Research, v. B64, p. 159-69.

Startzman, R. A., and R. A. Wattenbarger, 1985, An Improved Computation Procedure for Risk Analysis Problems With Unusual Probability Functions: SPE 13722, SPE Hydrocarbon Economics and Evaluation Symposium.

Strong, P. C., G. R. Wood, S. C. Lang, A. Jollands, E. Karalaus, and J. Kassan, 2001, Moomba Area Patchawarra Study, Santos, p. 59.

Strong, P. C., G. R. Wood, S. C. Lang, A. Jollands, E. Karalaus, and J. Kassan, 2002, High Resolution Palaeogeographic Mapping of the Fulvial-Lacustrine Patchawarra Formation in the Cooper Basin, South Australia: APPEA Journal, v. 42, p. 65-81.

Tahmhane, D., L. Wang, and P. M. Wong, 1999, The Role of Geology In Stochastic Reservoir Modeling: The Future Trends: SPE 54307, SPE Asia Pacific Oil and Gas Conference and Exhibition.

Taylor, P. J., 1997, Modeling the U.S. Oil Industry: How Much Oil is Left?: Journal of Petroleum Technology, p. 502-507.

Thompson, R. S., J. D. Wright, and S. A. Digert, 1987, The Error in Estimating Reserves Using Decline Curves: SPE 16295, SPE Hydrocarbon Economics and Evaluation Symposium.

Towler, B. F., 2002, Fundamental Principles of Reservoir Engineering: SPE Textbook, v. Vol 8: Richardson, Texas, USA, SPE, 232 p.

Tye, R. S., and J. J. Hickey, 2001, Permeability characterization of distributary mouth bar sandstone in Prudhoe Bay field, Alsaka: How horizontal cores reduce risk in developing deltaic reservoirs: American Association of Petroleum Geologists, v. 85, p. 459-475.

Vasiliev, S. V., 2001, Peat Accumulation rates in West Siberia: West Siberian Peatlands and Carbon Cycle: Past and Present. Proceedings, International Field Symposium, Noyabrsk, p. pp. 58-9.

Veevers, J. J., 2000, Billion-Year Earth History of Australia and Neighbors in Gondwanaland: Sydney, GEMOC Press.

List of Symbols and Abbreviations

1P Development Scenario Case-1
2P Development Scenario Case-2
3P Development Scenario Case-3
3D Three Dimensional
bbl Standard Oil Barrel
Bcf Billion Standard Cubic Feet
Bg Gas Formation Volume Factor
Bo Oil Formation Volume Factor
BPD Oil Barrel Per Day
cc Correlation Coefficient
cdf Cumulate Density Function
cf Cubic Feet
CLT Central Limit Theory
COV Coefficient of Variance
DST Drill Steam Test
DT Sonic Log
FVF Formation Volume Factor
GDV Geologically Driven Volumetrics
GOC Gas Oil Contact
GR Gamma Ray Logs
GRV Gross Reservoir Volume
Mbbl Million Standard Oil Barrels
Mcfd Million Standard Cubic Feet Per Day
N/G Net Gross Ratio
OGIP Original Gas In Place
OHIP Original Hydrocarbon In Place
OOIP Original Oil In Place
OWC Oil Water Contact
P10 10% confidence that there will be this hydrocarbon amount or more
P50 50% confidence that there will be this hydrocarbon amount or more
P90 90% confidence that there will be this hydrocarbon amount or more
scf/bbl Standard Cubic Fee Per Standard Oil Barrel
Sw Water Saturation
δ Standard Deviation
ϕ Porosity
μ Mean

Appendix 1

Reservoir interval tops for wells used to generate the 3D stochastic model

Well Name	X-Location	Y-Location	Subsea Depth	Marker Name
BARINA_1	393790.33	6868961.38	7049.25	VC00
BARINA_1	393790.32	6868961.37	7058.45	VL05
BARINA_1	393790.27	6868961.35	7082.11	VC10
BARINA_1	393790.19	6868961.30	7100.34	VL11
BARINA_1	393790.15	6868961.28	7127.20	VC15
BARINA_1	393790.02	6868961.21	7150.46	VC20
BARINA_1	393789.94	6868961.17	7166.98	VL22
BARINA_1	393789.88	6868961.14	7221.49	VC25
BARINA_1	393789.86	6868961.13	7257.32	VC30
BARINA_1	393789.84	6868961.12	7264.80	PPER
BARINA_2	394152.28	6867460.07	7099.31	VC00
BARINA_2	394153.39	6867455.02	7112.48	VL05
BARINA_2	394153.48	6867454.69	7119.88	VC10
BARINA_2	394153.69	6867453.94	7162.95	VL11
BARINA_2	394153.78	6867453.60	7190.38	VC15
BARINA_2	394154.04	6867452.66	7217.92	VC20
BARINA_2	394154.16	6867452.23	7243.73	VL22
BARINA_2	394154.28	6867451.80	7294.18	VC25
BARINA_2	394154.37	6867451.51	7332.80	VC30
BARINA_2	394154.37	6867451.51	7360.20	VC35
BARINA_2	394154.37	6867451.51	7385.20	PPER
BARINA_2	394154.37	6867451.51	7510.00	TD
BARINA_3	394725.69	6869568.05	6999.31	VC00
BARINA_3	394724.08	6869569.98	7011.70	VL05
BARINA_3	394724.04	6869569.99	7041.07	VC10
BARINA_3	394723.91	6869570.02	7065.13	VL11
BARINA_3	394723.70	6869570.07	7085.31	VC15
BARINA_3	394723.59	6869570.09	7112.20	VC20
BARINA_3	394723.34	6869570.16	7128.89	VL22
BARINA_3	394723.24	6869570.18	7169.14	VC25
BARINA_3	394723.24	6869570.18	7179.70	PPER
BARINA_3	394723.24	6869570.18	7293.00	TD
BARINA_4	394203.55	6868264.09	7040.75	VC00
BARINA_4	394205.99	6868263.13	7052.36	VL05
BARINA_4	394206.23	6868263.17	7068.86	VC10
BARINA_4	394206.49	6868263.21	7098.37	VL11
BARINA_4	394206.64	6868263.24	7121.58	VC15
BARINA_4	394207.06	6868263.31	7156.07	VC20
BARINA_4	394207.27	6868263.35	7182.37	VL22
BARINA_4	394207.57	6868263.39	7228.33	VC25
BARINA_4	394207.72	6868263.41	7259.49	VC30
BARINA_4	394207.87	6868263.43	7278.49	PPER
BARINA_4	394208.02	6868263.45	7370.00	TD
BARINA_5	392655.69	6868380.11	6999.54	VC00
BARINA_5	392651.89	6868381.83	7010.41	VL05
BARINA_5	392651.84	6868381.92	7035.93	VC10
BARINA_5	392651.74	6868382.09	7050.57	VL11
BARINA_5	392651.51	6868382.48	7085.99	VC15
BARINA_5	392651.38	6868382.72	7113.46	VC20
BARINA_5	392651.12	6868383.16	7142.34	VL22

Well Name	X-Location	Y-Location	Subsea Depth	Marker Name
BARINA_5	392650.62	6868384.06	7187.40	VC25
BARINA_5	392650.37	6868384.51	7217.41	VC30
BARINA_5	392649.87	6868385.41	7232.36	PPER
BARINA_5	392650.12	6868384.96	7232.36	VC35
BARINA_5	392649.62	6868385.86	7387.00	TD
BARINA_6	392391.70	6869176.10	7033.09	VC00
BARINA_6	392391.70	6869176.10	7046.65	VL05
BARINA_6	392391.70	6869176.10	7069.30	VC10
BARINA_6	392391.70	6869176.10	7086.39	VL11
BARINA_6	392391.70	6869176.10	7118.87	VC15
BARINA_6	392391.70	6869176.10	7147.88	VC20
BARINA_6	392391.70	6869176.10	7168.38	VL22
BARINA_6	392391.70	6869176.10	7235.34	VC25
BARINA_6	392391.70	6869176.10	7258.52	VC30
BARINA_6	392391.70	6869176.10	7280.59	VC35
BARINA_6	392391.70	6869176.10	7303.17	PPER
BARINA_6	392391.70	6869176.10	7507.20	TD
BARINA_7	392260.60	6866962.60	7057.58	VC00
BARINA_7	392260.60	6866962.60	7070.85	VL05
BARINA_7	392260.60	6866962.60	7098.61	VC10
BARINA_7	392260.60	6866962.60	7116.49	VL11
BARINA_7	392260.60	6866962.60	7156.13	VC15
BARINA_7	392260.60	6866962.60	7183.36	VC20
BARINA_7	392260.60	6866962.60	7210.43	VL22
BARINA_7	392260.60	6866962.60	7242.36	VC25
BARINA_7	392260.60	6866962.60	7284.45	VC30
BARINA_7	392260.60	6866962.60	7313.49	VC35
BARINA_7	392260.60	6866962.60	7362.35	PPER
BARINA_7	392260.60	6866962.60	7523.20	TD
COWAN_1	406668.50	6866630.20	6970.29	VC00
COWAN_1	406668.50	6866630.20	6984.29	VL05
COWAN_1	406668.50	6866630.20	7027.57	VC10
COWAN_1	406668.50	6866630.20	7030.00	VL11
COWAN_2	405934.60	6865873.22	7135.07	VC00
COWAN_2	405934.60	6865873.49	7150.86	VL05
COWAN_2	405934.60	6865873.85	7170.72	VC10
COWAN_2	405934.60	6865874.15	7192.87	VL11
COWAN_2	405934.60	6865874.46	7223.67	VC15
COWAN_2	405934.60	6865874.78	7253.49	VC20
COWAN_2	405934.60	6865875.09	7263.64	VL22
COWAN_2	405934.60	6865876.04	7287.18	VC25
COWAN_2	405934.60	6865876.35	7303.00	VC30
COWAN_2	405934.60	6865876.67	7305.20	VU45
COWAN_2	405934.60	6865876.98	7305.25	PPER
COWAN_2	405934.60	6865877.30	7489.00	TD
COWAN_3	406263.55	6867353.73	7214.00	VC00
COWAN_3	406263.81	6867353.52	7233.09	VL05
COWAN_3	406264.23	6867353.19	7259.83	VC10
COWAN_3	406265.23	6867352.38	7287.58	VL11
COWAN_3	406265.82	6867351.92	7316.60	VC15

Well Name	X-Location	Y-Location	Subsea Depth	Marker Name
COWAN_3	406266.13	6867351.67	7348.42	VC20
COWAN_3	406266.66	6867351.24	7356.57	VL22
COWAN_3	406275.49	6867345.52	7397.56	VC25
COWAN_3	406272.03	6867347.25	7430.80	VC30
COWAN_3	406273.00	6867346.52	7479.30	VU45
COWAN_3	406273.97	6867345.78	7480.28	PPER
COWAN_3	406274.95	6867345.05	7979.00	TD
COWAN_4	407235.75	6866324.47	7288.51	VC00
COWAN_4	407235.30	6866324.79	7309.13	VL05
COWAN_4	407234.56	6866325.33	7349.87	VC10
COWAN_4	407233.51	6866326.10	7367.94	VL11
COWAN_4	407232.51	6866326.83	7406.39	VC15
COWAN_4	407232.21	6866327.05	7441.01	VC20
COWAN_4	407231.82	6866327.33	7451.45	VL22
COWAN_4	407229.16	6866329.27	7476.14	VC25
COWAN_4	407228.41	6866329.82	7511.30	VC30
COWAN_4	407227.66	6866330.36	7557.00	VU45
COWAN_4	407226.92	6866330.91	7678.00	TD
DARALINGIE_1	399394.80	6862516.00	6854.00	VC00
DARALINGIE_1	399394.80	6862516.00	6866.47	VL05
DARALINGIE_1	399394.80	6862516.00	6898.55	VC10
DARALINGIE_1	399394.80	6862516.00	6909.24	VL11
DARALINGIE_1	399394.80	6862516.00	6934.18	VC15
DARALINGIE_1	399394.80	6862516.00	6957.94	VC20
DARALINGIE_1	399394.80	6862516.00	6986.95	VL22
DARALINGIE_1	399394.80	6862516.00	7013.90	VC25
DARALINGIE_1	399394.80	6862516.00	7037.68	VC30
DARALINGIE_1	399394.80	6862516.00	7093.13	PPER
DARALINGIE_1	399394.80	6862516.00	7329.00	TD
DARALINGIE_10	401922.20	6861773.90	6968.00	VC00
DARALINGIE_10	401922.20	6861773.90	6979.16	VL05
DARALINGIE_10	401922.20	6861773.90	7006.17	VC10
DARALINGIE_10	401922.20	6861773.90	7022.06	VL11
DARALINGIE_10	401922.20	6861773.90	7050.03	VC15
DARALINGIE_10	401922.20	6861773.90	7063.72	VC20
DARALINGIE_10	401922.20	6861773.90	7162.60	TD
DARALINGIE_11	394008.70	6862227.90	7036.80	VC00
DARALINGIE_11	394008.70	6862227.90	7053.91	VL05
DARALINGIE_11	394008.70	6862227.90	7085.38	VC10
DARALINGIE_11	394008.70	6862227.90	7102.64	VL11
DARALINGIE_11	394008.70	6862227.90	7147.82	VC15
DARALINGIE_11	394008.70	6862227.90	7172.70	VC20
DARALINGIE_11	394008.70	6862227.90	7206.99	VL22
DARALINGIE_11	394008.70	6862227.90	7258.70	VC25
DARALINGIE_11	394008.70	6862227.90	7293.52	VC30
DARALINGIE_11	394008.70	6862227.90	7359.54	VC35
DARALINGIE_11	394008.70	6862227.90	7480.10	VU45
DARALINGIE_11	394008.70	6862227.90	7480.51	PPER
DARALINGIE_11	394008.70	6862227.90	7625.00	TD
DARALINGIE_12	397849.90	6862776.60	7103.00	VC00

Well Name	X-Location	Y-Location	Subsea Depth	Marker Name
DARALINGIE_12	397849.90	6862776.60	7118.97	VL05
DARALINGIE_12	397849.90	6862776.60	7151.30	VC10
DARALINGIE_12	397849.90	6862776.60	7164.96	VL11
DARALINGIE_12	397849.90	6862776.60	7198.22	VC15
DARALINGIE_12	397849.90	6862776.60	7226.31	VC20
DARALINGIE_12	397849.90	6862776.60	7259.44	VL22
DARALINGIE_12	397849.90	6862776.60	7315.56	VC25
DARALINGIE_12	397849.90	6862776.60	7347.95	VC30
DARALINGIE_12	397849.90	6862776.60	7409.60	VC35
DARALINGIE_12	397849.90	6862776.60	7485.66	PPER
DARALINGIE_12	397849.90	6862776.60	7642.00	TD
DARALINGIE_13	399054.30	6864299.40	7109.00	VC00
DARALINGIE_13	399054.30	6864299.40	7119.90	VL05
DARALINGIE_13	399054.30	6864299.40	7145.60	VC10
DARALINGIE_13	399054.30	6864299.40	7163.90	VL11
DARALINGIE_13	399054.30	6864299.40	7190.00	VC15
DARALINGIE_13	399054.30	6864299.40	7226.81	VC20
DARALINGIE_13	399054.30	6864299.40	7265.50	VL22
DARALINGIE_13	399054.30	6864299.40	7292.62	VC25
DARALINGIE_13	399054.30	6864299.40	7328.48	VC30
DARALINGIE_13	399054.30	6864299.40	7345.81	VC35
DARALINGIE_13	399054.30	6864299.40	7372.89	PPER
DARALINGIE_13	399054.30	6864299.40	7657.70	TD
DARALINGIE_14	395931.70	6860856.00	7041.00	VC00
DARALINGIE_14	395931.70	6860856.00	7052.54	VL05
DARALINGIE_14	395931.70	6860856.00	7080.27	VC10
DARALINGIE_14	395931.70	6860856.00	7096.72	VL11
DARALINGIE_14	395931.70	6860856.00	7132.94	VC15
DARALINGIE_14	395931.70	6860856.00	7159.68	VC20
DARALINGIE_14	395931.70	6860856.00	7204.37	VL22
DARALINGIE_14	395931.70	6860856.00	7238.68	VC25
DARALINGIE_14	395931.70	6860856.00	7304.24	VC30
DARALINGIE_14	395931.70	6860856.00	7332.77	VC35
DARALINGIE_14	395931.70	6860856.00	7415.53	PPER
DARALINGIE_14	395931.70	6860856.00	7651.05	TD
DARALINGIE_15	395231.80	6863132.90	7113.00	VC00
DARALINGIE_15	395231.80	6863132.90	7130.12	VL05
DARALINGIE_15	395231.80	6863132.90	7160.33	VC10
DARALINGIE_15	395231.80	6863132.90	7177.59	VL11
DARALINGIE_15	395231.80	6863132.90	7204.72	VC15
DARALINGIE_15	395231.80	6863132.90	7256.15	VC20
DARALINGIE_15	395231.80	6863132.90	7282.24	VL22
DARALINGIE_15	395231.80	6863132.90	7312.47	VC25
DARALINGIE_15	395231.80	6863132.90	7349.36	VC30
DARALINGIE_15	395231.80	6863132.90	7419.58	VC35
DARALINGIE_15	395231.80	6863132.90	7703.80	TD
DARALINGIE_16	397693.10	6865696.40	7114.00	VC00
DARALINGIE_16	397693.10	6865696.40	7128.41	VL05
DARALINGIE_16	397693.10	6865696.40	7151.08	VC10
DARALINGIE_16	397693.10	6865696.40	7174.19	VL11

Well Name	X-Location	Y-Location	Subsea Depth	Marker Name
DARALINGIE_16	397693.10	6865696.40	7198.63	VC15
DARALINGIE_16	397693.10	6865696.40	7245.48	VC20
DARALINGIE_16	397693.10	6865696.40	7284.03	VL22
DARALINGIE_16	397693.10	6865696.40	7308.23	VC25
DARALINGIE_16	397693.10	6865696.40	7349.66	VC30
DARALINGIE_16	397693.10	6865696.40	7380.25	VC35
DARALINGIE_16	397693.10	6865696.40	7407.19	PPER
DARALINGIE_16	397693.10	6865696.40	7549.30	TD
DARALINGIE_17	6867314.90	7228.00	7228.00	VC00
DARALINGIE_17	6867314.90	7228.00	7238.38	VL05
DARALINGIE_17	6867314.90	7228.00	7259.29	VC10
DARALINGIE_17	6867314.90	7228.00	7288.82	VL11
DARALINGIE_17	6867314.90	7228.00	7309.32	VC15
DARALINGIE_17	6867314.90	7228.00	7353.23	VC20
DARALINGIE_17	6867314.90	7228.00	7364.08	VL22
DARALINGIE_17	6867314.90	7228.00	7403.76	VC25
DARALINGIE_17	6867314.90	7228.00	7449.94	VC30
DARALINGIE_17	6867314.90	7228.00	7478.46	VC35
DARALINGIE_17	6867314.90	7228.00	7652.00	TD
DARALINGIE_18	396844.40	6859614.40	7163.20	VC00
DARALINGIE_18	396844.40	6859614.40	7174.10	VL05
DARALINGIE_18	396844.40	6859614.40	7211.58	VC10
DARALINGIE_18	396844.40	6859614.40	7234.66	VL11
DARALINGIE_18	396844.40	6859614.40	7270.93	VC15
DARALINGIE_18	396844.40	6859614.40	7301.27	VC20
DARALINGIE_18	396844.40	6859614.40	7357.46	VL22
DARALINGIE_18	396844.40	6859614.40	7390.63	VC25
DARALINGIE_18	396844.40	6859614.40	7437.68	VC30
DARALINGIE_18	396844.40	6859614.40	7531.49	VC35
DARALINGIE_18	396844.40	6859614.40	7722.13	PPER
DARALINGIE_18	396844.40	6859614.40	8064.00	TD
DARALINGIE_19	395501.40	6860385.00	7192.00	VC00
DARALINGIE_19	395501.40	6860385.00	7205.82	VL05
DARALINGIE_19	395501.40	6860385.00	7242.19	VC10
DARALINGIE_19	395501.40	6860385.00	7261.92	VL11
DARALINGIE_19	395501.40	6860385.00	7304.21	VC15
DARALINGIE_19	395501.40	6860385.00	7330.36	VC20
DARALINGIE_19	395501.40	6860385.00	7364.32	VL22
DARALINGIE_19	395501.40	6860385.00	7412.44	VC25
DARALINGIE_19	395501.40	6860385.00	7446.00	VC30
DARALINGIE_19	395501.40	6860385.00	7542.63	VC35
DARALINGIE_19	395501.40	6860385.00	7708.50	PPER
DARALINGIE_19	395501.40	6860385.00	8118.40	TD
DARALINGIE_2	398648.60	6859473.00	7220.14	VC00
DARALINGIE_2	398648.60	6859473.00	7239.88	VL05
DARALINGIE_2	398648.60	6859473.00	7280.18	VC10
DARALINGIE_2	398648.60	6859473.00	7296.97	VL11
DARALINGIE_2	398648.60	6859473.00	7320.47	VC15
DARALINGIE_2	398648.60	6859473.00	7362.84	VC20
DARALINGIE_2	398648.60	6859473.00	7396.60	VL22

Well Name	X-Location	Y-Location	Subsea Depth	Marker Name
DARALINGIE_2	398648.60	6859473.00	7456.07	VC25
DARALINGIE_2	398648.60	6859473.00	7530.38	VC30
DARALINGIE_2	398648.60	6859473.00	7566.61	VC35
DARALINGIE_2	398648.60	6859473.00	7648.06	PPER
DARALINGIE_2	398648.60	6859473.00	7924.00	TD
DARALINGIE_20	399885.70	6866687.40	7228.08	VC00
DARALINGIE_20	399885.70	6866687.40	7241.61	VL05
DARALINGIE_20	399885.70	6866687.40	7274.42	VC10
DARALINGIE_20	399885.70	6866687.40	7294.51	VL11
DARALINGIE_20	399885.70	6866687.40	7308.04	VC15
DARALINGIE_20	399885.70	6866687.40	7349.87	VC20
DARALINGIE_20	399885.70	6866687.40	7363.82	VL22
DARALINGIE_20	399885.70	6866687.40	7401.54	VC25
DARALINGIE_20	399885.70	6866687.40	7453.63	VC30
DARALINGIE_20	399885.70	6866687.40	7472.90	VC35
DARALINGIE_20	399885.70	6866687.40	7671.20	TD
DARALINGIE_21	403104.50	6860682.20	7303.00	VC00
DARALINGIE_21	403104.50	6860682.20	7313.00	VL05
DARALINGIE_21	403104.50	6860682.20	7339.89	VC10
DARALINGIE_21	403104.50	6860682.20	7356.56	VL11
DARALINGIE_21	403104.50	6860682.20	7387.08	VC15
DARALINGIE_21	403104.50	6860682.20	7399.43	VC20
DARALINGIE_21	403104.50	6860682.20	7412.47	VL22
DARALINGIE_21	403104.50	6860682.20	7438.56	VC25
DARALINGIE_21	403104.50	6860682.20	7496.30	VC35
DARALINGIE_21	403104.50	6860682.20	7498.67	PPER
DARALINGIE_21	403104.50	6860682.20	7721.00	TD
DARALINGIE_22	397153.50	6863402.50	7186.03	VC00
DARALINGIE_22	397153.50	6863402.50	7202.79	VL05
DARALINGIE_22	397153.50	6863402.50	7233.17	VC10
DARALINGIE_22	397153.50	6863402.50	7250.28	VL11
DARALINGIE_22	397153.50	6863402.50	7275.07	VC15
DARALINGIE_22	397153.50	6863402.50	7313.48	VC20
DARALINGIE_22	397153.50	6863402.50	7331.99	VL22
DARALINGIE_22	397153.50	6863402.50	7385.07	VC25
DARALINGIE_22	397153.50	6863402.50	7436.10	VC30
DARALINGIE_22	397153.50	6863402.50	7502.54	VC35
DARALINGIE_22	397153.50	6863402.50	7829.70	TD
DARALINGIE_23	398580.40	6865261.80	7169.00	VC00
DARALINGIE_23	398580.40	6865261.80	7180.05	VL05
DARALINGIE_23	398580.40	6865261.80	7202.40	VC10
DARALINGIE_23	398580.40	6865261.80	7218.30	VL11
DARALINGIE_23	398580.40	6865261.80	7244.10	VC15
DARALINGIE_23	398580.40	6865261.80	7282.14	VC20
DARALINGIE_23	398580.40	6865261.80	7300.33	VL22
DARALINGIE_23	398580.40	6865261.80	7349.28	VC25
DARALINGIE_23	398580.40	6865261.80	7391.24	VC30
DARALINGIE_23	398580.40	6865261.80	7406.50	VC35
DARALINGIE_23	398580.40	6865261.80	7441.70	PPER
DARALINGIE_23	398580.40	6865261.80	7595.60	TD

Well Name	X-Location	Y-Location	Subsea Depth	Marker Name
DARALINGIE_24	403017.00	6864207.00	7265.04	VC00
DARALINGIE_24	403017.00	6864207.00	7286.47	VL05
DARALINGIE_24	403017.00	6864207.00	7298.70	VC10
DARALINGIE_24	403017.00	6864207.00	7338.95	VL11
DARALINGIE_24	403017.00	6864207.00	7367.12	VC15
DARALINGIE_24	403017.00	6864207.00	7409.14	VC20
DARALINGIE_24	403017.00	6864207.00	7425.07	VL22
DARALINGIE_24	403017.00	6864207.00	7463.75	VC25
DARALINGIE_24	403017.00	6864207.00	7482.77	VC30
DARALINGIE_24	403017.00	6864207.00	7546.76	VC35
DARALINGIE_24	403017.00	6864207.00	7602.90	PPER
DARALINGIE_24	403017.00	6864207.00	7744.00	TD
DARALINGIE_25	393650.78	6862922.71	6994.00	VC00
DARALINGIE_25	393650.78	6862922.71	7016.70	VL05
DARALINGIE_25	393650.78	6862922.71	7031.04	VC10
DARALINGIE_25	393650.78	6862922.71	7044.49	VL11
DARALINGIE_25	393650.78	6862922.71	7088.85	VC15
DARALINGIE_25	393650.78	6862922.71	7118.73	VC20
DARALINGIE_25	393650.78	6862922.71	7136.28	VL22
DARALINGIE_25	393650.78	6862922.71	7172.21	VC25
DARALINGIE_25	393650.78	6862922.71	7204.92	VC30
DARALINGIE_25	393650.78	6862922.71	7263.40	VC35
DARALINGIE_25	393650.78	6862922.71	7320.89	PPER
DARALINGIE_25	393650.78	6862922.71	7434.40	TD
DARALINGIE_3	395930.60	6864508.60	7047.00	VC00
DARALINGIE_3	395930.60	6864508.60	7062.58	VL05
DARALINGIE_3	395930.60	6864508.60	7099.25	VC10
DARALINGIE_3	395930.60	6864508.60	7114.61	VL11
DARALINGIE_3	395930.60	6864508.60	7136.61	VC15
DARALINGIE_3	395930.60	6864508.60	7172.23	VC20
DARALINGIE_3	395930.60	6864508.60	7201.56	VL22
DARALINGIE_3	395930.60	6864508.60	7239.62	VC25
DARALINGIE_3	395930.60	6864508.60	7273.84	VC30
DARALINGIE_3	395930.60	6864508.60	7330.06	VC35
DARALINGIE_3	395930.60	6864508.60	7367.70	VU45
DARALINGIE_3	395930.60	6864508.60	7433.90	TD
DARALINGIE_4	400152.10	6867715.80	7230.19	VC00
DARALINGIE_4	400152.10	6867715.80	7238.39	VL05
DARALINGIE_4	400152.10	6867715.80	7256.85	VC10
DARALINGIE_4	400152.10	6867715.80	7284.73	VL11
DARALINGIE_4	400152.10	6867715.80	7299.91	VC15
DARALINGIE_4	400152.10	6867715.80	7329.43	VC20
DARALINGIE_4	400152.10	6867715.80	7337.33	VL22
DARALINGIE_4	400152.10	6867715.80	7382.33	VC25
DARALINGIE_4	400152.10	6867715.80	7422.93	VC30
DARALINGIE_4	400152.10	6867715.80	7448.36	VC35
DARALINGIE_4	400152.10	6867715.80	7572.00	TD
DARALINGIE_5	399737.50	6861069.90	6794.61	VC00
DARALINGIE_5	399737.50	6861069.90	6804.22	VL05
DARALINGIE_5	399737.50	6861069.90	6824.44	VC10

Well Name	X-Location	Y-Location	Subsea Depth	Marker Name
DARALINGIE_5	399737.50	6861069.90	6842.22	VL11
DARALINGIE_5	399737.50	6861069.90	6856.44	VC15
DARALINGIE_5	399737.50	6861069.90	7061.00	TD
DARALINGIE_6	396753.40	6861777.30	7045.44	VC00
DARALINGIE_6	396753.40	6861777.30	7054.48	VL05
DARALINGIE_6	396753.40	6861777.30	7078.58	VC10
DARALINGIE_6	396753.40	6861777.30	7096.03	VL11
DARALINGIE_6	396753.40	6861777.30	7110.55	VC15
DARALINGIE_6	396753.40	6861777.30	7141.95	VC20
DARALINGIE_6	396753.40	6861777.30	7159.66	VL22
DARALINGIE_6	396753.40	6861777.30	7195.07	VC25
DARALINGIE_6	396753.40	6861777.30	7218.68	VC30
DARALINGIE_6	396753.40	6861777.30	7301.00	TD
DARALINGIE_7	401152.60	6863604.70	7147.16	VC00
DARALINGIE_7	401152.60	6863604.70	7157.85	VL05
DARALINGIE_7	401152.60	6863604.70	7188.78	VC10
DARALINGIE_7	401152.60	6863604.70	7201.21	VL11
DARALINGIE_7	401152.60	6863604.70	7225.67	VC15
DARALINGIE_7	401152.60	6863604.70	7252.88	VC20
DARALINGIE_7	401152.60	6863604.70	7272.91	VL22
DARALINGIE_7	401152.60	6863604.70	7323.81	VC25
DARALINGIE_7	401152.60	6863604.70	7361.18	VC30
DARALINGIE_7	401152.60	6863604.70	7405.02	VC35
DARALINGIE_7	401152.60	6863604.70	7436.26	PPER
DARALINGIE_7	401152.60	6863604.70	7570.00	TD
DARALINGIE_8	403077.50	6863367.30	7022.50	VC00
DARALINGIE_8	403077.50	6863367.30	7040.27	VL05
DARALINGIE_8	403077.50	6863367.30	7061.68	VC10
DARALINGIE_8	403077.50	6863367.30	7083.90	VL11
DARALINGIE_8	403077.50	6863367.30	7117.43	VC15
DARALINGIE_8	403077.50	6863367.30	7140.12	VC20
DARALINGIE_8	403077.50	6863367.30	7146.71	VL22
DARALINGIE_8	403077.50	6863367.30	7173.75	VC25
DARALINGIE_8	403077.50	6863367.30	7204.16	VC30
DARALINGIE_8	403077.50	6863367.30	7216.90	VC35
DARALINGIE_8	403077.50	6863367.30	7228.70	VU45
DARALINGIE_8	403077.50	6863367.30	7374.00	TD
DARALINGIE_9	397769.20	6860285.10	7027.04	VC00
DARALINGIE_9	397769.20	6860285.10	7034.94	VL05
DARALINGIE_9	397769.20	6860285.10	7062.54	VC10
DARALINGIE_9	397769.20	6860285.10	7089.20	VL11
DARALINGIE_9	397769.20	6860285.10	7124.74	VC15
DARALINGIE_9	397769.20	6860285.10	7157.20	VC20
DARALINGIE_9	397769.20	6860285.10	7179.20	VL22
DARALINGIE_9	397769.20	6860285.10	7241.70	VC25
DARALINGIE_9	397769.20	6860285.10	7313.15	VC30
DARALINGIE_9	397769.20	6860285.10	7338.67	VC35
DARALINGIE_9	397769.20	6860285.10	7432.31	PPER
DARALINGIE_9	397769.20	6860285.10	7539.20	TD
DEINA_1	400754.30	6858837.60	7230.00	VC00

Well Name	X-Location	Y-Location	Subsea Depth	Marker Name
DEINA_1	400754.30	6858837.60	7239.19	VL05
DEINA_1	400754.30	6858837.60	7272.68	VC10
DEINA_1	400754.30	6858837.60	7295.09	VL11
DEINA_1	400754.30	6858837.60	7317.50	VC15
DEINA_1	400754.30	6858837.60	7344.65	VC20
DEINA_1	400754.30	6858837.60	7370.64	VL22
DEINA_1	400754.30	6858837.60	7428.97	VC25
DEINA_1	400754.30	6858837.60	7477.53	VC30
DEINA_1	400754.30	6858837.60	7500.01	VC35
DEINA_1	400754.30	6858837.60	7515.71	PPER
DEINA_1	400754.30	6858837.60	7883.73	TD
FARINA_1	396466.80	6870815.99	7154.02	VC00
FARINA_1	396466.80	6870815.99	7171.01	VL05
FARINA_1	396466.80	6870815.99	7183.75	VC10
FARINA_1	396466.80	6870815.99	7217.37	VL11
FARINA_1	396466.80	6870815.99	7230.11	VC15
FARINA_1	396466.80	6870815.99	7273.64	VC20
FARINA_1	396466.80	6870815.99	7294.17	VL22
FARINA_1	396466.80	6870815.99	7326.73	PPER
FARINA_1	396466.80	6870815.99	7548.90	TD
FARINA_2	394284.48	6870230.25	7208.04	VC00
FARINA_2	394284.48	6870230.25	7219.36	VL05
FARINA_2	394284.48	6870230.25	7251.57	VC10
FARINA_2	394284.48	6870230.25	7280.94	VL11
FARINA_2	394284.48	6870230.25	7312.44	VC15
FARINA_2	394284.48	6870230.25	7350.66	VC20
FARINA_2	394284.48	6870230.25	7361.50	VL22
FARINA_2	394284.48	6870230.25	7429.63	VC25
FARINA_2	394284.48	6870230.25	7460.86	VC30
FARINA_2	394284.48	6870230.25	7475.20	VC35
FARINA_2	394284.48	6870230.25	7490.49	PPER
FARINA_2	394284.48	6870230.25	7826.50	TD
KOREE_SOUTH_1	398785.29	6852226.36	6767.17	VC00
KOREE_SOUTH_1	398785.29	6852226.36	6782.86	VL05
KOREE_SOUTH_1	398785.29	6852226.36	6814.23	VC10
KOREE_SOUTH_1	398785.29	6852226.36	6831.51	VL11
KOREE_SOUTH_1	398785.29	6852226.36	6855.90	VC15
KOREE_SOUTH_1	398785.29	6852226.36	6868.70	VC20
KOREE_SOUTH_1	398785.29	6852226.36	6881.81	VL22
KOREE_SOUTH_1	398785.29	6852226.36	6926.02	VC25
KOREE_SOUTH_1	398785.29	6852226.36	6958.03	VC30
KOREE_SOUTH_1	398785.29	6852226.36	6990.65	VC35
KOREE_SOUTH_1	398785.29	6852226.36	7139.10	TD
YAPENI_1	391273.80	6863404.30	6902.01	VC00
YAPENI_1	391273.80	6863404.30	6919.95	VL05
YAPENI_1	391273.80	6863404.30	6947.95	VC10
YAPENI_1	391273.80	6863404.30	6966.19	VL11
YAPENI_1	391273.80	6863404.30	6993.93	VC15
YAPENI_1	391273.80	6863404.30	7012.61	VC20
YAPENI_1	391273.80	6863404.30	7025.53	VL22

Well Name	X-Location	Y-Location	Subsea Depth	Marker Name
YAPENI_1	391273.80	6863404.30	7050.82	VC25
YAPENI_1	391273.80	6863404.30	7114.13	VC30
YAPENI_1	391273.80	6863404.30	7223.59	PPER
YAPENI_1	391273.80	6863404.30	7371.70	TD
YAPENI_2	391804.90	6862889.00	7125.99	VC00
YAPENI_2	391804.90	6862889.00	7140.33	VL05
YAPENI_2	391804.90	6862889.00	7169.01	VC10
YAPENI_2	391804.90	6862889.00	7196.80	VL11
YAPENI_2	391804.90	6862889.00	7231.94	VC15
YAPENI_2	391804.90	6862889.00	7256.37	VC20
YAPENI_2	391804.90	6862889.00	7272.11	VL22
YAPENI_2	391804.90	6862889.00	7299.87	VC25
YAPENI_2	391804.90	6862889.00	7362.30	VC30
YAPENI_2	391804.90	6862889.00	7423.87	VC35
YAPENI_2	391804.90	6862889.00	7587.21	PPER
YAPENI_2	391804.90	6862889.00	7729.10	TD

Appendix 2

Modeling algorithms used in this study

(Source: Roxar RMS V7.5 user manual)

Facies modelling theory

Introduction

This appendix provides a more detailed mathematical description of the implemented methods for the following facies modelling tools:

- Facies:Belts
- Facies:Composite
- Facies correlations
- Facies:Indicators

A list of references and further reading is included at the end of the appendix.

Facies:Belts model descriptions

Using a truncated Gaussian simulation algorithm to generate facies belts is based on establishing a 3D trend parameter, the simulation a continuous Gaussian residual field, followed by a discretisation of the trend and residual field into classes (facies) according to a set of truncation rules. These tasks are performed differently for *Proportions* mode and *Stacked belts* (and *Trend and threshold*) modes.

Stacked belts and Trend & threshold modes

In this mode, a trend for the continuous Gaussian variable is established from the conceptual geological model together with discretisation rules.

This combination of trend and discretisation rules is such that if the trend itself were discretised, the resulting facies distribution would be according to the conceptual geological model. However, only truncating the trend would not generate interfingering of the various facies and would not condition correctly to any wells in the model, therefore a Gaussian residual field is simulated and added to the established trend. This simulated residual ensures well conditioning and that the interfingering is according to the conceptual geological model after the discretisation.

The procedure is illustrated for a one-dimensional example in Figure D.4. This figure illustrates one grid layer in a vertical cross-section, where:

- The trend established from the geological model is shown as the dashed line

- The discretisation rules are shown as the horizontal dotted lines
- The generated continuous variable (combination of trend and residual) is shown as a solid line.

The vertical dotted lines show the transition between different facies as a result of the discretisation of the generated continuous variable.

Mathematically, the truncation of the simulation result (the Gaussian field) is expressed in Equation D.16,

$$F(x) = i \quad \text{if} \quad t_{i-1}(x) < Z(x) < t_i(x) \tag{D.16}$$

where *F(x)* is the facies, *Z(x)* is the Gaussian field and $t_i(x)$ is the discretisation rules in position *x*.

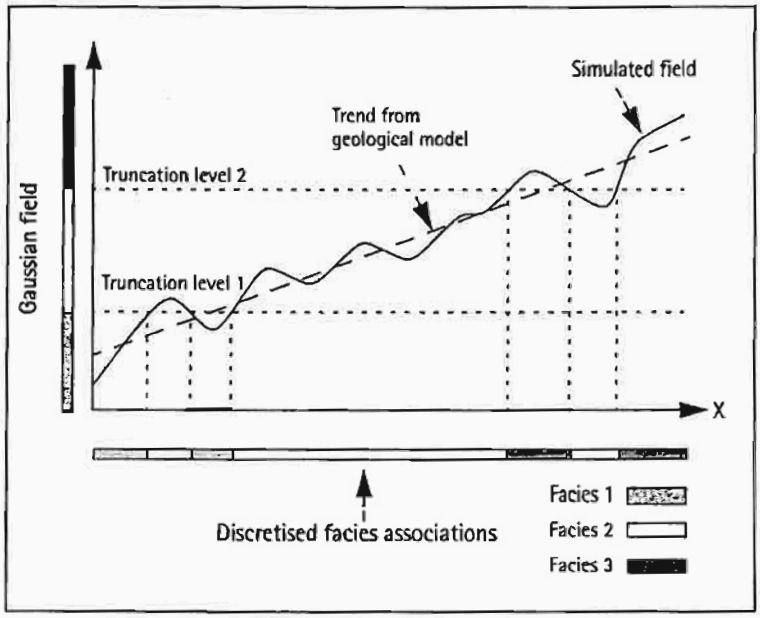

Figure D.4 Illustration of the truncated Gaussian model in Stacked belts mode

Proportions mode

In this mode, rather than having a non-constant 3D trend and constant truncation rules (horizontal lines in Figure D.4), the trend is equal to zero everywhere, but the proportion curves or cubes given as input is converted to non-horizontal truncations rules. A Gaussian field with a zero expectation value and a unit variance is now simulated for the residual. This is illustrated in Figure D.5. Note that for the Lenses option, the truncation rules are still constant (horizontal truncation lines as in Figure D.4.).

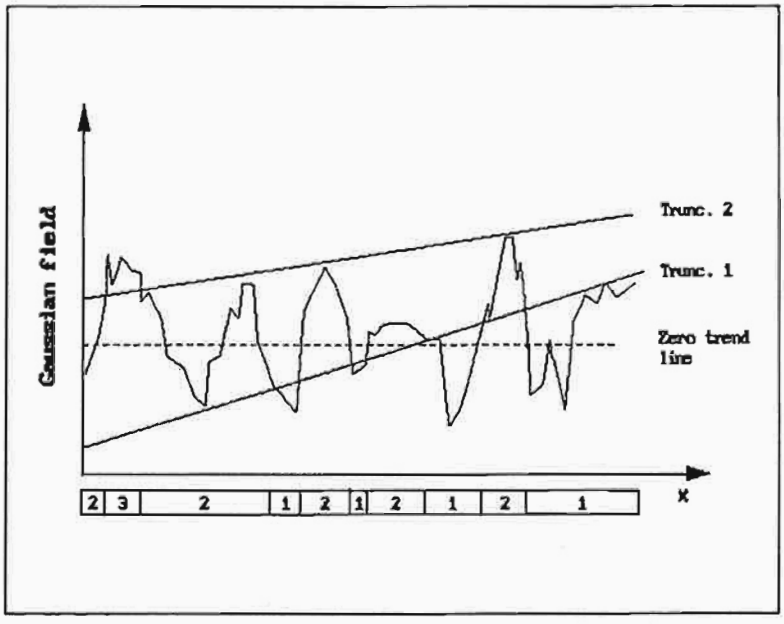

Figure D.5 Illustration of the truncated Gaussian model in Proportions mode

Facies:Composite model description

This section provides a technical description of the Facies:Composite model and the simulation algorithm, and a mathematical description of the user-defined shapes.

The model

Facies:Composite (General Marked Point process) is used for the modelling of bodies of different facies and shapes. One of the facies present in each subgrid must be defined as the background facies.

The facies distribution in the reservoir is described by a marked point process, which is an object-based stochastic model. Objects with random size, orientation and shape are placed randomly in the simulation volume. The density of the number of objects can however vary within the simbox, according to optional user-defined trends and seismic. The number of objects reach a quantity such that a target facies proportion or number of bodies is obtained. Attributes such as size and shape will also follow a distribution, specified in the parameter setting. If objects are observed in the wells, a conditional simulation is performed. Both unconditional and conditional objects which intersect the wells will then be simulated.

A marked point process is described by a *point*, which is a random position in the 3D volume given by the grid, and the *mark*, which is a stochastic description of the body positioned at that point.

In the model, each body (object) is specified with the following parameters:

- The *point:*
  - A reference position,
- The *mark*, being:
  - The length and width of the body
  - The expected height of the body

- The horizontal and vertical rotation of the body relative to the reservoir simulation box
- The top and bottom of the body specified in a fine local grid covering the body

The distribution of both the points and the marks may follow specified trends: for example, to have higher intensity of points or to have larger objects in special parts of the reservoir.

The length, width and expected height have a multi-Gaussian distribution. The same is true for the horizontal and vertical rotation. The top and bottom of the body are correlated Gaussian fields.

The distribution of the reference position is specified through four quantities:

- **Relative intensity functions.** One relative intensity function can be specified for each facies (except the background facies). Combined with the restrictions specified (see below), the relative intensity gives the absolute intensity which is used during simulation.

  If no repulsion function or seismic is specified, then the absolute intensity function gives, as a function of position, the expected number of bodies per volume unit. Thus, the relative (and absolute) intensity function should be used to introduce a trend in the number of bodies.

  If repulsions are specified, the interpretation of the intensity functions are no longer as simple, but a higher intensity at a position still makes it more probable for a body to be at that position. Intensity functions should normally not be used together with seismic conditioning, as these two ways of controlling the distribution of facies contain much the same information and may interfere with each other. Intensity functions cannot be specified if the restriction local volume fractions are specified.

- **Repulsion functions.** One repulsion function can be specified for each pair of facies (except the background facies). The repulsion between bodies can specify that two bodies (of the specified facies) should have a small probability of occurring close to each other.

- **Seismic.** A seismic map or 3D cube can be given, together with piecewise linear curves (Facies probability functions) describing the probability for object facies, as a function of the seismic attribute value. One such curve is specified for each of the object facies that are to be conditioned on the seismic information.

- **Restrictions.** Only one type of restriction is implemented. This restriction is that the volume fraction of a facies should be within a given interval. One such restriction is specified for each facies (except the background facies). A volume fraction can be global or local. If it is global the simulation will converge against the specified volume fraction calculated in the whole reservoir. If it is local the simulation will converge locally against the volume fractions specified in the given trends.

The previously-mentioned bodies of different facies can have different shapes. For each facies one shape must be chosen. It is possible to use both

predefined and user-defined stochastic shapes. The possible shapes are as follows:

- Rectangle
- Cone
- Ellipsoid
- General
- Axial
- Angular

For a further description of the possible shapes, see "Shape" on page 1212, "User-defined object shapes" on page 1237. A mathematical description of the user-defined shapes is given in "Shape theory" on page 1996.

Simulation algorithm

The complexity of many geological environments demands an advanced Monte-Carlo simulation method. Facies:Composite uses a Metropolis-Hastings algorithm with simulated annealing. This is an iterative algorithm which converges against the distribution for the specified geological model.

The initial states of the programs when simulation starts are empty reservoirs filled with background. In each iteration a change in the reservoir is proposed and thereafter accepted with a probability dependent upon the model chosen. In the implemented algorithm, three different procedures are used to draw the potential new states:

- Add a new body.
- Remove one of the old bodies.
- Change one of the old bodies.

Whether the proposed change is accepted or not is a stochastic function, depending on the acceptance probability. The acceptance probability is again a function of the ratio between the probability of the proposed reservoir and the probability of the reservoir in the previous iteration. A proposed change to a reservoir more in accordance with the geological model will therefore have a high probability of being accepted.

The probability of a reservoir is a function of how well the reservoir fits the specified model. That is, how well the reservoir fits the geological model, to which amount well and seismic information is honoured and how close the facies proportions are to the target volume proportions. Each potential new state in the Metropolis-Hastings algorithm is chosen such that it fulfils the well observations. Thus the well observations are always fulfilled during simulation.

Since we start with empty reservoirs in the first iteration the proposed reservoirs will typically contradict with target volume proportions. Therefore little attention is paid to these constraints in the beginning of the simulation, and gradually more weight will be put on them. This behaviour is obtained by using simulated annealing. We introduce a temperature parameter in the simulation, where high temperature means little weight on the constraints and low temperature means high weight.

The temperature is at maximum in the first iteration, and is lowered in each iteration according to a user defined annealing function. In Facies:Composite this function is implicitly defined by the minimum and maximum number of iterations together with the start temperature and temperature at minimum number of iterations.

The Metropolis-Hasting algorithm with simulated annealing forces the simulation to converge against the distribution for the specified reservoir. However, it is possible that the simulation ends without convergence. The resulting reservoirs may then contradict to trend and seismic information, and the target volume proportions may not be reached.

The simulation of the Gaussian random fields describing the top and bottom of the bodies is done first after the iterative Metropolis-Hastings algorithm is finished. This approach has been chosen because otherwise Gaussian fields would have to be simulated in each iteration in the iterative algorithm, which would have required a lot more computer resources than the approach chosen. In order to do this, a few minor approximations have been made. The most important is that when computing volume fractions (used in restrictions) the expected form of the bodies is used rather than the actual form taking into account the Gaussian fields describing the top and bottom.

Shape theory

This section provides a mathematical description of user-defined shapes in Facies:Composite.

Axial shape

The axial shape type is a stochastic shape, so parameters for individual residual fields for the lateral extent of the objects can be specified.

The parameterisation of an *Axial* type object is as follows:

Two trend functions for width $w(x)$ and centre position $c(x)$ as function of the x coordinate is supplied. The two edges:

$$Y_1 = (c(x) + R_c(x)) - 0{,}5(w(x) + R_w(x)) \tag{70.1}$$

and

$$Y_2 = (c(x) + R_c(x)) + 0{,}5(w(x) + R_w(x)) \tag{70.2}$$

represent the left and right edge of the object as seen in an xy projection looking in positive x direction from the origin. ($R_c(x)$ and $R_w(x)$ are 1D Gaussian residual fields for the centre and width, respectively.) The trend functions for centre and width must be defined such that $Y_1(x)$ and $Y_2(x)$ are both between -0.5 and 0.5 when the residual fields are 0, to ensure that the prototype shape is within a unit cube.

The user can also supply two thickness functions along the x axis, giving:

- The thickness from the local z=0 plane to the top $T^x_{top}(x)$
- The thickness from z=0 plane to the bottom $T^x_{bottom}(x)$

Note that the sum of the thicknesses must be in the interval from 0 to 1 everywhere.

The user can also specify how the thicknesses vary as function of the local y coordinate (that is, normal to the x axis). The two thickness functions are:

- The thickness from the local z=0 plane to top $T^{Y}_{top}(y)$
- The thickness from z=0 to bottom $T^{Y}_{bottom}(y)$

If thicknesses along the x axis are also specified, the resulting thickness is the product $T_{top}(x, y) = T_{top}{}^{X}(x)T_{top}{}^{Y}(y)$ for the top thickness and correspondingly for the bottom.

Since the object's shape varies with the left and right edges, the position of the specified thickness points in y direction is defined to be equally spaced between the left and right edges and rescaled for each x. The specified thicknesses must be non-negative and the sum must be in the interval from 0 to 1. A least one point must have positive total thickness. Default thickness if this profile is omitted is 0.5+0.5=1.0 for all y.

Angular shape

The parameterisation of an *Angular* type object is similar to that for an axial shape (see previous section). The main difference is that the geometry is specified as function of angle and radius (polar coordinates), instead of x and y coordinates.

Facies correlations theory

Facies correlation in Irap RMS allows for correct coupling based on object geometry and wells, because the decision of whether an observation should be included or not is made after (for example) the channel location is drawn. A prior computation of the likelihood of two observations belonging to the same channel is a very complicated task. However, computing the likelihood of including a channel observation, given the channel location in an area, is a much simpler task because many of the parameters have already been determined.

Providing each observation is included in (for example) the channel or crevasse with the correct probability, the couplings will also be correctly distributed according to the model. However, there might be other geological information indicating that some observations are from the same object, and others are definitely not (Skorstad et al.).

Correlation weights

This section provides information on the theory behind the probabilistic interpretation of correlation weights, used in the facies correlation.

When using correlation weights in Facies:Channels and Facies:Composite, it is important to realise that the weight is only a scaling of the geometrical coupling probability. Only the extreme cases with $w = 1$ or $w = 0$ disregards the geometrical probability. This probability, which here is denoted by $q_{\text{configuration}}$ is the probability of a configuration in a model without weights (equivalent with all weights equal to 0.5). This probability is given by the model and data, and is considered a constant in the following.

The scaling is also very non-linear. To see how it works, consider the case with two observations. Then q is the probability that they are coupled

without weights. Let p be the probability of coupling with weight, and the correlation weight be w. The relationship in its simplest form is then

(D.17)

$$\frac{p}{1-p} = \frac{q}{1-q} \times \frac{w}{1-w}$$

This expression shows that the ratio between the probability of coupling and the probability of not coupling is scaled with a factor $w/(1-w)$. This ratio can also be obtained by taking the number of realizations with coupling and dividing on the number of realizations without.

To get a better idea of what this means, consider Figure D.6. This figure shows p as a function of w for different values of q, each curve representing one value of q. The q-value for a curve can be read by looking at the point where $W = 0.5$, since $p = q$ at this point. As the plot shows, the curve changes shape with q. For $q = 0.5$ it is a straight line, given by $p = w$. For larger values of q, the coupling probability increases most at a value of w smaller than 0.5, and vice versa. As q approaches zero, the coupling probability will also be almost zero for most weights, but increase rapidly as w approaches 1. The point at which this occurs can be arbitrarily close to 1, depending on the value of q.

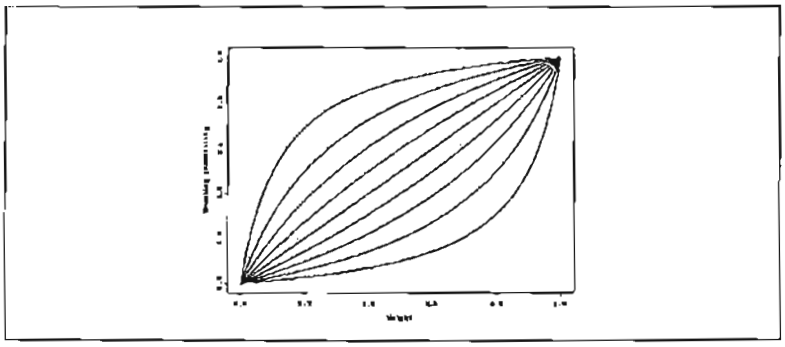

Figure D.6 Coupling probability against weights

This means that the weights should not in any way be interpreted as probabilities, but as a scaling of intrinsic probabilities built into the model. The weights scale the ratio between realizations with and without couplings, as shown in Equation D.17.

With more than two observations, the situation becomes more complex. Consider the coupling probability for the observations A and B, p_{AB}. The geometrical probability is q_{AB}, and the weight factor between these observations is w_{AB}. Let there be at least one more observation. We then have

(D.18)

In general, p_{AB} can be found from

$$p_{AB} = \sum_{c:A,B \text{ coupled}} q_c w_c \Big/ \left(\sum_c q_c w_c \right) \tag{D.19}$$

The sum in the enumerator is taken over all configurations where A and B are coupled, and the sum in the denominator is taken over all configurations. (By configuration we mean a given set of couplings.) The factor q_c is the geometrical probability of the configuration c, and w_c is given by

$$w_c = \left(\prod_{i,j \text{ coupled in } c} w_{ij} \right) \prod_{i,j \text{ not coupled in} c} 1 - w_{ij} \tag{D.20}$$

This means that p_{AB} contains w_{AB} as a factor, and (not as obvious) that 1 - w_{AB} is a factor in 1 - p_{AB}.

Essentially the behaviour is as before: Adjusting w_{AB} adjusts the ratio between realizations where A and B are coupled and not. However, the constant term q is now replaced with s and t, which in turn depends on all other weights. This means that adjusting the weight between two other observations may also affect the coupling probability for A and B. These effects are very hard to map, and the most useful approach to the use of weights is to consider Equation D.17, and make iterative adjustments if the interaction between weights is strong. This interaction will be stronger the more the weights are away from 0.5, and the larger the differences in the geometrical probability of the configurations are.

Correlation groups

Correlation weights can be defined between observations or observations belonging to separate groups. When correlation weights are defined in separate groups, then the following rules apply for the groups:

1. The groups must be disjoint: that is, no observation can be a group member of more than one group.
2. The observations that are not specified as members of any group form a 'rest group', with default values given by point 3 below.
3. Inside a group the default pairwise weights are 0.5. Between the groups the pairwise weights are 0.0.

When correlation weights are defined without specifying groups, then all observations will be treated as being in only one single group containing all observations.

Each group might be composed of one or more pairs of observations. For each pair of observation a correlation weight is defined. The specified value is not a probability, but a weight. For example, if observations A and B are in the same object, and the specified weight is 0.7, it means that the weight for A and B not to being in the same object is 0.3. The weights will be used to calculate the probabilities for A and B being in the same object. However

there can be different relationships between all pairs in one group: for example, that an observation C is not in the same object as A and B.

All pairwise weights are by default 0.5, so if no weights are specified, a weight of 0.5 will be used for the calculations.

For example, if there are six observations, ABCDEF, where the first three of them are definitely not in the same object as the other three, they can be set into two groups, ABC and DEF.

For defining the group ABC, the weights must be specified pairwise for that configuration. If then only two of the observations pairs have specified weights, for example:

weight 1 AB

weight 2 AC

and nothing more is specified, then this is equal to having set a weight of 0.5 for BC. The resulting weight for the three observations ABC to be connected is calculated as follows:

weight 1 * weight 2 * 0.5

The weight for none of the three being in contact would be calculated:

(1-weight 1) * (1- weight 2) * 0.5

Summarising all configurations will give a number unequal to 1:

x = weight 1 * (1-weight2) * 0.5 + weight2 * (1-weight1) * 0.5 + 0.5 * (1-weight1) * (1-weight2)

+ weight1 * weight2 * 0.5 + (1-weight1) * (1-weight2) * 0.5

The number x can then be used to calculate the probability of AB, AC and BC being in the same object by dividing weight1, weight2 and 0.5 by x.

However, the probability is not an overall probability. It will simply be used to scale probabilities of observations being correlated.

Facies:Indicators theory

The Facies:Indicators method works by Sequential Indicator Simulation (SIS). The sequential simulation works by visiting each point on the grid to be simulated, calculating the conditional distribution at that point and sampling from that distribution. The conditional distribution is the probability distribution for the facies at the point, given knowledge of the facies at nearby well locations and of previously simulated points nearby. By 'nearby' we mean within the search neighbourhood of the point to be simulated. The conditional distribution is found approximately using a kriging approach, with the exact methodology depending on the type of simulation that is being applied. In Irap RMS we use two types of simulation:

- SIS with Trends
- Sequential Indicator Cosimulation

The same basic simulation model is used for both types.

The basic SIS model

In Sequential Indicator Simulation (SIS)[2][5], a random path is first defined through the grid, so that each cell will be visited once.

The probability of each facies *i* at a location (grid cell) *x* is found by the following steps:

1. Set up an indicator for the facies *i*. That is, for each cell on the grid with facies information, set the value equal to 1 if it is facies *i* and equal to 0 if it is not facies *i*.
2. Using the indicator variogram for this facies (which is found by calculating the variogram of the indicator of the facies at the wells), krig the values of the facies at the location *x*. This value will usually lie between 0 and 1 since all the data are either 0 or 1. Moreover the value should be fairly close to the conditional probability of getting facies *i* at *x* given the facies information nearby (within the search neighbourhood).
3. Repeat this process for all facies. We now have an estimate of the conditional probability of each facies. However, there is no reason that the sum of these probabilities is equal to one. So the probabilities are normalized so that they sum to 1.
4. Finally, draw a facies at random from this estimated conditional distribution.

The procedure is repeated for each cell in the random path, paying attention to the availability of conditioning facies data in the previously simulated cells within the search neighbourhood. New facies realizations are obtained by reinitializing the random path through the model.

The algorithm automatically transforms the data from the 3D (sub)grid into an orthogonal shaped 'simulation box' while executing the simulation. Refer to "The simulation box" on page 1113 for details.

SIS with Trends

Sequential Indicator Simulation with Trends is a variation on the simple SIS method[2][5]. The version found in Irap RMS allows the user to use trends in the expected probability. This is important to allow for conditioning to vertical proportion curves and/or seismic data.

In this method a trend of probabilities is found for each facies. For example, for a seismic attribute, the relative probabilities of getting the various facies for a particular value of the seismic attribute is evaluated using well data (this is the facies probability function). These trends then become the expected values for our conditional distribution. In other words, when we are far away from hard data, our conditional distribution should resort to the values read from the facies probability function. However, when we are close to well data or to previously simulated points, the continuity expressed through the variogram and kriging should become more dominant. This is almost the same as the basic SIS method except that instead of a simple kriging, a kriging with trend is done. This ensures that far from hard data, the conditional distribution reverts back to the trend (or facies probability function).

Sequential Indicator Cosimulation

In Sequential Indicator Cosimulation, a collocated cokriging of the facies probabilities is done instead of a simple kriging. A description of the theory is given in Fichtl and Royer (1999)[4]. The idea behind cokriging is that the explicit correlation between the facies and the seismic data is calculated and used in the kriging process. If the correlation is found, empirically at the wells, to be zero, then the method reduces to a simple SIS method. In other words, with a zero correlation the seismic is not used as expected. The correlation is found by default by Irap RMS, but users have the choice of overriding the default correlation and inserting their own values.

It should be noted that there are non-obvious relationships between the correlations of the various facies and the seismic data. In particular for three or more facies it is not recommended that users try to input the correlations themselves. For the case of two facies some simple rules can help:

1. Assume that of the two facies, *i* and *j*, the mean seismic attribute value is lower for facies *i*. Also assume that the proportion of facies *i* is to be *p*. Then the proportion of facies *j* is *1-p*.
2. The correlation ρ of facies *j* with the seismic data will be positive while the correlation of facies *i* with the seismic will be negative and must be -ρ. Choosing values which are not the opposite of one another can lead to poor results.
3. There is usually an upper bound on the value of correlation that can exist between a facies and the seismic data. It is very unlikely that correlation values such as 0.9 will be observed. A maximum correlation can be found if we make the hypothesis that the distribution of the seismic values about their means are symmetric for both facies. Again, assuming that the proportion of the facies with the lower mean is *p*, then let *x* be the *p/2* quantile for the seismic data and let *y* be the *(1+p)/2* quantile. Then the maximum correlation is given by

$$\rho = \frac{(y-x)\sqrt{p(1-p)}}{\sigma_S} \qquad \text{(D.21)}$$

where σ_S is the standard deviation of the seismic data. While this value is only true when the seismic distributions are symmetric about

their means for both facies, it gives an approximate upper bound for other cases.

References and further reading

[1] Budding, M.C. et al. (1992). *3D Connectivity and Architecture in Sandstone Reservoirs*, SPE paper 22342 presented at the SPE International Meeting on Petroleum Engineering, Beijing, China, March 24-27, 1992.

[2] Cressie, N. (1991). *Statistics for Spatial Data*. John Wiley & Sons, New York, 900 pp.

[3] Damsleth, E. et al. (1992). A Two-Stage Stochastic Model Applied to a North Sea Reservoir, *Journal of Petroleum Technology*, April 1992.

[4] Fichtl, P. and Royer J-J. (1999). Facies based sequential indicator cosimulation: A collocated cokriging approach integrating seismic data. In *IAMG 99. Proc. 5th Intl conf of the Assoc for Math Geology*, Trondheim, Norway, 6-11 Aug 1999. Ed. Lippard S.J et al.

[5] Goovarts, P. (1997). *Geostatistics for Natural Resource evaluation*. Oxford University Press, 483 pp.

[6] Gundesø, R. and Egeland, O. (1990). SESIMIRA - A New Geological Tool for 3-D Modelling of Heterogeneous Reservoirs. In *North Sea Oil & Gas Reservoirs II*, Buller, A. T. and King, P. R. (eds.), Oxford U. Press, Oxford.

[7] Haldorsen, H. H. and Damsleth, E. (1990). Stochastic Modelling, *Journal of Petroleum Technology*, April 1990.

[8] Hatløy, A.S. (1994). Numerical Facies Modelling combining Deterministic and Stochastic Methods. In *Stochastic modelling and Geostatistics*, Yarus, J.M. and Chambers, R.L. (eds.), AAPG book, Computer Applications in Geology No. 3.

[9] Hove, K. et al. (1992). *From Stochastic Geological Description to Production Forecasting in Heterogeneous Layered Reservoirs*, SPE paper 24890 presented at the 1992 SPE Annual Technical Conference and Exhibition, Washington DC, October 4-7 and the 1993 SEG Annual Meeting and Exhibition, Washington DC, September 26-30.

[10] Skorstad, A., Hauge, R. and Holden, L. (1999). Well Conditioning in a Fluvial Reservoir Model. *Mathematical Geology*, Vol. 31, No. 7.

[11] Weber, K.J. and van Geuns, L.C. (1990). Framework for Constructing Clastic Reservoir Simulation Models, *Journal of Petroleum Technology*, October 1990.

Petrophysics method theory

Introduction

This appendix provides a more detailed and mathematical description of the implemented method for stochastic petrophysical modelling (see Chapter 46, "Petrophysical modelling"). It covers:

- Concepts
- Terminology
- Transformation
- Variogram models
- Correlation
- Kriging and simulation
- Cosimulation
- Types of modelling results
- References and further reading

More information on some aspects is given in Part VI, "Data analysis".

Concepts

Spatial data, such as petrophysical parameters, have a spatial correlation, meaning that the similarity between two locations depends on the distance between them: that is, the variance increases with increasing separate distance between two observations. Modelling in Irap RMS therefore takes advantage of geostatistics: the science of estimation, simulation and prediction of spatial data.

Another important characteristic of petrophysical parameters, utilized by the petrophysical modelling in Irap RMS, is that samples from petrophysical parameters can be transformed to a Gaussian (normal) distribution by the application of certain geological and statistical transformations.

The above leads to defining Gaussian fields for each petrophysical parameter. If facies heterogeneity is shown is be of importance in a reservoir study, one Gaussian field is defined for each petrophysical parameter for each facies association. The underlying definition is:

Parameter = Expectation + Residualfield

- The *expectation* term collects our geological knowledge and interpretations of the depositional environment, and in most cases this knowledge is gained through analysis of well logs, which leads to specifying the expectation of a petrophysical parameter through a stepwise transformation of well data. This process is often described by two diametrically different terms: *removing* or *including* geological trends until only the residual field of the well data remains.
- The *residual field* is a Gaussian field with an expectation of zero and a unit variance. It is the element of the petrophysical parameter that cannot be explained by systematic or low frequency geological features.

In order to transform the well data successfully, you must first calculate the data's statistical characteristics, and then build a sequence of transformations that perform both of the following tasks:

- Identify statistical deviations from the symmetrical, bell-shaped Gaussian distribution
- Incorporate any geological knowledge, such as trends and average parameter values

These transformations are applied to the well data before the petrophysical simulation is performed. After the simulation, the sequence of inverse transformations is applied automatically.

Terminology

This section defines the specific terms used in stochastic petrophysical modelling.

Note

In geostatistical terminology, "spatial variable" or "variable" is used instead of "petrophysical parameter" (or "parameter").

In the following definitions, the expressions listed in Table D.6 are used.

Table D.6: Expressions used in the definitions

Expression	Usage
$Z(x)$	Used for a variable Z in location x, where x is an (x,y,z)-point in 3-dimensional space
$Z_i(x)$ and $Z_j(x)$	Denote two different variables
$\mu(x)$	The expectation of $Z(x)$
h	Denotes the distance between two points (the lag)

Spatial variable

When a variable is distributed in space it is said to be spatial or regionalized. A spatial/regionalized variable is simply a function $f(x)$ that has a value for all x (i.e. x, y, z) points in 3-dimensional space.

Random variable

A random variable is a variable which takes numerical values according to a certain probability distribution.

Variance The variance is defined as the second order moment about the expectation $\mu(x)$, i.e.

$$\sigma(x)^2 = \mathrm{VAR}[Z(x)] = E\left\{[Z(x)-\mu(x)]^2\right\} \tag{D.22}$$

The variance specifies the variability of the variable in the total reference space. The higher the variance, the more variability the variable has.

Covariance The covariance between two variables is defined as:

$$\mathrm{Cov}(Z_i, Z_j) = E\{[Z_i(x)-\mu_i(x)][Z_j(x)-\mu_j(x)]\} \tag{D.23}$$

This gives a measure of the dependency between the two variables Z_i and Z_j, and the variability in the variables.

Correlation Correlation between two variables is given by the correlation coefficients which can be computed from the covariance of the two variables and their variance:

$$\mathrm{Corr}\{Z_i, Z_j\} = \frac{\mathrm{Cov}\{Z_i, Z_j\}}{\sigma_i \cdot \sigma_j} = \rho ij \tag{D.24}$$

Note *Note that:* $-1 \le \rho ij \le 1$

If the correlation is positive, the values of the two variables tend to be small or high at the same time, but if the correlation is negative the value of variable Z_i tends to be small if variable Z_j is high (and *vice versa*). The closer to 1 or -1 the correlation is, the stronger these tendencies become.

Variogram The spatial variogram function is defined as the variance of the increment $[Z(x)-Z(x+h)]$, and is written:

$$\gamma(h) = \frac{1}{2}\mathrm{Var}\{Z(x)-Z(x+h)\} \tag{D.25}$$

This function gives the spatial variability of a variable. The smoothness or discontinuity of the variable may be modelled by the variogram. A more detailed definition is given in "Variogram models" on page 2009, and in Appendix G, "Variogram theory".

Spatial correlation The spatial correlation function $\rho(h)$ is a measure of the dependency between two values with inter-distance h. There is a close relationship to the variogram function. For second order stationarity this is valid:

$$\gamma(h) = \sigma^2(1-\rho(h)) \tag{D.26}$$

Spatial stationarity A random variable is said to be stationary in the strict sense if the set of distribution functions $P(Z(x_1)<z_1, \ldots, Z(x_k)<z_k)$ and $P(Z(x_1+h)<z_1, \ldots, Z(x_k+h)<z_k)$ is the same for all vectors h. This means that the variable has the same probability distribution in all locations and implies that the expectation is constant throughout the volume.

Second order stationarity A random variable is said to be second order stationary if the expectation and the spatial variogram are location independent.

Gaussian distribution Another name for the normal distribution.

Multi Gaussian fields It means that for all n, the n-tuple $(Z_1,..., Z_n)$ is multi Gaussian.

cdf The abbreviation "cdf" is used for the cumulative distribution function. The cumulative distribution gives the probability of $Z(x) < z$ for all z.

Isotropy A medium is said to be isotropic if its properties are direction independent.

Anisotropy A medium is said to be anisotropic if its properties vary differently in different directions.

Kriging A standard geostatistical method for interpolation between observations, also used synonymously with **Prediction**. In the literature it is often called geostatistical estimation. The technique gives the expected value at all positions in the reservoir and the observations are reproduced, but the field will be smoother than in the real reservoir.

Unconditional simulation This simulation technique produces a realistic field given the stochastic modelling job. No observations are used. The method may be used in order to evaluate the specified modelling job. It is often useful to see if an unconditional simulation of the modelling job generates a realistic field (realization).

Conditional simulation Conditional simulation uses both the methods mentioned above. The simulation gives a possible field where all the well observations are reproduced. Simulations of several fields are valuable for analysing the uncertainty of the reservoir performance prediction.

As both kriging and conditional simulation are based on the same stochastic modelling job there is a close relationship between the resulting fields: given a location, using the same observations and the same job parameters, the average of a large set of simulated values will approach the kriged value.

Transformation

There are two reasons for transforming the observed well data:

- To ensure that trends observed in wells are carried through to simulation at non-well locations
- After a suitable set of transformations, the variables can be assumed to be normally distributed, and then analysed by the usual methods for normally distributed random variables.

After estimation of modelling job parameters and kriging/simulation the field is transformed back again.

Let $Y_i(x)$ be a petrophysical variable i at position x, where $x = (x, y, z)$ is a point in 3-dimensional space. It is then assumed that after some suitable transformation specified by the user the variable will be normally distributed with zero expectation:

$$Z_i(x) = f_i[Y_i(x)] \tag{D.27}$$

where Z_i is a Gaussian field with expectation zero and $Z_i(x)$ is the value of the field in position x.

The function f_i may be defined by one or more of the transforms listed in Chapter 32, "Trend analysis & transformations".

Variogram models

Gaussian fields are defined for each of the petrophysical parameters that should be modelled. Gaussian fields are characterized by various statistical parameters, some of them being the *Variogram* parameters that specify, for each facies type, the local scale spatial variability of the residuals of the petrophysical parameters

The variogram parameters indicate to what degree the residual values in one position are related to the residual values in a position nearby, as a function of their separation distance.

Before geostatistical kriging or simulation can be performed, the properties of the Gaussian field Z must be specified by its spatial variogram function.

The experimental variogram is calculated using the empirical (well) data. It is a sample of the 'true' variogram that we would have if we sample all possible data in the reservoir. This 'true' variogram is called the theoretical variogram and is defined as

$$\gamma(x,\ x+h) = \frac{1}{2} \cdot \mathrm{Var}(Z_i(x) - Z_j(x+h)) \tag{D.28}$$

In Irap RMS, when we calculate and model variograms we try to reduce our data to stationarity first. Being Stationary means that the probability distributions are the same at each point in the reservoir. In particular this implies that the mean value is a constant. In other words we must remove the trends from the data (see "Trends" on page 1382 to see how this is achieved in Irap RMS). Mathematically, this can be written

$$E\{Z(x)\} = \mu; \text{all } x \in V \tag{D.29}$$

A second implication of stationarity is that the variogram should only depend on the separation between the two points and not on the individual points themselves. This means that the left hand side of equation Equation D.29 depends only on h, and we can rewrite Equation D.29 as

$$\gamma(h) = \frac{1}{2} \cdot \mathrm{Var}(Z_i(x) - Z_j(x+h)) \tag{D.30}$$

In the stationary case, it can be shown that the variogram can also be expressed in terms of the spatial correlation function $\rho(h)$ giving the dependency between two values with distance h (this holds to the stationary case):

$$\gamma(h) = \sigma^2(1 - \rho(h)) \tag{D.31}$$

where σ^2 is the variance of Z(x). Some properties of this function have important physical interpretations, as shown in Table D.7.

The shape of the variogram close to the origin indicates the variability of the spatial variable at small distances. A parabolic shape characterises a smoother variable than a linear shape.

Various physical characteristics can be modelled by the variogram function. Irap RMS supports several types of variogram function;

Table D.7: Properties of the variogram spatial correlation function

Property	Interpretation
Nugget	The value of $\sigma_n^2 = \lim_{h \to 0} \gamma(h)$, is the nugget, and reflects the degree of discontinuity in the variable. A high nugget gives a field with little correlation between the values at two close locations, but one can still have a smooth large scale variation.
Range	The limit distance at which two locations, $Z_i(x)$ and $Z_i(x')$, change from correlated to uncorrelated is called the range. However, if the correlation between $Z_i(x)$ and $Z_i(x')$ for asymptotic-type variograms (such as Gaussian) falls below 0.05, the Petrophysical model sets the correlation to 0 in order to save a lot of computational costs. The distance r where this occurs is the range of the variogram, and determines the zone of spatial correlation. For all $h > r$ the correlation, $\rho(h) = 0$, i.e. points which lie more than the range away from each other are independent of each other. Therefore the range is often called the correlation length. When the correlation drops to zero, the variogram value reaches its sill and it remains at this value for all higher values of h (see below for a definition of sill. This statement follows from Equation D.31) Note: This concept of range applies to stationary data. If a variogram is calculated on data with a trend, it is usually seen to increase without ever reaching a limit. In other words, when you see a variogram that does not arrive at a sill at some range value, you will usually have to apply some more transformations to make the data stationary.
Sill	The value of $\gamma_\infty = \lim_{h \to \infty} \gamma(h)$ is the sill, and reflects the variability in the variable over the total volume. The higher the sill the more variability there will be in the field. Note the close relation to the variance: the sill equals $\sigma_n^2 + \sigma^2$, where σ^2 is the variance of the actual variable, i.e. the sill is the nugget plus the variance. A non-unit sill can be specified when using a variogram model as input to Petrophysical modelling.

mathematical descriptions of these are given in Appendix G, "Variogram theory".

During simulation, the variogram ellipsoid is moved from cell to cell in the modelling grid. At any position, the points on and outside the variogram ellipsoid are treated as independent of the point in the centre of the ellipsoid. The calculation of the spatial variability between the values in the centre and neighbourhood cells (points internal to the ellipsoid) is performed using a rotated coordinate system with its origin in the centre of the ellipsoid and its axes in the parallel, normal, and vertical variogram directions.

The weight of a neighbour cell is found by kriging using the variogram values at *lag (h)*.

Let (x', y', z') be a point (neighbourhood cell) in this coordinate system, and let (x, y, z) be the centre of the ellipsoid. The argument to the

variogram function, the *lag (h)* separating a point from the centre of the ellipsoid, is then defined as:

$$h = \left(\left(\frac{x'-x}{rx}\right)^2 + \left(\frac{y'-y}{ry}\right)^2 + \left(\frac{z'-z}{rz}\right)^2\right)^{1/2} \quad \text{(D.32)}$$

where rx, ry and rz are ranges in the parallel, normal, and vertical directions respectively.

Since there might be many cells in the neighbourhood, their maximum number can be limited for the calculation.

Correlation

So far only the spatial correlation for the stochastic variable $Z(x)$ has been studied, in the form of the variogram. Information about the correlation or dependency between pairs of petrophysical variables is also of great interest. If there is some correlation between two variables, observations of one variable gives information on the other. This may be utilised in kriging and simulation. The correlation between pairs of variables is defined by a matrix of correlation coefficients:

$$\mathrm{Corr}\{Z_i(x), Z_j(x)\} = \rho_{ij} \quad \text{(D.33)}$$

where ρ_{ij} gives the correlation between the variables Z_i and Z_j. Note that:

$$-1 < \rho_{ij} < 1 \quad i \neq j \quad \text{(D.34)}$$

and

$$\rho_{ii} = 1 \quad \text{(D.35)}$$

If the correlation is positive the values of the two variables tend to be small or high at the same time, but if the correlation is negative the value of variable Z_i tends to be small if variable Z_j is high. The closer to 1 or -1 the correlation is, the stronger these tendencies become. 0 correlation means that the variables are independent.

If matrix elements off the diagonal are very close to 1 some numerical problems may occur, and simulation is impossible. This is not usually a problem as a good reason for specifying, for example 0.99 correlation between two variables seldom exists. If the correlation is that high, there is hardly any need to simulate both variables.

A correlation specified in the petrophysical model is the linear correlation between two *residual fields*. The residual field for a parameter is that part of the variability in the data that remains when geological effects have been taken into account by applying the transformations sequence (see above).

When cosimulating, the correlated parameters must have the same variogram types and ranges specified.

Kriging and simulation

In Irap RMS two geostatistical methods are available: kriging (prediction) and simulation. Both methods may be unconditioned or conditioned on observations of petrophysical variables. All methods are based on the same

petrophysical modelling job. An example of kriging and conditional simulation is given in Figure D.7.

The variables under study are the spatial variables, $\{z(\mathbf{x});\mathbf{x}\varepsilon V\}$, where $\mathbf{x} = (x, y, z)$ is a vector in the 3-dimensional reference space. The spatial variable is considered as one realization of a random function $\{z(\mathbf{x});\mathbf{x}\varepsilon V\}$, and is normally known only for a finite number of points, $\{z(\mathbf{x}_i);\mathbf{x}_i\varepsilon V, i = 1...N\}$.

Spatial stationarity is assumed for the random function, which implies that the expectations are constant throughout the volume and that the spatial variability is location independent and can be defined by a variogram function $\gamma(h)$ only dependent on the distance h between two points in the volume

If several variables are to be modelled, a variogram function must be defined for each variable. In addition, correlation between variables may be defined. This may be specified by the covariance matrix. (To ensure that the covariance matrix is always positive definite, it is required that all variables have the same variogram range and variogram model type in each facies type.)

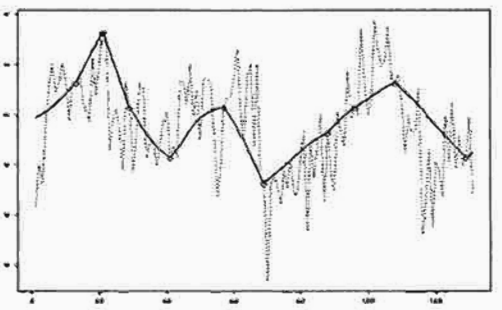

Figure D.7 Comparison: kriging (solid line) and conditional simulation (dotted line). The observations are also marked.

Kriging

The kriging methods used in Irap RMS are standard geostatistical methods. The general problem in kriging is to estimate $Z(\mathbf{x}_o)$, where $\mathbf{x}_o$ is an arbitrary location in the volume under study, from the observations $\{Z(\mathbf{x}_i); i = 1, N\}$. The kriging is really an interpolation between the observations and a kriged field will have the following properties:

1. It is unique and is the expected values given the observation.
2. It is the best linear estimate in the least squares sense when the variogram of the variable is known.
3. It coincides with the true variable in the observation locations.
4. It usually appears much smoother than the true field. Its variogram function will not be identical to the variogram function of the true variable. The variogram function will show less variability and more smoothness than the true one.

The interpolated values are given as a weighted average/linear combination of the observations. The weights used in the averaging depend on the spatial correlation between x_0 and the location of the observation x_i. If observations of other correlated variables exist the weight depends on those correlations too.

Neighbourhoods and kriging

The petrophysical modelling tool uses subsets of the data and dual kriging to achieve efficiency in speed and memory use while maintaining the accuracy in results. Dual kriging involves solving a linear equation system for a fixed subset of observations and re-use of this solution for many adjacent cells in a subvolume of the grid (Cressie, 1991). The main challenge in using this approach is to find "appropriate" subsets of the data.

The approach is illustrated in Figure D.8.

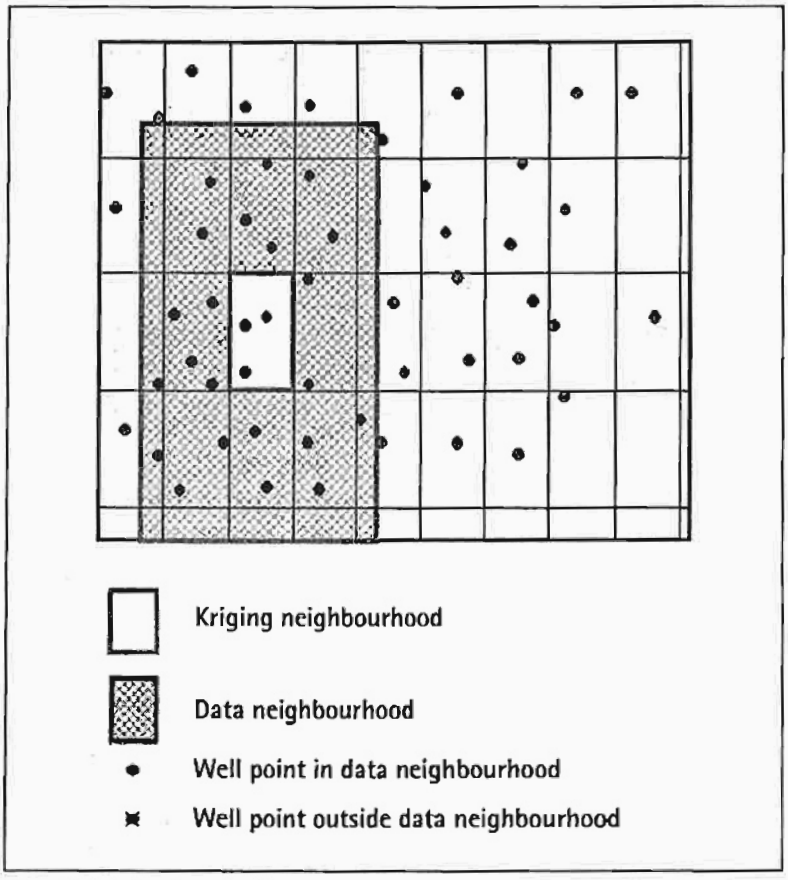

Figure D.8 Data subsets for kriging

The modelling grid is subdivided into equi-dimensional boxes called *kriging neighbourhoods*. A typical kriging neighbourhood will contain in the order of 1000 cells in 3D (e.g. 10*10*10). Each kriging neighbourhood is encased in a larger box called the *data neighbourhood*. Dual kriging is carried out using all observations in the data neighbourhood and applied to all cells

within the kriging neighbourhood. The kriging weights are calculated once for the kriging neighbourhoods instead of 1000 times.

The geometry of the kriging and data neighbourhoods is proportional to the ranges of the variogram.

The optimal size of the neighbourhoods is dependent on three main considerations.

1. The kriging neighbourhood should be as large as possible (to make use of dual kriging)
2. The data neighbourhood should be as small as possible (to speed up the kriging solution)
3. The data neighbourhood must be significantly larger than the kriging neighbourhood. This is to ensure that there is partial re-use of data between adjacent kriging neighbourhoods to avoid linear artefacts along the boundaries of the kriging neighbourhoods.

A smart algorithm is used to find sizes of the neighbourhoods that optimises performance and minimizes edge effects.

The kriging neighbourhoods are equi-dimensional for the entire modelling grid. The size of the data neighbourhoods, however, are dynamic and will change depending on the density of well observations in the proximity of the kriging neighbourhood. There is a target for the number of observations inside the data neighbourhood. This target is typically 50-1000. Larger targets will generally require more cpu time whereas smaller targets are generally faster but can introduce linear artefacts. The data neighbourhood will expand or reduce to meet the target. The data neighbourhood will never include data beyond one variogram range from the kriging neighbourhood.

Unconditional simulation

In Irap RMS an unconditional realization is simulated using the Fast Fourier Transform (FFT). The FFT is used to perform the convolution of a white noise field with a filter giving the correct correlation structure. A convolution is a simple product in the spectral domain and is therefore simple and fast. Moreover, the filter is a non-unique "square root" of the covariance function that is easily evaluated as the square root of the correlation function in the spectral domain. Thus, time consuming operations in space are trivial and fast operations in the spectral domain. The FFT algorithms are extremely fast and accurate so moving from the spatial to the spectral domain is fast.

FFT is a cyclic transformation. Thus in 1D, we operate on a circle, in 2D, we operate on a torus, and in 3D, opposite sides of the rectangular parallelepiped are attached. This means that the grids used in the FFT algorithm are cyclic and the moving average operation will make noise on opposite sides of the grid dependent. To avoid this dependence, the grid must be expanded by pads in all directions. The pads must be longer than the filter widths to guarantee independence between opposite sides of the grids. The filter sizes are determined by the range of the correlation function. Thus, ranges should be small compared to the grid lengths for fast performance.

This implies that the method does not work for variograms without range.

The FFT method can handle any stationary covariance function now matter how complicated it is as long as it has a finite range. This means that zonal anisotropy cannot be handled properly since the correlations never goes to zero along the principal axes. Any other kind of anisotropy is handled.

The method is described by Ripley [5] (on pages 108-110) for one-dimensional processes but it is trivially extendible to any dimension.

Conditional simulation

The procedure for conditional simulation was introduced as an alternative to kriging, and the objective was to avoid the smoothing tendency in the kriging [4]. The simulated variable has the following properties:

- It has the same distribution of values and the same variogram function as the true variable.
- It coincides with the true variable in the observation locations.
- It is not unique, since infinitely many variables will have the properties listed above.
- As the number of simulated fields increases the average of the simulated fields approaches the kriged.

The procedure of conditional simulation for one spatial variable is:

1. Perform unconditional simulation of a spatial variable $Z(x)$ normally distributed and with variogram $\gamma(h)$. This field satisfies the specified stochastic properties, but is does not interpolate the observations.
2. To ensure that the simulated variable passes through the observations, perform kriging on the unconditional simulated field to force it through the observations.

Cosimulation

The Petrophysical modelling tool allows you to perform two types of cosimulation:

- **Classic cosimulation:** If more than one petrophysical parameter is modelled at the same time, with correlations between them specified, these affect each other (see Figure D.9).
- **Co-located cosimulation:** The specified cosimulation parameter influences the result of the modelled petrophysical parameter (see Figure D.10). The co-located cosimulation parameter has values on the grid that are on identical locations to the modelled physical parameter.

  The cosimulation parameter is normally a seismic parameter. However, you can also specify a non-seismic parameter. For example, you could select a previously-modelled porosity parameter when modelling a permeability parameter. In this case, the permeability parameter will be affected by the porosity parameter, but not the other way round, which allows you to weight the influence of different parameters in the modelling.

Note

As an addition/alternative to seismic cosimulation, you can also condition *the result to seismic data by specifying a seismic parameter as a trend for a simulated parameter.*

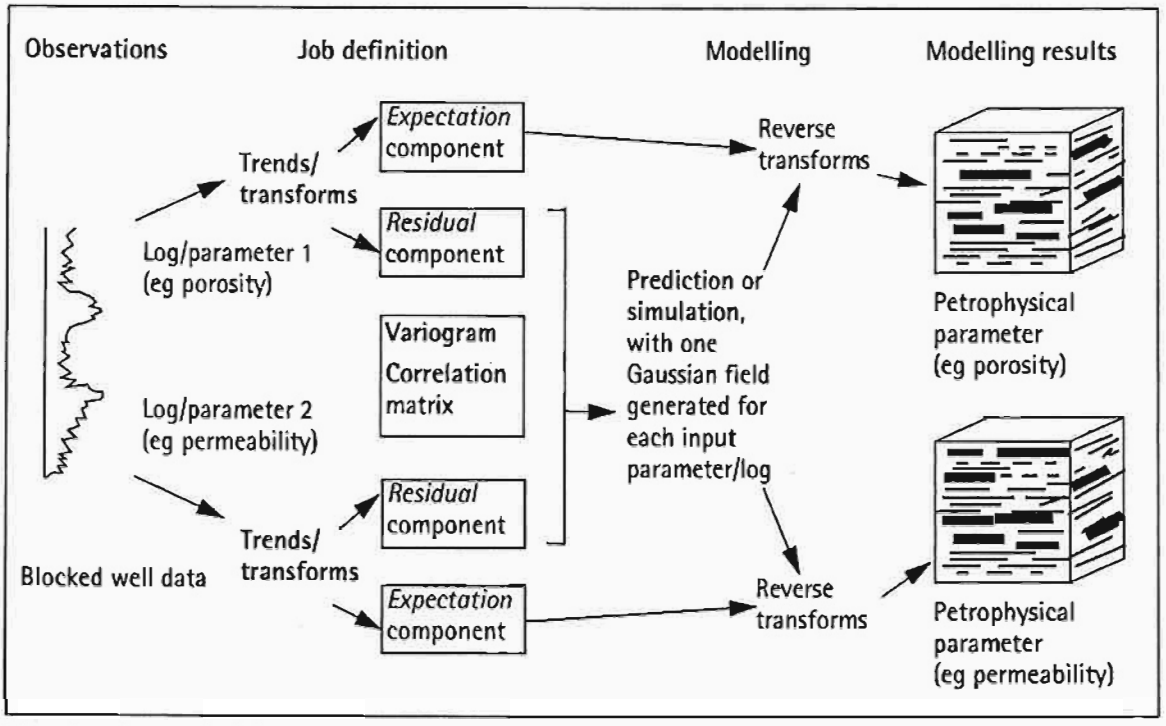

Figure D.9 The petrophysical modelling process, when modelling petrophysical parameters using classic cosimulation. Different subgrids and facies associations can be modelled separately, in the same way as when modelling uncorrelated parameters (see Figure 46.1 on page 1368)

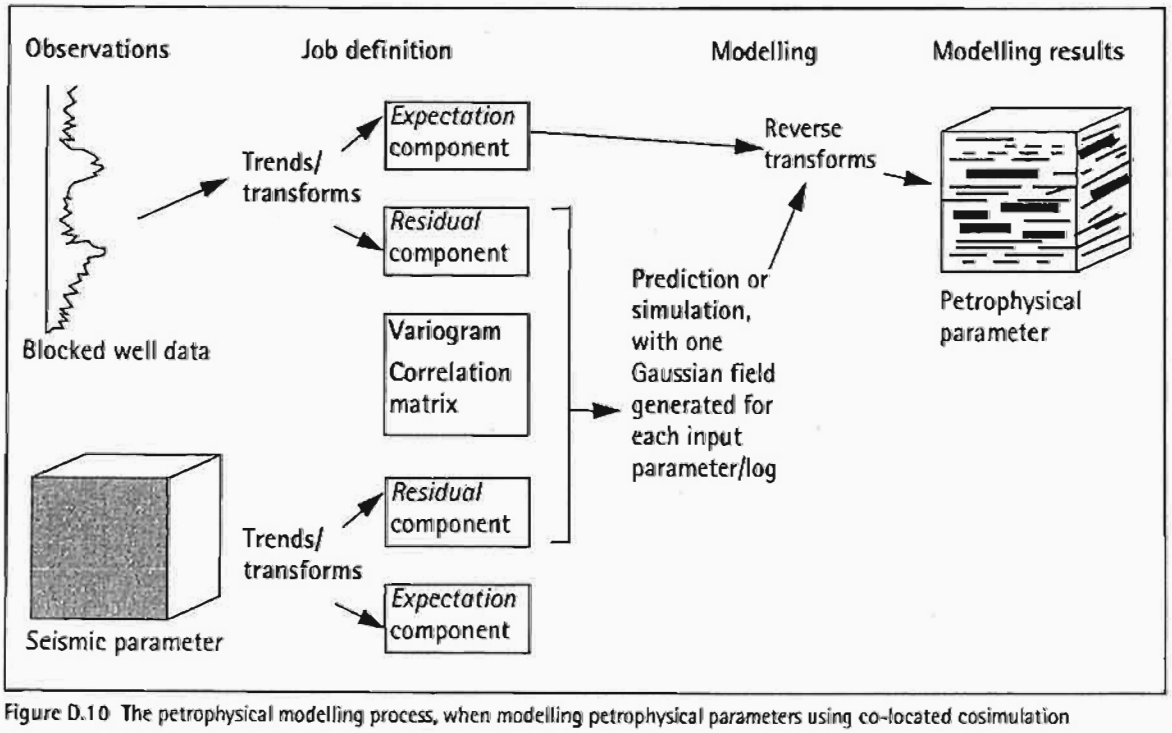

Figure D.10 The petrophysical modelling process, when modelling petrophysical parameters using co-located cosimulation

When cosimulating, the parameters must have the same variogram types and ranges specified.

Types of modelling results

Three types of modelling results are possible. These are described in Table 70.7, and typical appearances of modelling results, showing how the porosity value varies across the x axis of a 3D parameter, are shown in Figure D.11.

Table 70.7: Types of outcome from the petrophysical modelling

Model options			Name	Result	Technique
Prediction (Kriging)	Simulation	Conditioned to well data			
✓		✓	Expectation updated to well observations	Expectation of the parameter with the observations reproduced. The realization will be smoother than in the real reservoir.	A Kriging technique is applied to the difference between observations and the expectation.
	✓		Unconditional simulation	Simulated parameter with realistic heterogeneity (subject to the settings in the stochastic modelling job). The quality of the realization can be used to evaluate the specified modelling job.	The *residual field* is simulated and added to the expectation of the parameter.
	✓	✓	Conditional simulation	Simulated parameter with realistic heterogeneity and honouring the well observations. Simulations of several realizations are valuable for analysing the uncertainty of the reservoir performance prediction.	A Kriging technique is applied to the difference between the observations and the sum of the expectation and the simulated residual field.

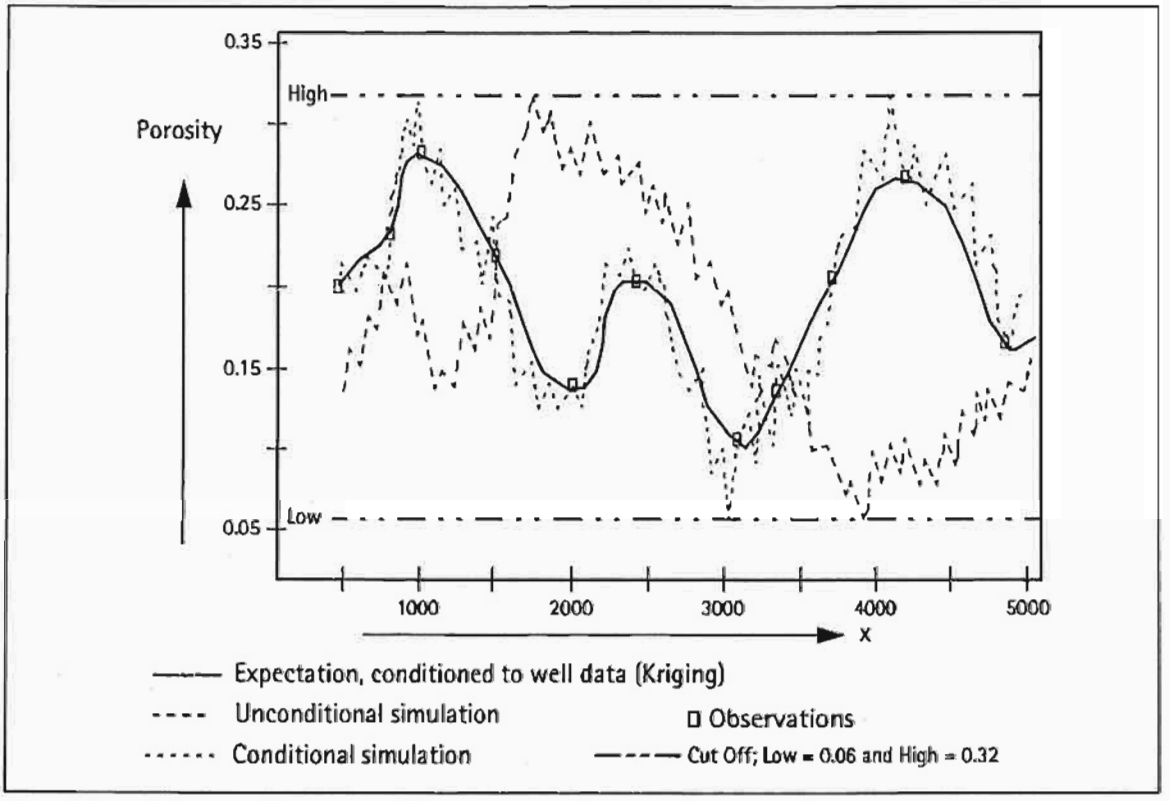

Figure D.11 Typical results of Kriging, unconditional & conditional simulation (see Table 70.7)

References and further reading

[1] Abrahamsen, P (1999). FFT algorithm for simulating Gaussian random fields. *SAND/10/99*, Norwegian Computing Center, Oslo.

[2] Christakos, G. (1992). *Random Field Models in Earth Sciences.* Academic Press, San Diego, 474 pp.

[3] Cressie, N. (1991). *Statistics for Spatial Data.* John Wiley & Sons, New York, 900 pp.

[4] Journel, A.G., and Huijbregts, Ch. J. (1978). *Mining Geostatistics.* Academic Press, New York.

[5] Ripley, B. D. (1987). *Stochastic simulation.* John Wiley & Sons, New York, 237 pp.

[6] Wood, A. T. A. and Chan. G. (1994). Simulation of stationary Gaussian processes in [0,1]d. *Journal of Computational and Graphical Statistics*, 3, 409 - 432.

Variogram theory

Introduction

This appendix provides a more detailed and mathematical description of the implemented methods for variogram analysis, related to Petrophysical modelling and facies modelling using indicator simulation. It covers:

- Terminology
- Variogram estimation
- The variogram function
- Variogram model types
- How the variogram is used during simulation

References and further reading are included at the end of the appendix.

Terminology

This section defines the specific terms used in variogram analysis of data.

Note

In geostatistical terminology, "spatial variable" or "variable" is used instead of "petrophysical parameter" (or "parameter").

In the following definitions, the expressions listed in Table D.8 are used.

Table D.8: Expressions used in the definitions

Expression	Usage
$Z(x)$	Used for a variable in location x, where x is an (x,y,z)-point in 3-dimensional space
$Z_i(x)$ and $Z_j(x)$	Denote two different variables
$\mu(x)$	The expectation of $Z(x)$
h	Denotes the distance between two points (the lag)

Spatial variable When a variable is distributed in space it is said to be spatial or regionalized. A spatial/regionalized variable is simply a function $f(x)$ that has a value for all x (i.e. x, y, z) points in 3-dimensional space.

Random variable A random variable is a variable which takes numerical values according to a certain probability distribution.

Variance The variance is defined as the second order moment about the expectation $\mu(x)$, i.e.

$$\sigma(x)^2 = \mathrm{VAR}[Z(x)] = E\left\{[Z(x) - \mu(x)]^2\right\} \tag{D.36}$$

The variance specifies the variability of the variable in the total reference space. The higher the variance, the more variability the variable has.

Covariance The covariance between two variables is defined as:

$$\mathrm{Cov}(Z_i, Z_j) = E\{[Z_i(x) - \mu_i(x)][Z_j(x) - \mu_j(x)]\} \tag{D.37}$$

This gives a measure of the dependency between the two variables Z_i and Z_j, and the variability in the variables.

Correlation Correlation between two variables is given by the correlation coefficients which can be computed from the covariance of the two variables and their variance:

$$\mathrm{Corr}\{Z_i, Z_j\} = \frac{\mathrm{Cov}\{Z_i, Z_j\}}{\sigma_i \cdot \sigma_j} = \rho ij \tag{D.38}$$

Note *Note that:* $-1 \le \rho ij \le 1$

If the correlation is positive, the values of the two variables tend to be small or high at the same time, but if the correlation is negative the value of variable Z_i tends to be small if variable Z_j is high (and *vice versa*). The closer to 1 or -1 the correlation is, the stronger these tendencies become.

Variogram The spatial variogram function is defined as the variance of the increment $[Z(x) - Z(x+h)]$, and is written:

$$\gamma(h) = \frac{1}{2}\mathrm{Var}\{Z(x) - Z(x+h)\} \tag{D.39}$$

This function gives the spatial variability of a variable. The smoothness or discontinuity of the variable may be modelled by the variogram. A more detailed definition is given in below.

Spatial correlation The spatial correlation function $\rho(h)$ is a measure of the dependency between two values with inter-distance h. There is a close relationship to the variogram function. For second order stationarity this is valid:

$$\gamma(h) = \sigma^2(1 - \rho(h)) \tag{D.40}$$

Spatial stationarity A random variable is said to be stationary in the strict sense if the set of distribution functions $P(Z(x_1) < z_1, \ldots, Z(x_k) < z_k)$ and $P(Z(x_1 + h) < z_1, \ldots, Z(x_k + h) < z_k)$ is the same for all vectors h. This means that the variable has the same probability distribution in all locations and implies that the expectation is constant throughout the volume.

Second order stationarity A random variable is said to be second order stationary if the expectation and the spatial variogram are location independent.

Gaussian distribution Another name for the normal distribution.

Multi Gaussian fields It means that for all n, the n-tuple $(Z_1, \ldots, Z_n)$ is multi Gaussian.

cdf The abbreviation "cdf" is used for the cumulative distribution function. The cumulative distribution gives the probability of $Z(\mathbf{x}) < z$ for all z.

Isotropy A medium is said to be isotropic if its properties are direction independent.

Anisotropy A medium is said to be anisotropic if its properties vary differently in different directions.

Kriging A standard geostatistical method for interpolation between observations. In the literature it is often called geostatistical estimation. The technique gives the expected value at all positions in the reservoir and the observations are reproduced, but the field will be smoother than in the real reservoir.

Variogram estimation

Irap RMS offers a choice of three methods for estimating variograms for continuous well logs. (For indicator variograms, only the Traditional method is available.)

Traditional estimator

The traditional estimator [3] is the most frequently used estimator in geostatistics. This estimator is characterised by:

- Certain optimality properties if representative sampling on a regular grid is performed. It is the minimum variance unbiased estimator among estimators of this form.
- The reliability decreases significantly with deviations from representative and regular sampling.

The traditional estimator is defined as:

$$\gamma^*(h) = \frac{1}{2 \cdot N_h} \sum_{(i,j) \epsilon D_h} (z(x_i) - z(x_j))^2 \qquad \text{(D.41)}$$

where N_h is the number of pairs collected in the lag D_h.

Optionally, a smoothing algorithm can be applied.

A schematic showing how the variogram is estimated, using the Traditional method, is given in Figure 70.8.

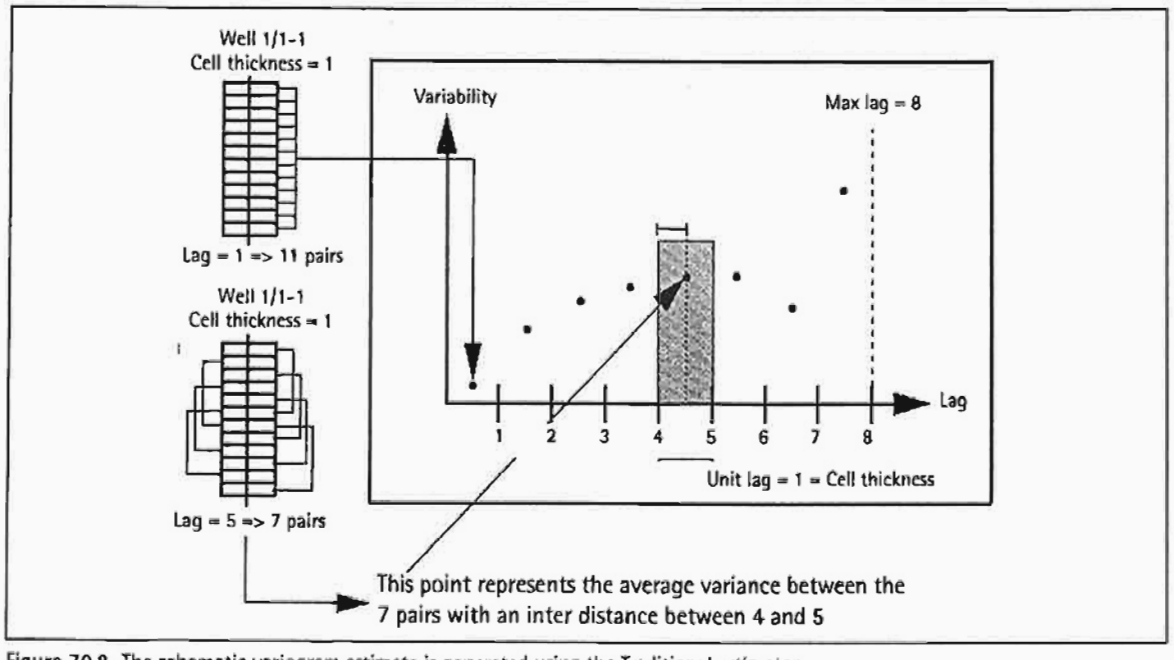

Figure 70.8 The schematic variogram estimate is generated using the Traditional estimator.

Robust estimator

A more robust estimator is available. This is described in Cressie (1993)[2].

Point cloud 'estimator'

This not an estimator in the strict sense: it simply gives you the variance in the measurements as a function of their lag.

The estimator plots

$$\frac{1}{2} \cdot (z(x_i) - z(x_j))^2 \tag{D.42}$$

for each pair of points (x_i and x_j) separated by the distance h.

The variogram function

Before geostatistical kriging or simulation can be performed, the properties of the Gaussian field Z must be specified by its spatial variogram function.

The experimental variogram is calculated using the empirical (well) data. It is a sample of the 'true' variogram that we would have if we sample all possible data in the reservoir. This 'true' variogram is called the theoretical variogram and is defined as

$$\gamma(x,\ x+h) = \frac{1}{2} \cdot \mathrm{Var}(Z_i(x) - Z_i(x+h)) \tag{D.43}$$

Now, in Irap RMS, when we calculate and model variograms we try to reduce our data to stationarity first. Being Stationary means that the probability distributions are the same at each point in the reservoir. In particular this implies that the mean value is a constant. In other words we must remove the trends from the data (see Chapter 32, "Trend analysis & transformations" to see how this is achieved in Irap RMS). Mathematically, this can be written

$$E\{Z(x)\} = \mu;\ \text{all}\ x \in V \tag{D.44}$$

A second implication of stationarity is that the variogram should only depend on the separation between the two points and not on the individual points themselves. This means that the left hand side of equation Equation D.44 depends only on h, and we can rewrite Equation D.44 as

$$\gamma(h) = \frac{1}{2} \cdot \mathrm{Var}(Z_i(x) - Z_i(x+h)) \tag{D.45}$$

In the stationary case, it can be shown that the variogram can also be expressed in terms of the spatial correlation function $\rho(h)$ giving the dependency between two values with distance h (this holds to the stationary case):

$$\gamma(h) = \sigma^2(1 - \rho(h)) \tag{D.46}$$

where σ^2 is the variance of Z(x). Some properties of this function have important physical interpretations, as shown in Table D.9.

The shape of the variogram close to the origin indicates the variability of the spatial variable at small distances. A parabolic shape characterises a smoother variable than a linear shape.

Table D.9: Properties of the variogram spatial correlation function

Property	Interpretation
Nugget	The value of $\sigma_n^2 = \lim_{h \to 0} \gamma(h)$, is the nugget, and reflects the degree of discontinuity in the variable. A high nugget gives a field with little correlation between the values at two close locations, but one can still have a smooth large scale variation.
Range	The limit distance at which two locations, $Z_i(x)$ and $Z_i(x')$, change from correlated to uncorrelated is called the range. However, if the correlation between $Z_i(x)$ and $Z_i(x')$ for asymptotic-type variograms (such as Gaussian) falls below 0.05, the Petrophysical model sets the correlation to 0 in order to save a lot of computational costs. The distance r where this occurs is the range of the variogram, and determines the zone of spatial correlation. For all $h > r$ the correlation, $\rho(h) = 0$, i.e. points which lie more than the range away from each other are independent of each other. Therefore the range is often called the correlation length. When the correlation drops to zero, the variogram value reaches its sill and it remains at this value for all higher values of h (see below for a definition of sill. This statement follows from Equation D.46) Note: This concept of range applies to stationary data. If a variogram is calculated on data with a trend, it is usually seen to increase without ever reaching a limit. In other words, when you see a variogram that does not arrive at a sill at some range value, you will usually have to apply some more transformations to make the data stationary.
Sill	The value of $\gamma_\infty = \lim_{h \to \infty} \gamma(h)$ is the sill, and reflects the variability in the variable over the total volume. The higher the sill the more variability there will be in the field. Note the close relation to the variance: the sill equals $\sigma_n^2 + \sigma^2$, where σ^2 is the variance of the actual variable, i.e. the sill is the nugget plus the variance. For transformed petrophysical log data, in an ideal situation the sill for all directions might be expected to be equal when the data are stationary, Gaussian, and not too far from being isotropic. However, in practice it is not always possible to arrive at this ideal situation: for example, sills may be different in different directions, indicating that the data is quite anisotropic. A non-unit sill can be specified when using a variogram model as input to Petrophysical modelling.

Variogram model types

Various physical characteristics [6] can be modelled by the variogram function. Due to the geostatistical method used in Irap RMS, the shape of the variogram function is restricted to the following classes for standard variograms:

- Spherical
- Gaussian
- Exponential
- General exponential, with the power satisfying $0 < power \leq 2$
- Hole effect (damped sine)
- Modified Bessel

and the following classes for indicator variograms:

- Spherical
- Exponential
- General exponential, but only with the power satisfying $0 < power \leq 1$

In addition, a nugget can be applied by specifying the White noise (nugget) variogram model type.

Information on the Spherical, Exponential, and Gaussian variogram functions are presented in the following subsections.

For information on General exponential, Hole effect (damped sine), and Modified Bessel variogram functions, refer to Abrahamsen (1997)[1].

Spherical variogram

This model defines a Gaussian field with a finite variability and range of correlation.

$$\gamma(h) = \sigma^2 \cdot \left(\frac{3}{2} - \frac{1}{2} \cdot \left\{ \frac{h}{r} \right\}^2 \right) \tag{D.47}$$

where

- σ^2 is the variance and r the range
- the sill is equal to $\sigma_n^2 + \sigma^2$
- for 3D variogram models, r is set equal to 1, and h is scaled incorporating the anisotropic ranges.

Exponential variogram

This model defines a Gaussian process with a finite variability and in practice a finite range of correlation.

$$\gamma(h) = \sigma^2 \cdot \left(1 - \exp\left\{ -\frac{h}{a} \right\} \right) \tag{D.48}$$

where

- σ^2 is the variance
- a is a parameter closely linked to the range used in practice. The exponential variogram gives correlation less than 0.05 for points with

inter-distance $h \geq 3 \cdot a$. The spatial correlation is therefore assumed to be zero for these points, i.e. the practical range is $r = 3 \cdot a$

- the sill equals $\sigma_n^2 + \sigma^2$, but no real range exists.
- for 3D variogram models, r is set equal to 1, and h is scaled incorporating the anisotropic ranges.

Gaussian variogram

This model defines a Gaussian process being infinitely times derivable. The correlation between two points with small inter-distance is therefore large, and a simulated field with this variogram is very smooth. Care should therefore be taken if one applies a Gaussian variogram with a large range compared with the grid increments. Numerical instabilities could occur. The variability is finite and in practice also the range of correlation.

$$\gamma'(h) = \sigma^2 \cdot \left(1 - \exp\left\{-\left(\frac{h}{a}\right)^2\right\}\right) \tag{D.49}$$

where

- σ^2 is the variance
- a is a parameter closely linked to the range used in practice. The Gaussian variogram gives correlation less than 0.05 for points with inter-distance $h \geq \sqrt{3} \cdot a$. The spatial correlation is therefore assumed to be zero for these points, i.e. the practical range is $r = \sqrt{3} \cdot a$
- the sill equals, $\sigma_n^2 + \sigma^2$, but no real range exists
- for 3D variogram models, r is set equal to 1, and h is scaled incorporating the anisotropic ranges.

How the variogram is used during simulation

During simulation, the variogram ellipsoid is moved from cell to cell in the modelling grid. At any position, the points on and outside the variogram ellipsoid are treated as independent of the point in the centre of the ellipsoid. The calculation of the spatial variability between the values in the centre and neighbourhood cells (points internal to the ellipsoid) is performed using a rotated coordinate system with its origin in the centre of the ellipsoid and its axes in the parallel, normal, and vertical variogram directions.

The weight of a neighbour cell is found by kriging using the variogram values at *lag (h)*.

Let (x', y', z') be a point (neighbourhood cell) in this coordinate system, and let (x, y, z) be the centre of the ellipsoid. The argument to the variogram function, the *lag (h)* separating a point from the centre of the ellipsoid, is then defined as:

$$h = \left(\left(\frac{x'-x}{rx}\right)^2 + \left(\frac{y'-y}{ry}\right)^2 + \left(\frac{z'-z}{rz}\right)^2\right)^{1/2} \tag{D.50}$$

where rx, ry and rz are ranges in the parallel, normal, and vertical directions respectively.

Since there might be many cells in the neighbourhood, their maximum number can be limited for the calculation.

References

[1] Abrahamsen, P 1997: *A Review of Gaussian Random Fields and Correlation Functions*, 2nd Ed., Report no. 917, Norwegian Computing Center, P.O.Box 114 Blindern, N-0314 Oslo, Norway, 64pp, ISBN 82-539-0435-5

[2] Cressie, N. A. C. 1993: *Statistics for Spatial data*, revised edition. Wiley series in probability and mathematical statistics.

[3] Matheron, G. 1965: *Les Variable Regionalisees et leur Estimation*, Masson & Cie, Paris

[4] Omre, K.H. 1984: *The Variogram and its Estimation*. Abstract of parts of PhD Thesis, Department of Applied Earth Sciences, Stanford University

[5] Omre, K.H. 1985: *User/technical documentation for the chain of variogram estimators CHAVAR*. NR-Note SAND/02/85, Norwegian Computing Center, Oslo.

[6] Omre, K.H. 1987: *Introduction to geostatistical theory and examples of practical applications*. NR-Note SAND/14/87, Norwegian Computing Center, Oslo.

[7] Omre, K.H., Sølna, K. and Tjelmeland, H., 1992: Simulation of random functions on large lattices. *Proceedings from the 4th Geostatistical Congress*, September 1992, Troia, Portugal.

Appendix 3

Slices through the 3D stochastic facies and porosity models

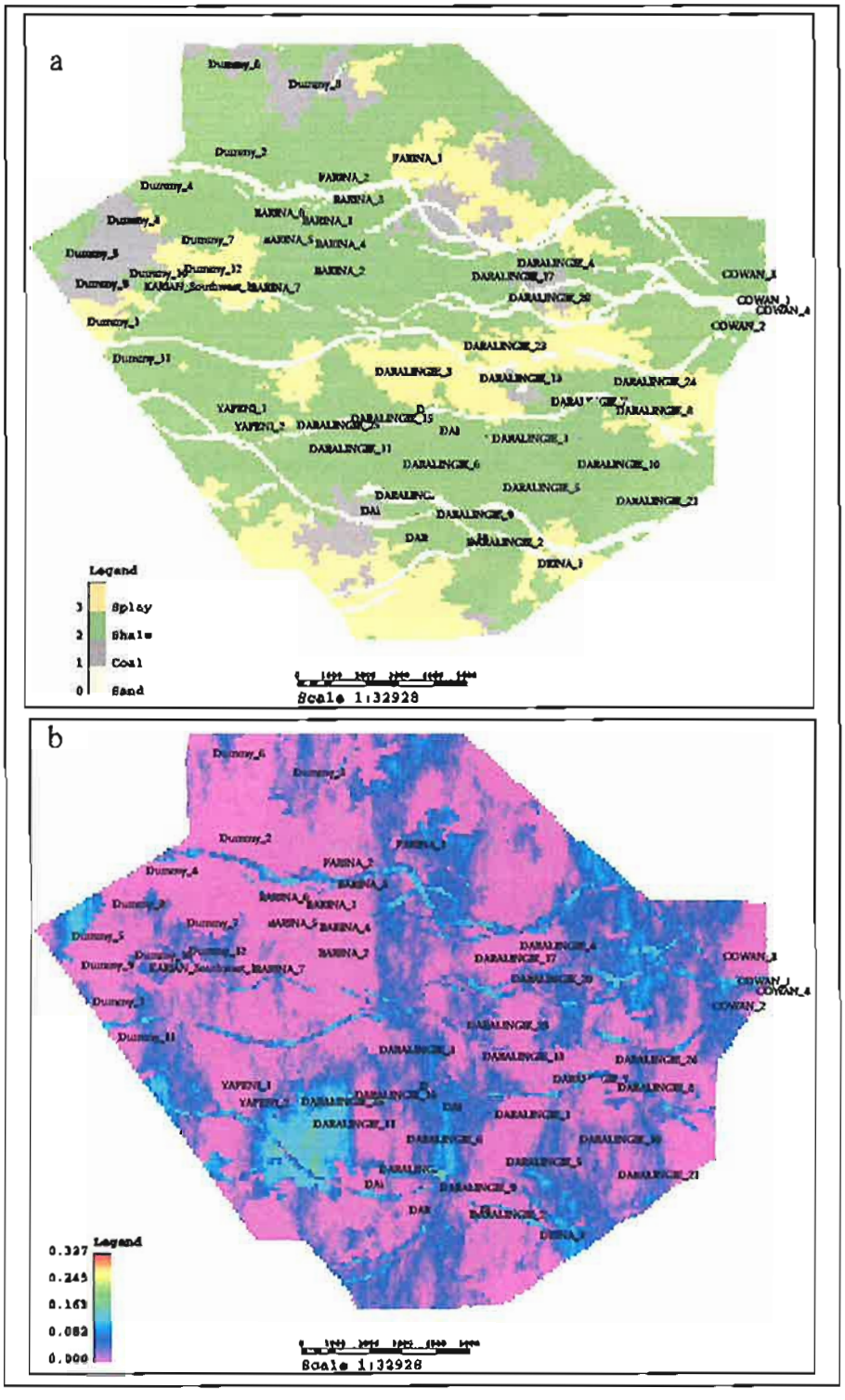

Figure A3.1: (a) A slice in the Daralingie Field facies model, (b) the porosity model in the VC00-VL05 reservoir interval.

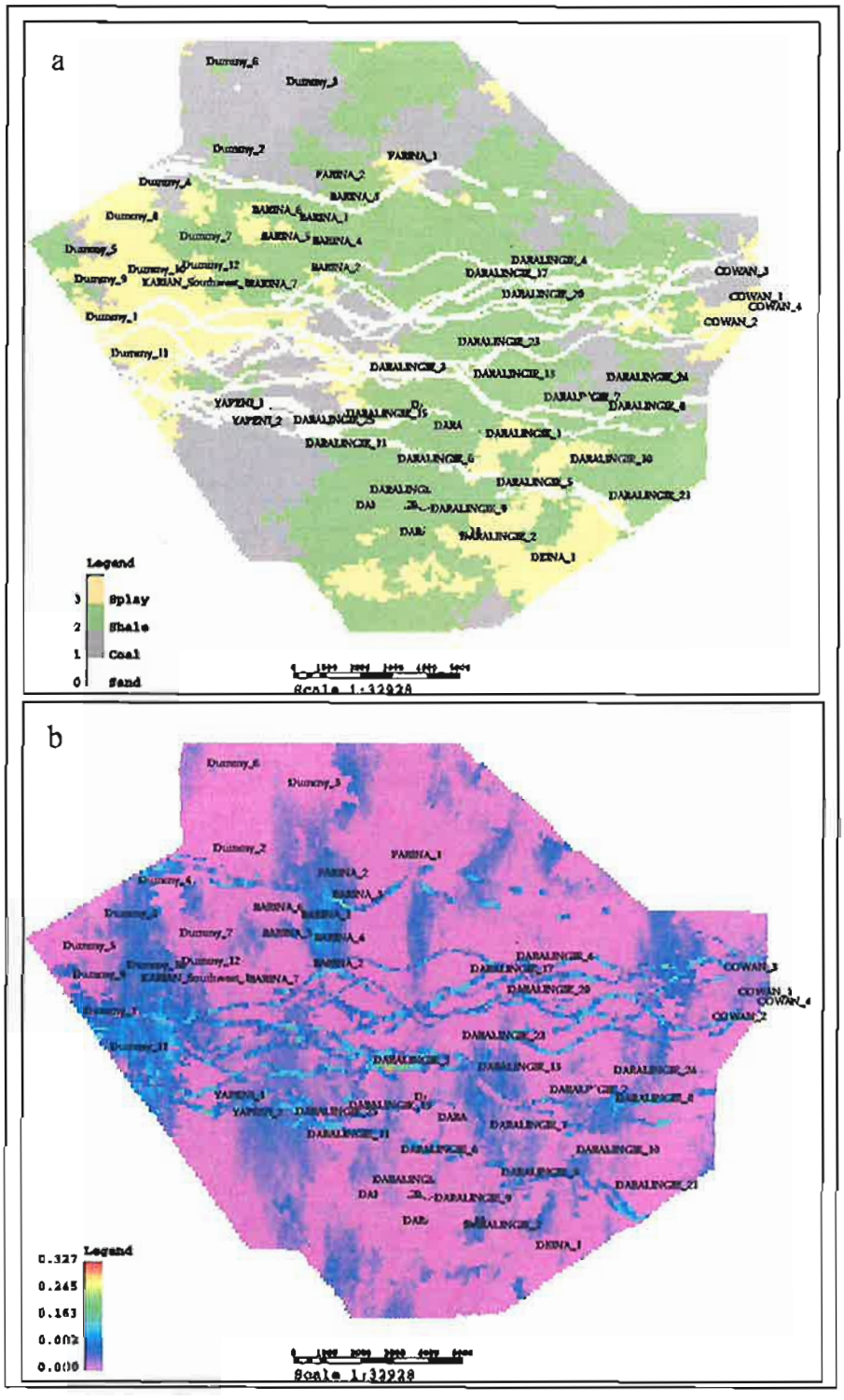

Figure A3.2: (a) A slice in the Daralingie Field facies model, (b) the porosity model in the VL05-VC10 reservoir interval.

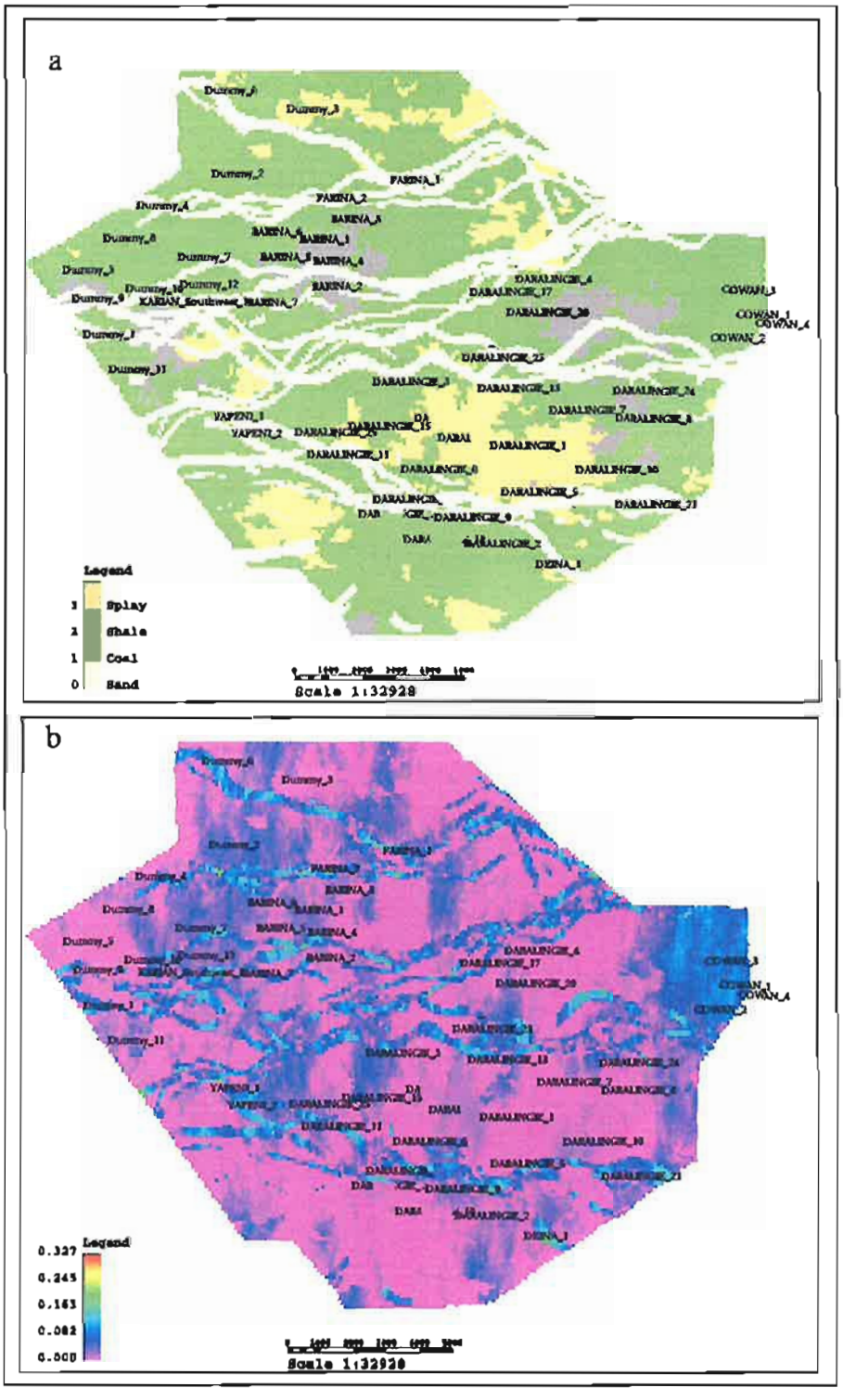

Figure A3.3: (a) A slice in the Daralingie Field facies model, (b) the porosity model in the VC10-VL11 reservoir interval.

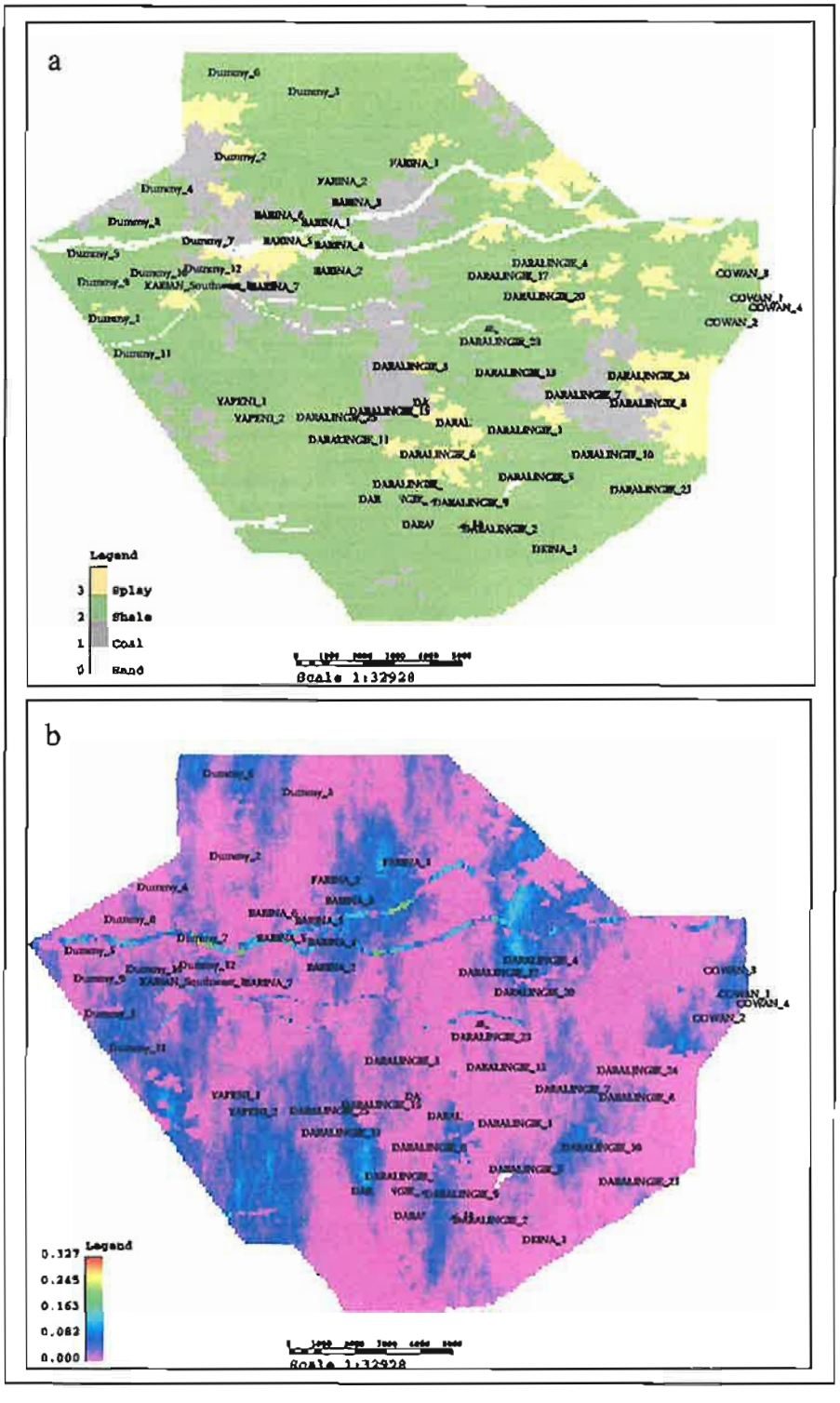

Figure A3.4: (a) A slice in the Daralingie Field facies model, (b) the porosity model in the VL11-VC15 reservoir interval.

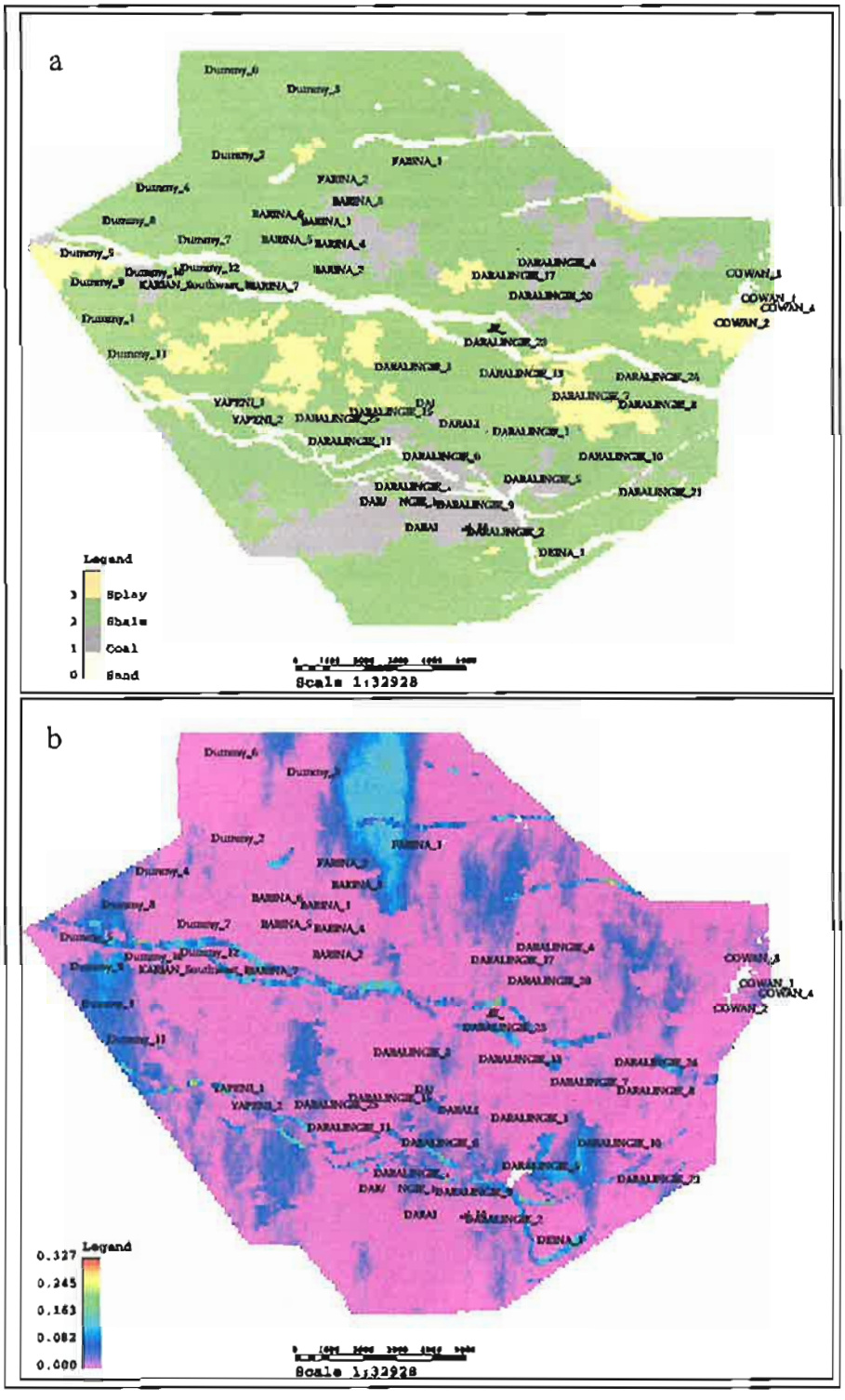

Figure A3.5: (a) A slice in the Daralingie Field facies model, (b) the porosity model in the VC15-VC20 reservoir interval.

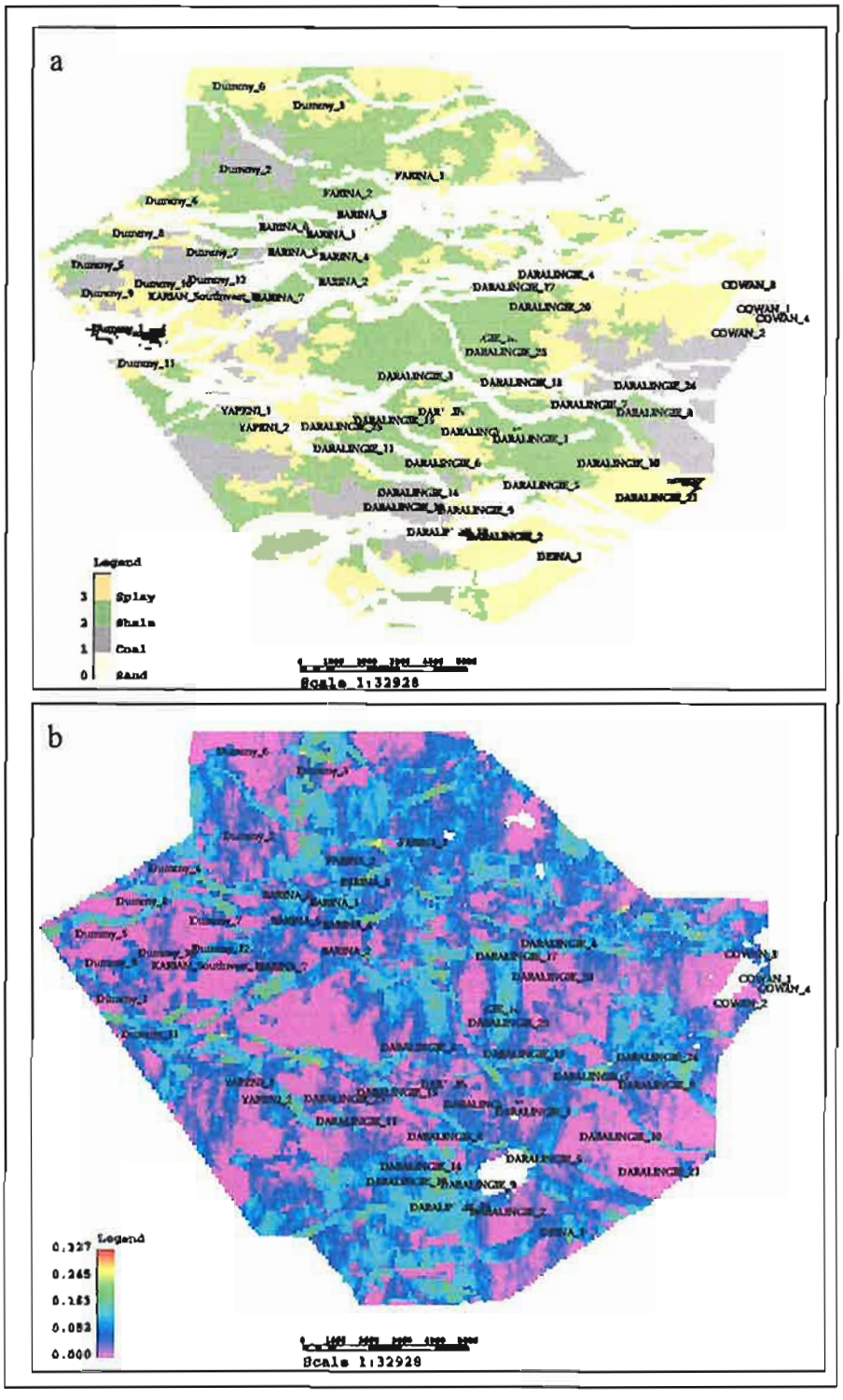

Figure A3.6: (a) A slice in the Daralingie Field facies model, (b) the porosity model in the VC20-VL22 reservoir interval.

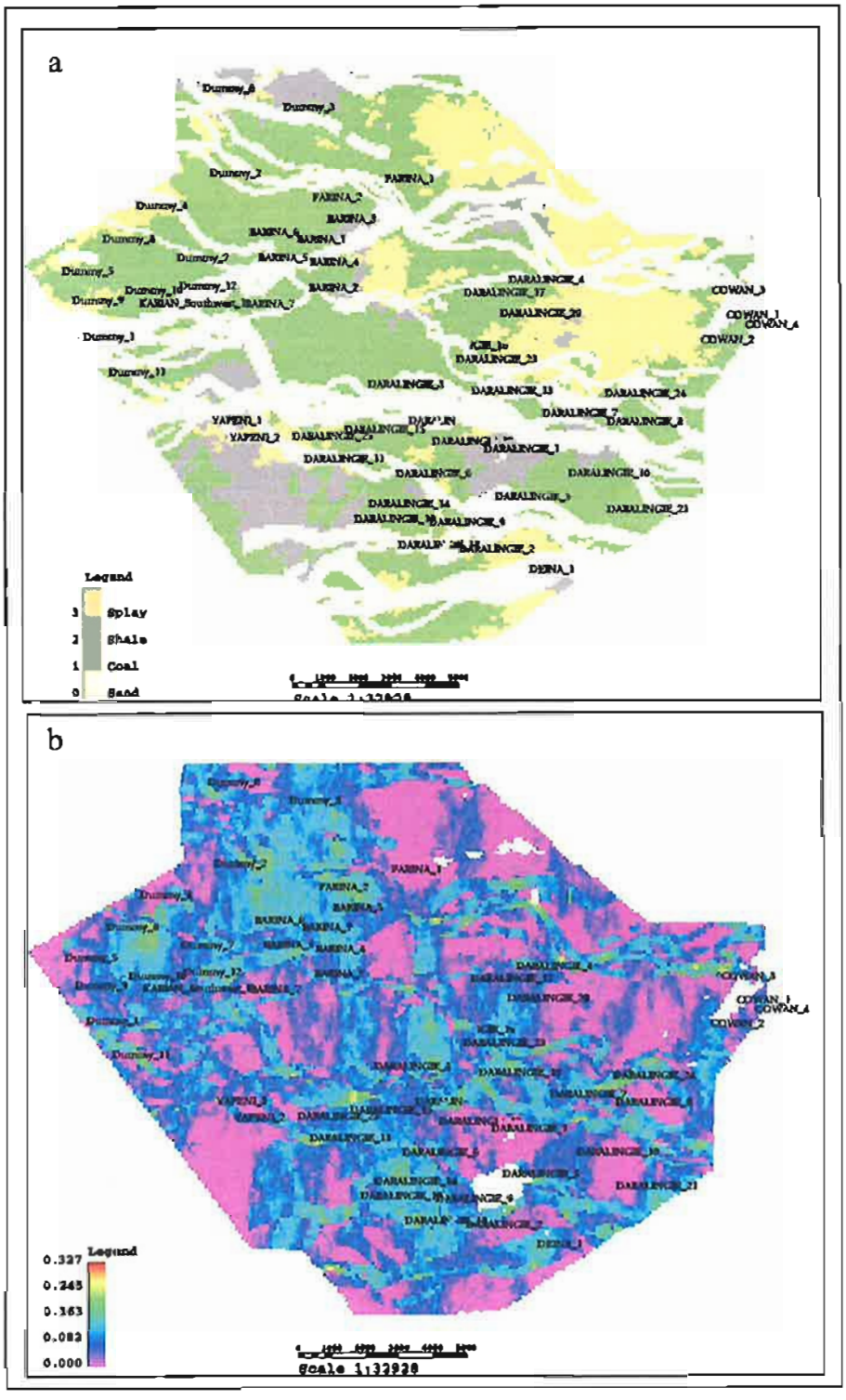

Figure A3.7: (a) A slice in the Daralingie Field facies model, (b) the porosity model in the VL22-VL25 reservoir interval.

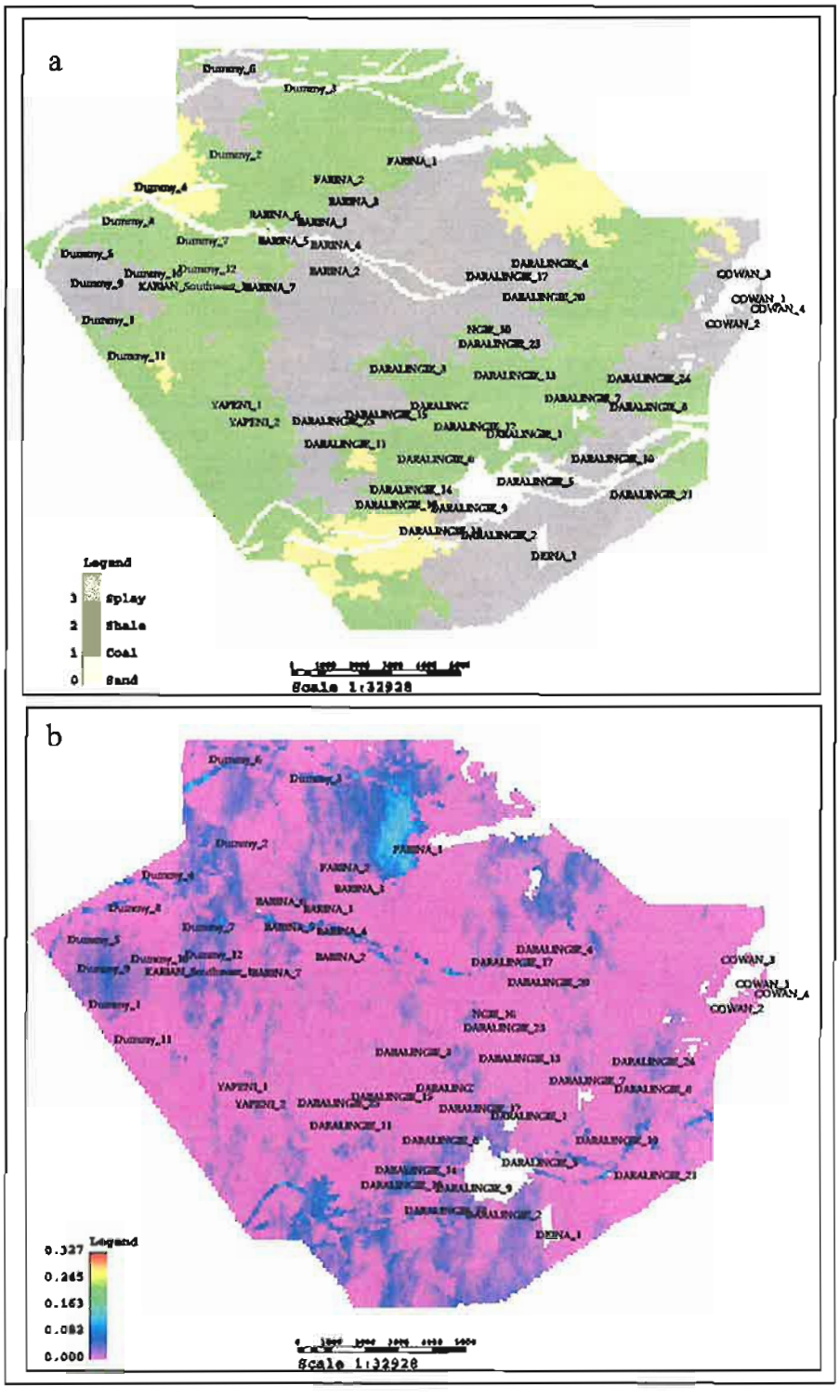

Figure A3.8: (a) A slice in the Daralingie Field facies model, (b) the porosity model in the VC25-VC30 reservoir interval.

Appendix 4

Modeling and Semivariograms settings in RMS

Channels Only

Tab	Description	
General	Output Format: Facies with body	
	Use all blocked wells	
	Condition on well data	
	Use Separate Subgrid Models	
	Multi-channel Mode	
	Channel: Sand	
	Background: Shale, Coal and Splay	
Simulation Settings	Minimum number of iterations: 1000	
	Monitor simulation: Yes	
	number of samples 100	
Volume Fractions	Type: Global	
	Value: define per subgrid as shown in tables xx	
	Tolerance: defined per subgrid as show in table xx	
	Channel position: 1	
Geometry	stacking pattern: Dispersed	
	Belt Dimensions	Belt thickness: N(15,3)
		Belt width (at top of belt): defined per subgrid as show in table xx
		Belt width (at base of belt): defined per subgrid as show in table xx
	Amplitude & Sinuosity (Channel-belts)	Amplitude: 2000
		Sinuosity: 1.05
	Number of channels in a belt	Value:3
		Tolerance: 1
	Channel dimensions	Thickness: N(8,4)
		Width: N(170,50)
		Correlation With-Thickness (0.1)
	Amplitude & Sinuosity (individual channels)	Amplitude: N(1200,200)
		Sinuosity: 1.05
	Orientation	Azimuth: N(90,10)
	Form/Repulsion	Channel form: Rigid
		Repulsion: None

Composite Model

Tab	Description	
General	Output Format: Facies only	
	Use all blocked wells	
	Condition on well data	
	Use Separate Subgrid Models	
	Model objects: Splay and Coal	
	Background: Shale	
	Erosion in wells: Yes	
Simulation Settings	Minimum number of iterations: Automatic	
	Monitor simulation: Yes	
	number of samples 100	
Volume Fractions	Type: Global	
	Value: define per subgrid as shown in tables xx	
	Tolerance: defined per subgrid as show in table xx	
	Relative intensity: 1	
Geometry	*Facies: Splay*	
	Shape: Rectangle	
	Reference Point: (0,0,0)	
	Size	Length: see table
		Width: see table
		Height: N(8,4)
	Orientation	Azimuth: N(90,10)
		Dip: N(0,0.1)
	Detailed Shape: Simple	Centerplane: 30
		Rugosity: 30
	Facies: Coal Shape: Ellipsoid Reference Point: (0,0,0)	
	Size	Length: see table
		Width: see table
		Height: N(8,4)
	Orientation	Azimuth: N(0,0.1)
		Dip: N(0,0.1)
	Detailed Shape: Simple	Centerplane: 30
		Rugosity: 30

Porosity Facies Based

Tab	Description	
General	Use all blocked wells	
	Parameters to be modeled: PHIE	
	Facies Data: Yes	
	Algorithm: Simulation	
	Separate subgrid models: Yes	
Simulation Settings	Kriging neighborhood: Default	
	Target number of data in local neighbor hoods: 250	
Distribution	User mode: Standard	
	Transformation type: Symmetric	
Transformation sequence	Automatic	
Variogram	*Log: PHIE Facies: Sand*	
	Standard deviation: Automatic	
	Variogram model: Standard	
	Type: Spherical	
	Anisotropy directions	Azimuth: 90
		Dip: 0
		Relative to body curvature
	Range	Parallel to azimuth: 5500 m
		Normal to azimuth: 2000 m
		Vertical: 10 ft
	Log: PHIE Facies: Coal	
	Standard deviation: Automatic	
	Variogram model: Standard	
	Type: Spherical	
	Range	Parallel to azimuth: 5500 m
		Normal to azimuth: 2000 m
		Vertical: 10 ft
	Log: PHIE Facies: Coal	
	Standard deviation: Automatic	
	Variogram model: Standard	
	Type: Spherical	
	Range	Parallel to azimuth: 5500 m
		Normal to azimuth: 2000 m

		Vertical: 10 ft
	Log: PHIE Facies: Coal	
	Standard deviation: Automatic	
	Variogram model: Standard	
	Type: Spherical	
	Range	Parallel to azimuth: 5500 m
		Normal to azimuth: 2000 m
		Vertical: 10 ft

Porosity only Model

Tab	Description	
General	Use all blocked wells	
	Parameters to be modeled: PHIE	
	Facies Data: No	
	Algorithm: Simulation	
	Separate subgrid models: Yes	
Simulation Settings	Kriging neighborhood: Default	
	Target number of data in local neighbor hoods: 250	
Distribution	User mode: Standard	
	Transformation type: Symmetric	
Transformation sequence	Automatic	
Variogram	Standard deviation: Automatic	
	Variogram model: Standard	
	Type: Spherical	
	Range	Parallel to azimuth: 5500 m
		Normal to azimuth: 2000 m
		Vertical: 10 ft

Appendix 5

Cross-plots of porosity and depositional facies for raw log data and the three stochastic models

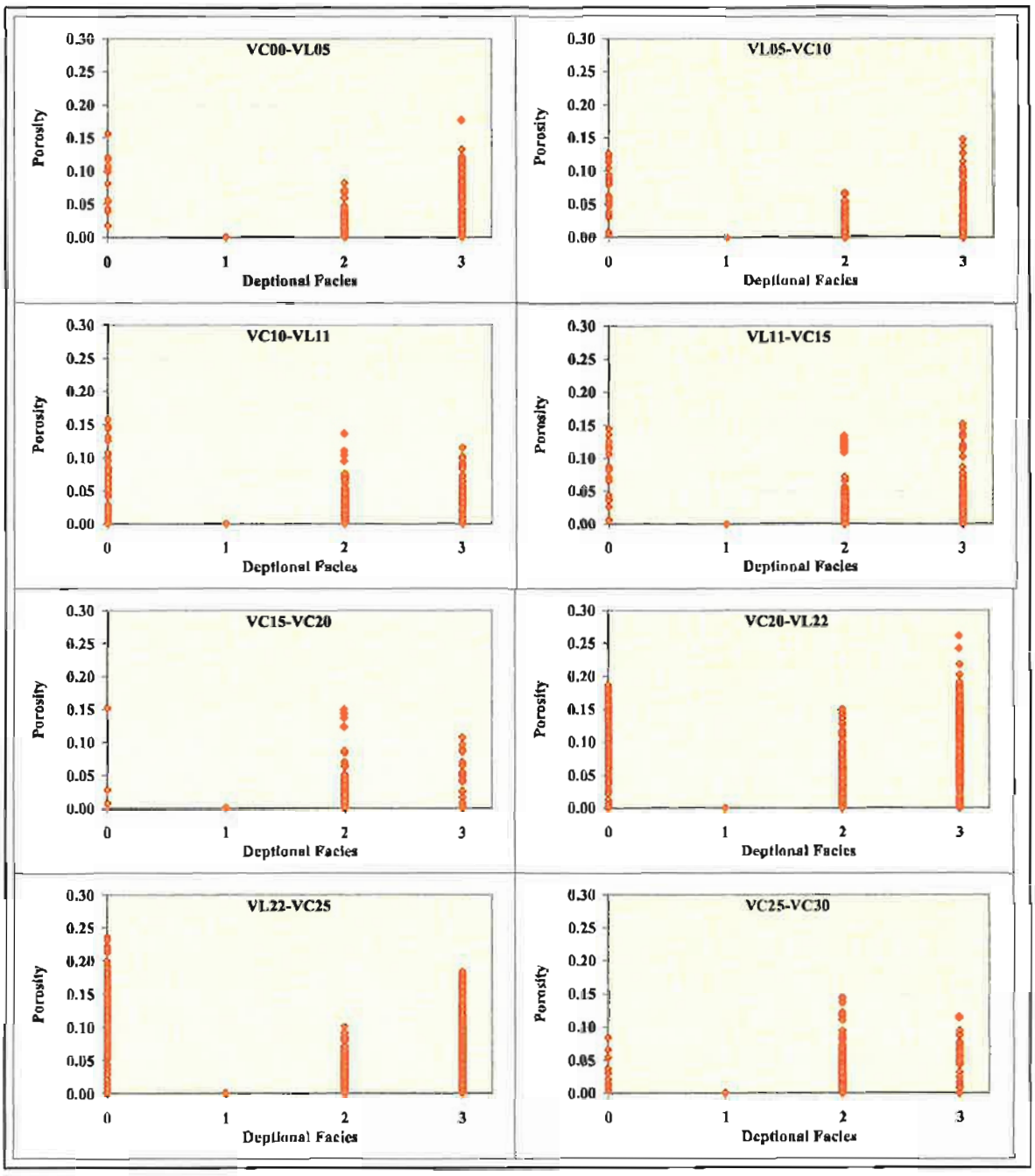

Figure A5.1: Cross-plots of porosity distribution in each facies in the well data for every reservoir interval the Daralingie Field

(Legned 0 = Channels, 1 = Coal, 2 = Shale, 3 = Spaly)

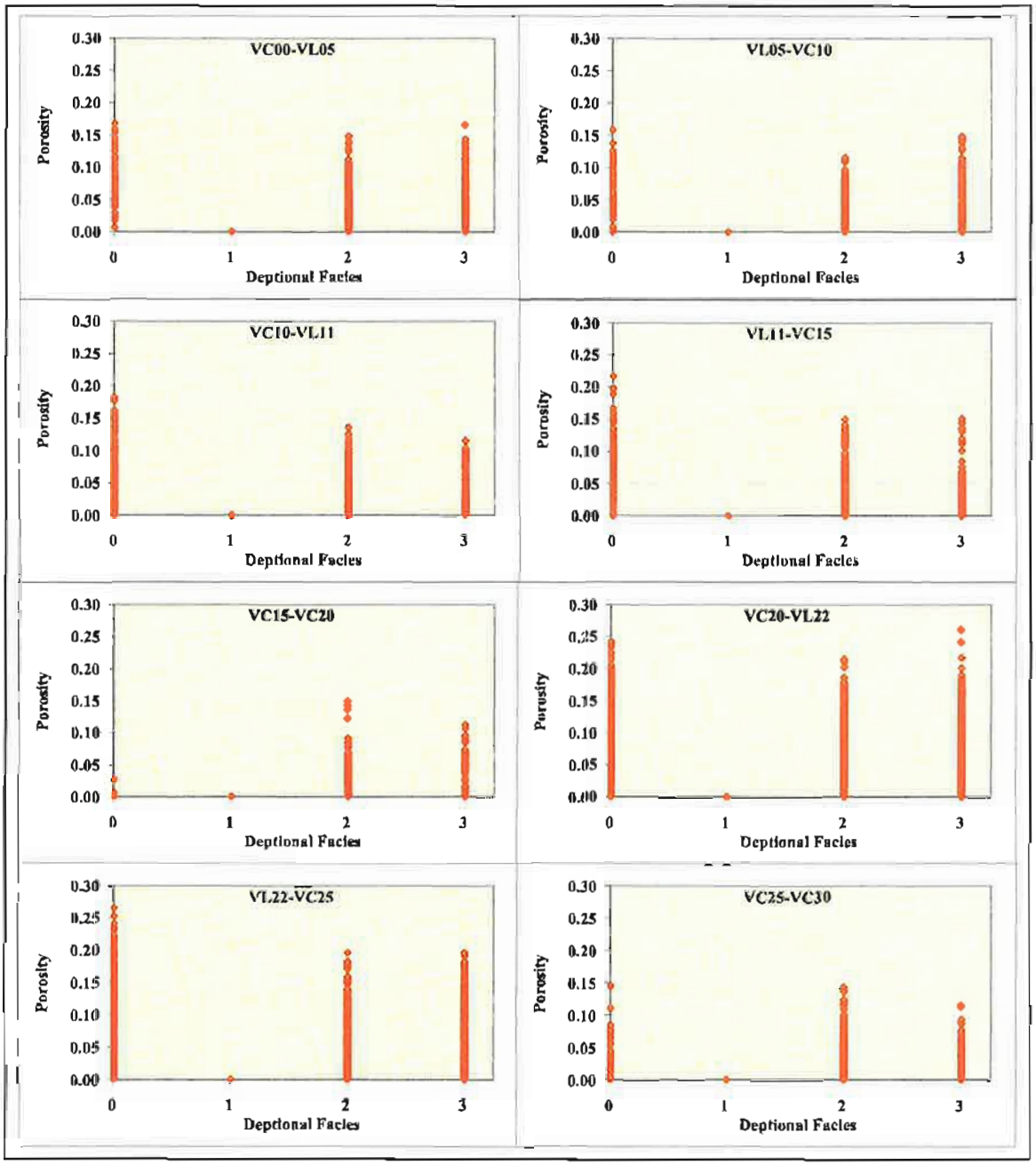

Figure A5.2: Cross-plots of porosity distribution in each facies in the porosity model-A for every reservoir interval the Daralingie Field

(Legned 0 = Channels, 1 = Coal, 2 = Shale, 3 = Spaly)

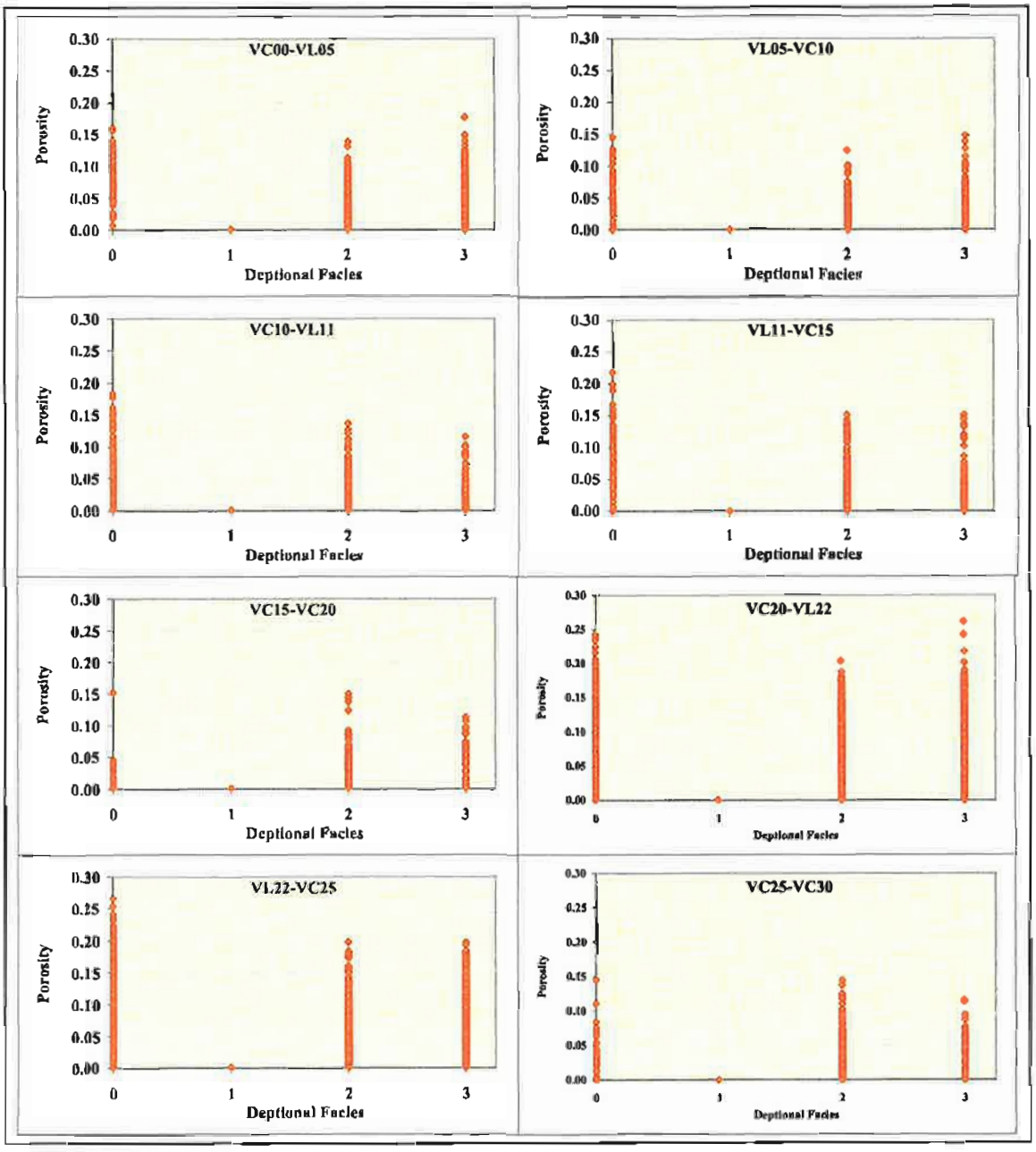

Figure A5.3: Cross-plots of porosity distribution in each facies in the porosity model-B for every reservoir interval the Daralingie Field

(Legned 0 = Channels, 1 = Coal, 2 = Shale, 3 = Spaly)

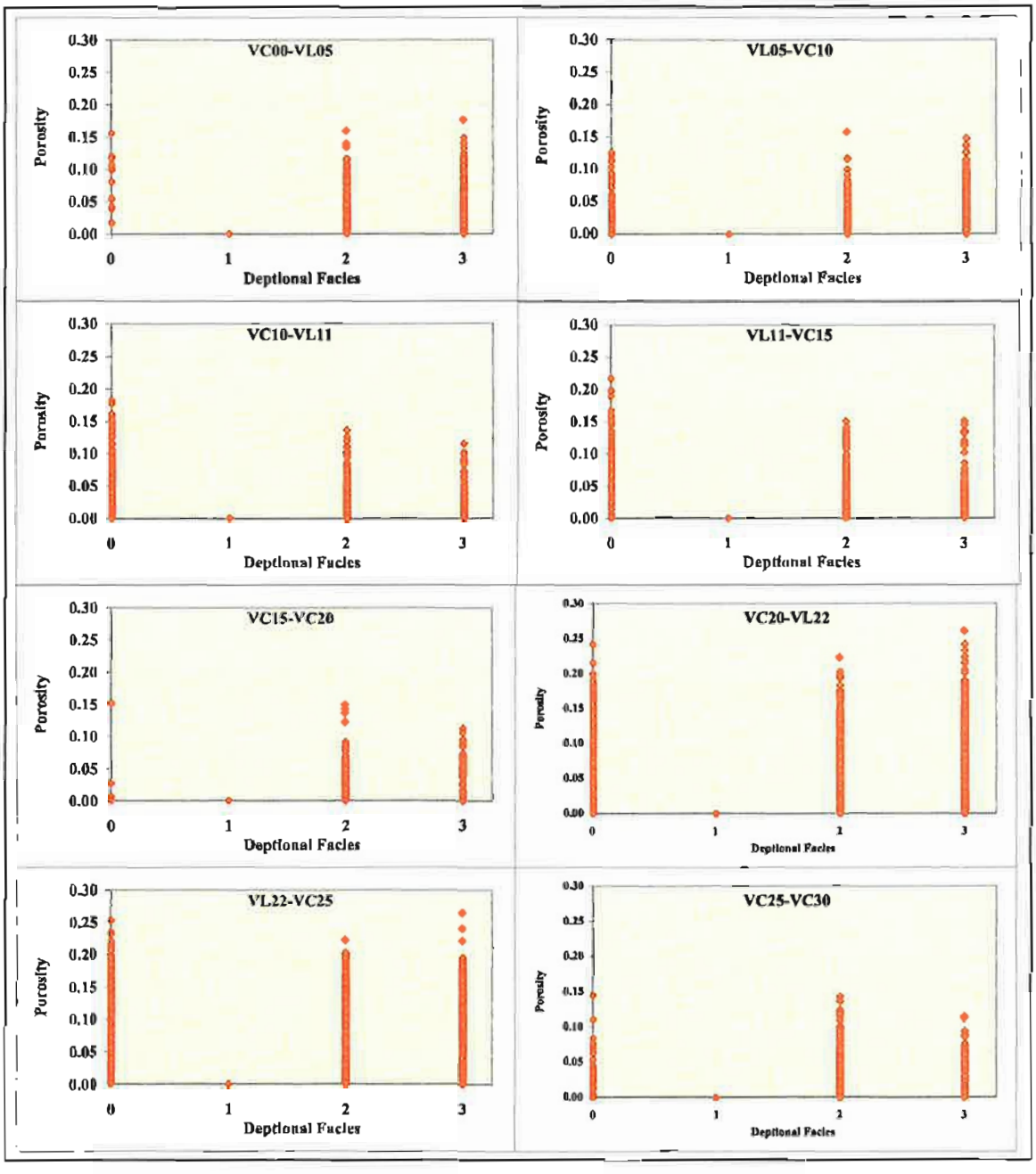

Figure A5.4: Cross-plots of porosity distribution in each facies in the porosity model-C for every reservoir interval the Daralingie Field

(Legned 0 = Channels, 1 = Coal, 2 = Shale, 3 = Spaly)

Appendix 6

The SPE/WPC reserves definitions of 1997

(Source: United Nations Economic Commission for Europe - http://daccessdds.un.org/doc/UNDOC/GEN/G03/307/10/PDF/G0330710.pdf)

The SPE/WPC reserves definitions of 1997

Preamble

Petroleum[3] is the world's major source of energy and is a key factor in the continued development of world economies. It is essential for future planning that governments and industry have a clear assessment of the quantities of petroleum available for production and quantities which are anticipated to become available within a practical time frame through additional field development, technological advances, or exploration. To achieve such an assessment, it is imperative that the industry adopt a consistent nomenclature for assessing the current and future quantities of petroleum expected to be recovered from naturally occurring underground accumulations. Such quantities are defined as reserves, and their assessment is of considerable importance to governments, international agencies, economists, bankers, and the international energy industry.

The terminology used in classifying petroleum substances and the various categories of reserves have been the subject of much study and discussion for many years. Attempts to standardize reserves terminology began in the mid 1930's when the American Petroleum Institute considered classification for petroleum and definitions of various reserves categories. Since then, the evolution of technology has yielded more precise engineering methods to determine reserves and has intensified the need for an improved nomenclature to achieve consistency among professionals working with reserves terminology. Working entirely separately, the Society of Petroleum Engineers (SPE) and the World Petroleum Congresses (WPC) produced strikingly similar sets of petroleum reserve definitions for known accumulations which were introduced in early 1987. These have become the preferred standards for reserves classification across the industry. Soon after, it became apparent to both organizations that these could be combined into a single set of definitions which could be used by the industry worldwide. Contacts between representatives of the two organizations started in 1987, shortly after the publication of the initial sets of definitions. During the World Petroleum Congress in June 1994, it was recognized that while any revisions to the current definitions would require the approval of the respective Boards of Directors, the effort to establish a worldwide nomenclature should be increased. A common nomenclature would present an enhanced opportunity for acceptance and would signify a common and unique stance on an essential technical and professional issue facing the international petroleum industry.

As a first step in the process, the organizations issued a joint statement which presented a broad set of principles on which reserves estimations and definitions should be based. A task force was established by the Boards of SPE and WPC to develop a common set of definitions based on this

---

[3] For the purpose of these definitions, the term petroleum refers to naturally occurring liquids and gases which are predominately comprised of hydrocarbon compounds. Petroleum may also contain non-hydrocarbon compounds in which sulphur, oxygen, and/or nitrogen atoms are combined with carbon and hydrogen. Common examples of non-hydrocarbons found in petroleum are nitrogen, carbon dioxide, and hydrogen sulphide.

statement of principles. The following joint statement of principles was published in the January 1996 issue of the SPE Journal of Petroleum Technology and in the June 1996 issue of the WPC Newsletter:

There is a growing awareness worldwide of the need for a consistent set of reserves definitions for use by governments and industry in the classification of petroleum reserves. Since their introduction in 1987, the Society of Petroleum Engineers and the World Petroleum Congresses reserves definitions have been standards for reserves classification and evaluation worldwide.

SPE and WPC have begun efforts toward achieving consistency in the classification of reserves. As a first step in this process, SPE and WPC issue the following joint statement of principles.

> *SPE and WPC recognize that both organizations have developed a widely accepted and simple nomenclature of petroleum reserves.*
>
> *SPE and WPC emphasize that the definitions are intended as standard, general guidelines for petroleum reserves classification which should allow for the proper comparison of quantities on a worldwide basis.*
>
> *SPE and WPC emphasize that, although the definition of petroleum reserves should not in any manner be construed to be compulsory or obligatory, countries and organizations should be encouraged to use the core definitions as defined in these principles and also to expand on these definitions according to special local conditions and circumstances.*
>
> *SPE and WPC recognize that suitable mathematical techniques can be used as required and that it is left to the country to fix the exact criteria for reasonable certainty of existence of petroleum reserves. No methods of calculation are excluded, however, if probabilistic methods are used, the chosen percentages should be unequivocally stated.*
>
> *SPE and WPC agree that the petroleum nomenclature as proposed applies only to known discovered hydrocarbon accumulations and their associated potential deposits.*
>
> *SPE and WPC stress that petroleum proved reserves should be based on current economic conditions, including all factors affecting the viability of the projects. SPE and WPC recognize that the term is general and not restricted to costs and price only. Probable and possible reserves could be based on anticipated developments and/or the extrapolation of current economic conditions.*
>
> *SPE and WPC accept that petroleum reserves definitions are not static and will evolve.*

A conscious effort was made to keep the recommended terminology as close to current common usage as possible in order to minimize the impact of previously reported quantities and changes required to bring about wide acceptance. The proposed terminology is not intended as a precise system of definitions and evaluation procedures to satisfy all situations. Due to the many forms of occurrence of petroleum, the wide range of characteristics, the uncertainty associated with the

geological environment, and the constant evolution of evaluation technologies, a precise classification system is not practical. Furthermore, the complexity required for a precise system would detract from its understanding by those involved in petroleum matters. As a result, the recommended definitions do not represent a major change from the current SPE and WPC definitions which have become the standards across the industry. It is hoped that the recommended terminology will integrate the two sets of definitions and achieve better consistency in reserves data across the international industry.

Reserves derived under these definitions rely on the integrity, skill, and judgment of the evaluator and are affected by the geological complexity, stage of development, degree of depletion of the reservoirs, and amount of available data. Use of these definitions should sharpen the distinction between the various classifications and provide more consistent reserves reporting.

Definitions

Reserves are those quantities of petroleum which are anticipated to be commercially recovered from known accumulations from a given date forward. All reserve estimates involve some degree of uncertainty. The uncertainty depends chiefly on the amount of reliable geologic and engineering data available at the time of the estimate and the interpretation of these data. The relative degree of uncertainty may be conveyed by placing reserves into one of two principal classifications, either proved or unproved. Unproved reserves are less certain to be recovered than proved reserves and may be further sub-classified as probable and possible reserves to denote progressively increasing uncertainty in their recoverability.

The intent of SPE and WPC in approving additional classifications beyond proved reserves is to facilitate consistency among professionals using such terms. In presenting these definitions, neither organization is recommending public disclosure of reserves classified as unproved. Public disclosure of the quantities classified as unproved reserves is left to the discretion of the countries or companies involved.

Estimation of reserves is done under conditions of uncertainty. The method of estimation is called deterministic if a single best estimate of reserves is made based on known geological, engineering, and economic data. The method of estimation is called probabilistic when the known geological, engineering, and economic data are used to generate a range of estimates and their associated probabilities. Identifying reserves as proved, probable, and possible has been the most frequent classification method and gives an indication of the probability of recovery. Because of potential differences in uncertainty, caution should be exercised when aggregating reserves of different classifications.

Reserves estimates will generally be revised as additional geologic or engineering data becomes available or as economic conditions change. Reserves do not include quantities of petroleum being held in inventory, and may be reduced for usage or processing losses if required for financial reporting.

Reserves may be attributed to either natural energy or improved recovery methods. Improved recovery methods include all methods for supplementing natural energy or altering natural forces in the reservoir to increase ultimate recovery. Examples of such methods are pressure maintenance, cycling, waterflooding, thermal methods, chemical flooding, and the use of miscible and immiscible displacement fluids. Other improved recovery methods may be developed in the future as petroleum technology continues to evolve.

Proved Reserves

Proved reserves are those quantities of petroleum which, by analysis of geological and engineering data, can be estimated with reasonable certainty to be commercially recoverable, from a given date forward, from known reservoirs and under current economic conditions, operating methods, and government regulations. Proved reserves can be categorized as developed or undeveloped.

If deterministic methods are used, the term reasonable certainty is intended to express a high degree of confidence that the quantities will be recovered. If probabilistic methods are used, there should be at least a 90% probability that the quantities actually recovered will equal or exceed the estimate.

Establishment of current economic conditions should include relevant historical petroleum prices and associated costs and may involve an averaging period that is consistent with the purpose of the reserve estimate, appropriate contract obligations, corporate procedures, and government regulations involved in reporting these reserves.

In general, reserves are considered proved if the commercial producibility of the reservoir is supported by actual production or formation tests. In this context, the term proved refers to the actual quantities of petroleum reserves and not just the productivity of the well or reservoir. In certain cases, proved reserves may be assigned on the basis of well logs and/or core analysis that indicate the subject reservoir is hydrocarbon bearing and is analogous to reservoirs in the same area that are producing or have demonstrated the ability to produce on formation tests.

The area of the reservoir considered as proved includes (1) the area delineated by drilling and defined by fluid contacts, if any, and (2) the undrilled portions of the reservoir that can reasonably be judged as commercially productive on the basis of available geological and engineering data. In the absence of data on fluid contacts, the lowest known occurrence of hydrocarbons controls the proved limit unless otherwise indicated by definitive geological, engineering or performance data.

Reserves may be classified as proved if facilities to process and transport those reserves to market are operational at the time of the estimate or there is a reasonable expectation that such facilities will be installed. Reserves in undeveloped locations may be classified as proved undeveloped provided (1) the locations are direct offsets to wells that have indicated commercial production in the objective formation, (2) it is reasonably certain such locations are within the known proved productive limits of the objective formation, (3) the locations conform to existing well spacing regulations where applicable, and (4) it is reasonably certain the locations will be developed. Reserves from other locations are categorized as proved undeveloped only where interpretations of geological and

engineering data from wells indicate with reasonable certainty that the objective formation is laterally continuous and contains commercially recoverable petroleum at locations beyond direct offsets.

Reserves which are to be produced through the application of established improved recovery methods are included in the proved classification when (1) successful testing by a pilot project or favorable response of an installed program in the same or an analogous reservoir with similar rock and fluid properties provides support for the analysis on which the project was based, and, (2) it is reasonably certain that the project will proceed. Reserves to be recovered by improved recovery methods that have yet to be established through commercially successful applications are included in the proved classification only (1) after a favorable production response from the subject reservoir from either (a) a representative pilot or (b) an installed program where the response provides support for the analysis on which the project is based and (2) it is reasonably certain the project will proceed.

Unproved Reserves

Unproved reserves are based on geologic and/or engineering data similar to that used in estimates of proved reserves; but technical, contractual, economic, or regulatory uncertainties preclude such reserves being classified as proved. Unproved reserves may be further classified as probable reserves and possible reserves.

Unproved reserves may be estimated assuming future economic conditions different from those prevailing at the time of the estimate. The effect of possible future improvements in economic conditions and technological developments can be expressed by allocating appropriate quantities of reserves to the probable and possible classifications.

Probable Reserves

Probable reserves are those unproved reserves which analysis of geological and engineering data suggests are more likely than not to be recoverable. In this context, when probabilistic methods are used, there should be at least a 50% probability that the quantities actually recovered will equal or exceed the sum of estimated proved plus probable reserves.

In general, probable reserves may include (1) reserves anticipated to be proved by normal step-out drilling where sub-surface control is inadequate to classify these reserves as proved, (2) reserves in formations that appear to be productive based on well log characteristics but lack core data or definitive tests and which are not analogous to producing or proved reservoirs in the area, (3) incremental reserves attributable to infill drilling that could have been classified as proved if closer statutory spacing had been approved at the time of the estimate, (4) reserves attributable to improved recovery methods that have been established by repeated commercially successful applications when (a) a project or pilot is planned but not in operation and (b) rock, fluid, and reservoir characteristics appear favorable for commercial application, (5) reserves in an area of the formation that appears to be separated from the proved area by faulting and the geologic interpretation indicates the subject area is structurally higher than the proved area, (6) reserves attributable to a future workover, treatment, re-treatment, change of equipment, or other mechanical procedures, where such procedure has not been proved successful in wells which exhibit similar

behaviour in analogous reservoirs, and (7) incremental reserves in proved reservoirs where an alternative interpretation of performance or volumetric data indicates more reserves than can be classified as proved.

Possible Reserves

Possible reserves are those unproved reserves which analysis of geological and engineering data suggests are less likely to be recoverable than probable reserves. In this context, when probabilistic methods are used, there should be at least a 10% probability that the quantities actually recovered will equal or exceed the sum of estimated proved plus probable plus possible reserves.

In general, possible reserves may include (1) reserves which, based on geological interpretations, could possibly exist beyond areas classified as probable, (2) reserves in formations that appear to be petroleum bearing based on log and core analysis but may not be productive at commercial rates, (3) incremental reserves attributed to infill drilling that are subject to technical uncertainty, (4) reserves attributed to improved recovery methods when (a) a project or pilot is planned but not in operation and (b) rock, fluid, and reservoir characteristics are such that a reasonable doubt exists that the project will be commercial, and (5) reserves in an area of the formation that appears to be separated from the proved area by faulting and geological interpretation indicates the subject area is structurally lower than the proved area.

Reserve Status Categories

Reserve status categories define the development and producing status of wells and reservoirs.

Developed: Developed reserves are expected to be recovered from existing wells including reserves behind pipe. Improved recovery reserves are considered developed only after the necessary equipment has been installed, or when the costs to do so are relatively minor. Developed reserves may be sub-categorized as producing or non-producing.

> ***Producing:*** Reserves subcategorized as producing are expected to be recovered from completion intervals which are open and producing at the time of the estimate. Improved recovery reserves are considered producing only after the improved recovery project is in operation.
>
> ***Non-producing:*** Reserves subcategorized as non-producing include shut-in and behind-pipe reserves. Shut-in reserves are expected to be recovered from (1) completion intervals which are open at the time of the estimate but which have not started producing, (2) wells which were shut-in for market conditions or pipeline connections, or (3) wells not capable of production for mechanical reasons. Behind-pipe reserves are expected to be recovered from zones in existing wells, which will require additional completion work or future recompletion prior to the start of production.

Undeveloped Reserves: Undeveloped reserves are expected to be recovered: (1) from new wells on undrilled acreage, (2) from deepening existing wells to a different reservoir, or (3) where a relatively

large expenditure is required to (a) recomplete an existing well or (b) install production or transportation facilities for primary or improved recovery projects.

Approved by the Board of Directors, Society of Petroleum Engineers (SPE) Inc., and the Executive Board, World Petroleum Congresses (WPC), March 1997.

Appendix 7

The SPE/WPC/AAPG 2000 resource classification of 2000

(Source: United Nations Economic Commission for Europe - http://daccessdds.un.org/doc/UNDOC/GEN/G03/307/10/PDF/G0330710.pdf)

The SPE/WPC/AAPG resource classification of 2000

Resources

In March 1997, the Society of Petroleum Engineers (SPE) and the World Petroleum Congresses (WPC) approved a set of petroleum* reserves definitions which represented a major step forward in their mutual desire to improve the level of consistency in reserves estimation and reporting on a worldwide basis. As a further development, the SPE and WPC recognized the potential benefits to be obtained by supplementing those definitions to cover the entire resource base, including those quantities of petroleum contained in accumulations that are currently sub-commercial or that have yet to be discovered. These other resources represent potential future additions to reserves and are therefore important to both countries and companies for planning and portfolio management purposes. In addition, the American Association of Petroleum Geologists (AAPG) participated in the development of these definitions and joined SPE and WPC as a sponsoring organization.

In 1987, the WPC published its report "Classification and Nomenclature Systems for Petroleum and Petroleum Reserves," which included definitions for all categories of resources. The WPC report, together with definitions by other industry organizations and recognition of current industry practice, provided the basis for the system outlined here.

Nothing in the following resource definitions should be construed as modifying the existing definitions for petroleum reserves as approved by the SPE/WPC in March 1997.

As with unproved (i.e. probable and possible) reserves, the intent of the SPE and WPC in approving additional classifications beyond proved reserves is to facilitate consistency among professionals using such terms. In presenting these definitions, neither organization is recommending public disclosure of quantities classified as resources. Such disclosure is left to the discretion of the countries or companies involved.

Estimates derived under these definitions rely on the integrity, skill, and judgement of the evaluator and are affected by the geological complexity, stage of exploration or development, degree of depletion of the reservoirs, and amount of available data. Use of the definitions should sharpen the distinction between various classifications and provide more consistent resources reporting.

DEFINITIONS. The resource classification system is summarized in Figure 1 and the relevant definitions are given below. Elsewhere, resources have been defined as including all quantities of petroleum which are estimated to be initially-in-place; however, some users consider only the estimated recoverable portion to constitute a resource. In these definitions, the quantities estimated to be initially-in-place are defined as Total Petroleum-initially-in-place, Discovered Petroleum-initially-in-place and Undiscovered Petroleum-initially-in-place, and the recoverable

portions are defined separately as Reserves, Contingent Resources and Prospective Resources. In any event, it should be understood that reserves constitute a subset of resources, being those quantities that are discovered (i.e. in known accumulations), recoverable, commercial and remaining.

TOTAL PETROLEUM-INITIALLY-IN-PLACE. Total Petroleum-initially-in-place is that quantity of petroleum which is estimated to exist originally in naturally occurring accumulations. Total Petroleum-initially-in-place is, therefore, that quantity of petroleum which is estimated, on a given date, to be contained in known accumulations, plus those quantities already produced therefrom, plus those estimated quantities in accumulations yet to be discovered. Total Petroleum-initially-in-place may be subdivided into Discovered Petroleum-initially-in-place and Undiscovered Petroleum-initially-in-place, with Discovered Petroleum-initially-in-place being limited to known accumulations.

It is recognized that all Petroleum-initially-in-place quantities may constitute potentially recoverable resources since the estimation of the proportion which may be recoverable can be subject to significant uncertainty and will change with variations in commercial circumstances, technological developments and data availability. A portion of those quantities classified as Unrecoverable may become recoverable resources in the future as commercial circumstances change, technological developments occur, or additional data are acquired.

DISCOVERED PETROLEUM-INITIALLY-IN-PLACE. Discovered Petroleum-initially-in-place is that quantity of petroleum which is estimated, on a given date, to be contained in known accumulations, plus those quantities already produced therefrom. Discovered Petroleum-initially-in-place may be subdivided into Commercial and Sub-commercial categories, with the estimated potentially recoverable portion being classified as Reserves and Contingent Resources respectively, as defined below.

RESERVES. Reserves are defined as those quantities of petroleum which are anticipated to be commercially recovered from known accumulations from a given date forward. Reference should be made to the full SPE/WPC Petroleum Reserves Definitions for the complete definitions and guidelines.

Estimated recoverable quantities from known accumulations which do not fulfil the requirement of commerciality should be classified as Contingent Resources, as defined below. The definition of commerciality for an accumulation will vary according to local conditions and circumstances and is left to the discretion of the country or company concerned. However, reserves must still be categorized according to the specific criteria of the SPE/WPC definitions and therefore proved reserves will be limited to those quantities that are commercial under current economic conditions, while probable and possible reserves may be based on future economic conditions. In general, quantities should not be classified as reserves unless there is an expectation that the accumulation will be developed and placed on production within a reasonable timeframe.

In certain circumstances, reserves may be assigned even though development may not occur for some time. An example of this would be where fields are dedicated to a long-term supply contract and will only be developed as and when they are required to satisfy that contract.

CONTINGENT RESOURCES. Contingent Resources are those quantities of petroleum which are estimated, on a given date, to be potentially recoverable from known accumulations, but which are not currently considered to be commercially recoverable.

It is recognized that some ambiguity may exist between the definitions of contingent resources and unproved reserves. This is a reflection of variations in current industry practice. It is recommended that if the degree of commitment is not such that the accumulation is expected to be developed and placed on production within a reasonable timeframe, the estimated recoverable volumes for the accumulation be classified as contingent resources.

Contingent Resources may include, for example, accumulations for which there is currently no viable market, or where commercial recovery is dependent on the development of new technology, or where evaluation of the accumulation is still at an early stage.

UNDISCOVERED PETROLEUM-INITIALLY-IN-PLACE. Undiscovered Petroleum-initially-in-place is that quantity of petroleum which is estimated, on a given date, to be contained in accumulations yet to be discovered. The estimated potentially recoverable portion of Undiscovered Petroleum-initially-in-place is classified as Prospective Resources, as defined below.

PROSPECTIVE RESOURCES. Prospective Resources are those quantities of petroleum which are estimated, on a given date, to be potentially recoverable from undiscovered accumulations.

ESTIMATED ULTIMATE RECOVERY. Estimated Ultimate Recovery (EUR) is not a resource category as such, but a term which may be applied to an individual accumulation of any status/maturity (discovered or undiscovered). Estimated Ultimate Recovery is defined as those quantities of petroleum which are estimated, on a given date, to be potentially recoverable from an accumulation, plus those quantities already produced therefrom.

AGGREGATION. Petroleum quantities classified as Reserves, Contingent Resources or Prospective Resources should not be aggregated with each other without due consideration of the significant differences in the criteria associated with their classification. In particular, there may be a significant risk that accumulations containing Contingent Resources or Prospective Resources will not achieve commercial production.

RANGE OF UNCERTAINTY. The Range of Uncertainty, as shown in Figure 1, reflects a reasonable range of estimated potentially recoverable volumes for an individual accumulation. Any estimation of resource quantities for an accumulation is subject to both technical and commercial uncertainties, and should, in general, be quoted as a range. In the case of reserves, and where appropriate, this range of uncertainty can be reflected in estimates for Proved Reserves (1P), Proved plus Probable Reserves (2P) and Proved plus Probable plus Possible Reserves (3P) scenarios. For other resource categories, the terms Low Estimate, Best Estimate and High Estimate are recommended.

The term "Best Estimate" is used here as a generic expression for the estimate considered to be the closest to the quantity that will actually be recovered from the accumulation between the date of the estimate and the time of abandonment. If probabilistic methods are used, this term would generally be a measure of central tendency of the uncertainty distribution (most likely/mode,

median/P50 or mean). The terms "Low Estimate" and "High Estimate" should provide a reasonable assessment of the range of uncertainty in the Best Estimate.

For undiscovered accumulations (Prospective Resources) the range will, in general, be substantially greater than the ranges for discovered accumulations. In all cases, however, the actual range will be dependent on the amount and quality of data (both technical and commercial) which is available for that accumulation. As more data become available for a specific accumulation (e.g. additional wells, reservoir performance data) the range of uncertainty in EUR for that accumulation should be reduced.

RESOURCES CLASSIFICATION SYSTEM

Graphical Representation

Figure 1 is a graphical representation of the definitions. The horizontal axis represents the range of uncertainty in the estimated potentially recoverable volume for an accumulation, whereas the vertical axis represents the level of status/maturity of the accumulation. Many organizations choose to further sub-divide each resource category using the vertical axis to classify accumulations on the basis of the commercial decisions required to move an accumulation towards production.

As indicated in Figure 1, the Low, Best and High Estimates of potentially recoverable volumes should reflect some comparability with the reserves categories of Proved, Proved plus Probable and Proved plus Probable plus Possible, respectively. While there may be a significant risk that sub-commercial or undiscovered accumulations will not achieve commercial production, it is useful to consider the range of potentially recoverable volumes independently of such a risk.If probabilistic methods are used, these estimated quantities should be based on methodologies analogous to those applicable to the definitions of reserves; therefore, in general, there should be at least a 90% probability that, assuming the accumulation is developed, the quantities actually recovered will equal or exceed the Low Estimate. In addition, an equivalent probability value of 10% should, in general, be used for the High Estimate. Where deterministic methods are used, a similar analogy to the reserves definitions should be followed.

As one possible example, consider an accumulation that is currently not commercial due solely to the lack of a market. The estimated recoverable volumes are classified as Contingent Resources, with Low, Best and High estimates. Where a market is subsequently developed, and in the absence of any new technical data, the accumulation moves up into the Reserves category and the Proved Reserves estimate would be expected to approximate the previous Low Estimate.

FIGURE 1 - RESOURCE CLASSIFICATION SYSTEM

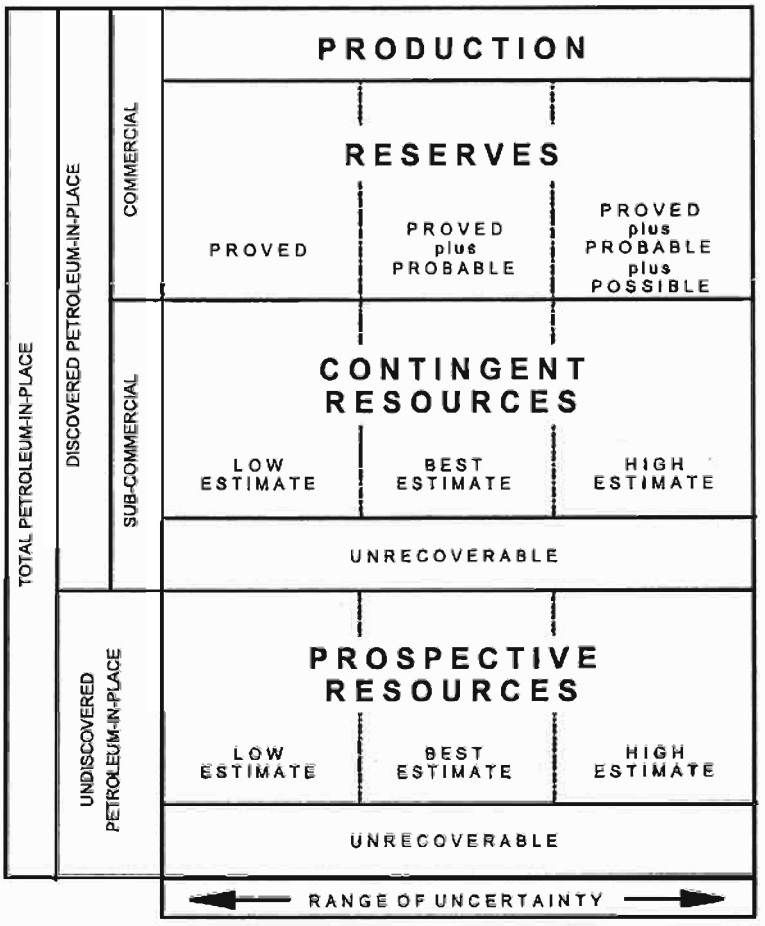

Appendix 8

United Nations Framework Draft Definitions of Reserves

(Source: United Nations Economic Commission for Europe - http://daccessdds.un.org/doc/UNDOC/GEN/G03/307/10/PDF/G0330710.pdf)

DRAFT DEFINITIONS

Reference	Term	Definition
Merriam-Webster online	Commercial	Suitable, adequate, or prepared for the exchange or buying and selling of commodities on a large scale involving transportation from place to place
New	Committed project	A project where the parties who have the rights to undertake it have done so. Projects are committed when they produce hydrocarbons, are developed, or are in development. Undeveloped projects are committed only when the relevant parties have undertaken to carry them out within a reasonable timeframe, or when decisions of the parties and prior committed projects de facto provide a commitment to define and execute them later. These commitments should be unconditional, except for timing that may be dependent on the development of prior committed projects. An example of this would be where fields are dedicated to a long-term supply contract and will only be developed as and when they are required to satisfy the contract.
New	Contingent	Dependent upon conditions that may or may not be fulfilled.
New	Contingent project	Project dependent upon conditions that may or may not be fulfilled.
Adapted from SPE	Contingent resources	Contingent resources are those quantities of petroleum which are estimated, on a given date, to be potentially recoverable from known accumulations, but which are not currently considered to be commercially recoverable. A discovered resource will remain contingent as long as there is no prudent basis for making a commitment to produce it. When such a basis exists, the resources will remain contingent until the commitment is made (explicitly or de facto). Contingent Resources may include, for example, accumulations for which there is currently no viable market, or where commercial recovery is dependent on the development of new technology, or where evaluation of the accumulation is still at an early stage.
Adapted from SPE	Developed projects	Developed projects are those from which reserves are expected to be recovered from existing wells including reserves behind pipe. Developed projects are committed and may be sub-categorized as producing or non-producing.
New	Discovered (on the geology axis)	Discoveries where the geologic conditions in which petroleum occurs have been observed directly through drilling, but where they are not known to the extent required for the geology to be considered explored and delineated.

Reference	Term	Definition
Adapted from NPD	Discovery	A discovery is one petroleum accumulation (also called deposit or pool), or several petroleum accumulations collectively that have been discovered in the same wildcat well, in which there has been established a probability of the existence of mobile petroleum (includes both a commercial and a technical discovery) through testing, sampling or logging. This includes the hydrodynamically accumulated as well as the distributed or continuous resources. Examples of such distributed or continuous resources are heavy oil, basin centre gas, gas hydrates, coal bed methane, etc.
New	Exploration project	Exploration (prospecting) of undiscovered quantities of petroleum that are estimated, on a give date, to be potentially recoverable.
New	Explored and delineated geology	Discoveries where the geologic conditions, fluid properties and flow characteristics are well enough known to form the basis for a development commitment for the production of reserves.
New	Field	A field is one or more discoveries together that are comprised in one plan for development and operation.
Webster New World Dictionary	Hydrocarbons	Any compound containing only hydrogen and carbon: benzene and methane are hydrocarbons.
Adapted from NDP	Lead	A lead is a petroleum trap (or more than one trap) where the quantity and quality of available data are inadequate to map and delimit the reservoir rock volume.
New	Lead/play under exploration	A lead or play for which a decision has been taken to gather geological, geophysical, geochemical and other adequate data to map and delimit the reservoir. The pupose shall be to prepare a decision of whether or not to proceed to direct detection of petroleum through drilling.
New	Lead or play under reconnaissance	Unexplored lead or play under reconnaissance or without exploration effort.
New	Not commercial	Not commercial under current economic conditions and fiscal terms, nor under such conditions and terms that may be expected in the future based on current information.
SPE has been requested to consider refining the definition with respect to the heavy fractions	Petroleum	All liquid and gaseous hydrocarbons, including gas hydrates and bitumen which exist in their natural state in the subsoil, as well as other substances produced in association with such hydrocarbons.

Reference	Term	Definition
Adapted from NPD	Play	A play is a geographically and stratigraphically delimited area where a specific set of geological factors exists that are required for petroleum to be found in commercial quantities. Such geological factors are reservoir rock, trap, mature source rock and migration paths. The trap must have formed before termination of the migration of petroleum. All discoveries and prospects within the same play are characterised by the specific set of geological factors of the play. *Confirmed play* contains at least one discovery of commercial quantities of petroleum. It is thus confirmed that the critical geological factors are simultaneously present for the play. *Unconfirmed play* is a play in which no petroleum has been discovered, either because exploration has still not started, or because only dry wells have been drilled in the play.
New	Produced Petroleum	Petroleum removed from its natural state in the subsoil, properly processed and measured at its reference point.
New	Project in development	A committed project whose plan for development has been approved as required and where the development works have started or are imminent.
New	Project in planning	A project where a decision to develop a full plan for development and operation has been taken. Normally, critical elements that may prevent development will have been eliminated before planning of the full development starts.
New	Project not very likely	Discovered and technically recoverable petroleum resources for which a project to recover them is not very likely, even in the long term. This includes resources in small, untested discoveries whose recovery seems unlikely. This category contains petroleum resources that require substantial changes in technology, prices, etc., to be recovered profitably, and where it is not very likely that the changes required would take place.
NPD:	Prospect	A prospect is a possible petroleum trap with a mappable, delimited reservoir rock volume.
New	Prospect matured for drilling	A prospect for which the decision to explore by drilling has been taken.
New	Prospect not matured for drilling	A prospect for which the decision to explore by drilling has not been taken.
New	Prospective resources	Prospective resources are those quantities of petroleum that are postulated from geological information and theory, on a given date, to be potentially recoverable from outside of known oil and gas fields.

Reference	Term	Definition
SPE	Proved reserves	Proved reserves are those quantities of petroleum which, by analysis of geological and engineering data, can be estimated with reasonable certainty to be commercially recoverable, from a given date forward, from known reservoirs and under current economic conditions, operating methods, and government regulations. Proved reserves can be categorized as developed or undeveloped. If deterministic methods are used, the term reasonable certainty is intended to express a high degree of confidence that the quantities will be recovered. If probabilistic methods are used, there should be at least a 90% probability that the quantities actually recovered will equal or exceed the estimate. Establishment of current economic conditions should include relevant historical petroleum prices and associated costs and may involve an averaging period that is consistent with the purpose of the reserve estimate, appropriate contract obligations, corporate procedures, and government regulations involved in reporting these reserves. In general, reserves are considered proved if the commercial producibility of the reservoir is supported by actual production or formation tests. In this context, the term proved refers to the actual quantities of petroleum reserves and not just the productivity of the well or reservoir. In certain cases, proved reserves may be assigned on the basis of well logs and/or core analysis that indicate the subject reservoir is hydrocarbon bearing and is analogous to reservoirs in the same area that are producing or have demonstrated the ability to produce on formation tests. The area of the reservoir considered as proved includes (1) the area delineated by drilling and defined by fluid contacts, if any, and (2) the undrilled portions of the reservoir that can reasonably be judged as commercially productive on the basis of available geological and engineering data. In the absence of data on fluid contacts, the lowest known occurrence of hydrocarbons controls the proved limit unless otherwise indicated by definitive geological, engineering or performance data. Reserves may be classified as proved if facilities to process and transport those reserves to market are operational at the time of the estimate or there is a reasonable expectation that such facilities will be installed. Reserves in undeveloped locations may be classified as proved undeveloped provided (1) the locations are direct offsets to wells that have indicated commercial production in the objective formation, (2) it is reasonably certain such locations are within the known proved productive limits of the

Reference	Term	Definition
		objective formation, (3) the locations conform to existing well spacing regulations where applicable, and (4) it is reasonably certain the locations will be developed. Reserves from other locations are categorized as proved undeveloped only where interpretations of geological and engineering data from wells indicate with reasonable certainty that the objective formation is laterally continuous and contains commercially recoverable petroleum at locations beyond direct offsets. Reserves which are to be produced through the application of established improved recovery methods are included in the proved classification when (1) successful testing by a pilot project or favorable response of an installed program in the same or an analogous reservoir with similar rock and fluid properties provides support for the analysis on which the project was based, and, (2) it is reasonably certain that the project will proceed. Reserves to be recovered by improved recovery methods that have yet to be established through commercially successful applications are included in the proved classification only (1) after a favorable production response from the subject reservoir from either (a) a representative pilot or (b) an installed program where the response provides support for the analysis on which the project is based and (2) it is reasonably certain the project will proceed
New	Proved geology	Geology is considered proved when it is known to the extent and detail specified in the definition of proved reserves.
Adapted from SPE	Reserves	Reserves are those quantities of petroleum that are anticipated to be commercially recovered from known accumulations from a given date forward as a result of development and production commitments.
New	Resources	Resources are comprised of reserves, contingent resources and prospective resources.
New	Standard commercial conditions	Standard economic conditions are fixed by agreement or regulation. They normally include relevant historical petroleum prices and associated costs (including listed future prices) and may involve an averaging period that is consistent with the purpose of the reserve estimate, appropriate contract obligations, corporate procedures, and government regulations involved in reporting these reserves.
New	Unclarified project	A project that has been properly evaluated, and where the possibility for development is high. The planning of a development project has not been initiated, normally pending the clarification of certain critical factors that may prevent successful development and production.

Reference	Term	Definition
New	Undefined project	New discovery where the evaluation of the acquired data are not yet evaluated. An undefined project may also be a possible, or conceptual improved recovery project aimed at improving the recovery that may be achieved through other, more firmly defined projects in the reserves or contingent resources categories.
New	Undeveloped project	Projects that the parties who have the right to undertake development and production are committed to undertake but where the plans are not yet prepared for approval and execution.
New	Unexplored lead or play	An unconfirmed lead or play where at most reconnaissance exploration has been conducted

Appendix 9

Statistical Properties for Distributions Used in This Study

(Source: @Risk v4.5 user manual)

Inverse Gaussian

RISKInvGauss(μ, λ)

Parameters:

μ	continuous parameter	μ > 0
λ	continous parameter	λ > 0

Domain:

x > 0	continuous

Density and Cumulative Functions:

$$f(x) = \sqrt{\frac{\lambda}{2\pi x^3}}\, e^{-\left[\frac{\lambda(x-\mu)^2}{2\mu^2 x}\right]}$$

$$F(x) = \Phi\left[\sqrt{\frac{\lambda}{x}}\left(\frac{x}{\mu}-1\right)\right] + e^{2\lambda/\mu}\,\Phi\left[-\sqrt{\frac{\lambda}{x}}\left(\frac{x}{\mu}+1\right)\right]$$

where Φ is the *Error Function*.

Mean:

$$\mu$$

Variance:

$$\frac{\mu^3}{\lambda}$$

Skewness:

$$3\sqrt{\frac{\mu}{\lambda}}$$

Kurtosis:

$$3+15\frac{\mu}{\lambda}$$

Mode:

$$\mu\left[\left(1+\frac{9\mu^2}{4\lambda^2}\right)-\frac{3\mu}{2\lambda}\right]$$

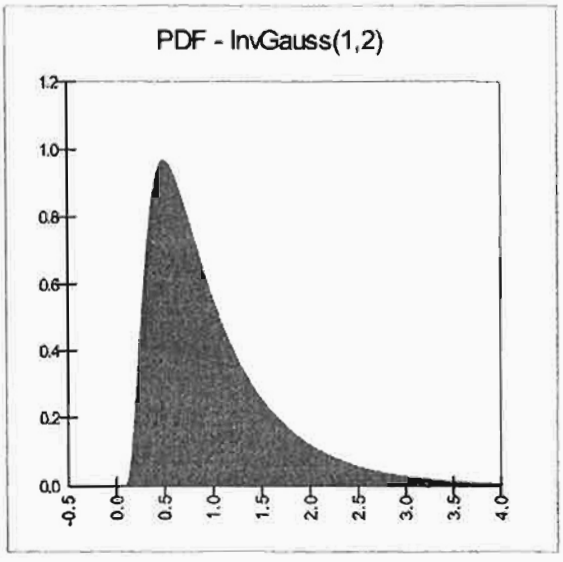

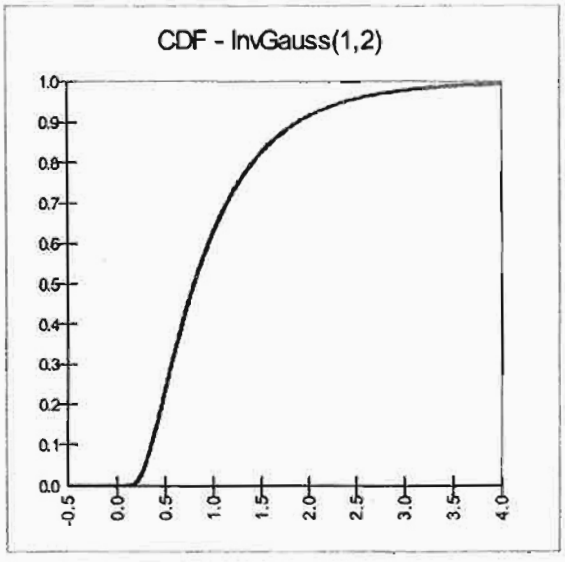

Logistic

RISKLogistic(α, β)

Parameters:

α	continuous location parameter	
β	continuous scale parameter	β > 0

Domain:

$-\infty \le x \le +\infty$	continuous

Density and Cumulative Functions:

$$f(x) = \frac{\operatorname{sech}^2\left(\frac{1}{2}\left(\frac{x-\alpha}{\beta}\right)\right)}{4\beta}$$

$$F(x) = \frac{1 + \tanh\left(\frac{1}{2}\left(\frac{x-\alpha}{\beta}\right)\right)}{2}$$

where "tanh" is the *Hyperbolic Tangent Function*.

Mean:

$$\alpha$$

Variance:

$$\frac{\pi^2\beta^2}{3}$$

Skewness:

0

Kurtosis:

4.2

Mode:

α

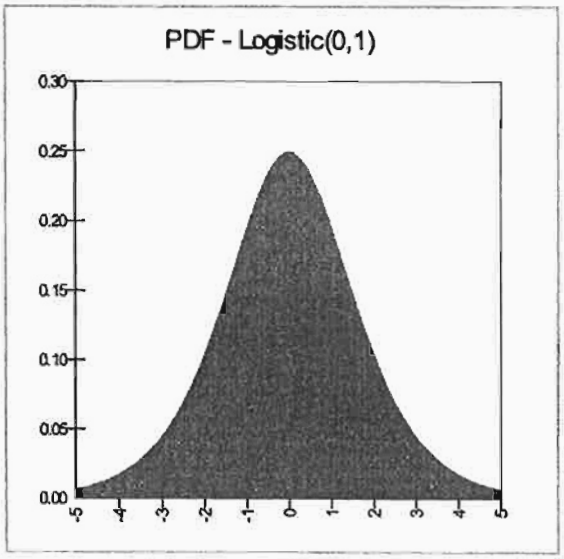

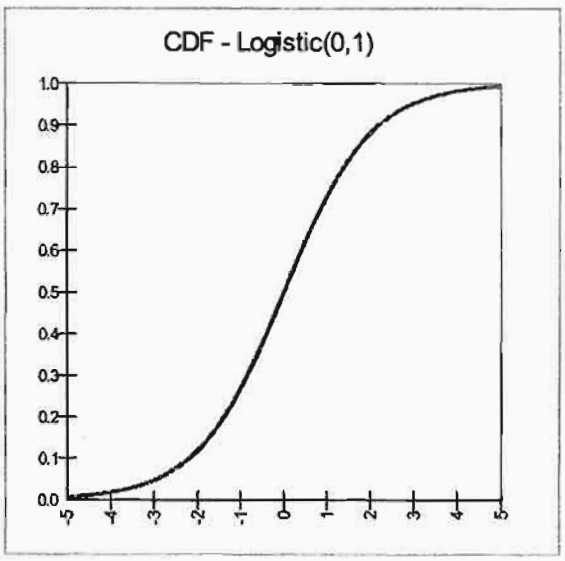

Lognormal (Format 1)

RISKLognorm(μ, σ)

Parameters:

μ	continuous parameter	$\mu > 0$
σ	continous parameter	$\sigma > 0$

Domain:

$0 \le x \le +\infty$ continuous

Density and Cumulative Functions:

$$f(x) = \frac{1}{x\sqrt{2\pi}\sigma'} e^{-\frac{1}{2}\left[\frac{\ln x - \mu'}{\sigma'}\right]^2}$$

$$F(x) = \Phi\left(\frac{\ln x - \mu'}{\sigma'}\right)$$

with $\mu' \equiv \ln\left[\frac{\mu^2}{\sqrt{\sigma^2 + \mu^2}}\right]$ and $\sigma' \equiv \frac{1}{2}\ln\left[1 + \left(\frac{\sigma}{\mu}\right)^2\right]$

where Φ is the *Error Function*.

Mean:

μ

Variance:

σ^2

Normal

RISKNormal(μ, σ)

Parameters:

μ	continuous location parameter	
σ	continuous scale parameter	σ > 0

Domain:

$-\infty \le x \le +\infty$	continuous

Density and Cumulative Functions:

$$f(x) = \frac{1}{\sqrt{2\pi}\sigma} e^{-\frac{1}{2}\left(\frac{x-\mu}{\sigma}\right)^2}$$

$$F(x) = \Phi\left(\frac{x-\mu}{\sigma}\right)$$

where Φ is the *Error Function*.

Mean:

μ

Variance:

σ^2

Skewness:

0

Kurtosis:

3

Mode:

μ

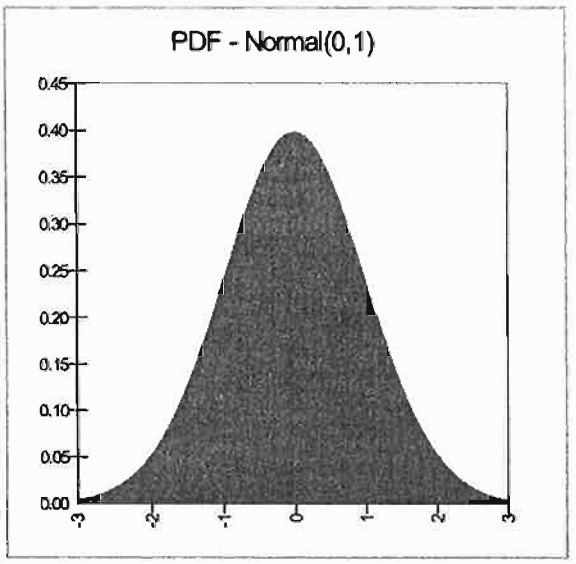

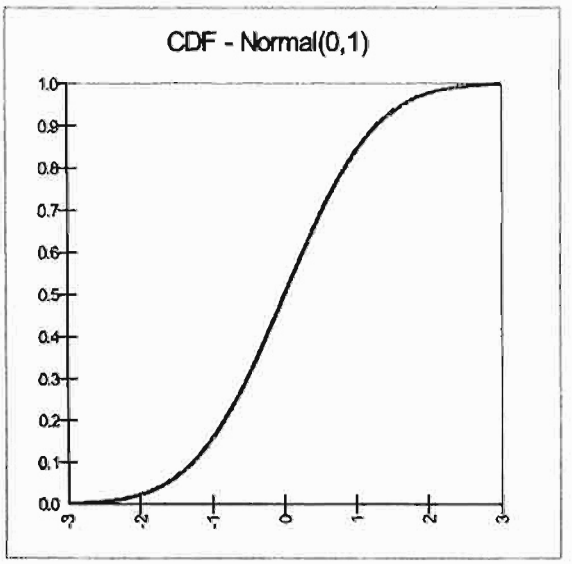

Triangular

RISKTriang(min, m.likely, max)

Parameters:

min	continuous boundary parameter	min < max
m.likely	continuous mode parameter	min ≤ m.likely ≤ max
max	continuous boundary parameter	

Domain:

$\min \le x \le \max$	continuous

Density and Cumulative Functions:

$$f(x) = \frac{2(x-\min)}{(\text{m.likely}-\min)(\max-\min)} \qquad \min \le x \le \text{m.likely}$$

$$f(x) = \frac{2(\max-x)}{(\max-\text{m.likely})(\max-\min)} \qquad \text{m.likely} \le x \le \max$$

$$F(x) = \frac{(x-\min)^2}{(\text{m.likely}-\min)(\max-\min)} \qquad \min \le x \le \text{m.likely}$$

$$F(x) = 1 - \frac{(\max-x)^2}{(\max-\text{m.likely})(\max-\min)} \qquad \text{m.likely} \le x \le \max$$

Mean:

$$\frac{\max + \text{m.likely} + \max}{3}$$

Variance:

$$\frac{\max^2 + \text{m.likely}^2 + \max^2 - (\max)(\text{m.likely}) - (\text{m.likely})(\min) - (\max)(\min)}{18}$$

Skewness:

$$\frac{2\sqrt{2}}{5}\frac{f\left(f^2-9\right)}{\left(f^2+3\right)^{3/2}} \qquad \text{where } f \equiv \frac{2(\text{m.likely}-\min)}{\max-\min} - 1$$

Kurtosis:

2.4

Mode:

m.likely

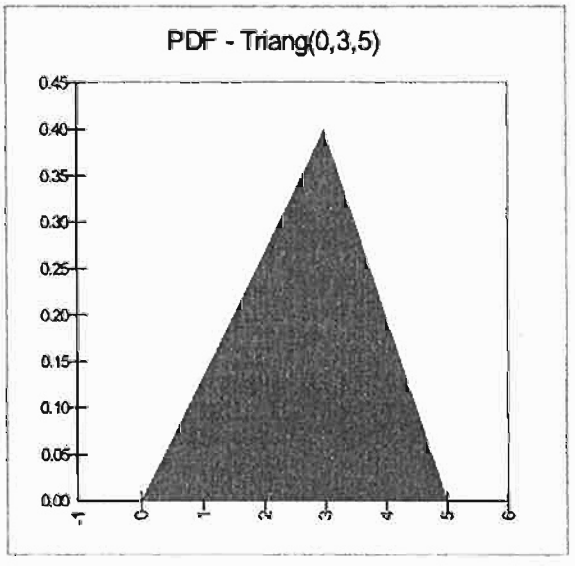

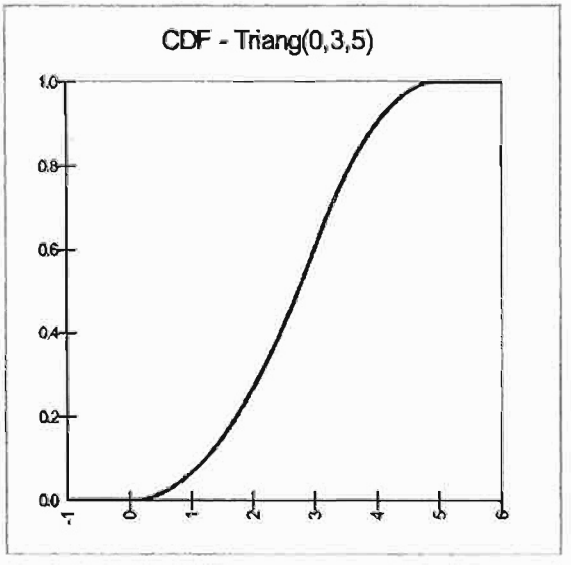

Weibull

RISKWeibull(α, β)

Parameters:

α	continuous shape parameter	$\alpha > 0$
β	continuous scale parameter	$\beta > 0$

Domain:

$0 \le x < +\infty$	continuous

Density and Cumulative Functions:

$$f(x) = \frac{\alpha x^{\alpha - 1}}{\beta^{\alpha}} e^{-(x/\beta)^{\alpha}}$$

$$F(x) = 1 - e^{-(x/\beta)^{\alpha}}$$

Mean:

$$b\Gamma\left(1 + \frac{1}{\alpha}\right)$$

where Γ is the *Gamma Function*.

Variance:

$$\beta^2\left[\Gamma\left(1 + \frac{2}{\alpha}\right) - \Gamma^2\left(1 + \frac{1}{\alpha}\right)\right]$$

where Γ is the *Gamma Function*.

Skewness:

$$\frac{\Gamma\left(1+\frac{3}{\alpha}\right)+3\Gamma\left(1+\frac{2}{\alpha}\right)\Gamma\left(1+\frac{1}{\alpha}\right)+2\Gamma^3\left(1+\frac{1}{\alpha}\right)}{\left[\Gamma\left(1+\frac{2}{\alpha}\right)-\Gamma^2\left(1+\frac{1}{\alpha}\right)\right]^{3/2}}$$

where Γ is the *Gamma Function*.

Mode:

$$\beta\left(1-\frac{1}{\alpha}\right)^{1/\alpha} \qquad \text{for } \alpha > 1$$

$$0 \qquad \text{for } \alpha \leq 1$$